



**HAL**  
open science

# Probabilistic models of impedance matrices. Application to dynamic soil-structure interaction

Régis Cottureau

► **To cite this version:**

Régis Cottureau. Probabilistic models of impedance matrices. Application to dynamic soil-structure interaction. Materials. Ecole Centrale Paris, 2007. English. NNT: . tel-00132950

**HAL Id: tel-00132950**

**<https://theses.hal.science/tel-00132950>**

Submitted on 23 Feb 2007

**HAL** is a multi-disciplinary open access archive for the deposit and dissemination of scientific research documents, whether they are published or not. The documents may come from teaching and research institutions in France or abroad, or from public or private research centers.

L'archive ouverte pluridisciplinaire **HAL**, est destinée au dépôt et à la diffusion de documents scientifiques de niveau recherche, publiés ou non, émanant des établissements d'enseignement et de recherche français ou étrangers, des laboratoires publics ou privés.

# Probabilistic models of impedance matrices.

Application to dynamic soil-structure interaction.

## THÈSE

présentée et soutenue publiquement le 18/01/2006

pour l'obtention du

**Doctorat de l'Ecole Centrale Paris**  
(spécialité mécanique)

par

Régis Cottereau

sous la direction du Prof. D. Clouteau et du Prof. C. Soize

### Composition du Jury

*Président :* Prof. L. Jézéquel (École Centrale Lyon)

*Rapporteurs :* Prof. E. Alarcón (Universidad Politécnica de Madrid, Spain)  
Prof. G. I. Schuëller (Leopold-Franzens University, Austria)

*Examineurs :* Prof. P. Labbé (EDF-SEPTEN)  
Prof. D. Clouteau (École Centrale Paris)  
Prof. C. Soize (Université de Marne-la-Vallée)



# Acknowledgments

It is a great pleasure for me to express my sincere gratitude to Prof. Didier Clouteau and Prof Christian Soize, who supervised this work. For the amazing amount of knowledge concurrently held, of which they tried to pass some on to me. For their organization in the joint supervision, which lacked the unnecessary inertia sometimes found in this type of collaboration. For the freedom they left me. And because it has been a real pleasure, scientific and human, to know them and to work with them.

I am very grateful to the thesis committee: Prof. Gerhart I. Schuëller, Prof. Enrique Alarcón, Prof. Louis Jézéquel, and Prof. Pierre Labbé. In particular, I am indebted to Prof. Gerhart I. Schuëller and Prof. Enrique Alarcón for accepting the tedious work of reviewing the manuscript.

Several people around the world have lent a helpful hand at some point during these four years. I list them here, in no particular order, and thank them heartily. Prof. Roger Ghanem, from USC, Prof. Eduardo Kausel, from MIT, Prof. Marc van Barel, from KU Leuven, Prof. Qiao and Dr. Wei, from McMaster University.

The steady collaboration with Prof. Geert Degrande, Dr. Geert Lombaert, Dr. Mattias Schevenels, and the other Ph.D. students at the department of Civil Engineering of KU Leuven was very fruitful. The campaign of measures that was conducted in February 2006 helped me discover that there was something beyond computers and numerical experiments. Thanks to you all !

There are far too many people at the Laboratoire MSSMat and at the École Centrale Paris I would like to thank to list them all here. However, I must acknowledge Prof. Denis Aubry and Prof. Didier Clouteau for offering me numerous opportunities to teach. Further, the company of Maarten, Jean-Michel, Guillaume, Oscar, Rémi, Anne-Sophie, Reza, Hamid, Haithem, Arnaud, Audrey, Jean-Philippe, David, Hachmi, Étienne, Bing, Steven, Damien, and many others made this time at ECP enjoyable as much as studios.

January 23, 2007, Paris



# Résumé

Dans de nombreux domaines d'application, comme en génie civil ou en aéronautique, les ingénieurs sont confrontés à des problèmes de dimensionnement de structures en contact avec un domaine infini. Pour ces problèmes, seule la structure intéresse réellement les ingénieurs, et le domaine extérieur n'a d'importance que par l'influence qu'il a sur cette structure. Une approche possible consiste à décomposer le domaine en deux, un sous-domaine pour la structure et un pour le domaine extérieur, les deux étant reliés par leur frontière commune. Le problème général est alors décomposé en deux problèmes locaux aux sous-domaines, et en un problème global, posé sur la frontière commune et défini, pour des problèmes linéaires, en termes d'impédance.

Les domaines infinis considérés dans ces applications sont souvent mal connus ou complexes à modéliser. Ainsi, pour les besoins de la résolution, l'hétérogénéité d'un sol réel est souvent représentée par un modèle de couches horizontales. Les estimations obtenues à partir d'un tel modèle sont différentes de la réalité, et cette différence est qualifiée d'erreur de modélisation. En outre, une fois le modèle choisi, la simple taille des domaines considérés rend compliquée et coûteuse une éventuelle campagne d'essais pour la caractérisation des paramètres du modèle. Les erreurs induites sont alors qualifiées de paramétriques. Pour certains domaines, comme le sol, ces erreurs, de modélisation et paramétriques, peuvent être importantes. On a alors recours à des approches probabilistes pour essayer de les prendre en compte.

Le but principal de cette thèse est de développer un modèle probabiliste des matrices d'impédance, d'abord dans un cadre général, puis dans le cas particulier des problèmes d'interaction dynamique sol-structure. Les applications proposées, dans le cadre d'une collaboration avec EDF R&D, concernent le dimensionnement parasismique des ouvrages de grande taille, et notamment les bâtiments-réacteurs de centrales nucléaires.

Le Chap. 2 présente un panorama des principaux outils et méthodes utilisés en modélisation probabiliste pour la mécanique. Dans le but d'appliquer ces techniques à la construction de modèles de matrices d'impédance pour des domaines de grande taille, et éventuellement présentant de hauts niveaux d'incertitude, une méthode non-paramétrique, récemment développée par Soize [2000, 2001], semble particulièrement intéressante. Dans cette méthode, les incertitudes sont prises en compte au niveau des matrices du système dynamique plutôt qu'au niveau des paramètres de ces matrices, ce qui permet de rendre compte des erreurs de modélisation autant que des erreurs paramétriques. En pratique, les matrices de masse, d'amortissement et de rigidité du système dynamique sont remplacées par des matrices aléatoires. Leur loi est construite à partir du principe du maximum d'entropie, avec comme contraintes la donnée d'un modèle moyen, la stricte positivité des matrices, et une condition d'intégrabilité de leur inverse. Chacune des matrices aléatoires est contrôlée par un unique paramètre de dispersion.

La définition d'une matrice d'impédance est donnée au Chap. 3, et ses propriétés principales y sont décrites, dont notamment la causalité. Un modèle déterministe de matrice d'impédance est alors introduit, suivant Chabas and Soize [1987], assurant la vérification de ces propriétés. Dans le cadre de ce modèle, les matrices d'impédance sont construites comme la condensation sur la frontière d'un système dynamique plus grand, dont les degrés de liberté supplémentaires sont dits cachés. Plus précisément, la matrice d'impédance est écrite sous la forme

$$[Z(\omega)] = [S_\Gamma(\omega)] - [S_c(\omega)][S_h(\omega)]^{-1}[S_c(\omega)]^T, \quad (1)$$

où la matrice de rigidité dynamique  $[S(\omega)]$  est décomposée en blocs

$$\begin{bmatrix} [S_\Gamma(\omega)] & [S_c(\omega)] \\ [S_c(\omega)]^T & [S_h(\omega)] \end{bmatrix} = -\omega^2 \begin{bmatrix} [M_\Gamma] & [M_c] \\ [M_c]^T & [M_h] \end{bmatrix} + i\omega \begin{bmatrix} [D_\Gamma] & [D_c] \\ [D_c]^T & [D_h] \end{bmatrix} + \begin{bmatrix} [K_\Gamma] & [K_c] \\ [K_c]^T & [K_h] \end{bmatrix}, \quad (2)$$

et où "Γ" fait référence aux degrés de liberté définis sur la fondation, "h" aux degrés de liberté cachés, et "c" au couplage entre les deux. Les matrices de masse  $[M]$ , d'amortissement  $[D]$  et de rigidité  $[K]$  de ce système dynamique sont alors remplacées par des matrices aléatoires  $[M]$ ,  $[D]$ , et  $[K]$  pour construire le modèle probabiliste non-paramétrique de la matrice d'impédance  $[Z(\omega)]$ . L'utilisation du modèle à variables cachées assure que toutes les réalisations du modèle probabiliste vérifient les propriétés de base des matrices d'impédance. La construction de ce modèle probabiliste des matrices d'impédance est le principal apport de cette thèse.

Cette construction par la méthode non-paramétrique nécessite la constitution préalable d'un modèle moyen, donné sous la forme d'un modèle à variables cachées. Le deuxième apport de la thèse réside donc dans une méthode d'identification, à partir d'impédances calculées numériquement, du modèle à variables cachées correspondant. Cette identification, qui fait l'objet du Chap. 4, est faite en deux étapes. La première est l'interpolation de la matrice d'impédance sur une base polynomiale rationnelle. Cette étape peut être effectuée par de nombreux algorithmes développés dans la littérature, dont un en particulier est choisi pour les applications de cette thèse. La seconde étape, développée spécifiquement dans le cadre de cette thèse, décrit l'identification des matrices du modèle à variables cachées à partir de l'interpolation de la matrice d'impédance. Cette seconde étape n'induit pas d'approximation supplémentaire de la matrice impédance, par rapport à la première étape. En revanche, plusieurs triplets équivalents de matrices  $\{[M], [D], [K]\}$  existent pour une même matrice d'impédance, ce qui conduit à choisir une forme particulière pour l'identification. On remarque, par ailleurs, que les matrices d'impédance utilisées peuvent avoir pour origine non seulement des calculs numériques, mais également des mesures expérimentales, ou même être directement des fonctions tabulées.

Le dernier chapitre de cette thèse, particularise les concepts décrits dans les chapitres précédents au cas d'un problème d'interaction dynamique sol-structure. En particulier, les méthodes spécifiques de calcul des matrices d'impédance utilisées dans ces problèmes, et les approches probabilistes rencontrées dans la littérature, y sont décrites. Par rapport à d'autres modèles, et notamment ceux à masses concentrées, le modèle à variables cachées semble intéressant car il considère pleinement le caractère matricielle de la matrice d'impédance. Cela lui permet d'être utilisé de façon plus générale, et notamment pour des fondations flexibles.

La première application des idées développées dans cette thèse considère un problème classique en interaction dynamique sol-structure: une fondation enterrée dans une couche de sol homogène sur un demi-espace rigide. A partir du problème homogène, on construit deux modèles probabilistes de l'impédance de fondation: un paramétrique et un non-paramétrique. Le premier requiert le maillage de toute la zone considérée comme hétérogène, qui se limite donc, pour des raisons de coût de calcul, à une partie du sol placée juste sous la fondation. Dans cette zone, les paramètres de Lamé sont modélisés par des champs aléatoires. Le deuxième modèle, non-paramétrique, est celui développé dans cette thèse. Malgré les différences d'approche, de nombreux points communs apparaissent dans les résultats analysés (Fig. 1). On illustre par ailleurs le lien entre la modélisation probabiliste des paramètres physiques du problème et celle de la matrice d'impédance, dans le cas paramétrique, et la non-localisation des incertitudes, dans le cas non-paramétrique.

La deuxième application de cette thèse se concentre sur un problème plus industriel de dimensionnement d'un bâtiment-réacteur au séisme. La matrice d'impédance de fondation est modélisée par la méthode développée dans cette thèse, et le bâtiment est modélisé de façon déterministe. Les résultats

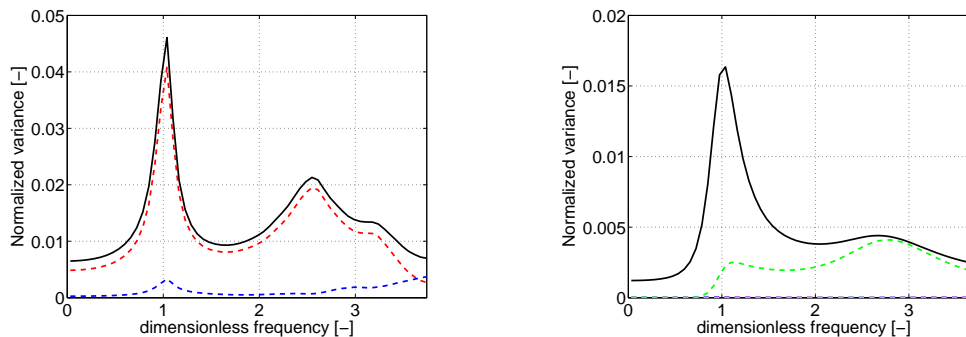


Figure 1: Variance normalisée (trait plein noir) du terme de pompage de la matrice d'impédance pour un modèle (a) paramétrique, et (b) non-paramétrique, et contribution des premiers modes de la matrice de covariance (traits discontinus).

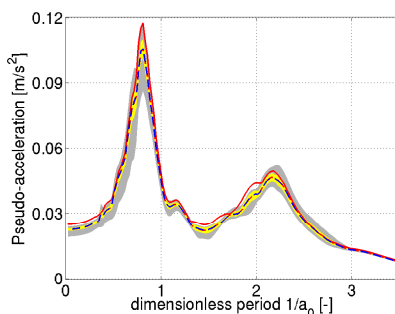


Figure 2: Spectre de plancher en haut du bâtiment-réacteur pour un modèle déterministe (ligne continue rouge), un modèle à variables cachées (ligne discontinue bleue), et un modèle probabiliste (moyenne en ligne rouge discontinue et intervalle de confiance à 90%, en jaune pour  $\delta = 0.1$  et en gris pour  $\delta = 0.3$ ) de l'impédance.

obtenus montrent l'intérêt de tels modèles probabilistes du sol pour le dimensionnement de ces structures. Ainsi, on obtient une modélisation probabiliste des spectres de plancher, pour différents niveaux d'incertitude (Fig. 2). Cependant, comme dans l'application précédente, des progrès restent encore à faire concernant l'identification du modèle à variables cachées, et plusieurs propositions sont faites à cette fin.

A partir des idées présentées dans cette thèse, plusieurs pistes pour des développements futurs sont ouvertes. Notamment, l'identification des modèles à variables cachées pour d'autres systèmes que ceux considérés ici est envisagée. A court terme, des travaux sur la caractérisation des paramètres physiques contrôlant le comportement dynamique des fondations sur pieux [Taherzadeh and Clouteau, 2006] pourraient être complétés par l'identification des modèles à variables cachées correspondant. A plus long terme, l'identification de tels modèles à partir de mesures expérimentales paraît intéressante.



# Contents

<b>Acknowledgements</b>	<b>i</b>
<b>Résumé</b>	<b>iii</b>
<b>1 Introduction</b>	<b>1</b>
1.1 Domain decomposition and impedances . . . . .	1
1.1.1 The domain decomposition technique . . . . .	1
1.1.2 A first glance at the impedance . . . . .	3
1.2 Uncertainties in mechanical problems . . . . .	6
1.2.1 Sources of uncertainties . . . . .	6
1.2.2 Why use probabilistic models and methods? . . . . .	7
1.2.3 Development of stochastic mechanics . . . . .	8
1.3 Objectives and outline of this dissertation . . . . .	8
<b>2 Stochastic modeling and solving in mechanics</b>	<b>11</b>
2.1 Tools for stochastic modeling . . . . .	11
2.1.1 Random variables, processes, and fields . . . . .	11
2.1.2 Measures of correlation . . . . .	14
2.1.3 Representation of random processes . . . . .	14
2.2 Tools and techniques for the resolution of stochastic mechanical problems . . . . .	19
2.2.1 Analytical tools and techniques . . . . .	20
2.2.2 Computational tools and techniques . . . . .	23
2.2.3 Reliability analyses . . . . .	25
2.3 Summary . . . . .	27
<b>3 Probabilistic models of impedance matrices</b>	<b>29</b>
3.1 Models of the impedance samples . . . . .	29
3.1.1 Definition of the impedance . . . . .	29
3.1.2 Numerical methods for the computation of the impedance matrix . . . . .	33
3.1.3 Properties of the impedance . . . . .	34
3.1.4 The hidden state variables model . . . . .	36
3.2 Probabilistic model of the impedance . . . . .	38
3.2.1 Nonparametric approach to the modeling of uncertainties . . . . .	38
3.2.2 The random matrices ensembles . . . . .	39
3.2.3 Nonparametric model of the impedance matrix . . . . .	41
3.3 Practical construction of the probabilistic model of an impedance matrix . . . . .	42

<b>4</b>	<b>Identification of the hidden state variables model of the impedance matrix</b>	<b>45</b>
4.1	Methodology for the identification of hidden variables models . . . . .	45
4.1.1	General issues . . . . .	45
4.1.2	Methodology for the identification of hidden variables models . . . . .	46
4.1.3	Choice of the number of hidden variables . . . . .	47
4.1.4	The cost function . . . . .	47
4.1.5	Choice of the interpolation method . . . . .	48
4.2	Weighted discrete linear least square rational approximation using orthogonal vectors of polynomials . . . . .	49
4.2.1	The space of vectors of polynomials . . . . .	49
4.2.2	Principle of the method . . . . .	50
4.2.3	Cost and optimization of the algorithm . . . . .	51
4.3	The identification problem . . . . .	52
4.3.1	Non-uniqueness of the solution . . . . .	52
4.3.2	Identification . . . . .	54
4.4	Validation of the identification . . . . .	56
4.4.1	Direct identification . . . . .	57
4.4.2	Influence of the frequency band . . . . .	61
4.4.3	Influence of the number of impedance channels . . . . .	62
4.4.4	Influence of noise . . . . .	62
4.4.5	Influence of non-diagonal damping . . . . .	63
4.5	Summary . . . . .	64
<b>5</b>	<b>Probabilistic models of the impedance matrix in Soil-Structure Interaction problems</b>	<b>67</b>
5.1	Domain decomposition in Soil-Structure Interaction problems . . . . .	67
5.1.1	Domain Decomposition approach to SSI . . . . .	67
5.1.2	Kinematic and Inertial interaction in SSI problems . . . . .	70
5.1.3	The impedance matrix in SSI problems . . . . .	71
5.1.4	Computation of the impedance matrix in SSI problems . . . . .	73
5.2	Probabilistic models and methods in Soil-Structure Interaction problems . . . . .	80
5.2.1	Probabilistic models for earthquake engineering problems . . . . .	80
5.2.2	Probabilistic approaches in SSI problems . . . . .	86
5.3	Parametric and nonparametric models of the impedance matrix . . . . .	89
5.3.1	The homogeneous problem . . . . .	89
5.3.2	Parametric approach: MISSVAR software . . . . .	92
5.3.3	Nonparametric approach . . . . .	97
5.3.4	Comparisons . . . . .	102
5.4	Design of a building using a stochastic impedance matrix . . . . .	104
5.4.1	Industrial needs . . . . .	104
5.4.2	The classical deterministic approach . . . . .	105
5.4.3	Probabilistic model of the response of the building . . . . .	109
<b>6</b>	<b>Conclusions and perspectives</b>	<b>115</b>

<b>A Mathematical notations and definitions</b>	<b>119</b>
A.1 Notations . . . . .	119
A.2 Probability theory . . . . .	119
<b>List of Figures</b>	<b>125</b>
<b>List of Tables</b>	<b>131</b>
<b>List of Acronyms</b>	<b>133</b>
<b>Bibliography</b>	<b>135</b>



# Chapter 1

## Introduction

In many fields of applied mechanics and engineering, the problems considered are composed of several parts with (very) different properties. A classical resolution scheme consists in using Domain Decomposition (DD) techniques, splitting the global problem into several local ones interacting through boundary impedances. This approach, and the subsequent modeling of boundary impedance matrices, has been studied extensively in a deterministic framework. However, in many problems, the presence of large uncertainties - in the data or the models - makes the use of stochastic models appealing. Contributing in that direction, this dissertation aims at developing a novel approach to the probabilistic modeling of impedance matrices.

To ease the reading, the chapters of this dissertation are mainly independent. In particular, Chap. 2 provides a review of stochastic mechanics models and methods, and will be skipped advantageously by the reader already knowledgeable in that field. Chap. 3 is more essential in the sense that the core of our work, the introduction of a new probabilistic model of the impedance matrix, is presented there. It concentrates on theoretical modeling issues, and an important practical question is extracted to the following chapter. Chap. 4 thus considers a deterministic identification problem that arises in the construction of our modeling of the impedance. It does not require any stochastic background, and will more particularly interest readers of the modal identification community, as some of their tools are used. Finally, several applications are presented in Chap. 5, which is focused more on the fields of Soil-Structure Interaction (SSI) and earthquake engineering.

This present chapter discusses some issues that are of interest for the entire dissertation. Namely, a first introduction to the impedance matrix is presented, and the possible contributions of stochastic mechanics to its modeling are described.

### 1.1 Domain decomposition and impedances

In this first section, the goal is to give the reader a feel of DD, and the way impedance matrices naturally arise in this technique. A general mechanical problem is therefore considered, and the application of the DD method to this problem is expounded with little reference to mathematics. The impedance matrix is described in a similar manner, delaying the introduction of the details and a more sound mathematical setting until Chap. 3. An example is also provided, where the impedance matrix of a 2-Degree-of-Freedoms (DOFs) system is constructed.

#### 1.1.1 The domain decomposition technique

Let us consider a general mechanical problem, represented in Fig. 1.1(a), where we wish to compute, in a domain  $\Omega$ , possibly unbounded, the displacement field  $\mathbf{u}$ , or any other mechanical quantity. We restrict ourselves to the linear case, and suppose that there are Dirichlet boundary conditions on a part  $\Sigma_u$  of

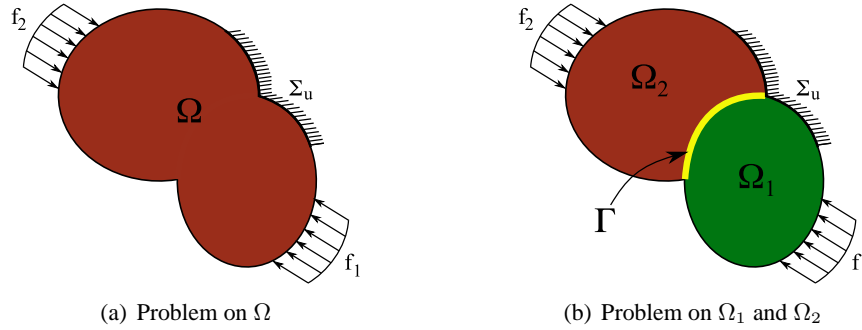


Figure 1.1: General mechanical problem posed on the entire domain  $\Omega$  and corresponding decomposed problem posed on subdomains  $\Omega_1$  and  $\Omega_2$  interacting through their common boundary  $\Gamma$ .

the boundary  $\partial\Omega$  of  $\Omega$ , and Neumann conditions on its complement  $\partial\Omega \setminus \Sigma_u$ . The set of equations that governs the behavior of this domain, including the boundary equations, and possibly radiation conditions if the domain is unbounded, is written in the general form:

$$\mathcal{E}_\Omega(\mathbf{u}) = \mathbf{0}. \quad (1.1)$$

The mechanical problem then consists in finding  $\mathbf{u}$  in a suitable functional space  $V(\Omega)$ , such that Eq. (1.1) is verified. In some cases, this problem is solvable by analytical means, and more generally, it is worked out using computational methods<sup>1</sup>. We only consider here the cases when analytical resolution is not an option, which is what happens for most industrial applications. The joint modeling of the entire domain  $\Omega$  is then required. When this domain is large and composed of parts with disparate mechanical parameters, it may result in complex modeling and costly resolution.

The DD technique is an alternative to such a direct approach. It consists in decomposing the domain  $\Omega$  into two (or more) subdomains  $\Omega_1$  and  $\Omega_2$ , introducing an additional boundary  $\Gamma$  between them, as represented on Fig. 1.1(b). The global problem of Eq. (1.1) is then transformed into two independent local problems, respectively on  $\Omega_1$  and  $\Omega_2$ , and an additional global problem defined on the interacting boundary  $\Gamma$  of the two subdomains:

$$\begin{cases} \mathcal{E}_{\Omega_1}(\mathbf{u}_1) = \mathbf{0} \\ \mathcal{E}_{\Omega_2}(\mathbf{u}_2) = \mathbf{0} \\ \mathcal{E}_\Gamma(\mathbf{u}_\Gamma) = \mathbf{0} \end{cases}, \quad (1.2)$$

where the fields  $\mathbf{u}_1$ ,  $\mathbf{u}_2$ , and  $\mathbf{u}_\Gamma$  are the restrictions of the displacement field  $\mathbf{u}$  respectively to  $\Omega_1$ ,  $\Omega_2$  and  $\Gamma$ .

A first important feature of the DD technique is that it explicitly allows the use of different models and resolution methods for the local problems on each of the subdomains. A bounded subdomain might therefore be modeled using a FE method where an unbounded subdomain would be represented using a Boundary Element (BE) method. Another interesting property of the DD method lies in the size of each of the derived problems in Eq. (1.2) compared to that of the original one in Eq. (1.1). Indeed, if we consider that the domain is modeled entirely using a FE method, and that the elements are not modified when performing the decomposition, then the number of DOFs of each of the resulting problems will be

<sup>1</sup>We obviously refer here to Finite Element (FE) methods, but other methods will also be described in Sec. 3.1.2, with a particular emphasis on those adapted for the modeling of large or unbounded domains.

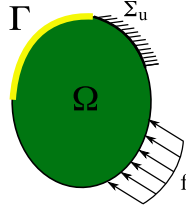


Figure 1.2: A domain  $\Omega_\ell$  and its boundary of interest  $\Gamma$ .

smaller than that of the original one. Since the first two problems can be computed independently, it means that the DD method is well adapted to parallel computing. Also, it allows for the design of larger systems, when size is the limiting factor of the computation. The third system to be solved in Eq. (1.2) is not independent of the other two, but its size is usually smaller because it is defined on a surface rather than a volume.

### 1.1.2 A first glance at the impedance

The formulation of the DD technique is made possible by the introduction of impedances for each of the subdomains  $\Omega_1$  and  $\Omega_2$ , with respect to the boundary  $\Gamma$ . Let us consider one of these local domains  $\Omega_\ell$  ( $\ell \in \{1, 2\}$ ), its boundary  $\partial\Omega_\ell$  and a bounded part  $\Gamma$  of  $\partial\Omega_\ell$  to which it is linked to the other subdomain (Fig. 1.2). The boundary conditions on  $\partial\Omega_\ell \setminus \Gamma$  are supposed, for a start, to be homogeneous.

For any imposed displacement field  $\mathbf{u}_\Gamma$  on the boundary  $\Gamma$ , the corresponding stress field  $\mathbf{f}_\Gamma$  can be computed, and is uniquely defined. A unique operator can therefore be defined that maps any displacement field  $\mathbf{u}_\Gamma$  on the boundary to the corresponding stress field  $\mathbf{f}_\Gamma$  on that boundary, provided that both these fields are defined in proper functional spaces. This operator  $\mathcal{Z}$  is called the impedance operator.

$$\mathcal{Z}(\mathbf{u}_\Gamma) = \mathbf{f}_\Gamma. \quad (1.3)$$

Impedance operators can be defined for the coupling of inputs and outputs of any system. They exist, for example, in electricity, where they usually relate the potential and the intensity of a passive system, and in fluid mechanics, where they relate fields of velocities and stresses. We will concentrate in this dissertation to the case of structural mechanics impedances, linking displacements and stresses. Choosing an appropriate finite dimensional subspace for  $\mathbf{u}_\Gamma$ , and using a classical Galerkin approach leads to approximations of the impedance operator  $\mathcal{Z}$  as an impedance matrix.

Going back to the problem of solving Eq. (1.2), the first two equations represent the computation of the impedance operators of each subdomain, respectively  $\mathcal{Z}_1$  and  $\mathcal{Z}_2$ , with respect to the same boundary  $\Gamma$ , with the loads in  $\Omega_1$  and  $\Omega_2$ , and the boundary conditions on  $\partial\Omega_1 \setminus \Gamma$  and  $\partial\Omega_2 \setminus \Gamma$  inherited from the global problem described in Eq. (1.1), assumed here homogeneous. The third equation of the system of Eq. (1.2) represents the global equilibrium equation of the boundary and arises when simultaneously equating the displacements and canceling the loads on the two sides of the boundary  $\Gamma$ . When there are nonhomogeneous boundary conditions on  $\partial\Omega_\ell \setminus \Gamma$ , the boundary conditions of the local problems, used to define the impedance operators, are still taken as homogeneous, and two additional problems are set to define, for each subdomain, equivalent loads  $\mathbf{f}_1$  and  $\mathbf{f}_2$  on the boundary. The global equilibrium equation is then written

$$\mathcal{Z}_1(\mathbf{u}_\Gamma) + \mathcal{Z}_2(\mathbf{u}_\Gamma) = \mathbf{f}_1 + \mathbf{f}_2. \quad (1.4)$$

This will be discussed in more details in Sec. 5.1, in the case of a SSI problem. In Chap. 3, the impedance operator and matrix will be defined in a more appropriate mathematical setting, but following the path sketched here.

### Box 1.1 A simple example of an impedance matrix

Let us compute the impedance of a simple 2-DOFs mass-spring-dashpot system with respect to one of its DOFs (Fig. 1.3). This system might represent the discretization of one of the subdomains of Fig. 1.1(b), e.g.  $\Omega_1$ , with one DOF on the boundary  $\Gamma$ , one internal DOF, and  $\partial\Omega_1 \setminus \Gamma = \Sigma_u$ .

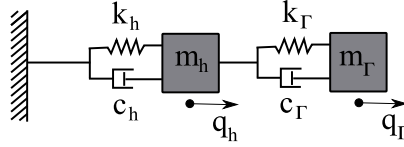


Figure 1.3: 2-DOFs series system.

Considering that the DOF of the boundary is loaded by a force  $f_\Gamma$ , possibly time-variant, the equation of motion for this system is

$$M\ddot{U}(t) + C\dot{U}(t) + KU(t) = F(t), \quad (1.5)$$

where the unknown vector is  $U(t) = [u_\Gamma(t), u_h(t)]^T$ , the loading vector is  $F(t) = [f_\Gamma(t), 0]^T$ , and the matrices of mass, stiffness and damping are defined by

$$M = \begin{bmatrix} m_\Gamma & 0 \\ 0 & m_h \end{bmatrix}, C = \begin{bmatrix} c_\Gamma & -c_\Gamma \\ -c_\Gamma & c_\Gamma + c_h \end{bmatrix}, K = \begin{bmatrix} k_\Gamma & -k_\Gamma \\ -k_\Gamma & k_\Gamma + k_h \end{bmatrix}. \quad (1.6)$$

It should be noted that, when the coefficients of the springs, dampers and masses are strictly positive, these matrices are positive definite. In the frequency domain, this equation translates to

$$(-\omega^2 M + i\omega C + K)U(\omega) = F(\omega), \quad (1.7)$$

where  $U$  and  $F$  are the Fourier transforms of the previous quantities. We will not use special notation for them as it is usually clear from the context which quantities are being used. This matrix equation corresponds to two scalar equations, the second of which yields

$$u_h(\omega) = \frac{i\omega c_\Gamma + k_\Gamma}{-\omega^2 m_h + i\omega(c_\Gamma + c_h) + (k_\Gamma + k_h)} u_\Gamma(\omega). \quad (1.8)$$

Injecting that relation in the first equation of the matrix system, the impedance is defined as

$$Z(\omega) = \frac{f_\Gamma(\omega)}{u_\Gamma(\omega)} = -\omega^2 m_\Gamma + i\omega c_\Gamma + k_\Gamma - \frac{(i\omega c_\Gamma + k_\Gamma)^2}{-\omega^2 m_h + i\omega(c_\Gamma + c_h) + (k_\Gamma + k_h)} \quad (1.9)$$

This quantity is the Schur complement of the dynamic impedance matrix  $A(\omega) = -\omega^2 M + i\omega C + K$ , with respect to the first DOF.

For positive coefficients of the springs, dampers and masses, the real parts of the poles of that impedance are negative, and the impedance corresponds to a causal stable second order filter that maps  $u_\Gamma$  to  $f_\Gamma$ . These notions will be discussed in more detail in Chap. 3. The impedance for that system can finally be written in an normalized form,

$$z(x) = 1 - \mu x^2 + 2i\xi\zeta x - \alpha_k \frac{(1 + 2i\xi\zeta x)^2}{1 - x^2 + 2i\zeta x}, \quad (1.10)$$

The normalized coefficients in this equation are defined by  $k_0 = k_\Gamma$ ,  $z(\omega) = Z(\omega)/k_0$ ,  $\omega_0 = \sqrt{m_h/(k_\Gamma + k_h)}$ ,  $x = \omega/\omega_0$ ,  $\zeta = \omega_0(c_\Gamma + c_h)/(2(k_\Gamma + k_h))$ ,  $\alpha_m = m_\Gamma/m_h$ ,  $\alpha_c = c_\Gamma/(c_\Gamma + c_h)$ ,  $\alpha_k = k_\Gamma/(k_\Gamma + k_h)$ ,  $\xi = \alpha_c/\alpha_k$ , and  $\mu = \alpha_m/\alpha_k$ .

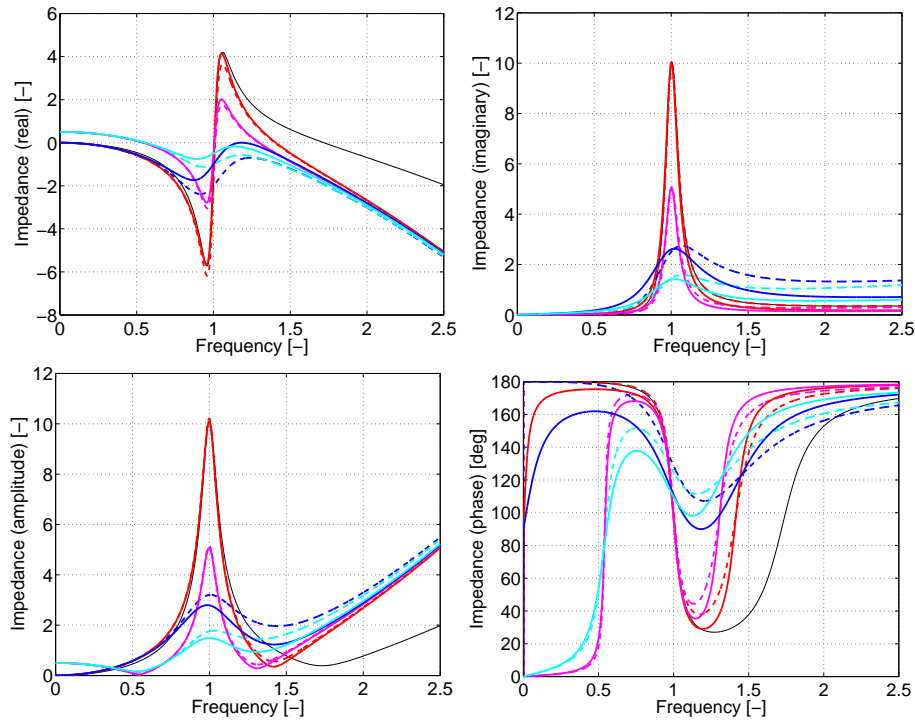


Figure 1.4: (a) real part, (b) imaginary part, (c) amplitude, and (d) phase of the impedance in Eq. (1.10), for  $\mu = 1$ ,  $\xi = 0.5$  (solid lines) or  $\xi = 1$  (dashed lines),  $\zeta = 0.05$  (red and magenta lines) or  $\zeta = 0.2$  (blue and cyan lines), and  $\alpha_k = 0.5$  (cyan and magenta lines) or  $\alpha_k = 1$  (blue and red lines). The black solid line is the same as the red dashed line, with  $\mu = 0.5$ .

On Fig. 1.4, the real and imaginary parts, the amplitude and the phase of the normalized impedance are drawn for a set of values of the parameters. It seems that  $\xi$  has little impact on the value of the impedance, except when  $\zeta$  itself is important. The behavior in the low frequency domain is controlled by  $\alpha_k$  (when considering the non-normalized impedance,  $k_\Gamma$  is also decisive), and that in the high frequency domain by  $\mu$  (for the real part and the amplitude) and the product  $\xi\zeta$  (for the imaginary

part). Finally, the static value of the imaginary part is always null, which is a consequence of the causality of the impedance.

## 1.2 Uncertainties in mechanical problems

This type of computation of the impedance matrices, and the DD techniques, are now well understood, and widely used. Over the years, and depending on the type of applications considered, many models and computational methods for impedance matrices have been devised. One lingering problem remains though: how are the possible errors and uncertainties taken into account in these models? In the case of large heterogeneous domains, such as soils for example, full characterization of the mechanical properties would require extensive experimentations that are not available in practice, so that this question is particularly significant. In this section, some of the main sources of uncertainty and errors in mechanical problems are reviewed, along with possible contributions from probabilistic methods.

These issues are discussed in a general setting in Kline [1985] and Favre [1998, 2000]. In the former, a classification of possible applications of probabilistic methods is presented, and, in the latter, the different sources of uncertainties and errors in soil mechanics problems are systematically categorized. The limits of such classifications, where some criteria are not measurable, are highlighted in Favre [1998].

### 1.2.1 Sources of uncertainties

The main types of uncertainties that will be considered in this dissertation can usually be separated in uncertainties on the model on the one hand, and errors on the parameters of that model on the other. Although the words "error" and "uncertainty" are often casually exchanged, they refer here to the fact that the parameter errors can usually be reduced using more information on the system, while model uncertainties cannot. An additional type of error, more customary in computational mechanics, is that arising from unsound sampling or discretization of the continuous fields that are considered in the models. This type of numerical error can usually be controlled by an appropriate refinement of the discretization, like in FE methods for example. Similarly, in Monte Carlo Sampling (MCS) methods<sup>2</sup>, the convergence of the moments of the solution can be bounded theoretically, and the number of samples necessary to reach a given reliability can be assessed beforehand. Numerical errors will not be considered in this dissertation, and all the numerical schemes that will be used will be supposed to have converged with respect to this type of error.

Model uncertainties arise from the fact that, to compute the response of a mechanical problem, the engineer chooses a particular model, that does not necessarily represent in an accurate way the real behavior of the mechanical system at hand. Thus, for example, the choice for a given material of a linear strain-stress relation rather than a nonlinear one, which will give rise to large model errors when considered with large strains, and less with small strains. Other examples of this type of error include the simplified boundary conditions (perfect interface contact for example), and the homogeneity of the material considered. These model uncertainties are difficult to quantify because they depend heavily on the type of problem, and their impact on the estimated response of a mechanical system is not obvious.

The second type of errors, the parameter errors, relates to the fact that the parameters of a chosen model are rarely perfectly evaluated. This discrepancy arises from several sources: inaccurate instrumentation and experimental setups, tare errors of the instruments, operator-dependent experimental measures,

---

<sup>2</sup>The application of the MCS method in the resolution of stochastic mechanics problems is described in Sec. 2.2.2.

reshuffling of the samples during their transport to the testing laboratory, choice of the number and location of the samples to be measured, among others. These last two examples are particularly important when considering large heterogeneous domains, like soils. These parameter errors can usually be lowered using better and more numerous instruments or experiments, but this has an important subsequent cost that most projects cannot afford.

There is a strong link between model uncertainties and parameter errors. Indeed, a refined model usually involves more parameters than a simpler one. Hence, the parameters of a simple model will often be easy to measure and the overabundant data will be used to increase the accuracy of the estimation. On the other hand, complicated models will require more data to be fitted, and their accuracy will probably depend more heavily on possible erroneous measures within the data set. The difficulty in probabilistic mechanics therefore lies in the simultaneous estimation of model errors and parameter uncertainties.

### 1.2.2 Why use probabilistic models and methods?

The goal of a probabilistic method is to provide a way to take into account one or more of these sources of uncertainty and to quantify their impact on the output of a mechanical system. Randomness is introduced in the problem, and the output is therefore given in terms of a Probability Density Function (PDF) rather than a deterministic value, or else, in terms of a set of possible values with their appropriate weight. A classical question is the difference between a fundamental randomness, which is supposed to describe an inherent property of the system, and modeled randomness, which arises from the choice of modeling a complicated, but deterministic, system using a probabilistic approach. Although it relates to the link between model errors and parameter uncertainties discussed above, this question is mainly philosophical: is the issue of a heads or tails game uncertain because of luck, or is it only that we fail to incorporate in our models all the necessary parameters to predict its output? Does the spatial variability of a mechanical parameter in a soil deposit contain some random origin, or is it purely deterministic, but out of the range of our modeling capacities? This issue will not be treated in this dissertation.

Probabilistic approaches are not procedures with which the engineers are familiar as these methods fully acknowledge their inability to estimate the solution of a problem in a perfectly exact manner. However, in most problems, engineers are provided with real systems modeled in a somehow inappropriate way, and the parameters of which are difficult to estimate. The use of a deterministic method in these cases will give a solution, probably false, with no means to quantify its accuracy, while a probabilistic method will give a set of possible values, with their respective probability. The engineer can then choose an estimator of the quantity he is interested in, for example the mean value, the most probable value, or a 95% quantile, and get a notion of the accuracy of that estimation, for example with the standard deviation.

This apparent superiority of probabilistic methods over deterministic ones should however not be seen as intrinsic. As the former are much more demanding than the latter, both theoretically and numerically, they should be used only when the levels of uncertainty are large enough. Moreover, they should not be seen as a solution *per se*, since the probabilistic information of the response of a stochastic mechanical problem is only a consequence of the model that has been chosen to represent the random parameters of this system. This means that the experimental validation of the hypotheses made during the modeling process is as important for probabilistic methods as for deterministic ones. Unfortunately, the validation processes associated are dissimilar, and still lack a lot of maturity and experience in the case of stochastic methods. Probabilistic approaches are therefore a powerful way to take into account the uncertainties arising in mechanical problems, but they should be used with much care, and with experimental validation as a foremost concern.

### 1.2.3 Development of stochastic mechanics

For a long time, probabilistic methods have been disregarded as they go against the traditional knowledge and understanding of the engineers. Uncertainty, though, has been recognized for a long time, and often taken care of with safety factors, either on the resistance or the loads of the mechanical systems. The values of these safety factors are usually derived from common practice and experience. Another approach consists in computing characteristic responses for the mechanical system, corresponding to values of the parameters estimated using statistics, for example mean and quantiles. Although this can often be encountered in the literature (see for example Simos and Costantino [2004] for a recent application in SSI), it is theoretically wrong for nonlinear systems.

The first attempts at quantifying the output of structural mechanics problems in a probabilistic sense were made in random vibration problems, where the response of a deterministic structure to a random loading is considered. Most resolution schemes<sup>3</sup> are based on analytical techniques and applied to the resolution of small nonlinear systems submitted to idealized white noise. These methods are not well-suited for applications in an industrial context, as they are often limited to a few DOFs, and the solutions are derived under very restricting hypotheses, such as normal distribution of the solution.

Today, the emphasis in probabilistic structural mechanics is more on the development of numerical (approximate) methods to model efficiently large systems. In that matter, the most interesting and versatile techniques is the Stochastic Finite Element (SFE) method, possibly coupled with a MCS method. The development of both these techniques has paralleled that of the computers, and they remain the subject of considerable attention, as they are still expensive in comparison to classical, deterministic methods. Nevertheless, probabilistic methods are now common in many industries, and have been acknowledged recently in civil engineering, with the introduction of the Eurocode 7.

Although they work for large systems with reasonable variability, these methods remain too limited for many applications. Particularly, unbounded natural media, such as soils, often show very large levels of fluctuations of the mechanical parameters, and their sheer size complicates the discretization of the mechanical operators and fields. Both the size and the high variability eventually require more parameters to be dealt with, and this in turn, complicates the validation process. Stochastic mechanics in these large heterogeneous domains is therefore still at a maturing stage, and this is where this dissertation aims at making progress.

## 1.3 Objectives and outline of this dissertation

From an engineering point of view, these unbounded media are studied only because of their influence on the surrounding mechanical systems. For example, the mechanical behavior of the soil is studied because we want the houses that are built on top of it to resist a possible earthquake. The flow of propellant exiting a turbine is studied to improve the efficiency of the related motor. The medium itself is not important, only its impact on the engineering system is. DD techniques are particularly adequate in that case. As we saw earlier, large heterogeneous media are often inaccurately represented, so that probabilistic methods seem an interesting option for their modeling. The main goal of this dissertation is therefore to unfold a novel approach to the stochastic modeling of impedance matrices, with a particular focus on large or unbounded heterogeneous domains. This will be treated in particular in Chap. 3.

The outline of this document is as follows, the chapters being, for the most part, independent:

---

<sup>3</sup>Although they are not directly useful for our problem, these methods are described in more detail in Sec. 2.2, for their historical relevance.

- In Chap. 2, a review of stochastic methods and models is first presented. These models are evaluated with respect to their ability to represent large or unbounded domains, heavily heterogeneous, and the methods on their capability to solve the associated stochastic problems. This evaluation hints at the use of the nonparametric method for the modeling, and at the MCS method for the resolution.
- The core of the dissertation is presented in Chap. 3. The impedance matrix is first defined in a sound mathematical setting, and its properties analyzed. These properties lead us in the choice of the hidden variables model for the representation of the samples of the random impedance matrices. The construction of the probabilistic model of the impedance matrix is then completed by using the nonparametric approach.
- The construction of the probabilistic model of an impedance matrix for a given mechanical problem is seen in Chap. 3 to require the identification of the hidden variables model of a related mean problem. This deterministic identification issue is treated in Chap. 4, in two steps: a general interpolation problem, and the identification of the matrices of mass, damping and stiffness of the hidden variables model from the interpolated impedance matrix.
- Finally, Chap. 5 concentrates on the particularization and computation of our probabilistic model of impedance matrices to the fields of SSI and earthquake engineering. In particular, two important applications are considered, where our approach is successively compared to a more classical SFE approach, and used in the seismic design of a strategic building.

Two aspects of this work are particularly innovative. Firstly, in Chap. 3, the joint use of the hidden state variables model and the nonparametric approach to random uncertainties problems allows impedance matrices to be constructed for large heterogeneous domains, which were previously not as easily accessible to modeling. This aspect is complemented by the comparison, in Sec. 5.3, of our approach to a SFE approach. Secondly, in Chap. 4, a new result is introduced for the exact mapping of an impedance function in a rational fraction form to the matrices of mass, damping and stiffness of the corresponding hidden variables model. The novelty of that results lies in its validity for multidimensional settings.



# Chapter 2

## Stochastic modeling and solving in mechanics

This chapter completes the previous one with a review of the classical tools and methods in stochastic mechanics. It is intended at highlighting the complexity of this type of approach, both in terms of modeling (Sec. 2.1) and solving (Sec. 2.2). Indeed, the definition of a probabilistic model in mechanics involves the introduction of additional parameters. The mean of a random parameter is usually directly extended from the value of the corresponding deterministic parameter, but the quantification of covariance and correlation is a new problem, exclusive to stochastic modeling. Once the probabilistic model has been defined, the resulting probabilistic problem also has to be solved with suitable methods, and this step is usually mathematically more involved than the corresponding step for deterministic problem.

Further, this chapter is a preparation for the choice, in the next chapter, of the stochastic model for the impedance matrix. It should therefore be read with the goal of the dissertation in mind, which is to construct a probabilistic model of the impedance matrix usable for large heterogeneous domains. We will see that most classical probabilistic approaches are not appropriate in that case. The reader already proficient in stochastic mechanics will probably want to skip the developments of this chapter, which is mainly bibliographical, and start over at Sec. 2.3, where the aspects of the review most relevant to this dissertation are summarized.

### 2.1 Tools for stochastic modeling

In this section, the tools for stochastic modeling are introduced. This includes random variables, that are the counterpart of deterministic parameters, and stochastic processes and fields, that are the counterparts of functions, respectively, of time, and space. For the latter, we will particularly concentrate on the measures of correlation, which describe the closeness of the values of a process at two separate times, and on the obstacles in its modeling. The focus of this section is rather physical than mathematical, and more accurate definitions can be found in App. A.2, or in Soize [1988a].

#### 2.1.1 Random variables, processes, and fields

In short, a random variable is a function from a set of possible causes to a set of possible consequences, associated with a probability measure specifying the relative likeliness of the different causes, and inducing the relative likeliness of the consequences. This means that probabilities are not defined on the outcomes of our variable of interest, but rather on some virtual underlying set of causes for these outcomes. Considering the example of a dice roll, the probabilities are not defined directly on the outcomes  $(1, \dots, 6)$  of the dice. They are rather defined on the space of the causes of these values, which might

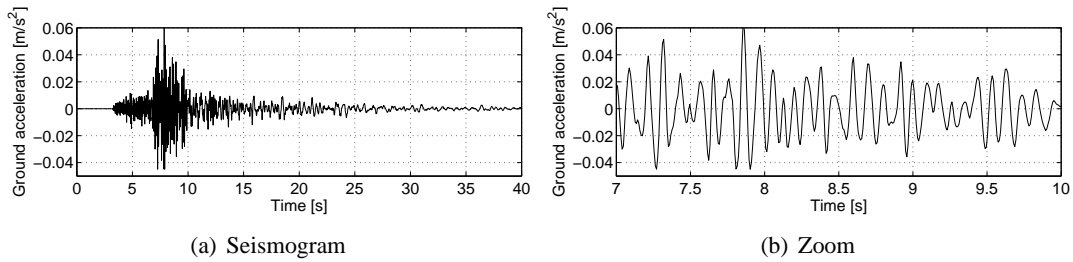


Figure 2.1: Example of an earthquake ground motion recorded during a Magnitude 4.2 earthquake in Grenoble (France) on January 11, 1999 [Ambraseys et al., 2001] at the Campus Universitaire site.

include the weight distribution of the dice, the way it was thrown, or the slope of the table on which it is rolling. In practice, this space is never defined, nor considered<sup>1</sup>.

Although many classical examples in probability theory consider variables with values on a finite set of numbers, like the dice described above, probabilities may be defined for variables with values in any space. In particular, we will consider in this dissertation positive-definite matrix-valued random variables. Whatever the space they span, random variables are adequate for the quantification of uncertainty in the sense that several values of the same variable are explicitly possible. However, some information on the probability measure - usually the Probability Density Function - has to be introduced.

In practice, this information is not easy to obtain because most observable parameters have a unique value when measured. Nevertheless, PDFs are usually introduced in the literature with little justification. Particularly, the Gaussian distribution is widely encountered, sometimes justified by the central limit theorem, mainly because of its definition by only the mean and standard deviation, and for its readiness of use in analytical stochastic calculus. However, this distribution is not appropriate for many parameters, because it gives a weight to all values, even though physical considerations exclude some (a mass, for example, cannot be negative). As the statistical information on the output of a system depends on that of the parameters, this input information should be chosen with care, and justified by appropriate experimental validations and physical considerations.

Random variables are the appropriate mathematical objects to quantify the uncertainty on mechanical constants, and the corresponding probabilistic objects for quantities varying with time are stochastic processes. Fundamentally, stochastic processes are studied as multidimensional random variables, each variable being the value of the process at a given time. Hence, at a given fixed time, the equivalent of the PDF can be defined, considering the random process at that time to be a random variable, independently of its value at other times. This equivalent function is called a first order marginal law and can be defined at any given time. As the values of a random process at distinct times are usually not independent, higher order marginal laws, taking into account that dependency, are necessary to define completely that process. The models for the first order marginal laws are direct extensions of those of the PDFs for random variables, and the modeling difficulties rather concentrate on the models of higher order marginal laws. Usually only the correlation between two instants is considered as the data sets available for the identification of higher order correlations are too small. Nevertheless it should be stressed that the knowledge of all marginal laws is theoretically necessary to define completely a stochastic process.

Many physical quantities can be modeled by stochastic processes: the wind pressure at a point on the

<sup>1</sup>However, this definition is interesting in regard of the discussion of Sec. 1.2.2 about the difference between fundamental randomness and inaccurate modeling.

surface of a high building, a seismograph recorded by an accelerometer (see Fig. 2.1 for an example), the wave motion at a point at sea, or the coastal wave height at a given point on a beach, for example. For space-dependent rather than time-dependent random processes, the usual denomination is random field instead of random process, but both quantities are studied essentially in the same manner. Examples of random fields include the fluctuating properties of a soil, the thickness of an imperfect shell, or the roughness of a road. For the simplicity of the presentation, all further references to stochastic processes in this section should be read as reference to both stochastic processes and random fields.

### Box 2.1 Examples of Probability Density Functions

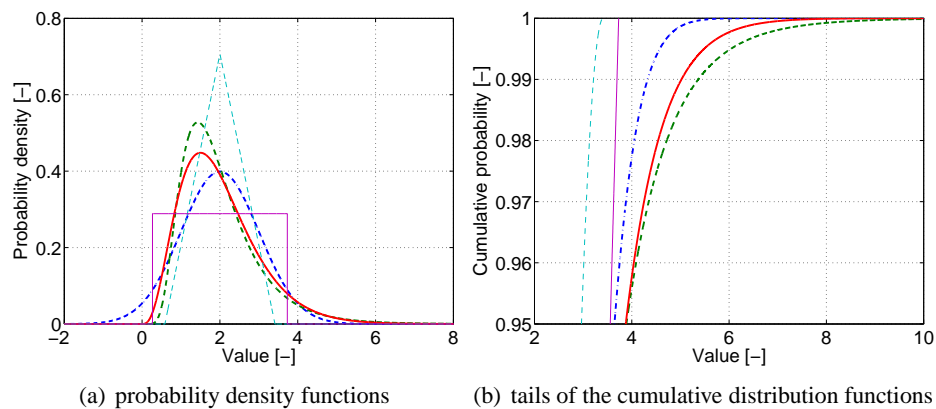


Figure 2.2: PDFs and tails of the cumulative distribution functions for some distributions with the same mean ( $\mu = 2$ ) and standard deviation ( $\sigma = 1$ ): Normal (dash-dotted blue line), lognormal (dashed green line), Gamma (solid red line), uniform (solid magenta thin line), and symmetric triangular (cyan dashed thin line).

In Fig. 2.2(a), examples of common PDFs corresponding to the same mean and standard deviation, are drawn (the definitions and values of the parameters are defined in Sec. A.2). It can be observed that, although the first two statistical moments are the same, there are significant variations between these distributions. Particularly, the differences in the tails imply that the estimation of the probability of a rare event is very dependent on the choice of the distribution. If, for example, the mechanical quantity that is modeled on Fig. 2.2(b) must remain under a given value with a probability of 99%, large differences will arise from considering a triangular rather than a lognormal distribution. This aspect is important in civil engineering because the probabilities of failure are precisely wished to be restrained to low levels.

### 2.1.2 Measures of correlation

The quantities that are most frequently used to measure the strength of the likeness of the values at two instants of a random process are the autocorrelation and covariance functions<sup>2</sup>. Relative high numbers for these functions mean that the values of the random process at the two instants are, statistically, close, although random. For a real-valued random process<sup>3</sup>  $\mathbf{X}$ , the autocorrelation is defined as  $R(t_1, t_2) = E\{\mathbf{X}(t_1)\mathbf{X}(t_2)\}$ , where  $E\{\cdot\}$  represents the mathematical expectation, and the covariance is the autocorrelation of the centered process  $\mathbf{X}(t) - E\{\mathbf{X}(t)\}$ .

When the mean of a random process is constant with time and its covariance function depends only on  $\Delta t = t_2 - t_1$ , it is qualified as mean-square stationary<sup>4</sup> (or mean-square homogeneous, for random fields). For these processes, models of the correlation structure are often introduced in terms of the correlation coefficient function and the spectral density function. The former is the covariance normalized by the covariance at the origin  $\Delta t = t_2 - t_1 = 0$ , and the latter is the Fourier transform in terms of  $\Delta t$  of the covariance. In these models of the correlation structure, a scale of fluctuation is usually defined, to indicate by a single scalar the strength of the correlation: the values of the process at two times separated by less than that lag are correlated, while for two instants further apart, the values are uncorrelated. This single scalar also allows a simpler experimental identification of the correlation structure.

Just like the choice of the PDF for a random variable is important and sometimes overlooked, the choice of a particular model of the correlation structure for a random process often remains unjustified in the literature. That choice should however be made carefully because it has consequences on the trajectories of the corresponding random process, particularly on their continuity. In general, for each field of application, numerous models of the correlation function have been developed in the literature<sup>5</sup>. They are sometimes derived from physical considerations, introducing the quantities that affect the randomness of the data as parameters, or simply by data-fitting with a very general interpolation basis. The latter approach lacks physical insight and the derived models of the correlation are therefore difficult to generalize from one problem to the other.

### 2.1.3 Representation of random processes

As we wish to apply probabilistic methods in a numerical environment, we have to address both the issues of the generation of samples of random quantities and of the discretization of the statistical dimension on finite dimensional bases. The first issue is important in MCS methods, where realizations of random variables or processes must be generated with a prescribed distribution and for the lowest possible computational cost. The second issue is important for all methods where continuous fields are approximated by their projection on finite dimensional bases, in particular the SFE methods. Various representations of stochastic processes have been designed, among which the spectral representation and the Auto-Regressive, Moving Average (ARMA) models are the most used for the generation of samples of Gaussian random processes, and the Karhunen-Loève (KL) and Polynomial Chaos (PC) expansions are the most used for general representations and for the discretization of random processes along the statistical axis. These four methods will be briefly presented here, and other techniques can be found with references in Shinozuka and Deodatis [1996] and Zerva and Zervas [2002, Sec. 6].

<sup>2</sup>These quantities are only defined for second-order random processes, as defined in App. A.2

<sup>3</sup>We will try, whenever possible, to use bold capital letters to identify random quantities from deterministic ones.

<sup>4</sup>Although it is not theoretically equivalent, mean-square stationarity is often referred to simply as stationarity.

<sup>5</sup>We will review some of these models for earthquake ground motions and soil parameter fields in Sec. 5.2.1.

### Box 2.2 Examples of Correlation Functions

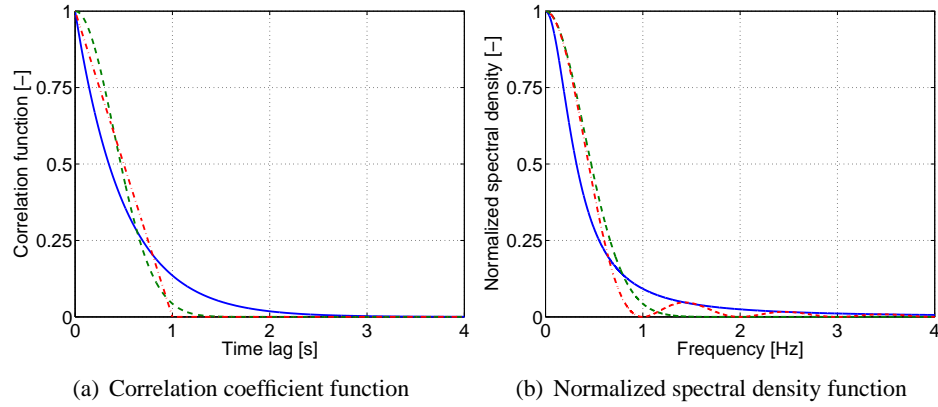


Figure 2.3: (a) Correlation function and (b) normalized spectral density function for several models with the same scale of fluctuation ( $\tau = 1$ s): exponential model (solid blue line), squared exponential model (dashed green line) and triangular model (dash-dotted red line).

Although many correlation structures have been proposed in the literature, one seems to appear more often: the exponential correlation function. It is defined (for a mean-square stationary random process  $\mathbf{X}$ ) as

$$\rho(\Delta t = t_2 - t_1) = \frac{\mathbb{E}\{(\mathbf{X}(t_1) - m_{\mathbf{X}})(\mathbf{X}(t_2) - m_{\mathbf{X}})\}}{\mathbb{E}\{(\mathbf{X}(0) - m_{\mathbf{X}})^2\}} = \exp\left(-2\frac{|\Delta t|}{\tau}\right), \quad (2.1)$$

where  $\tau$  is the scale of fluctuation, and  $m_{\mathbf{X}} = \mathbb{E}\{\mathbf{X}(t)\}$  is independent of time  $t$ , and  $\mathbb{E}\{(\mathbf{X}(0) - m_{\mathbf{X}})^2\} = \mathbb{E}\{(\mathbf{X}(t_2) - m_{\mathbf{X}})^2\} = \mathbb{E}\{(\mathbf{X}(t_1) - m_{\mathbf{X}})^2\}$ , because  $\mathbf{X}$  is mean-square stationary. The corresponding spectral density function for this model is

$$S(\omega) = \frac{1}{2\pi} \int_{\mathbb{R}} \exp(-i\omega\Delta t)\rho(\Delta t)d\Delta t = \frac{2\tau}{\pi(4 + \omega^2\tau^2)}. \quad (2.2)$$

On Fig. 2.3, the correlation function, and the corresponding spectral density function, for this exponential model, as well as for the squared exponential and triangular models, are represented. Graphically, these models seem very dissimilar, but it is not as clear as for the PDF of a design random variable whether this really has an important impact on reliability considerations.

In these short presentations of the four main representation methods, only one-dimensional, univariate stationary random processes are considered, but all four methods can be extended to multidimensional, multivariate nonstationary problems. The nonstationarity, which is important when modeling earthquake ground motion, is usually addressed either using modulations of stationary processes or by

splitting up the time domain into smaller subdomains on which the random process is seen as the restriction on a bounded interval of a stationary process. Also, the problem of the generation of samples of random variables of prescribed PDF are not considered here. Only the specific complexity arising from the consideration of random processes rather than random variables is addressed.

### Representation methods for the generation of Gaussian processes

The first method we will consider here is the spectral representation method. We will then turn to ARMA models. The basic idea of the spectral representation method [Shinozuka, 1972] is to expand a Gaussian random process on a set of cosine functions with increasing frequencies and random phases, such that the spectral density of the series converges to the given spectral density of the random process. Let us consider an unidimensional, univariate, Gaussian random process  $\mathbf{X}$ , with given spectral density  $S(\omega)$ . A discretization of the frequency domain has to be chosen with step  $\Delta\omega$  and values  $\{\omega_k\}_{1 \leq k \leq p}$ , so that a cut-off frequency is implicitly introduced, which has to be chosen high enough so that the spectral density is well represented. The spectral representation of order  $p$  of  $\mathbf{X}$  is

$$\mathbf{X}_p(t) = 2 \sum_{k=1}^p \sqrt{S(\omega_k)\Delta\omega} \cos(\omega_k t - \Xi_k), \quad (2.3)$$

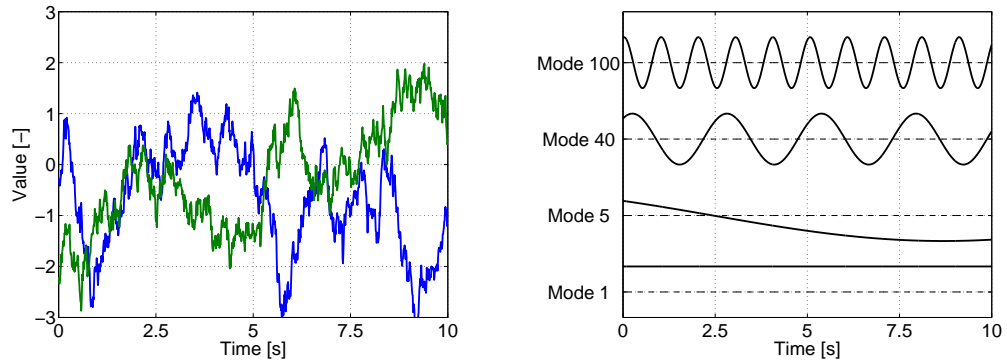
where the  $\{\Xi_k\}_{1 \leq k \leq p}$  are mutually independent random angles distributed uniformly on  $[0, 2\pi[$ . The random process  $\mathbf{X}_p(t)$  is asymptotically Gaussian when  $p$  tends to infinity, because of the Central Limit Theorem. The periodic character of this representation, which is artificially introduced, means that the step  $\Delta\omega$  has to be chosen small enough so that the period is large compared to the length of the path we wish to generate. An interesting aspect of this representation is that Eq. (2.3) can be written under an equivalent form which allows the use of the Fast Fourier Transform (FFT) for the generation of samples. The simulation time is therefore dramatically lowered. The multidimensional case is described, in great details, in Shinozuka and Deodatis [1996], and the case of non-Gaussian processes is considered in Yamazaki and Shinozuka [1988]. Applications to seismic ground motion can be found in Deodatis [1996].

The ARMA models for stationary discrete-time random processes represent a wide class of models, and are composed of two separate parts: the Auto-Regressive (AR) and the Moving Average (MA). The AR part describes the value of the considered process at a given time as a weighted sum of its values at previous times. The MA part describes the parameter as a weighted sum of random variables of given distribution, usually Gaussian. The ARMA model uses both parts, AR and MA, and the  $(n, p)$ -model of a discrete-time random process  $\mathbf{X}$  at time  $t_\ell$  is represented as a weighted sum of its values at previous times and of a random disturbance:

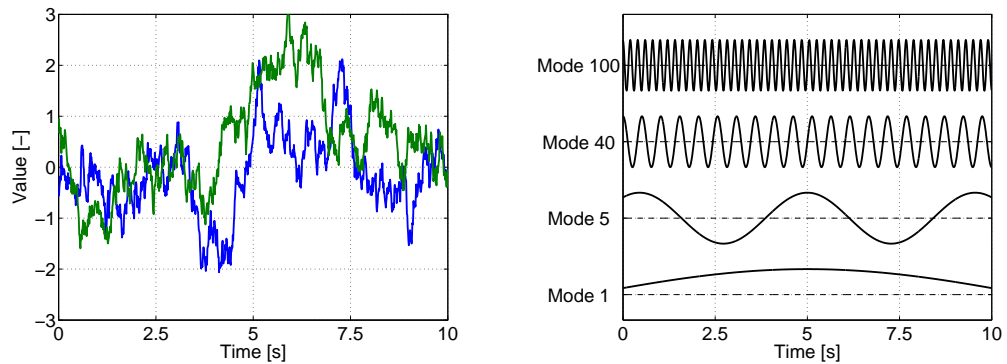
$$\mathbf{X}_{n,p}(t_\ell) = \sum_{k=1}^n \alpha_k \mathbf{X}(t_{\ell-k}) + \sum_{k=1}^p \beta_k \Xi_k, \quad (2.4)$$

where the  $\{\Xi_k\}_{1 \leq k \leq p}$  are random variables with given distributions, and the  $\{\alpha_k\}_{1 \leq k \leq n}$  and  $\{\beta_k\}_{1 \leq k \leq p}$  are coefficients that have to be determined by appropriate methods. The identification of these sets from experimental data is the main issue of ARMA modeling and many regression methods have been developed. Some of these are reviewed in Mignolet [1993], and in Kozin [1988] with a special emphasis on ARMA models for earthquake ground motions applications, for which the processes are nonstationary.

### Box 2.3 Examples of synthetic random processes



(a) Realizations and modes with the spectral representation method)



(b) Realizations and modes with the (KL expansion method)

Figure 2.4: Realizations of an exponentially-correlated stationary Gaussian random process ( $\tau = 2$  s) synthesized by (a) the spectral representation method and (b) the KL expansion. Two paths are presented for each method, along with the modes used for the first of the two paths.

Here are four samples of the same centered Gaussian random process, which is the restriction on a bounded time interval of an exponentially-correlated stationary process. Two samples are obtained using the spectral representation method and two using the KL expansion method. When using the former method, it is necessary to choose the underlying cut-off frequency high enough so that the spectral density function is well represented, and to choose the frequency step small enough so that the length of the generated path is very small compared to the period of the generated signal. When using the KL expansion method the problem lies in the computation of the modes of the representation, which can, in many cases be done analytically.

### Representation methods for the approximation of processes along the statistical axis

Both the KL and the PC expansions are representations of the random process  $\mathbf{X}(t)$  in terms of a countable set of random variables and deterministic functions of the variable  $t$ . The two methods are different in the choice of the PDFs of the random variables and the set of (time-dependent) basis functions of the expansion. In the KL expansion, the set of basis functions is prescribed, while the PDFs of the random variables is not, and in the PC expansion, it is the contrary. Although these two representation methods are presented here, separately from the previous ones, they can also be used for generation purposes. The PC expansion, particularly allows the straightforward generation of samples of non-Gaussian random processes.

The KL decomposition was developed independently by Karhunen [1946] and Loève [1955] (see also Lévy [1948] and Ghanem and Spanos [1991]), and is a representation of a stochastic process as an infinite linear combination of deterministic orthogonal functions and pairwise uncorrelated random variables. When the autocorrelation  $R(t_1, t_2)$  is such that  $\int_{\mathbb{R}^2} |R(t_1, t_2)|^2 dt_1 dt_2 < +\infty$ , a linear integral operator can be defined on the space of square-integrable functions, with kernel  $R(t_1, t_2)$ , and which is compact, symmetric, positive, and Hilbert-Schmidt. Therefore this operator has a countable spectrum of non-negative eigenvalues  $\{\lambda_n\}_{n \geq 0}$ , and the corresponding eigenvectors  $\{x_n\}_{n \geq 0}$  form an orthonormal basis of the space of square-integrable functions. For a random process  $\mathbf{X}(t)$  whose autocorrelation is prescribed and verifies the above condition, its KL expansion is such that

$$\mathbf{X}(t) = \mathbb{E}\{\mathbf{X}(t)\} + \sum_{n=0}^{+\infty} \sqrt{\lambda_n} \Theta_n x_n(t), \quad (2.5)$$

where the  $\{\Theta_n\}_{n \geq 0}$  are a countable set of zero-mean orthonormal<sup>6</sup> random variables. For a general random process  $\mathbf{X}(t)$ , the PDF of the  $\{\Theta_n\}_{n \geq 0}$  has to be computed by projection of the random process on the basis functions  $x_n(t)$ . When  $\mathbf{X}(t)$  is a Gaussian process, however, the  $\{\Theta_n\}_{n \geq 0}$  are known to be zero-mean unit-variance Gaussian random variables. The expansion is usually truncated at order  $p$ , with

$$\mathbf{X}_p(t) = \mathbb{E}\{\mathbf{X}(t)\} + \sum_{n=0}^p \sqrt{\lambda_n} \Theta_n x_n(t). \quad (2.6)$$

One of the interesting properties of the KL expansion is that it minimizes, in the  $L^2$  sense, the error resulting from the truncation at order  $p$ . One of its difficulties is the computation of the eigenvectors of the expansion, but many analytical solutions can be found in the literature, including for the most classical cases, as well as efficient algorithms for the more complicated cases.

The PC expansion provides a representation for second-order random processes as an expansion on a given set of orthogonal polynomials of zero-mean random variables with given PDFs, the coordinates of the expansion being functions of time. Here, the orthogonality of the polynomials refers to the probability measure of the random variables. Several choices for the set of polynomials and the PDFs of the random variables are possible, but the most often encountered are Hermite polynomials of Gaussian random

---

<sup>6</sup>with respect to the probability measure.

variables. The form of the PC expansion is

$$\begin{aligned} \mathbf{X}(t) = \Gamma_0 x_0(t) + \sum_{i_1=1}^{+\infty} \Gamma_1(\Xi_{i_1}) x_{i_1}(t) + \sum_{i_1=1}^{+\infty} \sum_{i_2=1}^{i_1} \Gamma_2(\Xi_{i_1}, \Xi_{i_2}) x_{i_1 i_2}(t) \\ + \sum_{i_1=1}^{+\infty} \sum_{i_2=1}^{i_1} \sum_{i_3=1}^{i_2} \Gamma_3(\Xi_{i_1}, \Xi_{i_2}, \Xi_{i_3}) x_{i_1 i_2 i_3}(t) + \dots, \end{aligned} \quad (2.7)$$

where the  $\{\Xi_i\}_{i \geq 1}$  are independent normalized Gaussian random variables, the  $\{\Gamma_p\}_{p \geq 0}$  are multidimensional Hermite polynomials of order  $p$ , and the  $\{t \mapsto x_\alpha(t)\}$  are the coordinates<sup>7</sup> of the random process  $\mathbf{X}(t)$ . The truncation of the expansion after the Hermite polynomial of order  $p$ , and the consideration of a finite set of random variables  $\{\Xi_i\}_{1 \leq i \leq n}$  yields the  $n$ -dimensional PC approximation of order  $p$ . Increasing  $n$  corresponds to the assessment of higher frequency random fluctuations of the underlying stochastic process, and increasing  $p$  corresponds to the representation of a stronger nonlinear dependency of the underlying process on the random variables of the expansion. The PC expansion can be used, in conjunction with a deterministic basis, to compute random eigenvalues and eigenvectors of an uncertain structure [Dessombz et al., 2001].

In this section, we have reviewed some of the most important tools in probabilistic modeling. The main aspect that should be stressed is the complexity of the assessment of the PDFs of random variables, and that of set of marginal laws for random processes. In the literature, the choices of PDFs and marginal laws are often not justified. However, the probabilistic response of the system will depend on these choices, so that they should be made lightly. Particularly, these choices should be consistent with the physics of the problem at hand, and amenable to experimental identification.

## 2.2 Tools and techniques for the resolution of stochastic mechanical problems

Once the tools of stochastic modeling have been introduced, we review here some of the most salient tools and techniques that have been used for the resolution of stochastic mechanical problems. We start with analytical techniques, which were historically discussed first. They will be seen to be often limited, in terms either of class or of size of the problems they can be applied to. Most of these methods are used to solve random vibration problems, where a deterministic model is loaded by an excitation modeled as a stochastic process. However, they can, in some cases, also be used to represent randomness in the coefficients of the differential equations governing the behavior of the system, but this will not be described here. After this set of analytical methods, we then turn to computational approximate tools and techniques, particularly the MCS technique and the SFE method, which are more versatile and usable for the resolution of larger classes of problems.

This panorama is mainly based on the review papers by Lin et al. [1986], Ibrahim [1987], Soize [1988a], Manohar and Ibrahim [1999], Grigoriu [2000], Schuëller [2001] and Manolis [2002], on the journal special issues edited by Schuëller [1997], Kleiber [1999], Hicks [2005] and Mace et al. [2005], and on the Ph.D. dissertations of Savin [1999], van de Wouw [1999] and Puel [2004]. Again, the goal of the dissertation is to model impedance matrices for possibly large and heterogeneous domains, and this should be kept in mind while reading.

<sup>7</sup>These coordinates are the unknowns in the SFE method, presented below, so they are therefore usually approximated by their projection on a classical FE basis.

### 2.2.1 Analytical tools and techniques

In this section, we first consider linear filtering problems, where a deterministic Linear Time Invariant (LTI) system is loaded by an excitation modeled by a random process. We then discuss several techniques for the resolution of random vibration problems for deterministic nonlinear systems, for which the literature is very extensive. As exact analytical results are not available in most cases, these techniques introduce approximations which yield problems that can be solved analytically.

#### Linear filtering

In linear filtering theory, the response of the system is modeled as the linear convolution of a deterministic Impulse Response Function (IRF) and a stochastic signal. This represents the excitation of a deterministic LTI system by a stochastic load. If we suppose that the excitation  $\mathbf{f}$  can be modeled by a mean-square stationary and continuous random process on  $\mathbb{R}$ , with a given spectral density function  $[S_{\mathbf{f}}(\omega)]$ , and that the IRF  $h(t)$  or the deterministic system is square-integrable, then the output  $\mathbf{u}$  is also mean-square stationary. Its mean  $E\{\mathbf{u}\}$  and spectral density function  $[S_{\mathbf{u}}(\omega)]$  are then

$$E\{\mathbf{u}(t)\} = [H(0)] E\{\mathbf{f}(t)\}, \quad (2.8)$$

and

$$[S_{\mathbf{u}}(\omega)] = [H(\omega)][S_{\mathbf{f}}(\omega)][H(\omega)]^*, \quad (2.9)$$

where  $E\{\mathbf{u}(t)\}$  and  $E\{\mathbf{f}(t)\}$  are independent of  $t$  because  $\mathbf{u}$  and  $\mathbf{f}$  are mean-square stationary,  $[H(\omega)]$  is the Frequency Response Function (FRF) of the filter, and the Fourier Transform of  $h(t)$ .

#### Random vibration problems for nonlinear systems

When considering nonlinear systems, the characterization of the response is not as simple. Exact analytical results are not available in most cases, so that many approximate methods have been devised, some of which are presented in the following paragraphs. With the exception of the equivalent linearization techniques, the systems considered in these methods are usually limited to one, or a few, DOF(s), the type of nonlinearity is often of the polynomial type, and limited to the stiffness function, and, finally, the excitation is in most cases modeled by an idealized random process. The equation of motion for these systems, in the unidimensional case, and in the time domain, can be put in the form

$$\ddot{\mathbf{u}}(t) + \eta\dot{\mathbf{u}}(t) + g(\mathbf{u}(t)) = \mathbf{f}(t), \quad (2.10)$$

where  $\mathbf{u}$  is the unknown random displacement of the mass,  $g$  is some nonlinear function of the displacement,  $\eta$  is the mass-normalized damping coefficient, and  $\mathbf{f}$  is the random excitation.

#### Equivalent linearization methods for nonlinear systems

The equivalent linearization methods are a set of techniques in which the nonlinear system under stationary random loading is replaced by a linear system under the same loading, equivalent in some particular sense. More specifically, the system of Eq. (2.10) is replaced by

$$\ddot{\mathbf{v}}(t) + \eta\dot{\mathbf{v}}(t) + \kappa\mathbf{v}(t) = \mathbf{f}(t), \quad (2.11)$$

where  $\mathbf{v}$  is the unknown stationary displacement of the mass in the equivalent system,  $\eta$  and  $\mathbf{f}$  are unchanged, and  $\kappa$  is an equivalent stiffness in the sense that it minimizes the mean square difference

between the two equations (2.10) and (2.11). The value of  $\kappa$  is yielded by the expression of that definition. Practically, Eq. (2.10) is written  $\ddot{\mathbf{u}}(t) + \eta\dot{\mathbf{u}}(t) + \eta\mathbf{u}(t) = \mathbf{f}(t) + (\kappa\mathbf{u}(t) - g(\mathbf{u}(t)))$ , and the mean square of the difference between the nonlinear restoring force and the linear one,  $E[\Phi_{\mathbf{u}}^2(t)] = E[(\kappa\mathbf{u}(t) - g(\mathbf{u}(t)))^2]$  is minimized by canceling its derivative with respect to  $\kappa$ , yielding

$$\kappa = \frac{E[\mathbf{u}(t)g(\mathbf{u}(t))]}{E[\mathbf{u}(t)^2]}, \quad (2.12)$$

where stationarity arguments are called to justify the time independence of  $\kappa$ . This formulation was sometimes referred to as "true equivalent linearization", or "unrestricted linearization". The expectations in Eq. (2.12) involve the probability density function of the nonlinear response  $\mathbf{u}$ , which is unknown, therefore most authors suggest a Gaussian distribution with undetermined variance, yielding the "Gaussian equivalent linearization", or "restricted linearization". Once the value of the equivalent stiffness has been computed, the moments of the response  $\mathbf{v}$  can be computed from those of  $\mathbf{f}$ , using standard linear theory.

Other linearization methods choose to base the equivalence on other indicators, for example  $\Phi_{\mathbf{v}}(t) = \kappa\mathbf{v}(t) - g(\mathbf{v}(t))$ , and yield other values for the equivalent stiffness, as well as for the moments of the response. This disparity in the definitions of the equivalent linearization sometimes induced misunderstandings and some authors claimed there was an error in the classical equivalent linearization technique. This particular problem was settled in Crandall [2001], and the differences between the criteria were emphasized. All linearization techniques were deemed acceptable, but, unfortunately, no clue was given with respect to the *a priori* choice of one criterion or another for obtaining the best results for a given system. In Socha and Pawleta [2001], another comparison of two equivalent linearization methods is presented, and the two methods are shown to be different in nature, although yielding the same results in most cases considered.

Unlike other random vibration resolution methods, the linearization techniques can easily cope with multi-dimensional systems, many types of nonlinearities, including that depending on derivatives of the displacement, and any type of random loading. Therefore it has been the focus of a lot of attention and research. Unfortunately, these methods provide accurate results only for small nonlinearities and, because of the underlying Gaussian hypothesis, it cannot estimate accurately moments of higher order than the second, or the tail of the distribution of the response. More generally, there is a lack of theoretical proof for the accuracy of the response, both *a priori* and *a posteriori*. In Bernard [1998], the "Gaussian equivalent linearization" is even shown to be mathematically inaccurate, and an example is presented to illustrate that matter. More details on equivalent linearization techniques can be found in one of the founding articles [Caughey, 1963b], in the monograph by Roberts and Spanos [1990] and in several review articles [Socha and Soong, 1991, Socha, 2005, Crandall, 2006]. The application of the equivalent linearization to Multiple-Degrees-of-Freedom (MDOF) systems is described in Pradlwarter and Schuëller [1992].

### Perturbation technique

The perturbation technique for the resolution of nonlinear problems of random vibration is based on the assumption that the nonlinear stiffness function  $g$  of Eq. (2.10) does not deviate too much from linearity. It is then written  $g(\mathbf{u}(t)) = \kappa(\mathbf{u}(t) + \epsilon\gamma(\mathbf{u}(t)))$ , where  $\kappa$  is an equivalent stiffness<sup>8</sup>, and  $\epsilon$  is a small parameter in the sense that  $\epsilon\|\gamma(\mathbf{u}(t))\|_{\mathbb{R}} \ll \|\mathbf{u}(t)\|_{\mathbb{R}}$  at all times. The response  $\mathbf{u}$  is then expanded in

<sup>8</sup>which is not related to the equivalent stiffness computed by equivalent linearization techniques

terms of  $\epsilon$ ,  $\mathbf{u}(t) = \sum_{k=0}^N \mathbf{u}_k(t)\epsilon^k$ , as well as the nonlinear function  $\gamma(\mathbf{u}(t)) = \sum_{k=0}^N \partial_{\mathbf{u}}^k \gamma(\mathbf{u}_0(t))\epsilon^k$ , and introduced in Eq. (2.10). The cancellation of each term of the resulting polynomial in  $\epsilon$  yields the following set of equations:

$$\ddot{\mathbf{u}}_0(t) + \eta \dot{\mathbf{u}}_0(t) + \kappa \mathbf{u}_0(t) = \mathbf{f}(t) \quad (2.13)$$

$$\ddot{\mathbf{u}}_1(t) + \eta \dot{\mathbf{u}}_1(t) + \kappa \mathbf{u}_1(t) = \kappa \gamma(\mathbf{u}_0(t)) \quad (2.14)$$

$$\ddot{\mathbf{u}}_2(t) + \eta \dot{\mathbf{u}}_2(t) + \kappa \mathbf{u}_2(t) = \kappa \partial_{\mathbf{u}} \gamma(\mathbf{u}_0(t)) \quad (2.15)$$

(...) ,

that can be solved hierarchically to yield the set  $\{\mathbf{u}_k\}_{0 \leq k \leq N}$ . In the literature, the expansion is usually performed to the first order  $\mathbf{u} = \mathbf{u}_0 + \epsilon \mathbf{u}_1$ , and is therefore only valid for small nonlinearities. When the excitation is stationary, with given correlation function, the statistical moments of the response  $\mathbf{u}$  can be evaluated, as well as other statistics of the response, such as the expected frequency of zero crossings, the distribution of the peaks, or the distribution of the envelope [Crandall, 1963]. However, this expansion is not guaranteed to converge when the number of terms increases, and it might contain secular terms inducing instabilities of the approximate solution when higher order terms are considered. Even though it was extensively studied in the literature, this technique should not be trusted for studies beyond sensibility analyses.

### Fokker-Planck equation

Under general conditions, that will not be described here (see Soize [1994] for details in the general case and Caughey [1963a] for the example of an one-dimensional nonlinear system under white noise loading), the response  $\mathbf{u}$  of the system described by Eq. (2.10) can be described by a diffusion process, with almost surely continuous trajectories. The transition probability  $p_t$  of this diffusion process verifies a Fokker-Planck equation (or forward Kolmogorov equation)

$$\frac{\partial p_t}{\partial t} = - \sum_{i=1}^N \frac{\partial}{\partial y_i} (a_i p_t) + \frac{1}{2} \sum_{i=1}^N \sum_{j=1}^N \frac{\partial^2}{\partial y_i \partial y_j} (b_{ij} p_t) \quad (2.16)$$

where the drift vector  $[a] = (a_i)_{1 \leq i \leq N}$  and the diffusion matrix  $[b] = (b_{ij})_{1 \leq i, j \leq N}$  can be derived from the characteristics of the initial mechanical system. Analytical solutions of this equation can be derived in some limited cases, including the steady-state response of particular dynamic systems in any dimension [Soize, 1994]. However, in the general case, approximate numerical techniques have to be used, and they become cumbersome for multidimensional systems [Soize, 1988b].

### Moment methods

The moment methods are a class of methods based on the fact that a system of differential equations for the moments of the response  $\mathbf{u}$  can be constructed, from the equation of Itô [Soize, 1988a, p.50], or from the Fokker-Planck equation. This system constitutes an infinite hierarchy so that a closure scheme has to be chosen, where the word 'closure' refers to the fact that the infinite hierarchy of equations is truncated to yield a closed set of equations for the moments of lower order. The moments of higher order are then either cancelled, or written in terms of those of lower order. Several schemes have been proposed, none of them apparently general. The Gaussian Closure consists in expressing the higher order moments of the response in terms of the first two, with the relation they would have if the random process were

Gaussian. An alternative method, although related, the cumulant-neglect closure [Lin and Cai, 1995, p.283], is based on a similar infinite hierarchy of equations, but for the cumulants of the response rather than the moments. As the cumulants of order higher than two vanish for Gaussian processes, this method is deemed more appropriate when the response is 'almost' Gaussian. It is interesting to note that these approaches can be completed using other techniques to evaluate PDFs from the knowledge of the first moments. For example, in Sobczyk and Trębicki [1999], such a completion is performed using the Maximum Entropy Principle.

As a conclusion on this group of methods, it should be noted that they are limited in one or all of three aspects: the class of problems they can be applied to, the size of the systems for which they can reasonably solved, and the level of variability they can assess. As the industrial problems we wish to address involve complicated, large, systems with important variability, we will rather turn to another set of techniques, more versatile, that are presented in the next section.

### 2.2.2 Computational tools and techniques

Most models in deterministic computational mechanics are represented over a discretized space using a FE method. The idea of the SFE methods is to extend these concepts, and possibly the corresponding software, to stochastic mechanics problems. The random dimension is considered an additional dimension which is discretized to yield an alternative problem which can be solved by traditional FE resolution methods. The differences between the SFE methods are related to the way the problem is formulated, yielding alternatively intrusive or non-intrusive methods. The first type of methods induces the resolution of one very large deterministic system, and requires the writing of dedicated software. The second type of method relies on the MCS method, which is presented below, to repeatedly call for the resolution of a classical FE problem, using software already available. Since deterministic commercial FE softwares have now reached a very mature level of development, with hundreds of engineers working on the improvement of the numerical schemes underlying the codes, this second approach seems computationally appealing.

#### Monte Carlo Sampling method

The MCS method is a very general resolution technique, that can deal with complicated system, with many random variables or processes. Its basic steps are:

1. generate samples of the input random parameter vector following its prescribed set of marginal laws,
2. compute the response of the system for each realization independently, and,
3. compute statistics of the response using these response samples.

From these steps, it can be seen that the MCS method is very versatile, and can be readily used for any random problem for which the corresponding deterministic problem can be solved. It can be applied to very complicated, possibly nonlinear, MDOF problems of very large size, assuming that the corresponding deterministic software is available. The main problem - and limitation - of the MCS method derives from the computational time required to assess the statistics of the response, as it is the time necessary for one deterministic computation multiplied by the number of trials. This number depends on the level of accuracy desired for the response, and, if more than the first moments are sought, rapidly becomes

unrealistic. An interesting feature, though, is that the necessary number of trials to reach a given level of accuracy can be assessed beforehand.

The fast development of computers makes the MCS method quite appealing and widespread but, for costly problems, it is still mainly restricted to the assessment of the accuracy of other, approximate, methods. The costs associated with MCS techniques as described here can be somewhat lowered by variance reduction techniques which, through an appropriate choice of the realizations of the input parameter, allow for a reduction of the number of samples necessary to reach a given level of accuracy [Pradlwarter and Schuëller, 1997]. Also, the independence of the computation of the response for each realization makes the parallelization of MCS codes very straightforward [Johnson et al., 2003].

Apart from prohibitive computational cost and possible issues of the deterministic computation, the main difficulty lies in the generation of the realizations of the input random vector, which has to follow a given set of marginal laws. Some of the available methods for the generation of realizations of random variables are presented in Robert and Casella [1999], and the aspects concerning the generation of realizations of random processes were reviewed in Sec. 2.1.3. A complete example of the application of the MCS method for the resolution of a nonlinear mechanics problem with uncertainties is presented in Shinozuka [1972].

### Stochastic Finite Element method

We only present here the spectral approach to SFE methods, described in Ghanem and Spanos [1991], and which is intrusive. In that approach, the discretization of the random dimension is performed using the KL expansion for the random parameters of the differential equations of the system, and the PC expansion for the response, supposing the hypotheses of both expansions are verified. When the order of the polynomials of the PC expansion is limited to two, the equation for the system is therefore

$$\left( [K_0] + \sum_{i=0}^p \sqrt{\lambda_i} \Theta_i^{KL} [K_i] \right) \left( \Gamma_0 \mathbf{u}_0 + \sum_{i=1}^n \Gamma_1(\Xi_i^C) \mathbf{u}_i + \sum_{i=1}^n \sum_{j=1}^i \Gamma_2(\Xi_i^C, \Xi_j^C) \mathbf{u}_{ij} \right) = \mathbf{F}, \quad (2.17)$$

where the  $(\lambda_i)_{1 \leq i \leq p}$  and  $([K_i])_{1 \leq i \leq p}$  are the eigenvalues and eigenvectors of the covariance matrix of the random operator of the system, the  $(\Gamma_i)_{i \geq 0}$  are the Polynomial Chaoses, the  $(\Theta_i^{KL})_{1 \leq i \leq p}$  are a set of orthogonal random variables with given distributions, the  $(\Xi_i^C)_{1 \leq i \leq n}$  are independent normalized Gaussian random variables, and the  $(\mathbf{u}_i)_{0 \leq i \leq p}$  and  $\mathbf{u}_{ij}{}_{1 \leq i, j \leq p}$  are the unknown coordinates of the PC expansion. By further multiplying this equation by each of the polynomials of the expansion, and averaging, we get a very large set of equations that yield the coefficients  $(\mathbf{u}_i)_{0 \leq i \leq p}$  and  $\mathbf{u}_{ij}{}_{1 \leq i, j \leq p}$ . The form of the matrix of the system is particular, and that can be used to lower the computational time needed for its inversion, but it still remains very time consuming. More details on the spectral SFE method and the actual computation of the response can be found in the monograph by Ghanem and Spanos [1991]. The versatility of this method has permitted its use in a very large number of applications, for the modeling of different types of uncertainties. In particular, in Ghiocel and Ghanem [2002], the spectral SFE method is applied to a SSI problem, where a wide range of parameters, in the soil, the structure and the loading, are considered uncertain.

### Stochastic boundary elements methods

As BE techniques are widely used in SSI problems, we next present a few attempts that have been made at deriving Stochastic Boundary Element (SBE) formulations [Burczyński, 1994]. For a random superficial loading or a random displacement imposed on the boundary, the approach is quite similar to the

deterministic BE method. The random field is discretized on a given mesh, and the unknown random field on the boundary is related to the input random field on the boundary through matrices computed using integrals of deterministic Green's functions for the considered domain. The mean of the unknown random field is therefore directly the one computed with the deterministic BE method for the mean of the input field, and the covariance and cross-covariance matrices of the unknown random field are computed from those of the input field. An additional requirement in these methods, in comparison with deterministic BE methods, is that the mesh should be chosen so that the size of the cells be small compared to the correlation length of the input random field as well as compared to the wavelength.

When considering random properties of the medium, things get more complicated. If the fluctuations of the properties are small compared to the mean, then a perturbation approach can be applied. If not, the integral equation of the BE method can be recast in terms of a classical BE problem plus an additional integral on the entire volume [Savin and Clouteau, 2002]. Doing that, one loses the main advantage of the BE method, which is to mesh only the boundary of the considered domain. Finally, some attempts at identifying stochastic Green's functions have been made [Manolis and Karakostas, 2003].

### 2.2.3 Reliability analyses

The goal in stochastic mechanical problems is not really to derive the marginal laws of the response of the system, but rather to assess some probability of failure of a structure. This requires the definition of failure criterion, which can relate to minimum or maximum authorized displacements, strains or stresses in some particular places of the structure. This criterion is usually the combination of basic failure criteria, relating to particular failure modes of the structure, so that the global failure criterion can become very complicated for real industrial structures. The choice of this criterion depends on the particular application at hand and will not be discussed here. However, once it has been chosen, the computation of the failure probability with respect to this criterion can be performed mainly in two ways, which are presented hereafter. As reliability analyses typically consider very small probabilities of failure, it should be reminded, as illustrated in Box 2.1.1, that unsound modeling of the parameters may have a large impact on the estimations.

#### Sampling approach

Let us consider that the failure criterion is given in the form of a failure function  $g = \mathbf{R} - \mathbf{S}$ , where  $\mathbf{R}$  represents some measure of the resistance of the structure, and  $\mathbf{S}$  stands for the solicitation on that structure. This failure function separates a safe set, where the particular  $\mathbf{R}$  and  $\mathbf{S}$  induce a good behavior of the structure, and a failure set, where the structure fails to resist the solicitation. Both  $\mathbf{R}$  and  $\mathbf{S}$  depend on the mode of failure that has been chosen, so that real failure functions will usually be complicated combinations of basic function such as  $g$ . The probability of failure of the structure is then computed as the probability that  $g < 0$ .

Using the MCS method, that probability of failure can be derived straightforwardly. Drawing samples of the random parameters of the problem, the corresponding realizations of  $\mathbf{R}$  and  $\mathbf{S}$  can be estimated, and the structure seen to fail or not. By drawing a sufficient number of samples, the probability of failure can be readily estimated. However, these probabilities are usually very low, relating to higher-order moments of the response. The number of Monte Carlo trials necessary to perform accurately that estimation will therefore be usually very high. Although this was a very strong limitation of the sampling approach in the past, this technique has become more customary, as powerful computers are more widely available.

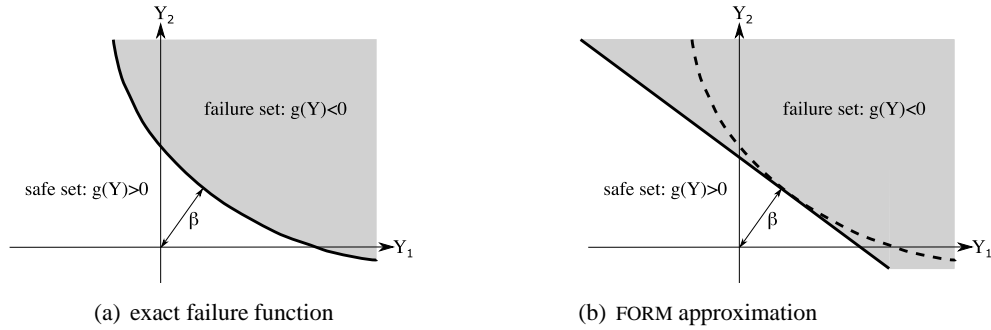


Figure 2.5: (a) Example of a failure function  $g$  in the plane of the parameters  $(Y_1, Y_2)$ , corresponding safe set and failure set, and reliability index  $\beta$ , and (b) FORM approximation of the same failure function and corresponding safe and failure sets.

### Approximate analytical approach

Another, approximate, approach to the computation of that probability of failure has been the subject of a very large interest in the community. Because this case can be easily represented graphically, we concentrate here on the particular case when the system depends on two random variables  $X_1$  and  $X_2$ . This method is probably the probabilistic method that is best known to structural engineers, mainly because it defines a reliability index  $\beta$  that allows in a certain sense the comparison of the reliability levels for separate structures.

The first issue of the reliability method is therefore the computation of that index, and this is performed in two steps. First, the random variables  $X_1$  and  $X_2$  are transformed into Gaussian zero-mean, unit-variance, random variables  $Y_1$  and  $Y_2$ , using an isoprobabilistic transformation. In that space, the origin corresponds to the mean state of the system, and the reliability index  $\beta$  corresponds to the shortest distance from the origin to the failure function<sup>9</sup>  $g(Y_1, Y_2) = 0$  (see Fig. 2.5(a)). This second step corresponds to a minimization problem, for which many methods have been devised, and yields at the same time  $\beta$  and the design point, which is the closest point to the origin on the failure function.

Once the design point has been encountered, two types of approximations are performed to yield the probability of failure  $P_f$ . The simplest one is the FORM, where the surface of failure is replaced by its tangent hyperplane at the design point. The probability of failure can then be computed from the knowledge of the reliability index with the simple formula

$$P_f = 1 - \Phi(\beta), \quad (2.18)$$

where  $\Phi$  is the normalized Gaussian distribution function. When the curvature of the failure surface is too important, so that the FORM yields a bad approximation, an enriched expansion can be performed, the Second-Order Reliability Method (SORM), which basically corresponds to a second order Taylor expansion, and for which formulas similar to Eq. (2.18) have been derived.

What was presented here was actually the computation of the probability of failure for a single mode of failure. For structural systems though, many modes of failure are possible, and that situation requires increased modeling. Let us consider a series system, for which the failure of one single component implies the failure of the entire structure, and a parallel system, where the failure of all components

<sup>9</sup>The function  $g$  is modified by the isoprobabilistic transformation but the same symbol is conserved for ease of reading.

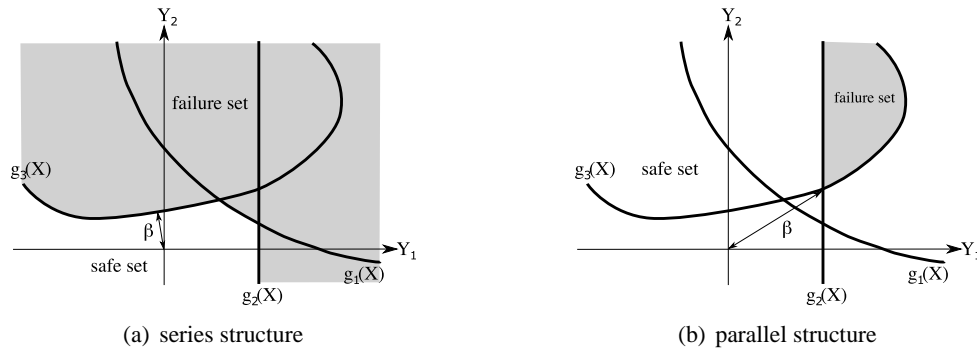


Figure 2.6: Failure surface, safe and failure sets, and reliability index for (a) a series structure and (b) a parallel structure.

simultaneously is necessary to yield the failure of the entire structure. The corresponding situations are drawn in Fig. 2.6, and are obviously much more complicated, if only because the global surface of failure is not a smooth function even when the surface of failure of each mode of failure is smooth. The minimization problem of finding the design point might be very badly conditioned. Besides, series and parallel systems are themselves simplifications of real structures, which can become very troublesome to deal with using the structural reliability method [Schuëller et al., 2004].

Nevertheless, the reliability methods have been undergoing very intensive study and many different related techniques have been developed, for many types of idealized structures. They were also shown to be suitable for industrial applications, with very large systems, and many randomized parameters, provided that appropriate numerical methods were used [Koutsourelakis et al., 2004, Pellissetti et al., 2006]. A monograph was recently written by Lemaire [2005] and review papers, with corresponding problems and limitations, can be found in chronological order in Ditlevsen and Bjerager [1986], Der Kiureghian [1996] and Rackwitz [2001]. A review and comparison of several softwares used in structural reliability can be found in Pellissetti and Schuëller [2006]

## 2.3 Summary

In the first part of this chapter, the main aspects of modeling in stochastic mechanics were presented. Most models in the literature seem to concentrate on low order modeling, for the statistical moments order, as well as for marginal laws order. An important reason for that is the difficult experimental identification of the higher order terms. Nevertheless, the influence of these terms is significant, particularly when considering rare events. This has to be kept in mind when representing a random variable or process, and the choice of a particular distribution or correlation model should not be made lightly.

In the second part, several stochastic approaches for mechanical problems were described. If we look back on this review recalling our aim of constructing a probabilistic model of the impedance matrix usable with large heterogeneous domains, most of these methods have to be discarded. Indeed, analytical approaches are too limited, in terms either of the level of variability they can assess, of the class of problems they can be applied to, or of the size of the problems that can be treated. SFE methods are widely used, but they are limited to bounded random domains<sup>10</sup>. SBE methods are not limited in that

<sup>10</sup>However, we will see in the field of SSI an application where a SFE method is used to model an heterogeneous soil, although

matter, but they are still restricted to very specific cases where the stochastic fundamental function can be computed. Finally, reliability approaches were considered, and the sampling technique was seen to be particularly appealing, provided that its cost could be afforded.

The question of the experimental assessment of high order moments and marginal laws, as well as the apparent deficiencies of the classical approaches for large heterogeneous domains, leads us to the choice of an alternative, more recent, method. In this nonparametric approach, a stochastic model of the matrices of mass, damping and stiffness of the system is introduced, and controlled by a small number of parameters. The algebraic properties of the realizations of these matrices are enforced so as not to allow non-physical samples. The modeling is performed in generalized bases for the displacements and stresses so that the size of the domain is not necessarily an issue, and the limited number of parameters makes the identification possible. Finally, this approach is compatible with a resolution by the MCS method, which was shown to be both practical, although costly, and mathematically sound. The construction of the probabilistic model of the impedance matrix using that nonparametric approach is the subject of the next chapter.

---

that heterogeneous soil is limited to a bounded part of the unbounded soil.

# Chapter 3

## Probabilistic models of impedance matrices

This chapter is the core of this dissertation. It presents the structure of the impedance matrix that will be used for the construction of the probabilistic model, and the construction itself. In a first section, the formal definition of the impedance matrix is given, along with its properties. The enforcement of these properties leads us to the introduction of a general frame for the samples of random impedance matrices: the hidden state variables model (Sec. 3.1.4). Considering the conclusions of the previous chapter, a non-parametric approach is then introduced for the probabilistic modeling of the random impedance matrices themselves. This strategy is presented, using tools introduced in the literature on vibrations of structures, and its application to our case is detailed (Sec. 3.2.1). The last section (Sec. 3.3) summarizes the steps of the practical construction of the probabilistic model of an impedance matrix.

### 3.1 Models of the impedance samples

In this first section, the impedance is defined in a deterministic setting. The problem is posed using continuous fields, which leads to the introduction of the impedance operator, and the discretization of these continuous fields yields the impedance matrix. The properties of this frequency-dependent matrix are studied, and the most classical methods for its computation are reviewed. Finally, the hidden variables model is introduced as an attempt to present a general framework enforcing these basic properties. As the properties of the impedance matrix have to be verified by both a deterministic model and realizations of a probabilistic model, this section should be read with both cases in mind.

#### 3.1.1 Definition of the impedance

The problem is set in the field of elastodynamics. It could equally have been derived in acoustics or fluid dynamics. However, in these cases, it is customary to define the impedance with respect to a velocity field rather than to a displacement field. We use here the classical definition in solid mechanics of the operator linking displacements and stresses. The setting considered (see Fig. 3.1) is very general, as in the introduction, and will be particularized for the field of SSI problems in Sec. 5.1. There,  $\Omega$  will represent the soil. We consider only the case of a viscoelastic medium without memory, so that these results are valid for bounded as well as unbounded domains. In the case of an undamped system, additional radiation conditions would have to be added to the system of Eq. (3.1), and the functional space defined in Eq. (3.2) would have to be modified<sup>1</sup>.

---

<sup>1</sup>Indeed, a mechanical wave propagating towards infinity, undamped, cannot be represented by a function in  $L^2(\Omega)$ , so that a larger functional space has to be introduced, and the radiation conditions can be seen as boundary conditions at infinity, preventing waves from entering the system from infinity.

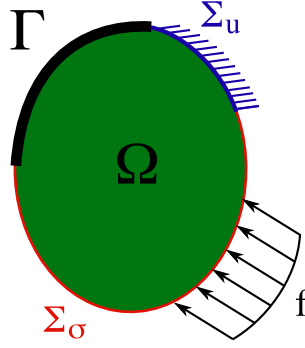


Figure 3.1: Setting of the Boundary Value Problem: (bounded) domain  $\Omega$  and boundary  $\Gamma$  with respect to which the impedance will be defined.

### Setting of the boundary value problem

Let  $\Omega$  be an open, bounded or unbounded, subset of  $\mathbb{R}^3$  with a smooth boundary  $\partial\Omega$ . This boundary is separated into  $\Gamma$ , with respect to which the impedance will be defined,  $\Sigma_\sigma$ , on which Neumann boundary conditions are imposed, and  $\Sigma_u$ , on which Dirichlet boundary conditions are enforced. These boundaries verify  $\Gamma \cup \Sigma_\sigma \cup \Sigma_u = \partial\Omega$  and  $\Gamma \cap \Sigma_\sigma = \Gamma \cap \Sigma_u = \Sigma_\sigma \cap \Sigma_u = \emptyset$ .

Let  $\mathbf{u} = [u_i]_{1 \leq i \leq 3}$  be a displacement field defined on  $\Omega$ , and  $\boldsymbol{\sigma} = [\sigma_{ij}]_{1 \leq i, j \leq 3}$  and  $\boldsymbol{\epsilon} = [\epsilon_{ij}]_{1 \leq i, j \leq 3}$  the corresponding linear stress and strain tensors. Let  $\mathbf{C}^e = [C_{ijkl}^e]_{1 \leq i, j, k, l \leq 3}$  and  $\mathbf{C}^d = [C_{ijkl}^d]_{1 \leq i, j, k, l \leq 3}$  be respectively the fourth order elastic and damping tensors of the materials in  $\Omega$ , having the usual properties of symmetry ( $C_{ijkl}^e = C_{jikl}^e = C_{klij}^e$  and  $C_{ijkl}^d = C_{jikl}^d = C_{klij}^d$ ) and positive-definiteness ( $C_{ijkl}^e e_{ij} e_{kl} \geq \alpha e_{ij} e_{ij}$  and  $C_{ijkl}^d e_{ij} e_{kl} \geq \beta e_{ij} e_{ij}$ , with  $\alpha, \beta > 0$  for any second order real symmetric tensor  $e$ ).

The local harmonic Boundary Value Problem (BVP) in  $\Omega$  consists in finding, for each  $\omega$  in  $\mathbb{R}$ , a displacement field  $\mathbf{u}$  such that, for all  $1 \leq i \leq 3$ ,

$$\begin{cases} \sigma_{ij,j}(\mathbf{u}) + \rho\omega^2 u_i = 0 & \text{in } \Omega \\ \sigma_{ij}(\mathbf{u}) n_j = \underline{f}_i & \text{on } \Sigma_\sigma \\ u_i = \underline{u}_i & \text{on } \Sigma_u \\ u_i = \phi_i & \text{on } \Gamma \end{cases}, \quad (3.1)$$

where  $\underline{f} = [f_i]_{1 \leq i \leq 3}$  is a given stress field, and  $\underline{u} = [u_i]_{1 \leq i \leq 3}$  and  $\phi = [\phi_i]_{1 \leq i \leq 3}$  are given displacement fields. Here Dirichlet boundary conditions are considered on  $\Gamma$ . Using Neumann conditions instead of the Dirichlet conditions would lead us to the definition of the flexibility operator, rather than to the definition of the impedance. It should also be noted that, in the linear case, the study of a problem with incident waves radiating from infinity - as in seismology - or with sources in  $\Omega$ , can be brought back to the study of a BVP, via superposition<sup>2</sup>.

<sup>2</sup>An example of this will be treated in Sec. 5.1, in the context of earthquake engineering.

### Variational formulation of the BVP

The classical complex Sobolev space of the square integrable complex functions defined on  $\Omega$ , with square integrable first derivative, is denoted  $H^1(\Omega)$ .

$$H^1(\Omega) = \{u \in L^2(\Omega), D^1 u \in L^2(\Omega)\}, \quad (3.2)$$

where  $D^1$  denotes the first order partial derivation operator.  $H^1(\Omega)$  is a complex Hilbert space when associated with the norm,  $\|\cdot\|_{H^1(\Omega)}$ , defined for  $u$  in  $H^1(\Omega)$  by

$$\|u\|_{H^1(\Omega)} = \left[ \int_{\Omega} \|u\|_{\mathbb{C}}^2 + \sum_i \|\partial_i u\|_{\mathbb{C}}^2 dx \right]^{1/2} \quad (3.3)$$

The space of the admissible solutions for the variational formulation of the BVP is  $V_{\Omega} = \{\mathbf{u} \in [H^1(\Omega)]^3\}$ . The continuous hermitian sesquilinear forms of mass, damping and stiffness are defined in  $V_{\Omega} \times V_{\Omega}$ , respectively, by<sup>3</sup>

$$m(\mathbf{u}, \delta \mathbf{u}) = \int_{\Omega} \rho u_i \overline{\delta u_i} dx, \quad (3.4)$$

$$k(\mathbf{u}, \delta \mathbf{u}) = \int_{\Omega} C_{ijkl}^e \epsilon_{ij}(\mathbf{u}) \epsilon_{kl}(\overline{\delta \mathbf{u}}) dx, \quad (3.5)$$

$$d(\mathbf{u}, \delta \mathbf{u}) = \int_{\Omega} C_{ijkl}^d \epsilon_{ij}(\mathbf{u}) \epsilon_{kl}(\overline{\delta \mathbf{u}}) dx. \quad (3.6)$$

The sesquilinear form of mass is positive definite. In the case of a bounded domain  $\Omega$ , the sesquilinear forms of stiffness and damping are only non-negative because the imposed displacement fields  $\phi$  on  $\Gamma$  and  $\underline{u}$  on  $\Sigma_u$  might allow rigid body modes inside  $\Omega$ . However, this particular case is treated extensively in Ohayon and Soize [1998] and will not be considered further in the dissertation. For an unbounded domain with a viscoelastic material, rigid body modes in  $\Omega$  require infinite energy so that the displacement field would then be outside of  $V_{\Omega}$ . For both cases, we therefore consider that the damping and stiffness sesquilinear forms are positive-definite. For a given frequency  $\omega$  in  $\mathbb{R}$ , the continuous sesquilinear form of dynamic stiffness is defined in  $V_{\Omega} \times V_{\Omega}$  by

$$s(\mathbf{u}, \delta \mathbf{u}; \omega) = -\omega^2 m(\mathbf{u}, \delta \mathbf{u}) + i\omega d(\mathbf{u}, \delta \mathbf{u}) + k(\mathbf{u}, \delta \mathbf{u}). \quad (3.7)$$

Considering an element  $\mathbf{u}$  of  $V_{\Omega}$ , its restriction<sup>4</sup> to boundary  $\Gamma$  is called the trace of  $\mathbf{u}$  on  $\Gamma$ , and denoted  $\mathbf{u}|_{\Gamma}$ . The space of the traces of the elements of  $V_{\Omega}$  on  $\Gamma$  is denoted  $V_{\Gamma}$ . The functional spaces  $V_{\Omega}^{\phi}$  and  $V_{\Omega}^0$  are then defined by

$$V_{\Omega}^{\phi} = \{\mathbf{u} \in V_{\Omega}, \mathbf{u}|_{\Sigma_u} = \underline{u}, \mathbf{u}|_{\Gamma} = \phi\}, \text{ and } V_{\Omega}^0 = \{\mathbf{u} \in V_{\Omega}, \mathbf{u}|_{\Sigma_u} = \mathbf{0}, \mathbf{u}|_{\Gamma} = \mathbf{0}\}. \quad (3.8)$$

The variational formulation of the BVP consists in finding, for  $\omega$  in  $\mathbb{R}$ ,  $\mathbf{u} \in V_{\Omega}^{\phi}$  such that

$$s(\mathbf{u}, \delta \mathbf{u}; \omega) = f(\delta \mathbf{u}; \omega), \quad \forall \delta \mathbf{u} \in V_{\Omega}^0, \quad (3.9)$$

where  $f$  is a continuous hermitian linear form defined, for  $\omega$  in  $\mathbb{R}$ , on  $V_{\Omega}$  by  $f(\delta \mathbf{u}; \omega) = \int_{\Sigma_{\sigma}} \underline{f}_i(\omega) \overline{\delta u_i} dS$ .

<sup>3</sup>In Eq. (3.4), and in the rest of this dissertation, the convention for summation over repeated indices is used.

<sup>4</sup>The restriction here is defined, since  $\Omega$  is open, as a limit for positions in  $\Omega$  tending towards positions in  $\Gamma$ .

### The impedance operator

In the static case, the ellipticity of the elastic tensor  $C^e$  ensures that the dynamic stiffness sesquilinear form  $s(\cdot, \cdot)$  is coercive. In the dynamic case, the ellipticity of the damping tensor  $C^d$  ensures that  $e^{i\pi/2}s(\cdot, \cdot)$  is coercive. In both cases, the Lax-Milgram theorem [Dautray and Lions, 1990] ensures that the variational formulation of the BVP has a unique solution, therefore defining for each  $\omega$  in  $\mathbb{R}$ , an unique operator  $\mathcal{T}(\omega)$  from  $V_\Gamma$  to  $V_\Omega^\phi$  such that

$$\mathbf{u} = \mathcal{T}(\omega)\phi. \quad (3.10)$$

The impedance operator is then defined, for each  $\omega$  in  $\mathbb{R}$ , from  $V_\Gamma$  into its antidual  $V_\Gamma'$ , for each  $\omega$  in  $\mathbb{R}$ , by

$$\langle \mathcal{Z}(\omega)\phi, \delta\phi \rangle_\Gamma = s(\mathcal{T}(\omega)\phi, \mathcal{T}(\omega)\delta\phi; \omega) \quad (3.11)$$

where  $\langle \cdot, \cdot \rangle_\Gamma$  is the antiduality product between  $V_\Gamma'$  and  $V_\Gamma$ .

### The impedance matrix

$\mathbf{u}$  and  $\delta\mathbf{u}$  can be approximated, with any desired level of accuracy, by their expansion on a finite Hilbert basis of functions defined on  $\Omega$ . The coordinates of these expansions are denoted  $\mathbf{u} = (u_1, u_2, \dots)$  and  $\delta\mathbf{u} = (\delta u_1, \delta u_2, \dots)$ . In that basis, the sesquilinear forms of mass, damping and stiffness are approximated respectively by the symmetric positive definite real matrices  $[M]$ ,  $[D]$  and  $[K]$ <sup>5</sup>, and the sesquilinear form of dynamic stiffness can be approximated by a second order polynomial with real matrix coefficients  $[S(\omega)] = -\omega^2[M] + i\omega[D] + [K]$ .

The fields  $\phi$  and  $\delta\phi$  can also be expanded on a Hilbert basis of functions defined on  $\Gamma$ , and compatible with the Hilbert basis defined on  $\Omega$ . Their projections are denoted  $\Phi = (\Phi_1, \Phi_2, \dots)$  and  $\delta\Phi = (\delta\Phi_1, \delta\Phi_2, \dots)$ . The previous matrices can then be block-decomposed, separating the DOFs defined on  $\Gamma$  from the DOFs defined in the interior of  $\Omega$ .

$$\begin{bmatrix} [S_\Gamma(\omega)] & [S_c(\omega)] \\ [S_c(\omega)]^T & [S_h(\omega)] \end{bmatrix} = -\omega^2 \begin{bmatrix} [M_\Gamma] & [M_c] \\ [M_c]^T & [M_h] \end{bmatrix} + i\omega \begin{bmatrix} [D_\Gamma] & [D_c] \\ [D_c]^T & [D_h] \end{bmatrix} + \begin{bmatrix} [K_\Gamma] & [K_c] \\ [K_c]^T & [K_h] \end{bmatrix} \quad (3.12)$$

In this block-decomposition, the index  $\Gamma$  stands for the boundary, the index 'h' stands for the interior of the domain, 'hidden' from the boundary, and the index 'c' stands for the coupling DOFs. For every frequency  $\omega \in \mathbb{R}$ , the impedance matrix  $[Z(\omega)]$ , approximation of the impedance operator  $\mathcal{Z}(\omega)$  in the Hilbert basis defined on  $\Gamma$ , is then the Schur complement of  $[S_h(\omega)]$  in  $[S(\omega)]$ .

$$[Z(\omega)] = [S_\Gamma(\omega)] - [S_c(\omega)][S_h(\omega)]^{-1}[S_c(\omega)]^T \quad (3.13)$$

In Eq. (3.12),  $[M_\Gamma]$ ,  $[D_\Gamma]$  and  $[K_\Gamma]$  are in  $\mathbb{M}_{n_\Gamma}^+(\mathbb{R})$ , the set of real  $n_\Gamma \times n_\Gamma$  positive-definite matrices,  $[M_c]$ ,  $[D_c]$  and  $[K_c]$  are in  $\mathbb{M}_{n_\Gamma n_h}(\mathbb{R})$ , the set of  $n_\Gamma \times n_h$  real matrices, and  $[M_h]$ ,  $[D_h]$  and  $[K_h]$  are in  $\mathbb{M}_{n_h}^+(\mathbb{R})$ , the set of real  $n_h \times n_h$  positive-definite matrices.

It was stated earlier that the definition of the impedance matrix that is given here, in a deterministic setting, could also be used for the realizations of a random impedance matrix. In that case, the matrix is seen as the projection of a realization of a random impedance operator on compatible Hilbert bases for the displacement fields. These bases should, however, be the same for two samples of the same random operator, so that these realizations are comparable. This difficulty will be further commented in Sec. 4.3, when discussing equivalent forms of the hidden variables model.

<sup>5</sup>As stated earlier, rigid body modes are not considered in this dissertation. For unbounded domains they are not acceptable as they would lead to displacements of infinite energy, out of  $V_\Omega$ , and for bounded domains, the definition of the impedance matrix for rigid body displacements of the boundary is treated in Ohayon and Soize [1998].

### 3.1.2 Numerical methods for the computation of the impedance matrix

The derivation of the impedance matrix described earlier shows that it requires the resolution of a classical mixed boundary value problem, considering Dirichlet boundary conditions on  $\Gamma$ . All classical methods are therefore usable, among which the FE method [Zienkiewicz et al., 2005] is, by far, the most often used. When the domain becomes large, or unbounded, an artificial boundary has to be introduced. This yields an interior domain, on which the FE computation is performed, and an exterior domain that has to be treated in some special way. Indeed the truncation of the domain means that waves would reflect on the exterior domain and pollute the solution in the interior domain. Many techniques have been derived in the literature to prevent that. Some of them are reviewed in Givoli [1992], Wolf and Song [1996], or in special journal issues on absorbing boundary conditions [Turkel, 1998, Magoulès and Harari, 2006]. In the first of these special issues, Tsynkov [1998] gives an extensive comparative overview of the main methods. These techniques can be gathered into three groups: global absorbing boundary conditions (ABCs), local ABCs, and absorbing layer.

Non-local absorbing boundary conditions consider the resolution of an exact problem, on the interior or on both the interior and the exterior domains. For example, an approach called the Non-Reflecting Boundary Condition method consists in representing the solution as a superposition of waves and to cancel all waves arriving from the external boundary. Another example, which has been derived under numerous forms, is the Dirichlet-to-Neumann (DtN) method, which consists in solving the exact problem on the exterior domain, analytically [Givoli and Keller, 1989], and to use the corresponding maps between displacements and stresses, as boundary conditions for the interior problem. These techniques are called non-local because they require some sort of integration over the entire exterior boundary. They are usually cumbersome to compute and most methods are limited to a particular type of geometry of the exterior boundary, but they are very accurate, as the exterior domain is taken into account exactly.

Local absorbing boundary conditions methods intend to relax the limitations of the previous techniques by defining the boundary conditions locally on each element of the exterior boundary. This leads to simpler and more easily implemented formulations, but sometimes induces an important loss in accuracy. Most formulations of local boundary conditions are derived as approximations of the global conditions, or by supposing some sort of simplified behavior of the waves hitting the exterior boundary. In that last case, it sometimes means that the domain has to be truncated further from the excitation than in global methods. To these local methods, one might add the so-called infinite element formulations, where a special type of element is derived with infinite size and whose behavior is controlled only by part of its boundary. A general framework, leading to both the infinite element formulation and the DtN method is described in Harari [1998].

Finally the last group of methods consists not in enforcing boundary conditions, but rather in extending the domain by a damping layer, which should ensure that the waves die out before they reach the exterior domain. The difficulty consists in introducing a new material, which will damp the incoming waves, without creating reflection inside the domain of interest. In that matter, the Perfectly Matched Layers (PMLs) method seems very efficient. An alternative to damping the waves is to slow them so that they reach the exterior boundary at later times and do not perturb the results of interest.

Besides these FE-based methods stands the BE method [Dominguez, 1993]. It appears quite natural for the computation of the impedance matrix, since the formulation is directly performed on the boundary. Besides, the discretization is only performed on that boundary, and in case of an unbounded domain, the radiation conditions are directly taken into account. The main problem of that method is the requirement of a fundamental solution, which restricts its use to homogeneous domains, or particular types of inhomogeneous domains.

The scaled boundary FE method [Wolf and Song, 2001] is an alternative approach which does not require a fundamental solution, and only requires the meshing of the boundary and enforces naturally the radiation condition. The principle is to consider that the domain is spanned by homothecies of the boundary, and consequently to parametrize the domain by a scaling variable and two variables describing the boundary. A classical weighted residual formulation then leads to a differential equation on the scaling variable, and to a FE-type equation on the boundary. The differential equation can, in most cases, be solved analytically. The main requirement for this method is a particular type of radial symmetry of the domain<sup>6</sup>.

### 3.1.3 Properties of the impedance

In the previous sections, some properties, like symmetry, were introduced for the matrices presented. They are examined further in this section, along with other important properties.

#### Symmetry

The definitions of the mass, damping and stiffness sesquilinear forms in Eq. (3.4)-(3.6), along with the symmetry of the elastic and damping tensors  $C^e$  and  $C^d$ , ensures that they are hermitian and positive definite. Using a real basis for the discretization of the operators makes the matrices of mass, damping and stiffness consequently real, symmetric, and positive definite. Their symmetry ensures then that of the dynamic stiffness matrix  $[S(\omega)]$ , for all frequencies  $\omega \in \mathbb{R}$ . Finally, from Eq. (3.13),

$$[Z(\omega)]^T = [S_\Gamma(\omega)]^T - ([S_c(\omega)][S_h(\omega)]^{-1}[S_c(\omega)]^T)^T \quad (3.14)$$

$$= [S_\Gamma(\omega)]^T - [S_c(\omega)][S_h(\omega)]^{-T}[S_c(\omega)]^T \quad (3.15)$$

$$= [S_\Gamma(\omega)] - [S_c(\omega)][S_h(\omega)]^{-1}[S_c(\omega)]^T = [Z(\omega)]. \quad (3.16)$$

The impedance matrix is therefore, for all  $\omega \in \mathbb{R}$ , a square complex symmetric matrix, in  $\mathbb{M}_{n_\Gamma}^S(\mathbb{C})$ .

#### Causality

A very important property of the impedance is that it corresponds in the time domain to a causal function. This represents the natural condition that an effect should never take place before the cause that creates it, that there is no stress on the boundary before a displacement has been imposed. This condition is usually written in the time domain, for a displacement field  $t \mapsto \phi(t)$ , and supposing that the inverse Fourier transform  $t \mapsto [\widehat{Z}(t)]$  of the impedance matrix  $\omega \mapsto [Z(\omega)]$  exists (in the sense of the distribution),

$$\phi(t) = \mathbf{0}, \forall t < 0 \Rightarrow ([\widehat{Z}] * \phi)(t) = \mathbf{0}, \forall t < 0, \quad (3.17)$$

where  $(f * g)(t) = \int_{\mathbb{R}} f(t')g(t-t')dt'$  is the convolution product of the functions  $t \mapsto f(t)$  and  $t \mapsto g(t)$ .

As we have been defining the impedance matrix in the frequency domain, this definition is not appropriate. It is however recalled that an equivalent definition [Dautray and Lions, 1990] exists in the frequency domain. It states that a function  $p \mapsto \hat{f}(p)$  with values in a Hilbert space  $\mathcal{H}$  is the Laplace transform of a causal function  $t \mapsto f(t)$  if and only if there exists a  $\xi_0 \in \mathbb{R}$  such that  $\hat{f}$  is holomorphic in  $\mathcal{C}_{\xi_0} = \{p = \xi + i\eta, \xi \in ]\xi_0, +\infty[, \eta \in \mathbb{R}\}$  and there exists a polynomial of  $|p|$ ,  $\text{Pol}(|p|)$ , such that

<sup>6</sup>Particularly, this method cannot be used for the computation of the impedance of a horizontally layered medium.

$\|f(p)\|_{\mathcal{H}} \leq \text{Pol}(|p|)$ , where  $\|\cdot\|_{\mathcal{H}}$  is the norm associated with  $\mathcal{H}$ , and the coefficients of  $\text{Pol}$  may depend on  $\xi_0$ .

The definitions of  $[S(\omega)]$  and  $[Z(\omega)]$  in the frequency domain are therefore extended to the domain of the complex frequencies with  $\omega = -ip$ ,  $p \in \mathbb{C}$ , which leads to the classical definition of the Laplace transforms of the dynamic stiffness matrix  $[\hat{S}(p)]$  and the impedance matrix  $[\hat{Z}(p)]$ . The positive definiteness of  $[M]$ ,  $[D]$  and  $[K]$  ensures that of  $[M_h]$ ,  $[D_h]$  and  $[K_h]$ . Therefore, for any complex vector  $\mathbf{x}$ ,  $\mathbf{x}^*[\hat{S}_h(p)]\mathbf{x} = p^2 m_{\mathbf{x}} + p d_{\mathbf{x}} + k_{\mathbf{x}}$ , with  $m_{\mathbf{x}} > 0$ ,  $d_{\mathbf{x}} > 0$ , and  $k_{\mathbf{x}} > 0$ <sup>7</sup>. The roots of that polynomial have negative real part, so that  $p \mapsto [\hat{S}_h(p)]$  is invertible on  $\mathbb{C}_{\xi_0}$ , when  $\xi_0 > 0$ . For the same reasons, and on the same space, the inverse of the determinant of  $[\hat{S}_h(p)]$  is bounded, so that  $p \mapsto \|[\hat{Z}(p)]\|_F$  can be bounded by a polynomial function of  $p$ . Since  $\xi_0 > 0$ ,  $p \mapsto [\hat{Z}(p)]$  is holomorphic in  $\mathbb{C}_{\xi_0}$ , then it corresponds in the time domain to a causal function.

### Stability

The condition of stability for the impedance matrix states that for a bounded input displacement, the stress on the boundary will remain bounded. It means that small variations around a given imposed displacement will not result in dramatic modifications in the induced stresses.

In the previous section, we showed that, for any complex vector  $\mathbf{x}$ , all roots of  $p \mapsto \mathbf{x}^*[\hat{S}_h(p)]\mathbf{x}$  have negative real part. The same can then be said of the poles of the inverse of the determinant of  $p \mapsto [\hat{S}_h(p)]$ , and these poles are the same as those of  $p \mapsto [Z(p)]$ . Let us then call these poles of the impedance matrix  $(p_i)_{1 \leq i \leq 2n_h}$ . After a pole residue expansion and inverse Laplace transform, the impedance matrix in the time domain can then be written formally as a weighted sum of exponential terms ( $t \mapsto \exp(p_i t)_{1 \leq i \leq 2n_h}$ ). Since the poles have negative real parts, a bounded displacement on the boundary yields bounded stresses. The impedance matrix, as defined above, is therefore stable.

### Damping system

Another physical property that the impedance matrix should enforce is that no energy is created within the domain  $\Omega$ . Energy is introduced in the system by the excitation but not created within  $\Omega$ . This property can be verified by checking that the rate of energy transmission through the boundary  $\Gamma$  is non-negative over a period.

Considering an harmonic input displacement vector  $\mathbf{u}(\omega) \cos(\omega t) = \Re\{\mathbf{u}(\omega) \exp(i\omega t)\}$ , with  $\mathbf{u}(\omega) \in \mathbb{R}$ , and the corresponding stress response  $\Re\{\mathbf{f}(\omega) \exp(i\omega t)\}$ , the rate of energy transmission  $\mathcal{E}_T$  over a period  $T = 2\pi/\omega$  is

$$\mathcal{E}_T = \frac{\omega}{2\pi} \int_0^{2\pi/\omega} \Re\{\mathbf{f}(\omega)^T \exp(i\omega t)\} \Re\{\dot{\mathbf{u}}(\omega) \exp(i\omega t)\} dt, \quad (3.18)$$

where the dot indicates time derivation. Using  $\mathbf{f}(\omega) = [Z(\omega)]\mathbf{u}(\omega)$ , and  $\dot{\mathbf{u}}(\omega) = i\omega\mathbf{u}(\omega)$  yields

$$\mathcal{E}_T = -\frac{\omega^2}{2\pi} \int_0^{2\pi/\omega} \mathbf{u}(\omega)^T \Re\{[Z(\omega)]^T \exp(i\omega t)\} \mathbf{u}(\omega) \sin(\omega t) dt \quad (3.19)$$

$$= -\frac{\omega^2}{2\pi} \int_0^{2\pi/\omega} \mathbf{u}(\omega)^T [\Re\{[Z(\omega)]\} \cos(\omega t) \sin(\omega t) - \Im\{[Z(\omega)]\} \sin^2(\omega t)] \mathbf{u}(\omega) dt \quad (3.20)$$

$$= \frac{\omega}{2\pi} \mathbf{u}(\omega)^T \Im\{[Z(\omega)]\} \mathbf{u}(\omega). \quad (3.21)$$

<sup>7</sup>The symmetry of  $[M_h]$ ,  $[D_h]$  and  $[K_h]$  is used here, so that  $\Re\{\mathbf{x}^T[\hat{S}_h]\Im\{\mathbf{x}\} = \Im\{\mathbf{x}\}^T[\hat{S}_h]\Re\{\mathbf{x}\}$ , and  $\mathbf{x}^*[\hat{S}_h]\mathbf{x} = \Re\{\mathbf{x}\}^T[\hat{S}_h]\Re\{\mathbf{x}\} + \Im\{\mathbf{x}\}^T[\hat{S}_h]\Im\{\mathbf{x}\}$

And therefore the non-negativity of the rate of energy transmission binds the imaginary part of the impedance matrix to be positive semi-definite.

No such result can be obtained for the real part of the impedance matrix. We will see on examples in the following chapters that the real part of the impedance can indeed become non-positive. In statics, though, the positive-definiteness of the stiffness matrix yields directly that of the impedance matrix. This can be extended by continuity to the low frequency range.

### 3.1.4 The hidden state variables model

The first requirement that should be asked of any reasonable model of the impedance matrix is that it enforces the basic properties that were described in the previous section. We will consider here mainly the causality, which will lead us to the choice of the hidden variables model, and then show that it also verifies the other properties. To enforce causality, several methods exist, corresponding to different points of view, and they are discussed here: the expansion on a basis of Hardy functions is a mathematical derivation, the Kramers-Kronig relations are widely used in physics, and finally we describe the alternative approach that we have chosen.

#### Expansion on a basis of Hardy functions

A first approach consists in trying to model the impedance as an expansion on a basis of some subspace of all Laplace transforms of causal functions, the space of Hardy functions. A function  $f$  defined on  $\mathbb{C}_{\xi_0} = \{p = \xi + i\eta, \xi > 0, \eta \in \mathbb{R}\}$  is said to be a Hardy function if it is holomorphic on  $\mathbb{C}_{\xi_0}$  and  $\sup_{a>0} \int_{\mathbb{R}} |f(\xi + i\eta)|^2 d\eta < +\infty$ . It can be shown [Pierce, 2001] that  $f$  is a Hardy function if and only if it is the Laplace transform of some square integrable causal function. A nice feature of that functional space is that it is equipped with an explicit orthonormal basis, the functions  $\{p \mapsto e_\ell(p)\}_{\ell \geq 0}$ , with

$$e_\ell(p) = \frac{(-1)^{\ell+1}}{\sqrt{\pi}} \left( \frac{1}{1-p} \right) \left( \frac{1+p}{1-p} \right)^\ell. \quad (3.22)$$

This space only contains square integrable functions, whereas the pseudodifferential part of the impedance matrix is not. The expansion of the impedance matrix in Eq would therefore be in the form  $[Z(p)] = p^2 [R_2] + p [R_1] + [R_0] + \sum_{\ell \geq 0} [Z_\ell] e_\ell(p)$ . Unfortunately, there is no algebraic information on the matrices  $\{[Z_\ell]\}_{\ell \geq 0}$ . Also, since this construction is purely mathematical, the coefficients of this expansion are not easily related to physical parameters of the system. More important, the rate of convergence of the infinite sum is not known so a very large number of terms might be required to yield a good approximation.

#### Kramers-Kronig relations

The Kramers-Kronig relations were originally developed for electromagnetic problems to link the real and imaginary parts of the polarization coefficients [Kramers, 1927] and of the index of refraction [Kronig, 1926], and were demonstrated without any explicit reference to causality. Later, they were shown (see Champeney [1973] for example for a demonstration) to be verified by any complex causal function, and they state that the real and imaginary parts of its Fourier transform  $\omega \mapsto f(\omega)$  verify, equivalently,

$$\Re \{f(\omega)\} = \frac{1}{\pi} \oint_{\mathbb{R}} \frac{\Im \{f(\omega')\}}{\omega - \omega'} d\omega', \quad (3.23)$$

or,

$$\Im \{f(\omega)\} = -\frac{1}{\pi} \oint_{\mathbb{R}} \frac{\Re\{f(\omega')\}}{\omega - \omega'} d\omega'. \quad (3.24)$$

They are widely used in experimental physics because, in many applications, the imaginary part of a quantity of interest can be measured experimentally, and then the whole function constructed with Eq. (3.23). Unfortunately, numerically, the real and imaginary parts of the impedance matrix cannot be computed separately. Therefore these relations can be used to prolongate an impedance matrix that was computed on a bounded frequency interval to the entire frequency domain [Dienstfrey and Greengard, 2001], but are not constructive for the modeling of an impedance matrix from scratch. Moreover these formulas apply only for functions  $f$  in  $L^1$ , which is obviously not the case for  $[Z]$ , and the accurate evaluation of the singular integral might require a large band of frequency, highly refined, to be studied.

### Hidden state variables model

Ultimately, a given algebraic structure can be proposed to construct an approximation of the boundary impedance matrix, satisfying *a priori* the desired causality condition. Following Chabas and Soize [1987], the structure of the boundary impedance matrix of a mechanical system of which the vibrations in the time domain are governed by a second-order differential equation with constant coefficients is chosen. This algebraic structure may not span the entire space of possible boundary impedance matrices arising from real physical systems and it is only a sufficient condition for causality to be satisfied. However, the similarities between this structure and the underlying system considered in Eq. (3.12) is appealing in the sense that the approach may give some interesting insights on the mechanical system hidden behind the boundary impedance matrix.

Let us therefore consider such a mechanical system and its discretization in  $n$  DOFs. We will denote  $n = n_\Gamma + n_h$ , where  $n_\Gamma$  is the number of DOFs of the part of the boundary with respect to which the boundary impedance matrix is constructed. In the frequency domain, the hypothesis in the time domain means that the dynamic stiffness  $\omega \mapsto [S(\omega)]$  is a second-order polynomial in  $(i\omega)$  with real matrix coefficients. Denoting  $[M]$ ,  $[D]$  and  $[K]$  in  $\mathbb{M}_n^+(\mathbb{R})$  those coefficients, we have

$$[S(\omega)] = -\omega^2[M] + i\omega[D] + [K], \quad (3.25)$$

and  $[Z(\omega)]$  is the condensation on the first  $n_\Gamma$  DOFs of  $[S(\omega)]$ . The block-decomposition of Eq. (3.25) yields

$$\begin{bmatrix} [S_\Gamma(\omega)] & [S_c(\omega)] \\ [S_c(\omega)]^T & [S_h(\omega)] \end{bmatrix} = -\omega^2 \begin{bmatrix} [M_\Gamma] & [M_c] \\ [M_c]^T & [M_h] \end{bmatrix} + i\omega \begin{bmatrix} [D_\Gamma] & [D_c] \\ [D_c]^T & [D_h] \end{bmatrix} + \begin{bmatrix} [K_\Gamma] & [K_c] \\ [K_c]^T & [K_h] \end{bmatrix}, \quad (3.26)$$

and the subsequent impedance is

$$[Z(\omega)] = [S_\Gamma(\omega)] - [S_c(\omega)][S_h(\omega)]^{-1}[S_c(\omega)]^T. \quad (3.27)$$

The name "hidden state variables model" comes from the fact that the DOFs on which the matrices  $[M]$ ,  $[D]$  and  $[K]$  are defined are not necessarily physical degrees of freedom, but rather state variables that are hidden in the background of the physical model. These matrices correspond to generalized mass, damping and stiffness matrices, but they are not necessarily the classical mass, damping and stiffness matrices, e.g. constructed using a FE method. Indeed it will be shown in Sec. 4.3.1 that there are infinitely many distinct sets of matrices  $\{[M], [D], [K]\}$  that correspond to the same impedance matrix.

Therefore, we are free to choose the set of generalized matrices  $[M]$ ,  $[D]$  and  $[K]$  as we wish in the set of matrices yielding the appropriate impedance.

More specifically, it will be shown that we can choose an equivalent form of the hidden variables model, where the hidden part is diagonal and with no coupling in mass<sup>8</sup>. In that case, the impedance can be written

$$[Z(\omega)] = [S_\Gamma(\omega)] - \sum_{\ell=1}^{n_h} \frac{(i\omega[D_c]^\ell + [K_c]^\ell)(i\omega[D_c]^\ell + [K_c]^\ell)^T}{-\omega^2 + id_\ell + k_\ell}, \quad (3.28)$$

where  $([D_c]^\ell)_{1 \leq \ell n_h}$  and  $([K_c]^\ell)_{1 \leq \ell n_h}$  are the  $\ell^{th}$  columns of  $[D_c]$  and  $[K_c]$ , and  $(d_\ell)_{1 \leq \ell n_h}$  and  $(k_\ell)_{1 \leq \ell n_h}$  are the diagonal elements of  $[D_h]$  and  $[K_h]$ . For a system with 1 DOF on the boundary and one internal, we retrieve exactly the example of Box 1.1.2.

As the structure of the hidden state variables model of the impedance is the same as that used in the definition of the impedance matrix in Sec. 3.1.1, the properties that were derived are valid for that model, provided that the matrices of the hidden variables model  $\{[M], [D], [K]\}$  are positive definite. Therefore the hidden state variables model of the impedance ensures that the impedance matrix is symmetric, causal, stable, and corresponds to a damped system.

## 3.2 Probabilistic model of the impedance

In the previous section, a general structure for samples of impedance matrices was presented. Our goal in this section is to present the probabilistic modeling of an impedance matrix, using both this hidden state variables model and the nonparametric approach to the modeling of uncertainty in mechanics.

### 3.2.1 Nonparametric approach to the modeling of uncertainties

Let us first recall the methods that were described in Chap. 2. All of these started from a probabilistic model of one or several parameters of the problem - *e.g.* the unit mass, Young's modulus, or the loading - and yielded the corresponding probabilistic model of the solution - *e.g.* the maximum displacement at some point. In that sense, they are called parametric methods. The uncertainty arises from the parameters and the method only provides a way to propagate that uncertainty to the quantity of interest. This approach excludes the consideration of model uncertainties, and it might become cumbersome when various uncertain parameters are incorporated simultaneously. The difficulties would start with the modeling, as complicated correlation models would then be required, but it would be particularly important when considering the identification of these multiple parameters and their correlation patterns from experimental measures.

The nonparametric approach to the modeling of uncertainties in mechanics was introduced by Soize [2000, 2001], and tackles the problem in a different way. Rather than assessing the uncertainty on given parameters, the method tries to provide a quantification of the uncertainties on a higher level, and specifically, in structural mechanics, at the level of the matrices of mass, damping and stiffness of the system. These matrices depend on the mechanical parameters, so that parametric uncertainties are accounted for, and, furthermore, model uncertainties are also assessed, although in a limited way.

The method therefore relies on random matrices, the PDFs of which are constructed by the Maximum Entropy Theorem [Shannon, 1948, Jaynes, 1957], using algebraic properties on the matrices, and their mean value as constraints. A unique parameter for each matrix is introduced that controls the dispersion

<sup>8</sup>In order to yield that result, an hypothesis is required on the damping part. That hypothesis is classical in structural mechanics and will be described in Sec. 4.3.1, and illustrated in Sec. 4.4.5

of the PDF. Since the mapping from the probabilistic models of the parameters to those of the matrices is bypassed, it is not possible to incorporate knowledge at the parametric level into the probabilistic model. However it is believed that this approach is in adequacy with the needs of simplicity and propriety of the probabilistic models. The simplicity is required in view of the necessary later identification of the parameters of that probabilistic model, and the propriety is meant in the sense that each realization of the random matrices will be physically acceptable.

The next section will provide a description of the main ensembles of random matrices that are used in the nonparametric method. Other such ensembles exist in the literature, *e.g.* the Gaussian Orthogonal Ensemble [Mehta, 1991], which has been used for a long time in theoretical physics, but these ensembles are not appropriate to model the positive matrices that are encountered in structural mechanics. We will work here with two ensembles that have been more recently introduced and are more adapted to the stiffness, mass and damping matrices of a dynamical system: the normalized positive-definite ensemble  $SG^+$  and the positive-definite ensemble  $SE^+$  [Soize, 2005].

The construction of the nonparametric probabilistic model of the impedance matrix is based on the replacement of the matrices of the hidden state variables model by random matrices. More specifically, the matrices  $[M]$ ,  $[D]$ ,  $[K]$ ,  $[S(\omega)]$  and  $[Z(\omega)]$  of Eq. (3.25) will be replaced by random matrices  $[\mathbf{M}]$ ,  $[\mathbf{D}]$ ,  $[\mathbf{K}]$ ,  $[\mathbf{S}(\omega)]$  and  $[\mathbf{Z}(\omega)]$ . The probabilistic model of each of the matrices  $[\mathbf{M}]$ ,  $[\mathbf{D}]$  and  $[\mathbf{K}]$  is constructed in  $SE^+$ , and those of  $[\mathbf{S}(\omega)]$  and  $[\mathbf{Z}(\omega)]$  are simply derived using statistics and Eq. (3.25)-(3.27). To improve the readability, we first recall the construction of these two ensembles  $SG^+$  and  $SE^+$ , and their main properties. Then, the construction of an approximation of the probability density function of the random impedance matrix  $[\mathbf{Z}(\omega)]$  by the MCS method is described.

### 3.2.2 The random matrices ensembles

There are two main random matrices ensembles,  $SG^+$  and  $SE^+$ , which differ only by the mean of the matrix which is modeled. In the former ensemble, all matrices have identity mean, whereas, in the latter ensemble any positive definite matrix can be specified as the mean. Obviously,  $SG^+ \subset SE^+$ . For both ensembles, the definition are recalled, and the probability density functions are derived. The definition of the dispersion parameter is also introduced, and the question of its identification is discussed.

#### The normalized positive definite ensemble of random matrices

The normalized positive-definite ensemble of random matrices, denoted  $SG^+$ , is defined as the set of the random matrices  $[\mathbf{G}_n]$  defined on a probability space  $(\mathcal{A}, \mathcal{T}, \mathcal{P})$ , with values in  $\mathbb{M}_n^+(\mathbb{R})$  verifying:

1.  $[\mathbf{G}_n] \in \mathbb{M}_n^+(\mathbb{R})$ , almost surely;
2. Matrix  $[\mathbf{G}_n]$  is a second-order random variable:  $E\{\|[\mathbf{G}_n]\|_F^2\} < +\infty$ ;
3. The mean value  $[\underline{G}_n]$  of  $[\mathbf{G}_n]$  is the identity matrix  $[I_n]$  in  $\mathbb{M}_n^+(\mathbb{R})$ :  $E\{[\mathbf{G}_n]\} = [\underline{G}_n] = [I_n]$ ;
4.  $[\mathbf{G}_n]$  is such that  $E\{\ln(\det[\mathbf{G}_n])\} = \nu_{G_n}$ ,  $|\nu_{G_n}| < +\infty$ .

As was proved in Soize [2001], the last constraint yields the fundamental property that the inverse of  $[\mathbf{G}_n]$  is also a second-order random variable:  $E\{\|[\mathbf{G}_n]^{-1}\|_F^2\} < +\infty$ . For the computation of the probability density function of  $[\mathbf{G}_n]$ , it was also shown that rather than considering  $\nu_{[\mathbf{G}_n]}$ , the value of which does not bear a simple physical meaning, it was interesting to replace it by a parameter  $\delta$ , which measures the dispersion of the probability model of the random matrix  $[\mathbf{G}_n]$  around the mean value  $[\underline{G}_n]$ .

### The positive-definite ensemble of random matrices

The normalized positive-definite ensemble of random matrices, denoted  $SE^+$ , was developed simultaneously with  $SG^+$ , the ensemble of normalized positive-definite ensemble of random matrices. The matrices  $[\mathbf{A}_n]$  in  $SE^+$  verify properties similar to those in  $SG^+$ , with any given matrix for the mean:

1.  $[\mathbf{A}_n] \in \mathbb{M}_n^+(\mathbb{R})$ , almost surely;
2. Matrix  $[\mathbf{A}_n]$  is a second-order random variable:  $E\{\|[\mathbf{A}_n]\|_F^2\} < +\infty$ ;
3. The mean value  $[\underline{A}_n]$  of  $[\mathbf{A}_n]$  is a given matrix in  $\mathbb{M}_n^+(\mathbb{R})$ :  $E\{[\mathbf{A}_n]\} = [\underline{A}_n]$ ;
4.  $[\mathbf{A}_n]$  is such that  $E\{\ln(\det[\mathbf{A}_n])\} = \nu_{A_n}$ ,  $|\nu_{A_n}| < +\infty$ .

Since  $[\underline{A}_n]$  is positive definite, there is an upper triangular matrix  $[\underline{L}_n]$  in  $\mathbb{M}_n(\mathbb{R})$  such that

$$[\underline{A}_n] = [\underline{L}_n]^T [\underline{L}_n] \quad (3.29)$$

and the ensemble  $SE^+$  can be defined as the set of random matrices  $[\mathbf{A}_n]$  which are written as

$$[\mathbf{A}_n] = [\underline{L}_n]^T [\mathbf{G}_n] [\underline{L}_n] \quad (3.30)$$

in which  $[\mathbf{G}_n]$  is in  $SG^+$ .

### The probability density function of random matrices in $SG^+$ and $SE^+$

Using Eq. (3.30), realizations of the matrices of  $SE^+$  can be computed from those of matrices of  $SG^+$ , so that only the PDF of the latter ensemble will be described. The PDF of a matrix in  $SG^+$  is therefore computed using the Maximum Entropy Theorem, with the constraints listed in the definition of the ensemble. It is defined with respect to the measure  $\tilde{d}G_n$  on the set  $\mathbb{M}_n^S(\mathbb{R})$  of  $n \times n$  real symmetric matrices, where  $\tilde{d}G_n$  is such that

$$\tilde{d}G_n = 2^{n(n-1)/4} \prod_{1 \leq i < j \leq n} d[G_n]_{ij} \quad (3.31)$$

where  $dG_n = \prod_{1 \leq i, j \leq n} d[G_n]_{ij}$  is the Lebesgue measure on  $\mathbb{R}^n$ . With the usual normalization condition on the probability density function, it can be shown to be [Soize, 2000, 2001]

$$p_{[\mathbf{G}_n]}([G_n]) = \mathbb{1}_{\mathbb{M}_n^+(\mathbb{R})}([G_n]) \times C_{[\mathbf{G}_n]} \times (\det[G_n])^{(n+1)(1-\delta^2)/(2\delta^2)} \times \exp\left\{-\frac{n+1}{2\delta^2} \text{tr}[G_n]\right\} \quad (3.32)$$

in which  $[G_n] \mapsto \mathbb{1}_{\mathbb{M}_n^+(\mathbb{R})}([G_n])$  is a function from  $\mathbb{M}_n(\mathbb{R})$  into  $\{0, 1\}$  that is equal to 1 when  $[G_n]$  is in  $\mathbb{M}_n^+(\mathbb{R})$  and 0 otherwise, and where constant  $C_{[\mathbf{G}_n]}$  is equal to

$$C_{[\mathbf{G}_n]} = \frac{(2\pi)^{-n(n-1)/4} \left(\frac{n+1}{2\delta^2}\right)^{n(n+1)/(2\delta^2)}}{\prod_{j=1}^n \Gamma\left(\frac{n+1}{2\delta^2} + \frac{1-j}{2}\right)}, \quad (3.33)$$

with  $z \mapsto \Gamma(z)$  the gamma function defined for  $z > 0$  by  $\Gamma(z) = \int_0^{+\infty} t^{z-1} e^{-t} dt$ . We will see further that realizations of matrices following this PDF can be drawn very efficiently.

### The dispersion parameter

The dispersion parameter  $\delta$  is a real parameter defined, for any random matrix  $[\mathbf{G}_n]$ , with mean value  $[\underline{G}_n]$ , by

$$\delta = \left\{ \frac{\mathbb{E}\{\|[\mathbf{G}_n] - [\underline{G}_n]\|_F^2\}}{\|[\underline{G}_n]\|_F^2} \right\}^{1/2}, \quad (3.34)$$

where  $\|\cdot\|_F$  is the Frobenius norm (see App. A.1). For matrices of  $SG^+$ , this definition reduces to

$$\delta = \frac{1}{n} \mathbb{E}\{\|[\mathbf{G}_n] - [I_n]\|_F^2\}^{1/2}, \quad (3.35)$$

The dispersion parameter should be chosen independent of  $n$  and such that

$$0 < \delta < \sqrt{\frac{n+1}{n+5}}, \quad (3.36)$$

to ensure that the condition on the integrability of the inverse of the random matrices is verified.

Several procedures for the estimation of  $\delta$  have been derived [Soize, 2005, Arnst et al., 2005], depending on the type of information available:

1. when no objective information is known about  $\delta$ , a sensitivity analysis must be performed with  $\delta$  as the parameter and its value estimated depending on the level of stochastic fluctuations (level of uncertainty);
2. when a sufficient amount of experimental data is available,  $\delta$  can be estimated using statistics;
3. when a parametric model has been constructed in the low-frequency range, where data uncertainties are, in general, more important than model uncertainties,  $\delta$  can be estimated through statistics on the first eigenfrequency;
4. when the uncertain system pertains to a class of systems for which  $\delta$  has already been studied, the same value can be re-used.

We will not go in this dissertation through the process of the estimation of  $\delta$  for our particular problems. In the numerical applications that will be considered in the following chapters, we will skip this identification and consider the value  $\delta = 0.1$  for all the matrices.

### 3.2.3 Nonparametric model of the impedance matrix

Before describing the way the nonparametric model of the impedance matrix is constructed, the issue of drawing realizations of the random matrices of mass, damping and stiffness is addressed. This means that the independence of the three random matrices has to be considered, and that an efficient way of drawing these realizations has to be described.

#### The probability model of a set of random matrices in $SE^+$

Indeed, we have described the PDFs of the three matrices of mass, damping and stiffness independently. But since they correspond to the same physical problem it could be argued that they should be dependent. And in fact they are, through their mean values, which are computed using the same mechanical

parameters. But concerning their probabilistic model, since we did not specify any particular condition of dependence, the Maximum Entropy Theorem describes the matrices as independent.

This can be written using a more mathematical formalism. Let us consider a set of  $m$  random matrices  $[\mathbf{A}_n^1], \dots, [\mathbf{A}_n^m]$  in  $SE^+$ , for which the mean values are given, but no correlation tensor between any two of the random matrices is provided. The Maximum Entropy Theorem can be used to show that the PDF  $([A_n^1], \dots, [A_n^m]) \mapsto p_{[\mathbf{A}_n^1], \dots, [\mathbf{A}_n^m]}([A_n^1], \dots, [A_n^m])$  from  $(\mathbb{M}_n^+(\mathbb{R}))^m$  into  $\mathbb{R}_+$  with respect to the measure  $\tilde{d}A_n^1 \times \dots \times \tilde{d}A_n^m$  on  $(\mathbb{M}_n^S(\mathbb{R}))^m$  is written as

$$p_{[\mathbf{A}_n^1], \dots, [\mathbf{A}_n^m]}([A_n^1], \dots, [A_n^m]) = p_{[\mathbf{A}_n^1]}([A_n^1]) \times \dots \times p_{[\mathbf{A}_n^m]}([A_n^m]), \quad (3.37)$$

which means that the  $[\mathbf{A}_n^1], \dots, [\mathbf{A}_n^m]$  are independent random matrices.

### **Algebraic representation of a random matrix $[\mathbf{G}_n]$ in $SG^+$ adapted for the construction of independent samples**

Having values in  $\mathbb{M}_n^+(\mathbb{R})$ ,  $[\mathbf{G}_n]$  can be written  $[\mathbf{G}_n] = [\mathbf{L}_n]^T[\mathbf{L}_n]$ , where  $[\mathbf{L}_n]$  is an upper triangular random matrix with values in  $\mathbb{M}_n(\mathbb{R})$ . Let us introduce  $\sigma_n = \delta(n+1)^{-1/2}$ . It can be shown that

1. random variables  $([\mathbf{L}_n]_{ij})_{1 \leq i \leq j \leq n}$  are independent;
2. for  $i < j$ ,  $[\mathbf{L}_n]_{ij}$  can be written  $[\mathbf{L}_n]_{ij} = \sigma_n U_{ij}$ , where  $U_{ij}$  is a Gaussian random variable with real values, zero mean and unit variance.
3. for  $i = j$ ,  $[\mathbf{L}_n]_{ii}$  can be written  $[\mathbf{L}_n]_{ii} = \sigma_n \sqrt{2V_i}$ , where  $V_i$  is a gamma random variable with positive real values and a probability density function  $p_{V_i}(v)$  (with respect to  $dv$ ) in the form

$$p_{V_i}(v) = \mathbb{1}_{\mathbb{R}^+}(v) \frac{1}{\Gamma\left(\frac{n+1}{2\delta^2} + \frac{1-i}{2}\right)} v^{\frac{n+1}{2\delta^2} - \frac{1+i}{2}} e^{-v} \quad (3.38)$$

This algebraic structure of  $[\mathbf{G}_n]$ , allows an efficient procedure to be defined for the Monte Carlo numerical simulation of random matrix  $[\mathbf{G}_n]$ .

### **The nonparametric model of random uncertainties for the impedance matrix**

The principle of construction of the nonparametric probabilistic model of random uncertainties for the impedance matrix consists in replacing the matrices of mass, damping and stiffness of the mean model defined in Sec. 3.1.4 by random matrices  $[\mathbf{M}]$ ,  $[\mathbf{D}]$ ,  $[\mathbf{K}]$  in  $SE^+$ . The mean value and a dispersion parameter have to be known for each of them. Using Monte Carlo techniques, independent samples of these matrices can be drawn and the corresponding dynamic stiffness matrix computed for all frequencies. The realizations  $\{[Z_\ell(\omega)]\}_{\ell \geq 1}$  of the impedance matrix  $[\mathbf{Z}(\omega)]$  corresponding to these triplets of realizations of  $\{([M]_\ell, [D]_\ell, [K]_\ell)\}_{\ell \geq 1}$  are then computed by condensation, for all frequencies, of the dynamic stiffness matrix on the DOFs of the boundary.

## **3.3 Practical construction of the probabilistic model of an impedance matrix**

In the first part of this chapter, a general structure for samples of the impedance matrix was presented, ensuring that its main properties are verified, and based on generalized matrices of mass, damping and

stiffness. The nonparametric approach to stochastic modeling consists in setting the PDFs of these matrices, ensuring that certain algebraic properties are verified. For the construction of these PDFs, the mean value and a dispersion parameter have to be supplied for each of the matrices. We discarded the problem of the identification of the dispersion parameters (see discussion in Sec. 3.2.2), but we still have to address that of the mean value of the matrices  $[M]$ ,  $[D]$ , and  $[K]$ . Indeed, the computation of impedance matrices, particularly on unbounded domains, often bypasses the explicit construction of these matrices. The identification of these mean matrices from a given impedance matrix will be the subject of the next chapter.

Practically, the construction of the probabilistic model of an impedance matrix follows these steps:

1. A deterministic computation method is chosen and the impedance matrix  $\{\{\tilde{Z}(\omega_\ell)\}\}_{1 \leq \ell \leq L}$  is evaluated at a finite set of frequencies  $(\omega_\ell)_{1 \leq \ell \leq L}$ . This computation method can be absolutely any method in the literature, and those most often used were recalled in Sec. 3.1.2. Alternatively, the impedance matrix can be measured experimentally, or even read from charts.
2. The mean matrices  $[M]$ ,  $[D]$ , and  $[K]$  are identified from the set of values of the impedance matrix  $\{\{\tilde{Z}(\omega_\ell)\}\}_{1 \leq \ell \leq L}$ . This step was not described in this section.
3. Supposing that the dispersion parameter has been identified for each random matrix  $[M]$ ,  $[D]$  and  $[K]$ , their PDFs are now available, and realizations of these matrices can be drawn, as described in Sec. 3.2.3.
4. For each set of realizations, the corresponding realization of the random impedance matrix  $[Z(\omega)]$  can be computed, using Eq. (3.27). The statistics on these realizations provide approximations of the marginal laws of  $[Z(\omega)]$ .

As announced, the last issue that has to be considered is that of the identification of the mean matrices from the input impedance matrix. This will be treated in the next chapter.



# Chapter 4

## Identification of the hidden state variables model of the impedance matrix

In the previous chapter, we presented the hidden state variables model for impedance matrices. It can be used to model deterministic impedance matrices, samples of random impedance matrices, and is the structural basis for the construction of our probabilistic model for impedance matrices. However, in the course of the construction of that stochastic model, we saw that it was necessary to provide the hidden variables model corresponding to a given mean matrix. When the domain that is considered is modeled by a FE method, the construction of the corresponding hidden variables model is straightforward. It only consists in projecting the matrices of mass, damping and stiffness in a given basis, both for the DOFs of the boundary, and for the internal DOFs. The Craig-Bampton reduction basis [Craig and Bampton, 1968] is one such example, where a Galerkin-type interface basis is considered on the boundary, and the internal DOFs are projected on the eigenmodes of the related fixed-interface problem. When the domain is unbounded however, the reduction is not that simple, because the impedances that are computed using classical methods are not given in terms of frequency-independent matrices. The description of the hidden variables model provides a structure for the frequency dependence, but its parameters, that is the values of the matrices of mass, damping and stiffness, have to be evaluated.

This chapter therefore concentrates on the computation of the matrices of the hidden variables model,  $[M]$ ,  $[D]$  and  $[K]$ , corresponding to an input impedance matrix, given by its values at a set of frequencies  $\{[Z(\omega_\ell)]\}_{1 \leq \ell \leq L}$ . This is a quite general problem, with many links to classical modal and system identification. The last section of this chapter presents an example on which several important aspects of the identification method are highlighted.

### 4.1 Methodology for the identification of hidden variables models

In this first section, the most salient issues of system and modal identification are presented, as well as the general methodology for the identification of the hidden variables model of a given impedance matrix. We will see that one step of that methodology is very general, so that many of the available algorithms in the literature can be re-used. This section starts with a review of general methods and representations, which should be read with that aspect in mind.

#### 4.1.1 General issues

First, a definition should be given for system and modal identification. We refer to system identification methods for the techniques which do not postulate *a priori* a form of the identified model, and where the identification is hence performed on a general basis. ARMA methods, for example, fall in this category. Modal identification methods, on the other hand, suppose that the model is given in terms of

modal frequency, modal damping, and modal participation vectors. The identification is then performed directly in terms of these parameters. From a physical point of view, modal identification techniques seem more interesting as they provide information on the dynamical behavior of the system. However, when considering impedance matrices, the identification of the internal modes may be unnecessary. We will see in Sec. 4.3.1 that, indeed, the modal frequencies and damping are important quantities for the identification of an impedance matrix, but that the eigenvectors are not relevant. More details on modal identification methods, with examples of frequently used techniques, can be found in Heylen et al. [1997]. Reviews of the main system identification methods are presented in Pintelon et al. [1994] and Guillaume et al. [1996], respectively for the Single-Input, Single-Output (SISO) and Multiple-Input, Multiple-Output (MIMO) cases.

In MIMO, which is the case we are interested in, several parametrizations are used, all usually enforcing the idea that poles are global quantities of a system. In the common-denominator approach, the impedance is modeled as the ratio of a matrix-valued numerator polynomial and a scalar denominator polynomial; in the left (respectively, right) matrix fraction parametrization, the impedance is written as the left- (respectively, right-) multiplication of a matrix by the inverse of another one; in the partial fraction description, the impedance is written as a pole-residue expansion, with matrix-valued residues. The first and last approaches are closely related, as will be seen in the following sections. The partial fraction description is often used in modal identification in the frequency domain [Balmès, 1996], as poles are readily parametrized.

Another important aspect when choosing an identification method concerns its domain of definition, time or frequency. We will restrict ourselves, as we have done in the entire dissertation, to the frequency domain, and to the corresponding algorithms. However, bridges exist between the time domain and the frequency domain, so that many methods can be used for both definition domains. In Allemang and Brown [1998], a common framework for most MIMO-identification methods is proposed, and the identification processes in the time and frequency domains are developed symmetrically. Likewise, Paronesso [1997] describes in parallel the identification of parametric models for FRFs and IRFs, using similar tools for both approaches. In a recent paper, Şafak [2006] makes a direct use of the time-frequency correspondence to construct a model in the time domain from data in the frequency domain.

Finally, a last issue is the choice of a deterministic or stochastic identification approach. The latter explicitly takes into account the possible pollution of the data by providing probabilistic models of the noise. These techniques seem to gain increasing attention as many identification methods lack accuracy when presented with noisy data. Pintelon and Schoukens [2001], for example, focus largely on these methods. Nevertheless, for the sake of simplicity, only deterministic methods will be presented here. When considering the identification of an experimentally measured impedance function, which is possible in the framework presented in this dissertation, but has not been done yet, this choice might become important.

#### 4.1.2 Methodology for the identification of hidden variables models

In system identification, the parameters that are identified are the coefficients of the projection of the desired quantity over a given basis, for example polynomial. In modal identification, the quantities that are sought are the modal parameters of the system: modal frequencies, modal damping, participation factors. Here, we are following an alternative, although related, approach, where we want to identify the values of matrices of mass, damping and stiffness. To make full use of the existing literature and algorithms on system identification, we have chosen to separate the identification process in two steps:

1. Firstly, a classical system identification is performed on the input impedance matrix, the model

being in a common denominator form,  $[\underline{Z}(\omega)] = [\underline{N}(\omega)]/q(\omega)$ . The parameters that are identified are the coefficients of the matrix-valued polynomial  $[\underline{N}(\omega)]$ , and the coefficients of the scalar polynomial  $q(\omega)$ . This identification is usually not exact, and some degree of approximation is introduced, controlled by the degree of the polynomials  $[\underline{N}(\omega)]$  and  $q(\omega)$ . This step of the identification will be subsequently called interpolation, to avoid confusion with the following.

2. Secondly, from the knowledge of the coefficients of the polynomials  $[\underline{N}(\omega)]$  and  $q(\omega)$ , the matrices of mass, damping and stiffness are identified. This step of the identification is performed exactly, and no further degree of approximation of the solution is introduced. During that step, modal frequencies and damping are identified.

The second step is one of the main novelties presented in this dissertation. Two aspects are particularly important: the non-uniqueness of the set  $\{[\underline{M}], [\underline{D}], [\underline{K}]\}$  for a given pair of polynomials  $[\underline{N}(\omega)]$  and  $q(\omega)$ , which calls for choices on the structure of the set, and the computation of the matrices themselves, once a structure of the set has been chosen. Both these aspects are studied in Sec. 4.3.

The main inconvenient of separating the identification process in that two-step form is that information on the matrices of mass, damping and stiffness, cannot be introduced as constraint on the interpolation. Particularly, the positive-definiteness of these matrices cannot be enforced. This means that the first estimation of these matrices, for a given input impedance matrix and a given level of approximation, might be non-positive-definite. This can usually be corrected *a posteriori*, if necessary by degrading the approximation, but there is no certainty then that the best approximate has been reached. However this approach allows the use of already existing and powerful algorithms, so that the possible loss of precision is deemed compensated. Also, this segmentation allows the approach to be directly applicable for input impedance matrices of different types: only the identification method of the first step has to be changed when considering an experimental impedance instead of a numerical result.

### 4.1.3 Choice of the number of hidden variables

The level of approximation of the identification process is controlled at the interpolation step, when choosing the degree of the polynomials  $[\underline{N}(\omega)]$  and  $q(\omega)$ . Considering the impedance matrix derived from a hidden variables model, as in Eq. (3.28), it is obvious that these orders are directly related to the number of hidden state variables in the model. Specifically, if  $n_N$  is the degree of the matrix-valued polynomial  $[\underline{N}(\omega)]$ ,  $n_q$  that of polynomial  $q(\omega)$ , and  $n_h$  is the number of hidden variables in the model, we have  $n_N = 2n_h + 2$  and  $n_q = 2n_h$ . Incidentally,  $n_N = n_q + 2$ . Several modal identification techniques, aimed at FRFs identification, require that  $n_N < n_q$ , so that they cannot be used in our framework. Most system identification methods, though, can be used.

In the rest of this chapter, the algorithms are presented supposing that the number  $n_h$  is known, which is not the case for an unknown system. It is normally obtained through an iterative process on the number of hidden variables. The process, starting at  $n_h = 1$ , is stopped when the cost function reaches a threshold chosen by the user. A balance has to be settled between higher accuracy and the possibility of identifying computational, or unphysical, modes.

### 4.1.4 The cost function

The basic idea of all system identification methods is to introduce an error function, usually the difference between the input data and the corresponding model, and to minimize it in some given sense. Often a Least Squares (LS) cost function is used, which means that the quantity that is minimized is the sum of

the squares of the error function. Denoting  $[\tilde{Z}(\omega)]$  the input matrix, and  $[Z(\omega)]$  the model that we are trying to identify, this LS approach yields the following cost function:

$$\epsilon = \sum_{\ell=1}^L \|[Z(\omega_\ell)] - [\tilde{Z}(\omega_\ell)]\|_F^2 = \sum_{\ell=1}^L \sum_{i=1}^{n_\Gamma} \sum_{j=1}^{n_\Gamma} \left( Z_{ij}(\omega_\ell) - \tilde{Z}_{ij}(\omega_\ell) \right)^2. \quad (4.1)$$

The direct minimization of this cost function is a difficult problem unless the modeled function  $[Z(\omega)]$  is linear in the parameters. In general, the presence of poles in the system will render this problem highly nonlinear. The direct computation of the minimum of the cost function is nevertheless possible, as shown for example in Chalko et al. [1996], but the result depends heavily on the accuracy of an initial estimate of the solution, and the process is numerically intensive.

A parallel approach, that has been later derived under many forms, originated in a paper by Levy [1959]. Instead of considering the nonlinear (-in-the-parameters) cost function, a linearized version is introduced. Using a common denominator description for the model impedance,  $[Z(\omega)] = [N(\omega)]/\underline{q}(\omega)$ , the new cost function to be minimized is

$$\epsilon_{LLS} = \sum_{\ell=1}^L w(\omega_\ell) \|[N(\omega_\ell)] - \underline{q}(\omega_\ell)[\tilde{Z}(\omega_\ell)]\|_F^2. \quad (4.2)$$

The weight  $w(\omega)$  is necessary for the correct evaluation of the poles of the system, which are the roots of  $\underline{q}(\omega)$ . Indeed, without it, the comparative importance of the term  $\|[N(\omega_\ell)] - \underline{q}(\omega_\ell)[\tilde{Z}(\omega_\ell)]\|_F^2$  gets very small when  $\omega_\ell$  approaches a pole. Sanathanan and Koerner [1963] therefore proposed to use an iterative scheme where the weight  $w(\omega)$  at a given step is taken as the inverse of the square norm of the denominator  $1/|\underline{q}(\omega)|^2$  evaluated at the previous step. Many choices of this weight function have been proposed in the literature, giving rise to as many identification methods [Pintelon et al., 1994]. Equivalent approaches exist when considering other parametrizations of the matrices. In Leuridan and Kundrat [1982], for example, the left-matrix fraction description is shown to lead to the determination of the coefficients of an ARMA model in the frequency domain.

#### 4.1.5 Choice of the interpolation method

Once a particular cost function has been chosen, a method for its actual minimization has to be selected. This choice should not be overlooked, and the main criterion that should lead us is the origin of the data. Indeed, when confronted to noisy data, most identification methods will fail. That aspect is important when designing, as we are, a framework that wishes to remain valid for the identification of hidden variables model of impedance matrices computed numerically, measured experimentally, or even read from charts. The characteristics of the data in each of these cases are very particular, and the "best" interpolation method will probably be different for each of them. Another aspect that might lead our choice is the computational cost, because almost all our computational time will be spent in this interpolation step.

We will present here only one particular interpolation method, that will be shown on an example to be very accurate when presented with noiseless data. Other valuable assets of this method are its conceptual clarity and the simplicity of its numerical implementation. It is a weighted discrete linear least square rational approximation using orthogonal vectors of polynomials, and is based on a rewriting of the cost function of Eq. (4.2) in a simpler form. Introductory papers on this paper include van Barel and Bultheel [1992, 1993] for the SISO case. An example of a MIMO implementation is described in Pintelon et al. [2004].

## 4.2 Weighted discrete linear least square rational approximation using orthogonal vectors of polynomials

The weighted discrete linear least square rational approximation using orthogonal vectors of polynomials starts from the formulation of Eq. (4.2), with the model to be fitted in a common denominator form, with matrix-valued polynomial  $[\underline{N}(\omega)]$  and scalar polynomial  $\underline{q}(\omega)$ . Both these polynomials are real polynomials<sup>1</sup> in powers of  $(i\omega)$ .

$$\epsilon_{LLS} = \sum_{\ell=1}^L w(\omega_\ell) \|[ \underline{N}(\omega_\ell) ] - \underline{q}(\omega_\ell) [\tilde{Z}(\omega_\ell)]\|_F^2. \quad (4.3)$$

The basic idea of the method is to introduce a space of vectors of polynomials that will allow us to rewrite the cost function as the minimization of the norm of a vector  $[P(\omega)]$ , under a simple constraint on its coordinates  $\{\alpha_\ell\}_{1 \leq \ell \leq m_2}$ .

$$\begin{cases} \min_{([\underline{N}], \underline{q})} \epsilon_{LLS} \equiv \min_{[P]} \|[P(\omega)]\|_W^2 \equiv \min_{\{\alpha_\ell\}_{1 \leq \ell \leq m_2}} \sum_{\ell=1}^{m_2} \alpha_\ell^2 \\ \alpha_{m_2} = 1 \end{cases}, \quad (4.4)$$

where  $m_2$  will be defined later. The minimization is straightforward, and numerically instantaneous. However, the computation of an orthonormal basis for the space of vectors of polynomials is required, and this is where most of the computational time will be spent. Before presenting in more details the developments sketched here, we will introduce the space of vectors of polynomials, and the corresponding scalar product, norm and orthonormal basis.

Although this is not a requirement of the method, we will restrict ourselves to the case where  $n_N = n_q + 2 = 2n_h + 2$ . The impedance matrix is  $n_\Gamma \times n_\Gamma$ .

### 4.2.1 The space of vectors of polynomials

For a given  $m$  in  $\mathbb{N}$ , let  $\mathbb{R}[i\omega]^m$  be the set of all the  $m$ -vectors whose elements are constituted of polynomials of  $(i\omega)$ , of any degree, and with real coefficients.  $[P_1(\omega)]$ ,  $[P_2(\omega)]$ , and  $[P_3(\omega)]$  are three examples of elements, respectively, of  $\mathbb{R}[i\omega]^3$ ,  $\mathbb{R}[i\omega]^3$ , and  $\mathbb{R}[i\omega]^4$ .

$$[P_1(\omega)] = \begin{bmatrix} (i\omega)^2 - 1 \\ (i\omega) + 2 \\ (i\omega)^7 \end{bmatrix}, [P_2(\omega)] = \begin{bmatrix} 1 \\ 0 \\ 0 \end{bmatrix}, [P_3(\omega)] = \begin{bmatrix} (i\omega)^2 - 1 \\ (i\omega) + 2 \\ (i\omega)^7 \\ 0 \end{bmatrix}. \quad (4.5)$$

A vector  $\Delta$  of  $\mathbb{N}^m$  is then introduced to control the degree of each of the elements of the vectors. Let then  $\mathbb{R}[i\omega]_\Delta^m \subset \mathbb{R}[i\omega]^m$  be the space of all  $m$ -vectors of polynomials of  $(i\omega)$  with real coefficients and degrees respectively  $\Delta(1)$  to  $\Delta(m)$ . The vectors of Eq. (4.5) are respectively in  $\mathbb{R}[i\omega]_{(2,1,7)}^3$ ,  $\mathbb{R}[i\omega]_{(0,0,0)}^3$ , and  $\mathbb{R}[i\omega]_{(2,1,7,0)}^4$ .

<sup>1</sup>Although it will not be further commented, it is customary in system identification to normalize both the data and the frequency, and to expand the data set to its complex conjugate for negative frequencies. The normalization of the frequency is used to prevent higher frequencies from being undeservedly represented, since we are considering powers of  $(i\omega)$ . The expansion of the data set provides an elegant way to enforce that the coefficients of  $[\underline{N}(\omega)]$  and  $\underline{q}(\omega)$  are real. In all applications presented hereafter, these principles have been followed.

To provide the space  $\mathbb{R}[i\omega]_{\Delta}^m$  with a (semi-) norm, we introduce a frequency-dependent matrix  $[W(\omega)]$ , with values in  $\mathbb{M}_m^{+0}(\mathbb{C})$ , the space of positive  $m \times m$  complex matrices. The hermitian sesquilinear form, for a given set of frequencies  $(\omega_\ell)_{1 \leq \ell \leq L}$ ,

$$([P_1], [P_2])_W = \Re \left\{ \sum_{\ell=1}^L [P_1(\omega_\ell)]^* [W(\omega_\ell)] [P_2(\omega_\ell)] \right\} \quad (4.6)$$

is a "semi-inner product" on  $\mathbb{R}[i\omega]_{\Delta}^m$ , in the sense that the corresponding form  $\|[P]\|_W = \sqrt{([P], [P])_W}$  is a semi-norm on the same space. Using that semi-inner product, it is possible<sup>2</sup> to construct an orthonormal basis  $\{[e_\ell(\omega)]\}_{1 \leq \ell \leq m'}$  of vectors of  $\mathbb{R}[i\omega]_{\Delta}^m$ , where  $m'$  depends on  $\Delta$ . The actual construction of the orthonormal basis can be performed using the Gram-Schmidt orthonormalization procedure [Golub and van Loan, 1983], starting from a given set of vectors of  $\mathbb{R}[i\omega]_{\Delta}^m$ .

#### 4.2.2 Principle of the method

The weighted discrete linear least square rational approximation using orthogonal vectors of polynomials consists in using the previous space of vectors of polynomials, with particular  $m$ ,  $\Delta$ , and  $[W(\omega)]$ . Namely, we choose  $m = n_{\Gamma}^2 + 1$ ,  $\Delta = (n_N, n_N, \dots, n_N, n_q) = (2n_h + 2, \dots, 2n_h + 2, 2n_h)$ , and

$$[W(\omega)] = \left( w(\omega) \begin{bmatrix} [I_{n_{\Gamma}^2}] & -\text{vec}([\tilde{Z}(\omega)]) \end{bmatrix} \right)^* \left( w(\omega) \begin{bmatrix} [I_{n_{\Gamma}^2}] & -\text{vec}([\tilde{Z}(\omega)]) \end{bmatrix} \right) \quad (4.7)$$

$$= w^2(\omega) \begin{bmatrix} [I_{n_{\Gamma}^2}] & -\text{vec}([\tilde{Z}(\omega)]) \\ -\text{vec}([\tilde{Z}(\omega)])^* & \|\tilde{Z}(\omega)\|_F^2 \end{bmatrix}, \quad (4.8)$$

where the operator  $\text{vec}(\cdot)$  applied to a matrix in  $\mathbb{M}_{n_{\Gamma}}(\mathbb{C})$  produces a  $n_{\Gamma}^2$ -vector by stacking the columns of the matrix one on top of the others. For any matrix  $[A]$  in  $\mathbb{M}_{n_{\Gamma}}(\mathbb{C})$ , it should be noted that  $\|[A]\|_F^2 = \text{vec}([A])^* \text{vec}([A])$ . Considering that the vector  $[P(\omega)]$ , in  $\mathbb{R}[i\omega]_{\Delta}^m$ , represents

$$[P(\omega)] = \begin{bmatrix} \text{vec}([\underline{N}(\omega)]) \\ \underline{q}(\omega) \end{bmatrix}, \quad (4.9)$$

and using the previous definitions, the cost function  $\epsilon_{LLS}$  can be rewritten

$$\epsilon_{LLS} = \|[P(\omega)]\|_W^2. \quad (4.10)$$

---

<sup>2</sup>Since  $\|\cdot\|_W$  is a semi-norm rather than a norm, problems might arise as some non-zero vectors have a zero norm. However, we will see that this possibility in our case is not a real difficulty.

The following set of  $m_2 = n_\Gamma^2(2n_h + 3) + 2n_h + 1$  vectors forms a non-orthonormal basis of  $\mathbb{R}[i\omega]_\Delta^m$ :

$$\begin{aligned} & \begin{bmatrix} 1 \\ 0 \\ 0 \\ \dots \\ 0 \\ 0 \end{bmatrix}, \begin{bmatrix} (i\omega) \\ 0 \\ 0 \\ \dots \\ 0 \\ 0 \end{bmatrix}, \begin{bmatrix} (i\omega)^2 \\ 0 \\ 0 \\ \dots \\ 0 \\ 0 \end{bmatrix}, \dots, \begin{bmatrix} (i\omega)^{2n_h+2} \\ 0 \\ 0 \\ \dots \\ 0 \\ 0 \end{bmatrix}, \begin{bmatrix} 0 \\ 1 \\ 0 \\ \dots \\ 0 \\ 0 \end{bmatrix}, \begin{bmatrix} 0 \\ (i\omega) \\ 0 \\ \dots \\ 0 \\ 0 \end{bmatrix}, \dots, \\ & \begin{bmatrix} 0 \\ 0 \\ 0 \\ \dots \\ (i\omega)^{2n_h+2} \\ 0 \end{bmatrix}, \begin{bmatrix} 0 \\ 0 \\ 0 \\ \dots \\ 0 \\ 1 \end{bmatrix}, \dots, \begin{bmatrix} 0 \\ 0 \\ 0 \\ \dots \\ 0 \\ (i\omega)^{2n_h-1} \end{bmatrix}, \begin{bmatrix} 0 \\ 0 \\ 0 \\ \dots \\ 0 \\ (i\omega)^{2n_h} \end{bmatrix}. \quad (4.11) \end{aligned}$$

The Gram-Schmidt orthonormalization procedure can be used to yield an orthonormal basis  $\{[e_\ell(\omega)]\}_{1 \leq \ell \leq m_2}$  of  $\mathbb{R}[i\omega]_\Delta^m$ . Since  $\|\cdot\|_W$  is only a semi-norm, it is possible that the orthonormalization procedure breaks. It only means that we have found a non-zero vector  $[P(\omega)]$  such that  $\|[P(\omega)]\|_W = 0$ , and consequently  $\epsilon_{LLS} = 0$ . A perfect solution of the original minimization problem has been encountered.

Expanding  $[P(\omega)]$  on that basis of vectors of polynomials, and denoting  $(\alpha_\ell)_{1 \leq \ell \leq m_2}$  its coordinates, we have  $[P(\omega)] = \sum_{\ell=1}^{m_2} \alpha_\ell [e_\ell(\omega)]$ , and

$$\epsilon_{LLS} = \sum_{\ell=1}^{m_2} \alpha_\ell^2. \quad (4.12)$$

The original minimization problem can therefore be replaced by the minimization of a sum of squares. The trivial solution  $\alpha_\ell = 0, 1 \leq \ell \leq m_2$ , comes from our use of the linearized cost function of Eq. (4.2) rather than that of Eq. (4.1). Indeed, if  $[\underline{N}(\omega)] = 0$ , and  $\underline{q}(\omega) = 0$ , then  $\epsilon_{LLS} = 0$ . Therefore the solution has to be constrained, for example by imposing that the coefficient of highest order of  $\underline{q}(\omega)$  be 1. Other constraints can be chosen, but this one can be implemented particularly nicely in terms of the coordinates  $\alpha_\ell$ . Indeed, if the basis was computed using the Gram-Schmidt procedure, which orthonormalizes each vector with respect to the previous ones, and starting from the basis of Eq. (4.11), then only the last vector of the basis will contain terms of order  $2n_\Gamma$  on its last dimension. Therefore, the constraint that the coefficient of highest order of  $\underline{q}(\omega)$  be 1 translates to  $\alpha_{m_2} = 1$ . Consequently the solution of the minimization of the cost function is therefore

$$\begin{cases} \alpha_\ell = 0, & 1 \leq \ell \leq m_2 - 1, \\ \alpha_{m_2} = 1 \end{cases}, \quad (4.13)$$

or, in terms of the polynomials of interest,

$$\begin{bmatrix} \text{vec}([\underline{N}(\omega)]) \\ \underline{q}(\omega) \end{bmatrix} = [P(\omega)] = [e_{m_2}(\omega)]. \quad (4.14)$$

### 4.2.3 Cost and optimization of the algorithm

The entire computational cost of this method lies in the construction of the orthonormal basis using the Gram-Schmidt method. As the space is of size  $m_2 = n_\Gamma^2(2n_h + 3) + 2n_h + 1$ , the computational time

increases with the number of impedance functions in the data set, as well as with the number of hidden variables. Also, since the computation of the semi-inner product  $(\cdot, \cdot)_W$  involves a sum on the frequency set, the refinement in the frequency range influences the CPU time, but to a lesser extent.

This algorithm has reached a more mature level of development than what is presented here. All issues are not discussed as it is not the purpose of this dissertation, and the reader is referred to the literature [Bultheel et al., 2005, 2004] on the subject. Among the issues concerning the optimization of this method, the parallelization of the process is treated in van Barel and Bultheel [1992] and the construction of the orthonormal basis using a recurrence relation between the elements of the basis is presented in van Barel and Bultheel [1993], both allowing for greater accuracy and speed.

### 4.3 The identification problem

The previous section presented a way to identify the polynomials  $[\underline{N}(\omega)]$  and  $\underline{q}(\omega)$  from the knowledge of  $\{\tilde{Z}(\omega_\ell)\}_{1 \leq \ell \leq L}$ . This section now introduces the identification of the set  $\{[\underline{M}], [\underline{D}], [\underline{K}]\}$  from the polynomials  $[\underline{N}(\omega)]$  and  $\underline{q}(\omega)$ . In Sec. 3.1.4, the hidden state variables model of an impedance matrix was presented in a very general manner, with no precision on the structure of the matrices  $\{[\underline{M}], [\underline{D}], [\underline{K}]\}$ , aside from their symmetry. We will see here that a particular structure can be enforced, with no loss of generality of the model. Basically, we will show that many distinct sets of matrices lead to the same impedance matrix so that we can choose a particular one for the identification. The first part of this section is dedicated to this non-uniqueness problem, and the related choice of the set  $\{[\underline{M}], [\underline{D}], [\underline{K}]\}$ , while the second part concentrates on the actual identification of the set from the values of the coefficients of the polynomials  $[\underline{N}(\omega)]$  and  $\underline{q}(\omega)$ .

#### 4.3.1 Non-uniqueness of the solution

The non-uniqueness problem presented here should not be mistaken for the more classical uniqueness problem in structural mechanics, that consists in studying the minimal number of excitations and observations required to identify uniquely a system. In Udwadia et al. [1978], it is shown that, for a N-DOFs damped shear beam building, the observation of the base motion and of the motion of the first floor are required to identify the stiffness and damping distributions, if the mass distribution is known beforehand. In Franco et al. [2004, 2006] these results are developed, allowing for simultaneous identification of the mass distribution. Our goal here is different, as we will show that we cannot have uniqueness, and we rather try to constrain the matrices to get fewer solutions to the identification problem. For a better understanding of the problem, we start with a small example, before stating the choice of the structures of the matrices  $\{[\underline{M}], [\underline{D}], [\underline{K}]\}$ .

#### Example of equivalent sets of matrices

Let us consider two sets of matrices  $\{[\underline{M}_1], [\underline{D}_1], [\underline{K}_1]\}$ , and  $\{[\underline{M}_2], [\underline{D}_2], [\underline{K}_2]\}$ , all in  $\mathbb{M}_n^+(\mathbb{R})$ , such that  $[\underline{M}_2] = [U][\underline{M}_1][U]^T$ ,  $[\underline{D}_2] = [U][\underline{D}_1][U]^T$ , and  $[\underline{K}_2] = [U][\underline{K}_1][U]^T$ , with

$$[U] = \begin{bmatrix} [I_{n_\Gamma}] & [0_{n_\Gamma n_h}] \\ [0_{n_h n_\Gamma}] & [G] \end{bmatrix}, \quad (4.15)$$

in  $\mathbb{M}_n(\mathbb{R})$ , and with  $[G]$  in  $\mathbb{M}_{n_h}^*(\mathbb{R})$ . The dynamic stiffness matrices corresponding to these two sets are therefore related, for any frequency  $\omega$ , by the relation  $[\underline{S}_2(\omega)] = -\omega^2[\underline{M}_2] + i\omega[\underline{D}_2] + [\underline{K}_2] =$

$[U][\underline{S}_1(\omega)][U]^T$ , and, consequently

$$[\underline{Z}_2(\omega)] = [\underline{S}_{\Gamma_2}(\omega)] - [\underline{S}_{c_2}(\omega)][\underline{S}_{h_2}(\omega)]^{-1}[\underline{S}_{c_2}(\omega)]^T \quad (4.16)$$

$$= [\underline{S}_{\Gamma_1}(\omega)] - [\underline{S}_{c_1}(\omega)][G][G]^{-1}[\underline{S}_{h_1}(\omega)]^{-1}[G]^{-T}[G]^T[\underline{S}_{c_1}(\omega)]^T \quad (4.17)$$

$$= [\underline{S}_{\Gamma_1}(\omega)] - [\underline{S}_{c_1}(\omega)][\underline{S}_{h_1}(\omega)]^{-1}[\underline{S}_{c_1}(\omega)]^T = [\underline{Z}_1(\omega)]. \quad (4.18)$$

We have therefore found two separate sets of matrices  $\{[\underline{M}_1], [\underline{D}_1], [\underline{K}_1]\}$  and  $\{[\underline{M}_2], [\underline{D}_2], [\underline{K}_2]\}$  that yield the exact same impedance matrix. If the only input for the identification is the impedance matrix, then these two sets are perfectly equivalent, and identifying one or the other is indifferent. If the structure of one of the sets of matrices makes its identification easier, then this one should be chosen. We will use this hereafter, by finding a larger group of equivalent sets, and then choosing among this group the set with the appropriate structure for our means.

### Choice of the structure of the matrices

We first show here that the same kind of equivalence can be found with a more general matrix  $[U]$ . Let us therefore use

$$[U] = \begin{bmatrix} [I_{n_\Gamma}] & [F] \\ [0_{n_h n_\Gamma}] & [G] \end{bmatrix}, \quad (4.19)$$

with  $[F]$  in  $M_{n_\Gamma n_h}(\mathbb{R})$ , and  $[G]$  in  $M_{n_h}^*(\mathbb{R})$ . As before, we have  $[\underline{S}_2(\omega)] = [U][\underline{S}_1(\omega)][U]^T$ , with this time

$$\begin{cases} [\underline{S}_{\Gamma_2}(\omega)] = [\underline{S}_{\Gamma_1}(\omega)] + [\underline{S}_{c_1}(\omega)][F]^T + [F][\underline{S}_{c_1}(\omega)]^T + [F][\underline{S}_{h_1}(\omega)][F]^T \\ [\underline{S}_{c_2}(\omega)] = [\underline{S}_{c_1}(\omega)][G]^T + [F][\underline{S}_{h_1}(\omega)][G]^T \\ [\underline{S}_{h_2}(\omega)] = [G][\underline{S}_{h_1}(\omega)][G]^T \end{cases}. \quad (4.20)$$

Since  $[G]$  and  $[\underline{S}_{h_1}(\omega)]$  are invertible, we have again

$$[\underline{Z}_2(\omega)] = [\underline{S}_{\Gamma_2}(\omega)] - [\underline{S}_{c_2}(\omega)][\underline{S}_{h_2}(\omega)]^{-1}[\underline{S}_{c_2}(\omega)]^T = [\underline{Z}_1(\omega)]. \quad (4.21)$$

Supposing the set of matrices  $\{[\underline{M}_1], [\underline{D}_1], [\underline{K}_1]\}$  is a good model for the system under study, we get an equivalent set  $\{[\underline{M}_2], [\underline{D}_2], [\underline{K}_2]\}$ , with the same impedance  $[\underline{Z}_2(\omega)] = [\underline{Z}_1(\omega)]$ , for each pair of matrices  $[F]$  and  $[G]$ . Let us then choose

$$\begin{cases} [F] = -[\underline{M}_{c_1}][\underline{M}_{h_1}]^{-1} \\ [G] = [\Phi] \end{cases}, \quad (4.22)$$

where  $[\Phi]$  is the matrix of the eigenvectors solutions of the generalized eigenvalue problem

$$[\underline{K}_{h_1}]\phi = \lambda[\underline{M}_{h_1}]\phi, \quad (4.23)$$

normalized with respect to the mass matrix  $[\underline{M}_{h_1}]$ . Eq. (4.20) are also true when the dynamic stiffness matrix  $[\underline{S}(\omega)]$  is replaced by either  $[\underline{M}]$ ,  $[\underline{D}]$ , or  $[\underline{K}]$ . For this choice of  $[F]$  and  $[G]$ , we therefore get that  $[\underline{M}_{h_2}] = [\Phi][\underline{M}_{h_1}][\Phi]^T = [I_{n_h}]$ ,  $[\underline{K}_{h_2}] = [\Phi][\underline{K}_{h_1}][\Phi]^T$  is diagonal, and  $[\underline{M}_{c_2}] = [0_{n_\Gamma n_h}]$ . It is usually supposed in structural mechanics that the damping matrix can be diagonalized in the same basis as the matrices of mass and stiffness, so that  $[\underline{D}_{h_2}] = [\Phi][\underline{D}_{h_1}][\Phi]^T$  is supposed to be diagonal. In Hasselman [1976] and Park et al. [1992], the adequacy of considering such a diagonal damping matrix is discussed

and criterions are given for that matter. However, we will not consider these here, but only observe on an example, in Sec. 4.4.5, that this hypothesis seems appropriate.

With no loss of generality (apart from the hypothesis on the damping matrix), we can therefore choose to identify the hidden variables model of an impedance matrix with matrices  $\{[\underline{M}], [\underline{D}], [\underline{K}]\}$  with the following structures

$$[\underline{M}] = \begin{bmatrix} [\underline{M}_\Gamma] & [0_{n_\Gamma n_h}] \\ [0_{n_h n_\Gamma}] & [I_{n_h}] \end{bmatrix}, [\underline{D}] = \begin{bmatrix} [\underline{D}_\Gamma] & [\underline{D}_c] \\ [\underline{D}_c]^T & [d_h] \end{bmatrix}, [\underline{K}] = \begin{bmatrix} [\underline{K}_\Gamma] & [\underline{K}_c] \\ [\underline{K}_c]^T & [k_h] \end{bmatrix}, \quad (4.24)$$

where  $[\underline{M}_\Gamma]$ ,  $[\underline{D}_\Gamma]$  and  $[\underline{K}_\Gamma]$  are in  $\mathbb{M}_{n_\Gamma}^+(\mathbb{R})$ ,  $[\underline{D}_c]$  and  $[\underline{K}_c]$  are in  $\mathbb{M}_{n_\Gamma n_h}(\mathbb{R})$ , and  $[d_h]$  and  $[k_h]$  are diagonal matrices of  $\mathbb{M}_{n_h}^+(\mathbb{R})$ . We further introduce the parameters  $(d_\ell)_{1 \leq \ell \leq n_h}$  and  $(k_\ell)_{1 \leq \ell \leq n_h}$  such that  $[d_h] = \text{diag}(d_\ell)_{1 \leq \ell \leq n_h}$  and  $[k_h] = \text{diag}(k_\ell)_{1 \leq \ell \leq n_h}$ .

### 4.3.2 Identification

We will here first write the impedance matrix in terms of the matrices  $\{[\underline{M}], [\underline{D}], [\underline{K}]\}$ , and then in terms of the polynomials  $[\underline{N}(\omega)]$  and  $q(\omega)$ . The identification of the matrices of the hidden variables model is based on the comparison of these two forms. Using Eq. (4.24), we have  $[\underline{S}_h(\omega)]^{-1} = \text{diag}(1/(-\omega^2 + i\omega d_\ell + k_\ell))_{1 \leq \ell \leq n_h}$ , and

$$[\underline{Z}(\omega)] = [\underline{S}_\Gamma(\omega)] - [\underline{S}_c(\omega)][\underline{S}_h(\omega)]^{-1}[\underline{S}_c(\omega)]^T \quad (4.25)$$

$$= -\omega^2[\underline{M}_\Gamma] + i\omega[\underline{D}_\Gamma] + [\underline{K}_\Gamma] - \sum_{\ell=1}^{n_h} \frac{(i\omega[\underline{D}_c]^\ell + [\underline{K}_c]^\ell)(i\omega[\underline{D}_c]^\ell + [\underline{K}_c]^\ell)^T}{-\omega^2 + i\omega d_\ell + k_\ell}, \quad (4.26)$$

where  $[\underline{D}_c]^\ell$  and  $[\underline{K}_c]^\ell$  represent the  $\ell^{\text{th}}$  columns of  $[\underline{D}_c]$  and  $[\underline{K}_c]$ . Expanding this equation, we get

$$\begin{aligned} [\underline{Z}(\omega)] = & -\omega^2[\underline{M}_\Gamma] + i\omega[\underline{D}_\Gamma] + \left( [\underline{K}_\Gamma] - \sum_{\ell=1}^{n_h} [\underline{D}_c]^\ell [\underline{D}_c]^{\ell T} \right) \\ & - \sum_{\ell=1}^{n_h} i\omega \frac{[\underline{D}_c]^\ell [\underline{K}_c]^{\ell T} + [\underline{K}_c]^\ell [\underline{D}_c]^{\ell T} - d_\ell [\underline{D}_c]^\ell [\underline{D}_c]^{\ell T}}{-\omega^2 + i\omega d_\ell + k_\ell} \\ & - \sum_{\ell=1}^{n_h} \frac{[\underline{K}_c]^\ell [\underline{K}_c]^{\ell T} - k_\ell [\underline{D}_c]^\ell [\underline{D}_c]^{\ell T}}{-\omega^2 + i\omega d_\ell + k_\ell} \end{aligned} \quad (4.27)$$

On the other hand, assuming that there are no real nor repeated poles, the matrix-valued rational function computed in Sec. 4.2 can be expanded in an unique pole-residue expansion:

$$[\underline{Z}(\omega)] = \frac{[\underline{N}(\omega)]}{q(\omega)} = -\omega^2[R_{-2}] + i\omega[R_{-1}] + [R_0] + \sum_{\ell=1}^{2n_h} \frac{[R_\ell]}{i\omega - p_\ell}, \quad (4.28)$$

where the  $([R_\ell])_{-2 \leq \ell \leq 0}$  are in  $\mathbb{M}_{n_\Gamma}^S(\mathbb{R})$  (by construction), the  $([R_\ell])_{1 \leq \ell \leq 2n_h}$  are in  $\mathbb{M}_{n_\Gamma}^S(\mathbb{C})$  and the poles  $(p_\ell)_{1 \leq \ell \leq 2n_h}$  are complex. Noting that each pair  $(p_\ell, [R_\ell])$  is associated with its associated complex conjugate pair  $(\overline{p_\ell}, \overline{[R_\ell]})$ , we reorder and regroup the terms of Eq. (4.28) as

$$\frac{[\underline{N}(\omega)]}{q(\omega)} = -\omega^2[R_{-2}] + i\omega[R_{-1}] + [R_0] + \sum_{\ell=1}^{n_h} \frac{2i\omega \Re\{[R_\ell]\} - 2\Re\{[R_\ell]\overline{p_\ell}\}}{-\omega^2 - 2i\omega \Re\{p_\ell\} + \|p_\ell\|^2}, \quad (4.29)$$

Comparing Eq. (4.27) and Eq. (4.29), which hold for all frequencies in  $\mathbb{R}$ , we get three sets of equations, to be solved one after the other:

1. the first one is an uncoupled system of  $2n_h + 2$  equations

$$\begin{cases} [\underline{M}_\Gamma] = [R_{-2}], \\ [\underline{D}_\Gamma] = [R_{-1}], \\ d_\ell = -2\Re\{p_\ell\}, \quad 1 \leq \ell \leq n_h, \\ k_\ell = \|p_\ell\|^2, \quad 1 \leq \ell \leq n_h, \end{cases} \quad (4.30)$$

that gives directly the values of  $[\underline{M}_\Gamma]$ ,  $[\underline{D}_\Gamma]$  and  $d_\ell$  and  $k_\ell$ , for  $1 \leq \ell \leq n_h$ ;

2. the second one is a coupled system of  $2n_h$  equations

$$\begin{cases} [\underline{K}_c]^\ell [\underline{K}_c]^{\ell T} - k_\ell [\underline{D}_c]^\ell [\underline{D}_c]^{\ell T} = 2\Re\{[R_\ell] \overline{p_\ell}\}, & 1 \leq \ell \leq n_h, \\ [\underline{D}_c]^\ell [\underline{K}_c]^{\ell T} + [\underline{K}_c]^\ell [\underline{D}_c]^{\ell T} - d_\ell [\underline{D}_c]^\ell [\underline{D}_c]^{\ell T} = -2\Re\{[R_\ell]\}, & 1 \leq \ell \leq n_h. \end{cases} \quad (4.31)$$

setting the values of the  $[\underline{D}_c]^\ell$  and  $[\underline{K}_c]^\ell$ , given those of  $d_\ell$  and  $k_\ell$ , for  $1 \leq \ell \leq n_h$ ;

3. finally, the third one gives directly the value of  $[\underline{K}_\Gamma]$  when the second system has been solved,

$$[\underline{K}_\Gamma] - \sum_{\ell=1}^{n_h} [\underline{D}_c]^\ell [\underline{D}_c]^{\ell T} = [R_0], \quad (4.32)$$

Of these three, the only system that has got to be explicitated is the second one. It is in fact partially decoupled, as the equations are coupled only in pairs for each  $\ell$ , for  $1 \leq \ell \leq n_h$ . The  $n_h$  systems of equations are all in the form

$$\begin{cases} [X][X]^T - \alpha \overline{\alpha} [Y][Y]^T = \overline{\alpha} [A] + \alpha \overline{[A]} \\ [X][Y]^T + [Y][X]^T + (\alpha + \overline{\alpha}) [Y][Y]^T = -([A] + \overline{[A]}) \end{cases} \quad (4.33)$$

where the  $[X]$  and  $[Y]$  are the unknowns, in  $\mathbb{M}_{n_\Gamma}(\mathbb{R})$ ,  $\alpha$  is a given complex scalar, and  $[A]$  is a given matrix in  $\mathbb{M}_{n_\Gamma}^S(\mathbb{C})$ . Obviously, for  $1 \leq \ell \leq n_h$ ,  $[X]$  corresponds to  $[\underline{K}_c]^\ell$ ,  $[Y]$  corresponds to  $[\underline{D}_c]^\ell$ ,  $\alpha$  to the pole  $p_\ell$ , and  $[A]$  to the corresponding residue  $[R_\ell]$ .

For any square complex symmetric (non-hermitian) matrix  $[U]$ , the Takagi factorization [Takagi, 1925, Horn and Johnson, 1990] is a special case of the singular decomposition, stating that there always exists a unitary matrix  $[Q]$  such that

$$[U] = [Q][\Sigma][Q]^T, \quad (4.34)$$

where  $[\Sigma]$  is the diagonal matrix of the singular values of  $[U]$ . Denoting  $[\sqrt{\Sigma}]$  the diagonal matrix of the square root of these singular values, and  $[L_u] = [Q][\sqrt{\Sigma}]$ , we have  $[L_u][L_u]^T = [U]$ . Going back to our problem of identifying  $[X]$  and  $[Y]$  in Eq. (4.33), it is always possible to find  $[L]$  in  $\mathbb{M}_n(\mathbb{C})$  such that

$$[L][L]^T = -2i \frac{[A]}{\Im\{\alpha\}}. \quad (4.35)$$

It is then a simple matter to check that the pair defined by

$$\begin{cases} [X] = \Im\{\alpha\} \Re\{[L]\} - \Re\{\alpha\} \Im\{[L]\} \\ [Y] = \Im\{[L]\} \end{cases} \quad (4.36)$$

is a solution of the system to Eq. (4.33). It should be noted that, in general,  $[X]$  and  $[Y]$  will be  $n_\Gamma \times n_\Gamma$  matrices, so that each pole will correspond to several columns and lines of the matrices of mass, damping, and stiffness.

This final step allows us to identify completely the matrices  $[M]$ ,  $[D]$  and  $[K]$  corresponding to the pair of polynomials  $[\underline{N}(\omega)]$  and  $\underline{q}(\omega)$ , and ultimately to an impedance matrix given at a discrete set of frequencies  $\{[\tilde{Z}(\omega_\ell)]_{1 \leq \ell \leq L}\}$ .

#### 4.4 Validation of the identification

We will try in this section to illustrate the main aspects of the identification method that was described in this chapter. We consider a simple 6-DOFs mechanical model, which will be referred to as the Input Model, and defined by its matrices of mass  $[\tilde{M}]$ , damping  $[\tilde{D}]$ , and stiffness  $[\tilde{K}]$ ,

$$\begin{aligned}
 [\tilde{M}] &= \begin{bmatrix} 4 & 3 & 0 & 0 & 0 & 0 \\ & 4 & 0 & 0 & 0 & 0 \\ & & 100 & 0 & 0 & 0 \\ & & & 100 & 0 & 0 \\ \text{(sym.)} & & & & 100 & 0 \\ & & & & & 100 \end{bmatrix}, \\
 [\tilde{D}] &= \begin{bmatrix} 1 & .2 & 1 & 0 & 4 & -3 \\ & 4 & 0 & 2 & -4 & 2 \\ & & 70 & 0 & 0 & 0 \\ & & & 30 & 0 & 0 \\ \text{(sym.)} & & & & 60 & 0 \\ & & & & & 80 \end{bmatrix} \times 10^{-1}, \\
 [\tilde{K}] &= \begin{bmatrix} 1.5 & .5 & 2 & -3 & -2 & 0 \\ & 5 & 2 & 0 & 2 & 2 \\ & & 4 & 0 & 0 & 0 \\ & & & 25 & 0 & 0 \\ \text{(sym.)} & & & & 49 & 0 \\ & & & & & 81 \end{bmatrix}. \quad (4.37)
 \end{aligned}$$

We compute the corresponding impedance matrix  $[\tilde{Z}(\omega)]$ , with respect to the first 2 DOFs, and for frequencies in the interval  $[0,1]$  rad/s. Since this  $2 \times 2$ -impedance matrix is symmetric, only three terms are independent, and are denoted (1,1), (1,2) and (2,2). The real part, imaginary part, amplitude and phase of these functions are drawn in Fig. 4.1, as a solid red line. In each of the following sections, we emphasize a particular aspect of the identification process, and all the results are summarized in Table 4.1, Table 4.2, and Table 4.3.

Each line of these tables represents one of the cases that will be considered, starting with the input system in the first line, and the direct identification with 1, 2, 3 or 4 hidden variables, in the following. In Table 4.1, the modal quantities are described, namely the modal frequencies and the modal dampings. These values,  $(\omega_\ell, \zeta_\ell)_{1 \leq \ell \leq n_h}$ , are directly related to the poles  $(p_\ell)_{1 \leq \ell \leq n_h}$  of the identified system, by  $|p_\ell|^2 = \omega_\ell^2$ , and  $-2\Re\{p_\ell\} = 2\omega_\ell\zeta_\ell$ . For each modal frequency, the columns of Table 4.2, and Table 4.3 then represent the coupling parts of the damping and stiffness matrices  $[D_c]$  and  $[K_c]$ . As the impedance matrix is  $2 \times 2$ , the coupling matrices corresponding to each modal frequency (or pole) are also  $2 \times 2$ .

This is why there are two columns for each modal frequency even though there was originally only one in the input system.

	Modal frequencies [rad/s]				Modal damping [%]			
	$\omega_1$	$\omega_2$	$\omega_3$	$\omega_4$	$\zeta_1$	$\zeta_2$	$\zeta_3$	$\zeta_4$
Input model	0.20	0.40	0.70	0.90	17.50	3.00	4.29	4.44
1 Hidden Variable (HV)	0.24	-	-	-	6.49	-	-	-
2 HVs	0.20	0.50	-	-	17.44	2.96	-	-
3 HVs	0.20	0.50	0.70	-	17.52	3.00	4.33	-
4 HVs	0.20	0.50	0.70	0.90	17.50	3.00	4.29	4.44
$B^*$ , 4 HVs	0.20	0.50	0.70	0.90	17.50	3.00	4.29	4.44
$B_L$ , 2 HVs	0.20	0.50	-	-	17.49	3.04	-	-
$B_L$ , 4 HVs	0.20	0.50	0.70	0.90	17.50	3.00	4.29	4.44
$B_H$ , 2 HVs	-	-	0.68	0.90	-	-	3.57	4.47
$B_H$ , 4 HVs	0.19	0.50	0.70	0.90	19.66	3.01	4.29	4.44
(1,1), 4 HVs	0.20	0.50	0.70	0.90	17.50	3.00	4.29	4.44
(1,1)-(2,2), 4 HVs	0.20	0.50	0.70	0.90	17.50	3.00	4.29	4.44
$\alpha = 0.05$ , 3 HVs	0.20	0.50	0.70		17.53	2.98	4.19	
$\alpha = 0.3$ , 3 HVs	0.20	0.50	0.86		16.39	2.93	0.27	
Non-diagonal $[\tilde{D}_h]$	0.20	0.50	0.70	0.90	17.52	2.99	4.29	4.44

Table 4.1: Modal parameters of the input system and of the identified systems.

The next section studies the identification of the hidden state variables model for the impedance matrix  $[\tilde{Z}(\omega)]$ , with no knowledge of the matrices  $[\tilde{M}]$ ,  $[\tilde{D}]$ , and  $[\tilde{K}]$ . Each of the following sections investigates a particular aspect of the identification process, and the possible difficulties that may arise.

#### 4.4.1 Direct identification

The identification is performed here, for 4 hidden variables, on the complete  $2 \times 2$ -impedance matrix  $[\tilde{Z}(\omega)]$ , using 101 frequency points equally spaced over the interval  $B_0 = [0,1]$  rad/s. The identified impedance functions are drawn in Fig. 4.1 and perfectly match the input functions. The CPU time necessary to perform the identification is negligible (a few seconds on a 1 GHz PowerPC G4 laptop). This time would increase with the number of frequency points considered, and, more importantly, with the number of impedance functions simultaneously identified. The structure of the coupling matrices is worth commenting: although we started from a system with lone poles, and therefore one column for each resonant frequency, the matrices identified have two columns for each resonant frequency. This is due to the structure of the identification, which allows *a priori* for each modal frequency an order of multiplicity equal to the size of the impedance matrix ( $n_\Gamma$  in general, 2 here). Nevertheless, when the number of hidden variables increases, the second columns goes to zero, and the multiplicity of each modal frequency to 1.

On Fig. 4.1, the hidden variables model obtained for 3 hidden variables is also drawn in dash-dotted blue line. The modal parameters of the models obtained for 1, 2, 3, and 4 hidden variables are described in Table 4.1, and the corresponding coupling matrices are listed in Table 4.2 and Table 4.3. It is interesting

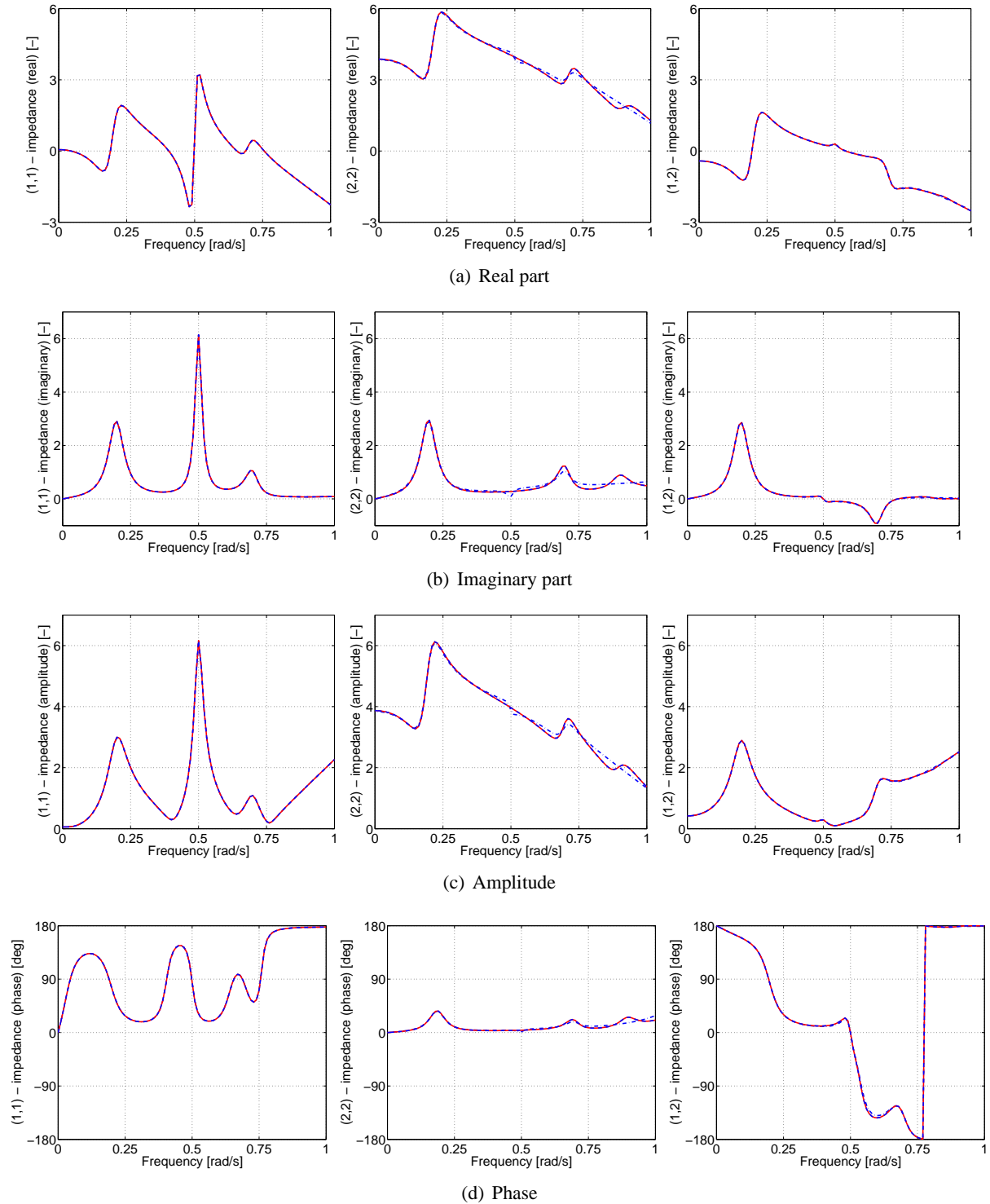


Figure 4.1: (a) Real part, (b) imaginary part, (c) amplitude, and (d) phase of the (1,1)-, (2,2)-, and (1,2)-elements of an example of impedance matrix (solid red line), and corresponding identified functions with 4 hidden state variables (dashed blue line), and 3 hidden state variables (dash-dotted blue line). The resonance frequencies of the input impedance are at 0.2, 0.4, 0.7, and 0.9 rad/s.

	$[D_c] (\times 10^{-2})$							
	$\omega_1$		$\omega_2$		$\omega_3$		$\omega_4$	
Input model	1.00	0	0.00	0	4.00	0	-3.00	0
	0.00	0	2.00	0	-4.00	0	2.00	0
1 HV	-19.31	1.40						
	-24.62	-60.44						
2 HVs	4.18	0.53	3.88	0.02				
	-2.65	-33.53	-6.89	-16.36				
3 HVs	1.04	-0.29	-0.01	0.00	-4.06	-0.25		
	0.20	19.07	-1.89	-12.98	4.89	-17.05		
4 HVs	1.00	0.00	0.00	0.00	-4.00	-0.00	-3.00	-0.00
	-0.00	-0.00	-2.00	0.00	4.00	-0.00	2.00	0.00
$B^*$ , 4 HVs	1.00	0.00	0.00	0.00	-4.00	-0.00	-3.00	-0.00
	-0.00	-0.00	-2.00	0.00	4.00	-0.00	2.00	0.00
$B_L$ , 2 HVs	1.01	0.06	0.01	0.00				
	-0.02	-3.77	-1.87	0.31				
$B_L$ , 4 HVs	1.00	-0.00	0.00	0.00	-4.00	0.00	-3.00	-0.08
	-0.00	0.00	-2.00	0.01	4.00	0.11	1.98	-0.50
$B_H$ , 2 HVs					-2.94	-0.04	-3.05	-0.35
					2.43	-0.04	2.31	0.49
$B_H$ , 4 HVs	1.01	2.59	-0.04	0.02	-4.01	-0.05	-3.00	-0.00
	-0.02	-12.70	-2.06	0.11	4.00	-0.24	2.00	0.00
(1,1), 4 HVs	1.00		0.00		-4.00		-3.00	
(1,1)-(2,2), 4 HVs	1.00	-0.00	-0.00	-0.00	-4.00	0.00	-3.00	-0.00
	0.00	-0.00	-0.00	2.00	0.00	4.00	-0.00	-2.00
$\alpha = 0.05$ , 3 HVs	0.29	0.00	-0.17	0.00	-5.48	0.00		
	1.30	0.00	-1.28	0.00	7.07	0.00		
$\alpha = 0.3$ , 3 HVs	9.93	3.21	4.93	0.00	-8.02	-0.33		
	-15.70	-49.90	-9.73	0.00	8.59	-3.89		
Non-diagonal $[\tilde{D}_h]$	-1.81	0.00	1.89	0.00	-4.00	-0.00	-3.00	-0.00
	-0.00	-0.00	-0.12	-0.00	4.00	-0.00	2.00	-0.00

Table 4.2: Coupling damping matrix,  $[D_c]$  of the input system and of the identified systems. The columns are organized so as to correspond to increasing modal frequencies, like in Table 4.1.

	$[K_c] (\times 10^{-1})$							
	$\omega_1$		$\omega_2$		$\omega_3$		$\omega_4$	
Input model	2.00	0	-3.00	0	-2.00	0	0.00	0
	2.00	0	0.00	0	2.00	0	2.00	0
1 HV	1.39	0.01						
	2.20	-0.25						
2 HVs	1.98	0.00	2.94	-0.00				
	2.03	-0.30	0.06	-0.37				
3 HVs	2.00	0.00	3.00	-0.00	2.01	-0.01		
	2.00	-0.09	0.01	-0.14	-1.95	-0.40		
4 HVs	2.00	0.00	3.00	-0.00	2.00	-0.00	-0.00	-0.00
	2.00	-0.00	0.00	-0.00	-2.00	-0.00	2.00	-0.00
$B^*$ , 4 HVs	2.00	0.00	3.00	-0.00	2.00	-0.00	0.00	0.00
	2.00	-0.00	0.00	-0.00	-2.00	-0.00	2.00	-0.00
$B_L$ , 2 HVs	2.00	0.00	3.03	-0.00				
	-2.00	-0.03	-0.03	-0.31				
$B_L$ , 4 HVs	2.00	0.00	3.00	0.00	2.00	-0.00	0.00	0.00
	2.00	-0.00	-0.00	-0.00	-2.00	-0.04	2.00	-0.06
$B_H$ , 2 HVs					2.74	-0.18	0.00	-0.07
					-1.92	-1.27	2.01	-0.02
$B_H$ , 4 HVs	1.97	0.01	3.02	0.00	2.00	-0.00	-0.00	-0.00
	2.02	-0.05	0.01	-0.16	-2.00	-0.01	2.00	0.00
(1,1), 4 HVs	2.00		3.00		2.00		-0.00	
(1,1)-(2,2), 4 HVs	2.00	-0.00	3.00	-0.00	2.00	-0.00	0.00	0.00
	-0.00	-2.00	-0.00	0.00	-0.00	-2.00	-0.00	-2.00
$\alpha = 0.05$ , 3 HVs	2.00	0.00	2.98	0.00	1.98	0.00		
	2.03	0.00	0.05	0.00	-1.92	0.00		
$\alpha = 0.3$ , 3 HVs	1.97	0.04	2.95	0.00	0.36	-0.03		
	1.94	-1.01	0.17	0.00	-0.10	-0.71		
Non-diagonal $[\tilde{D}_h]$	2.00	0.00	2.99	-0.00	2.00	-0.00	0.00	0.00
	2.00	-0.00	-0.01	-0.00	-2.00	-0.00	2.00	-0.00

Table 4.3: Coupling stiffness matrix,  $[K_c]$  of the input system and of the identified systems. The columns are organized so as to correspond to increasing modal frequencies, like in Table 4.1.

to note that each additional modal frequency is identified almost perfectly when an additional hidden variable is introduced. Although this is not a general behavior, it shows that the identification algorithm works well for the estimation of these parameters. Likewise, the coupling stiffness matrix goes smoothly toward the correct value when the number of hidden variables increases. However, for the coupling damping matrix, strong residuals remain until the perfect identification is encountered. This seems to show that this matrix is very sensitive to small changes in the impedance matrix, and should be monitored in the case of noisy data. Particularly, these high values of the extra-diagonal terms of the damping matrix may make it non-positive, *e.g.* for the identification with 1 and 2 hidden variables. Finally, it should be noted that the CPU time does not necessarily increase with the number of hidden variables. Indeed, as we are using an iterative algorithm, the perfect situation often converges a lot faster than when fewer hidden variables are used.

### 4.4.2 Influence of the frequency band

In this section we try to see the influence of the frequency band and the sampling parameters on the accuracy of the identification. All the results are presented in Table 4.1, Table 4.2, Table 4.3, and on Fig. 4.2, where they can be compared to the original impedance. On this last figure, only the real part has been shown to save space. The graphs for the imaginary part, the amplitude and the phase are similar.

We therefore perform the identification of the same system but using data evaluated for different samples of frequency points. The results presented previously were all obtained for data at 101 points equally space on  $B_0 = [0,1]$  rad/s. We will use here  $B^*$  which has the same bounds as  $B_0$ , but only 11 equally spaced points,  $B_L = [0.8,1]$  rad/s with 21 equally spaced points, and  $B_H = [0,0.5]$  rad/s, with 51 equally spaced points. The number of points for the last two cases means that the frequency step is the same as for  $B_0$ .

When considering  $B^*$ , it can be seen that the algorithm performs very well, even with such a coarse grid. With fewer frequency points, though, the identification deteriorates very rapidly. Similarly, for limited frequency bands, the algorithm is able to retrieve the modes that are outside of the studied frequency band quite well. When the number of hidden variables is lower than 4, the algorithm only fits the modes that are inside the band.

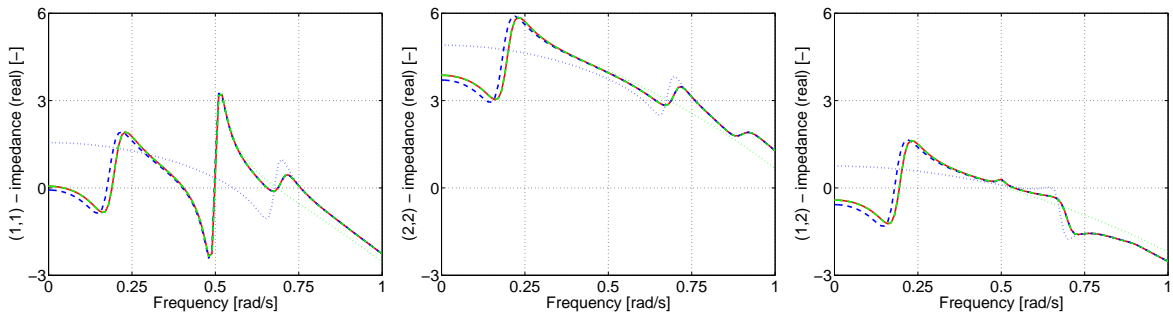


Figure 4.2: Real part of the (1,1)-, (2,2)-, and (1,2)-elements of the input impedance matrix (solid red line), and corresponding identified functions on  $B^*$  with 4 hidden variables (dotted magenta line), on  $B_L$  with 2 (dotted blue line) and 4 hidden variables (dashed blue line), and on  $B_H$  with 2 (dotted green line) and 4 hidden variables (dashed green line).

### 4.4.3 Influence of the number of impedance channels

In this section, we study the influence of the number of impedance channels used for the identification. Specifically, we perform the identification using only the element (1,1) of the impedance, on the one hand, and both elements (1,1) and (2,2), without the extra-diagonal terms, on the other hand. In both cases the modal frequencies and damping are evaluated perfectly, although visually the last mode does not show up on the drawing of element (1,1). In the first case, the first line of the coupling matrices is well retrieved and the second line is not identified. This seems logical as no data, neither on input nor on output, has been given on the second DOF. In the second case, the coupling matrices have the particularity to be  $2 \times 2$ -diagonal blocks, which means that, although the poles are shared, the two elements of the impedance are not coupled through  $[D_c]$  nor  $[K_c]$ . Again, this seems logical as we implicitly supposed, by not specifying it, that the element (1,2) of the impedance was zero.

### 4.4.4 Influence of noise

We try in this section to study the influence of noise on the data. We therefore generate a synthetic impedance matrix, by adding to the latter, independently at each frequency and for each element, a random value  $\alpha \times \mathbf{G}$ , where  $\alpha$  is 0.05 for the first case considered, and 0.3 in the second, and  $\mathbf{G}$  is a zero-mean unit-variance Gaussian random variable.

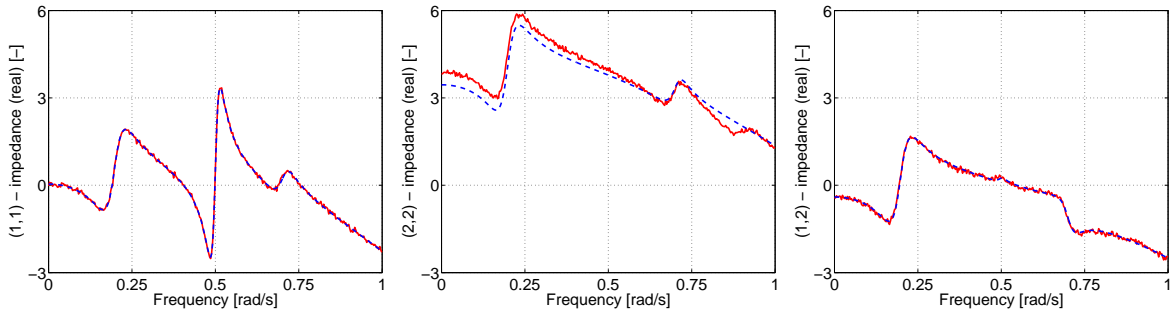


Figure 4.3: Real part of the (1,1)-, (2,2)-, and (1,2)-elements of the noisy input impedance matrix (solid red line), and corresponding identified functions (dashed blue line) in the case  $\alpha = 0.05$  (low noise).

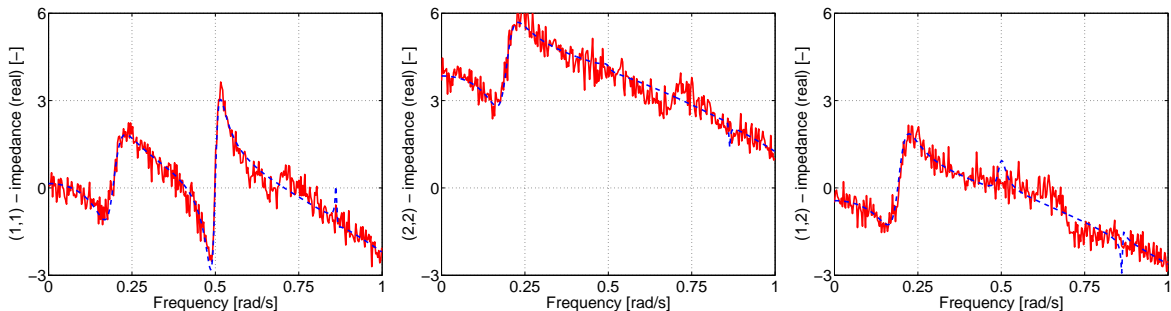


Figure 4.4: Real part of the (1,1)-, (2,2)-, and (1,2)-elements of the noisy input impedance matrix (solid red line), and corresponding identified functions (dashed blue line) in the case  $\alpha = 0.3$  (high noise).

For both cases, the results are quite inaccurate. The identification cannot be performed for 4 hidden variables, because it results in an unstable system, even for  $\alpha = 0.05$ . For 3 hidden variables, the modal frequencies are well identified, but the damping is rather erroneous. This results in a strange resonance in the identified impedance, particularly for  $\alpha = 0.3$ . The coupling damping matrices are also grossly inaccurate.

This inaccuracy in the identification method is due to our use of a Linear Least Squares (LLS) cost function, with an iterative scheme, that has trouble converging when fed with noisy data. A stochastic approach, where a model of the noise is introduced, would probably have been more appropriate here.

#### 4.4.5 Influence of non-diagonal damping

It should be noted that the matrices that have been chosen here for the input system are of the same form as those of the hidden state variables model (except a scaling of the hidden part), with a diagonal hidden part and no mass coupling. It was proved that any mechanical system defined by the set  $\{[\tilde{M}], [\tilde{D}], [\tilde{K}]\}$  could be put under this form, with no change in the impedance function, provided that the hidden part of  $[\tilde{D}]$  could be diagonalized in the same basis as the hidden parts of  $[\tilde{M}]$  and  $[\tilde{K}]$ . We try to study in this section what happens when such an hypothesis is not verified.

Let us consider the same matrices of mass  $[\tilde{M}]$  and stiffness  $[\tilde{K}]$  for the input system, now with the following damping matrix:

$$[\tilde{D}'] = \begin{bmatrix} 1 & .2 & 1 & 0 & 4 & -3 \\ & 4 & 0 & 2 & -4 & 2 \\ & & 70 & -20 & 0 & 0 \\ & & & 30 & 0 & 0 \\ \text{(sym.)} & & & & 60 & 0 \\ & & & & & 80 \end{bmatrix} \times 10^{-1}. \quad (4.38)$$

The only difference with the damping matrix used until now lies in its hidden part, which is non-diagonal. The impedance for this system  $\{[\tilde{M}], [\tilde{D}'], [\tilde{K}]\}$ , with respect to the first two DOFs, is computed and drawn on Fig. 4.5, again only for the real part.

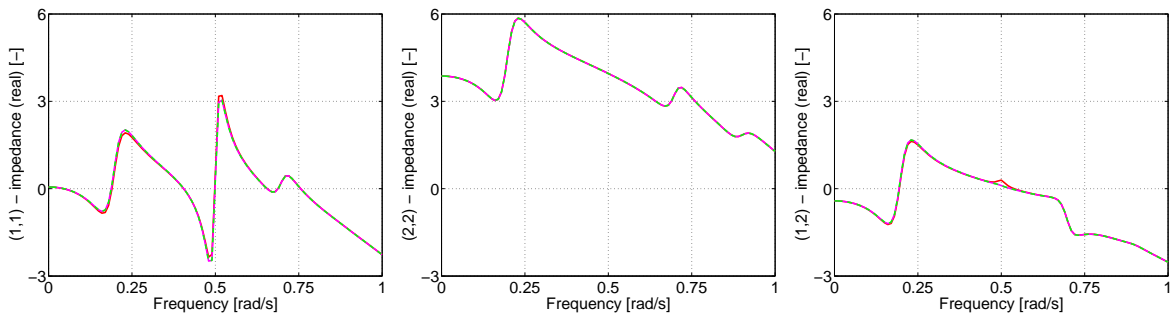


Figure 4.5: Real part of the (1,1)-, (2,2)-, and (1,2)-elements of the input impedance matrix for the original system (solid red line), for the system with non-diagonal  $[\tilde{D}_h]$  (solid magenta line), and for the hidden variables model identified from the latter (dashed blue line).

This modified impedance is used as input, and the corresponding hidden variables model is sought. It is interesting to note, on Fig. 4.5, that the identification is perfect, although we started from a system we

know not to verify the hypothesis for the diagonalization of  $[\tilde{D}_h]$ . The identified  $[\underline{D}]$ , and on a smaller scale  $[\underline{K}]$ , adjusted to meet the new system. This seems to indicate that the hypothesis we made is acceptable, although more research has to be done on this point to confirm it formally.

## 4.5 Summary

We presented in this section a method for the identification of the matrices of the hidden variables model,  $[\underline{M}]$ ,  $[\underline{D}]$  and  $[\underline{K}]$ , corresponding to an input impedance matrix, given by its values at a set of frequencies  $\{[Z(\omega_\ell)]\}_{1 \leq \ell \leq L}$ . This identification is performed in two steps: a general interpolation problem that can be solved by any of the many methods available in the literature, and the more specific construction of the matrices of mass, damping, and stiffness from the knowledge of the interpolated impedance. The latter step is performed analytically, while the second involves an approximation process.

The main inconvenient in separating the identification in such a manner is that, although the matrices of mass, damping and stiffness of the hidden variables model are known to be positive definite, this cannot be enforced during the interpolation process. In practice, this means that the result of the identification might be an unstable system, with negative elements on the diagonal of either  $[\underline{D}_h]$  or  $[\underline{K}_h]$ , or, more generally, that it might result in non-positive definite matrices. During the tests we ran, unstable systems arose only when the number of hidden variables was increased beyond that necessary for a good approximation of the impedance. It appeared that the interpolation method was then looking for poles with no physical significance, which resulted in an unstable identified system. In parallel, we often encountered non-positive definite damping matrices, for stable systems, even when the interpolation was visually almost perfect. This seems to be due to a particular sensitivity of the values of the damping matrix to very small errors on the imaginary part of the impedance, particularly in the low-frequency range, where it is close to zero. We tried to improve *a posteriori* the solution by fixing the poles and performing a LLS identification, using the exact cost function of Eq. (4.1) rather than the approximation of Eq. (4.2), but there was no noticeable amelioration. However, an appropriate choice of the weighting function  $w(\omega)$  in Eq. (4.2), forcing the identification to be very precise in the low frequency range seemed to resolve the issue in most cases.

These difficulties, due to our separation of the identification process into two steps, seem however to be balanced by the advantages of such a procedure. Indeed, it allows us to re-use the numerous methods available in the literature, selecting the most appropriate for each problem at hand. For example, for the identification of an impedance matrix measured experimentally, the interpolation method described here was shown to behave poorly. Another more appropriate approach could be used in that case for the interpolation part, without any modification of the second part of the identification process.

Another interesting issue that we did not investigate in this work is the influence of the size of the impedance matrix. By using more impedance channels, and therefore redundant information on the poles of the system, one expects to improve the accuracy of the identification. However this may result in important costs, as the method that we presented requires the construction of an orthonormal basis of vectors, the size of which depends heavily on the number of impedance channels used. Several methods exist to circumvent such difficulties, one of them being, for example, to consider only the highest terms of the Singular Value Decomposition (SVD) of the sum of the power spectra of the impedance matrix [Leuridan and Kundrat, 1982]. The accuracy of the Gram-Schmidt orthonormalization procedure would also have to be adequately monitored. Finally, a radical approach might be, as before, to use a method specifically designed for the purpose at hand, here the identification of large MDOF systems.

In conclusion, it should be noted that, although this identification method is described here only

with the goal of constructing a probabilistic model of the impedance matrix, its possible applications are numerous. Of particular interest to us, the use of the identified matrices for the design of nonlinear structures in SSI should be stressed. Indeed, the matrices of the hidden variables model are the same in the time domain as in the frequency domain, so that they can be used to model the influence of a (linear) soil on a nonlinear structure, the problem being solved in the time-domain. This will not be considered further here, and the next chapter concentrates on the construction of the probabilistic impedance matrix in SSI problems.



# Chapter 5

## Probabilistic models of the impedance matrix in Soil-Structure Interaction problems

In the previous chapters, we presented a general methodology to construct probabilistic models of the impedance matrix. The goal of this chapter is to particularize these concepts in the field of Soil-Structure Interaction. The first section is therefore concerned with the introduction of the vocabulary and conventions of that field, along with some specific methods used for the computation of soil impedance matrices. In the second section, we review some models and methods that were considered in the literature for the assessment of uncertainty in SSI problems. Particularly, the probabilistic treatment the soil parameters, and that of the seismic loading are discussed.

Finally, two applications will allow the reader to grasp the interest of our method: the first presents models of the probabilistic soil impedance matrix for a classical problem, and the second considers the influence of the randomness of the soil impedance matrix on the variability of the design variables for an industrial SSI problem. In the former, a circular embedded foundation in a layer of soil on a rigid bedrock is considered, and two probabilistic models of this problem are discussed: a SFE approach, and the nonparametric approach that was presented in this dissertation. In the latter problem, a realistic reactor-building is excited by a seismic wave, and the variability of the acceleration at the top of the building, due to the random soil impedance matrix, is studied.

### 5.1 Domain decomposition in Soil-Structure Interaction problems

In this section, we go over the general presentation of DD techniques that was given in the introduction (Sec. 1.1), and particularize it to the case of SSI. The modeling of the seismic loading is succinctly described, and the classical normalization scheme for the soil impedance matrix is presented. Finally, charts and lumped-parameter models, frequently used in practice, are introduced, as well as some notions about experimental measures of impedance matrices.

#### 5.1.1 Domain Decomposition approach to SSI

Let us consider the design problem of a building resting on a soil, and excited by a seismic wave (Fig. 5.1). Basically, the SSI can be defined as the acknowledgment that the dynamical behavior of that structure cannot be studied independently of the propagation of the seismic wave in the soil. Physically, when that wave reaches the structure, part of it is scattered, and part of it is stored in the structure, before it is either re-injected in the soil or dissipated. That means that the record of the ground motion in

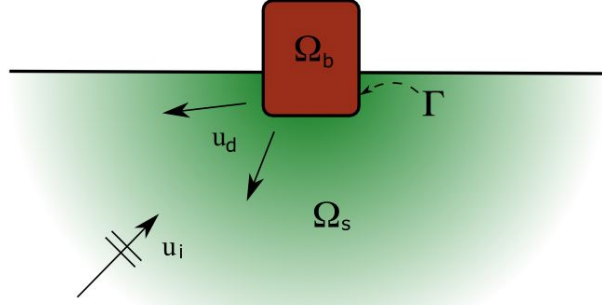


Figure 5.1: A typical soil-structure interaction problem: a building  $\Omega_b$  resting on a soil  $\Omega_s$ , and excited by a seismic wave. The displacement field in the soil  $\mathbf{u}$  is usually decomposed in an incident displacement field  $\mathbf{u}_i$  and a scattered displacement field  $\mathbf{u}_d$ , such that  $\mathbf{u} = \mathbf{u}_i + \mathbf{u}_d$ .

the free-field (far from any building) will be substantially different from that at the base of the building, in terms of amplitude, frequency-content, and duration. In terms of frequency-content, the resonance frequencies of the soil and the structure may be close, so that the global resonance frequency of the coupled system generally depends on both. When these resonance frequencies are far-apart, for example when the soil is stiff and the building light, then the effects of SSI are negligible and the study of the propagation of the seismic wave in the soil and that of the dynamical behavior of the structure can be performed independently.

The effects of SSI have been studied extensively and are now well understood. General introductions can be found in Wolf [1985], Clouteau [2000], and Pecker [2006, Chap. 10]. In these references, the SSI problem is treated in the frequency domain, and the soil is considered linear, which is an arguable assumption for strong motions excitation. Nevertheless, this approach is often used as it allows a resolution in terms of the superposition of simpler problems. Linear equivalent approaches have been developed [Pitilakis et al., 2005, Pitilakis, 2006], but the full consideration of the nonlinear character of the soil has to be performed in the time domain, as described in Wolf [1988]. Details and examples concerning the computational aspects of the SSI problems can be found in Clouteau and Aubry [2001].

The rest of this section concentrates on the detailing, in the particular case of a SSI problem, of the equations of the DD technique, described succinctly in Sec. 1.1.1. We use the same notations as in Eq. (3.1), and particularize the fields, tensors, and mechanical parameters, by superscripts "s" for the soil, and "b" for the building. All the displacement fields considered in the following equations verify homogeneous Neumann conditions on the non-coupling part of the boundary of their domain of definition, which is the interface between that domain and air. Specifically, we have

$$\begin{cases} \sigma_{ij}^s(\mathbf{u}_\alpha) n_j = 0 & \text{on } \partial\Omega_s \setminus \Gamma, \text{ for } 1 \leq i \leq 3 \\ \sigma_{ij}^b(\mathbf{u}_\beta) n_j = 0 & \text{on } \partial\Omega_b \setminus \Gamma, \text{ for } 1 \leq i \leq 3 \end{cases} \quad (5.1)$$

where  $\alpha \in \{s, inc, d, s\phi\}$ ,  $\beta \in \{b, b\phi, \psi\}$ , and the corresponding displacement fields are described further along. These equations will not be repeated in the following derivations.

We start with the consideration of the soil subdomain,  $\Omega_s$ . The total displacement field on that

domain is denoted by  $\mathbf{u}_s$ , and verifies

$$\begin{cases} \sigma_{ij,j}^s(\mathbf{u}_s) + \rho^s \omega^2 u_{si} = 0 & \text{in } \Omega_s, \text{ for } 1 \leq i \leq 3 \\ \mathbf{u}_s = \phi & \text{on } \Gamma \end{cases}, \quad (5.2)$$

where the displacement field on the boundary,  $\phi$ , is supposed to be given. The soil is excited by an incident seismic field, that is denoted  $\mathbf{u}_{\text{inc}}$ , and verifies

$$\sigma_{ij,j}^s(\mathbf{u}_{\text{inc}}) + \rho^s \omega^2 u_{\text{inc}i} = 0 \text{ in } \Omega_s, \text{ for } 1 \leq i \leq 3. \quad (5.3)$$

Physically, this field represents the displacement in the soil due to an earthquake in the free-field, far from any structure. In practice, it is defined by its value on the surface of the same soil, but without the structure. The total displacement in the soil is then decomposed as  $\mathbf{u}_s = \mathbf{u}_{\text{inc}} + \mathbf{u}_d + \mathbf{u}_{s\phi}$ , where  $\mathbf{u}_d$  is called the local scattered field,  $\mathbf{u}_{s\phi}$  is the radiated field, and  $\mathbf{u}_d + \mathbf{u}_{s\phi}$  is the scattered field.  $\mathbf{u}_d$  represents the part of the scattered field arising from a seismic wave hitting a fixed boundary  $\Gamma$ , and  $\mathbf{u}_{s\phi}$  the scattered field due to the displacement of the boundary  $\phi$ . They verify, respectively,

$$\begin{cases} \sigma_{ij,j}^s(\mathbf{u}_d) + \rho^s \omega^2 u_{di} = 0 & \text{in } \Omega_s, \text{ for } 1 \leq i \leq 3 \\ \mathbf{u}_d = -\mathbf{u}_{\text{inc}} & \text{on } \Gamma \end{cases}, \quad (5.4)$$

and

$$\begin{cases} \sigma_{ij,j}^s(\mathbf{u}_{s\phi}) + \rho^s \omega^2 u_{s\phi i} = 0 & \text{in } \Omega_s, \text{ for } 1 \leq i \leq 3 \\ \mathbf{u}_{s\phi} = \phi & \text{on } \Gamma \end{cases}. \quad (5.5)$$

The impedance operator  $\mathcal{Z}^s$  is then defined, for the radiated field, which is the field that arises from a displacement of the boundary, as

$$\langle \mathcal{Z}^s \phi, \delta \phi \rangle_\Gamma = \int_\Gamma \sigma_{ij}^s(\mathbf{u}_{s\phi}) \delta \phi_i n_j dS. \quad (5.6)$$

This definition is similar to that in Eq. (3.11). The superposition of the local scattered field and of the incident field, which stirs no displacement of the boundary, is used to define an equivalent loading  $\mathbf{f}$  on the boundary, as

$$\langle \mathbf{f}, \delta \phi \rangle_\Gamma = - \int_\Gamma \sigma_{ij}^s(\mathbf{u}_{\text{inc}} + \mathbf{u}_d) \delta \phi_i n_j dS. \quad (5.7)$$

By projection in appropriate bases, usually that of the rigid body displacements of the boundary, and as described in Sec. 3.1.1, the impedance operator is approximated by an impedance matrix  $[Z^s(\omega)]$ , and the equivalent seismic loading by a vector  $[F^s]$ . The computation of the impedance operator and the equivalent seismic loading are represented in Fig. 5.2, respectively on the second and first steps of the decomposition.

With respect to the building, we similarly introduce the total displacement field  $\mathbf{u}_b$ , which verifies

$$\begin{cases} \sigma_{ij,j}^b(\mathbf{u}_b) + \rho^b \omega^2 u_{bi} = 0 & \text{in } \Omega_b, \text{ for } 1 \leq i \leq 3 \\ \mathbf{u}_b = \phi & \text{on } \Gamma \end{cases}. \quad (5.8)$$

This displacement field is then classically decomposed into a fixed-interface displacement field  $\mathbf{u}_{b\psi}$  and a lift  $\mathbf{u}_{b\phi}$ , for which there is a displacement of the boundary, but no inertial forces induced in the building. These fields verify

$$\begin{cases} \sigma_{ij,j}^b(\mathbf{u}_{b\phi}) = 0 & \text{in } \Omega_b, \text{ for } 1 \leq i \leq 3 \\ \mathbf{u}_{b\phi} = \phi & \text{on } \Gamma \end{cases}. \quad (5.9)$$

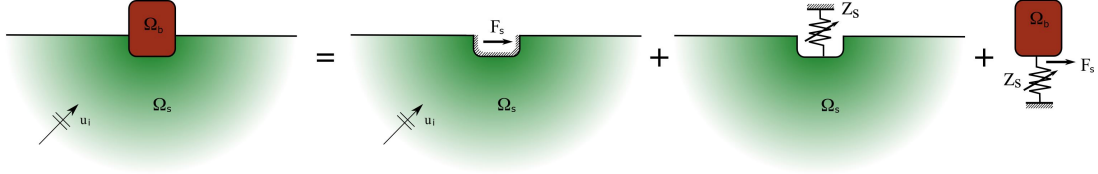


Figure 5.2: Decomposition of the SSI problem: computation of the equivalent seismic load  $\mathbf{F}^s$ , computation of the soil impedance  $[Z_s]$ , and resolution of the global problem on the structure.

and

$$\begin{cases} \sigma_{ij,j}^b(\mathbf{u}_\psi) + \rho^b \omega^2 u_{\psi i} = -\rho^b \omega^2 u_{b\phi i} & \text{in } \Omega_b, \text{ for } 1 \leq i \leq 3 \\ \mathbf{u}_\psi = 0 & \text{on } \Gamma \end{cases}, \quad (5.10)$$

For a rigid foundation, the static lift displacement field  $\mathbf{u}_{b\phi}$  typically corresponds to a rigid body displacement field of the entire building.

In the introduction (Sec. 1.1.1), we indicated that the impedance operator of each of the subdomain was computed, and that the global problem was then solved only on the interface. However, in SSI problems, the engineers are interested in post-treating the response inside the building, while the response in the soil is usually the subject of less attention. The global problem is therefore solved directly in the building, and the impedance operator and the equivalent seismic loading, defined on the boundary, are used as a particular type of boundary conditions. This situation is described in the rightmost part of the Fig. 5.2. The displacement field  $\mathbf{u}_b$  can be approximated in a finite dimensional Hilbert basis, compatible with that used for the soil impedance matrix and the equivalent seismic load vector. The corresponding stiffness, damping and mass sesquilinear forms are then approximated by matrices of mass  $[M^b]$ , damping  $[D^b]$  and stiffness  $[K^b]$ , as is described in Sec. 3.1.1. The problem can then be rewritten, separating the DOFs of the boundary from those of the interior of the building, and using the subscripts "Γ" and "h" to identify them, as

$$\begin{bmatrix} [S_\Gamma^b(\omega)] + [Z^s(\omega)] & [S_c^b(\omega)] \\ \text{(sym.)} & [S_h^b(\omega)] \end{bmatrix} \begin{bmatrix} [\mathbf{u}_\Gamma] \\ [\mathbf{u}_h] \end{bmatrix} = \begin{bmatrix} [\mathbf{F}^s] \\ [0_{n_h^b, 1}] \end{bmatrix} \quad (5.11)$$

where the superscripts "b" and "s" still refer, respectively, to the building and the soil,  $n_h^b$  is the number of eigenmodes used in the expansion of the fixed-base displacement field inside the building, and  $[S_\alpha^b(\omega)] = -\omega^2 [M_\alpha^b] + i\omega [D_\alpha^b] + [K_\alpha^b]$ , for  $\alpha \in \{\Gamma, c, h\}$ . The resolution of this matrix system yields directly the displacements inside the building.

### 5.1.2 Kinematic and Inertial interaction in SSI problems

An alternative approach to this formulation of the SSI problem comes from observing the influence of two physical phenomena: the Kinematic Interaction, and the Inertial Interaction. As the soil and the foundation have different stiffnesses, they tend to distort in different manners. The incident field in the soil is therefore filtered to meet the kinematical conditions imposed by the vicinity of the foundation. This filtering effect is known as Kinematic Interaction. Consider for example a rigid foundation: its presence imposes constraints on the possible relative displacements of the soil at two points on the soil-foundation boundary  $\Gamma$  (Fig. 5.1), and therefore yields a displacement field in the soil that is often quite different from that which would prevail in the absence of the foundation. In addition, the vibration of the

excited building generates inertial forces on the foundation, and eventually gives rise to more waves in the soil: this is the Inertial Interaction effect.

In practice, the kinematic interaction is defined as the movement that the foundation would undergo, were it to be massless and rid of the building. It is entirely defined by the vector  $[c_0(\omega)]$ , such that

$$[Z^s(\omega)][c_0(\omega)] = [F^s(\omega)]. \quad (5.12)$$

For surface foundations excited by a vertically propagating incident wave, there is no kinematic interaction, because the displacement field in the soil is compatible with the rigidity of the foundation, and hence the vector  $[c_0(\omega)]$  is directly the vector of the free-field displacements on the boundary. Otherwise,  $[c_0(\omega)]$  is the projection on a basis compatible with the kinematics of the foundation of that vector of free-field displacements on the boundary, oftentimes the basis of rigid body displacements of the foundation.

This definition of the kinematic interaction allows us to redefine the problem of Eq. (5.11) as a problem with imposed displacements, by eliminating  $[F^s(\omega)]$  using Eq. (5.12) and introducing  $[c] = [u_\Gamma] - [c_0(\omega)]$ . This yields

$$\begin{bmatrix} [S_\Gamma^b(\omega)] + [Z^s(\omega)] & [S_c^b(\omega)] \\ \text{(sym.)} & [S_h^b(\omega)] \end{bmatrix} \begin{bmatrix} [c] \\ [u_h^b] \end{bmatrix} = -[S^b(\omega)] \begin{bmatrix} [c_0(\omega)] \\ [0_{n_h^b,1}] \end{bmatrix}, \quad (5.13)$$

and  $[c]$  is the response of the building, in a moving frame characterized by  $[c_0(\omega)]$ , with imposed displacement at its base and with additional (frequency-dependent) stiffness on its foundation.

### 5.1.3 The impedance matrix in SSI problems

In most SSI problems, the foundations are rigid, and there are two horizontal axes of symmetry. A rigid embedded rectangular foundation in a horizontally layered soil is an example of such a symmetrical problem. This means that the impedance matrix, in the basis of the rigid body movements of the soil-structure interface, is not full. More precisely, only the diagonal terms, and the coupling terms between the horizontal translation along one of the axis of symmetry and the rotation around the other one, are non-zero. Denoting the axes x-axis and y-axis, the six diagonal terms of the impedance matrix are called x-shaking, y-shaking, pumping, x-rocking, y-rocking, and torsion. The coupling term between the translational movement along the x-axis and the rotation around the y-axis is called x-shaking-y-rocking coupling, and its counterpart y-shaking-x-rocking coupling. Furthermore, in all the (deterministic) examples that are studied in this dissertation, the foundation and the soil are axisymmetrical. In that case, the equivalence between the x-axis and the y-axis allows us to consider only five non-zero different terms, that are denoted simply shaking, pumping, rocking, torsion, and shaking-rocking coupling. The impedance matrix is then written

$$[Z(\omega)] = \begin{bmatrix} Z_s(\omega) & 0 & Z_{sr}(\omega) & 0 \\ & Z_p(\omega) & 0 & 0 \\ & & Z_r(\omega) & 0 \\ \text{(sym.)} & & & Z_t(\omega) \end{bmatrix}, \quad (5.14)$$

where  $Z_s(\omega)$ ,  $Z_p(\omega)$ ,  $Z_r(\omega)$ ,  $Z_t(\omega)$ , and  $Z_{sr}(\omega)$  are, respectively, the shaking, pumping, rocking, torsion, and shaking-rocking coupling elements.

When dealing with realizations of a random impedance matrix, these considerations are not true anymore. From a mathematical point of view, the realizations of the mass, damping and stiffness matrices

that are drawn using the nonparametric method are full, so that the corresponding impedance matrix is also *a priori* full. From a more physical point of view, what we are trying to see with these probabilistic models is, among other things, the influence of a possible inhomogeneity of the mechanical parameters. We cannot, with the nonparametric approach, observe that non-uniformity at the level of the parameters, but we still expect to get full impedance matrices. Furthermore, the inhomogeneity of the mechanical parameters in the soil means that the x-axis and the y-axis are not equivalent, so that we should really consider that the x-shaking and y-shaking, as well as the corresponding rocking and shaking-rocking coupling terms, are different for each sample of the random impedance matrix. Nevertheless, as the same information is given for each pair of terms for the construction of the probabilistic model, they should be statistically equivalent. The random impedance matrix is then written

$$[\mathbf{Z}(\omega)] = \begin{bmatrix} \mathbf{Z}_s(\omega) & \mathbf{Z}_{ss'}(\omega) & \mathbf{Z}_{sp}(\omega) & \mathbf{Z}_{sr}(\omega) & \mathbf{Z}_{sr'}(\omega) & \mathbf{Z}_{st}(\omega) \\ & \mathbf{Z}_{s'}(\omega) & \mathbf{Z}_{s'p}(\omega) & \mathbf{Z}_{s'r}(\omega) & \mathbf{Z}_{s'r'}(\omega) & \mathbf{Z}_{s't}(\omega) \\ & & \mathbf{Z}_p(\omega) & \mathbf{Z}_{pr}(\omega) & \mathbf{Z}_{pr'}(\omega) & \mathbf{Z}_{pt}(\omega) \\ & & & \mathbf{Z}_r(\omega) & \mathbf{Z}_{r'r'}(\omega) & \mathbf{Z}_{rt}(\omega) \\ & \text{(sym.)} & & & \mathbf{Z}_{r'}(\omega) & \mathbf{Z}_{r't}(\omega) \\ & & & & & \mathbf{Z}_t(\omega) \end{bmatrix}. \quad (5.15)$$

As we will consider in this chapter both deterministic and probabilistic models of the impedance matrix, we will discuss and plot not only the five terms mentioned in Eq. (5.14), but also the shaking-pumping coupling element  $\mathbf{Z}_{sp}(\omega)$ . We expect it to be zero at all frequencies for deterministic models, and possibly non-zero for probabilistic models. We will not plot separately the x-shaking and y-shaking (neither the corresponding rocking terms) because they are statistically equivalent, and neither additional extra-diagonal terms to avoid an overloading in the presentation. However, even though only six terms are plotted, all the samples of the impedance matrix that are drawn in the applications in Sec. 5.3.1 and Sec. 5.4 are full matrices in the form of Eq. (5.15).

For a more uniform presentation of the results in this chapter, and for easier comparisons, it is customary to normalize all the impedance matrices with a constant matrix  $[K_0]$ , called the static stiffness matrix. Also, it is classical to consider a normalized frequency  $a_0 = \omega c_s / r$ , where  $c_s$  is the shear velocity in the top layer of soil, and  $r$  is the radius of the foundation. Within a class of problems, this double normalization allows for easier comparisons of impedance matrices on soils with different mechanical properties. It should be noted that this is usually done term by term in the literature, concealing the non-diagonal feature of the matrix. We choose here a slightly different normalization in the form

$$[Z(a_0)] = [K_0]^{1/2} ([K(a_0)] + i[C(a_0)]) [K_0]^{1/2}, \quad (5.16)$$

where  $[K_0]$  is a diagonal matrix whose elements are computed using Table 5.1. Although it is recalled for comparisons with results of the literature, the last line of Table 5.1 is therefore not used. The quantities that will be plotted, and discussed, in this chapter are therefore the elements of the matrices  $[K(a_0)]$ , and  $[C(a_0)]$ , called respectively the stiffness and damping coefficients. These coefficients matrices should not be confused with the stiffness and damping matrices of the hidden variables model of the corresponding impedance. They inherit the structure of the impedance matrix, so that only the six terms described above will be considered for each of them. The values in Table 5.1, commonly accepted in the SSI community, are approximations of the elements of the actual static stiffness matrix, so that we expect the diagonal elements of  $[K(a_0 = 0)]$  to be close to unity. Also, the causality condition implies that the imaginary part of the impedance matrix cancels for  $\omega = 0$ , so that we should have  $[C(a_0 = 0)] = [0_6]$ .

In many applications in SSI problems, it is customary to model the soil using hysteretic damping, which induces a non-causal behavior of the impedance matrix. This is the case, in particular, for the

	Surface foundation	Embedded foundation
Shaking	$\frac{8Gr}{2-\nu}$	$\frac{8Gr}{2-\nu}(1 + \frac{r}{2H})(1 + \frac{2D}{3r})(1 + \frac{5D}{4H})$
Pumping	$\frac{4Gr}{1-\nu}$	$\frac{4Gr}{1-\nu}(1 + 1.28\frac{r}{H})(1 + \frac{D}{2r})(1 + (0.85 - 0.28\frac{D}{r})\frac{D/H}{1-D/H})$
Rocking	$\frac{8Gr^3}{3(1-\nu)}$	$\frac{8Gr^3}{3(1-\nu)}(1 + \frac{r}{6H})(1 + \frac{2D}{r})(1 + 0.7\frac{D}{H})$
Torsion	$\frac{16Gr^3}{3}$	$\frac{16Gr^3}{3}(1 + 2.67\frac{D}{r})$
Coupling	$\frac{8Gr^2}{2-\nu}$	$0.40\frac{8Gr}{2-\nu}(1 + \frac{r}{2H})(1 + \frac{2D}{3r})(1 + \frac{5D}{4H})D$

Table 5.1: Values of the elements of the static stiffness matrix  $[K_0]$  for a rigid circular surface and embedded foundations.  $G$  is the shear modulus,  $\nu$  is Poisson's ratio,  $r$  is the radius of the foundation,  $H$  is the height of the first layer, and  $D$  is the embedment height.

software MISS [Clouteau, 2003], that will be used further along. In order to still be able to analyze the results of these computations, and compare them with other results, a complex static stiffness matrix  $[K_0^*]$  is often considered, which replaces  $[K_0]$  in Eq. (5.16) by

$$[K_0^*] = [K_0](1 + i[\beta]), \quad (5.17)$$

where  $[\beta]$  a diagonal matrix in  $\mathbb{M}_4^S(\mathbb{R})$ , such that the diagonal elements of the damping coefficients matrix be zero at  $a_0 = 0$ . This is a straight generalization of the normalization of the impedance matrix in one-dimensional systems, and it is not perfectly adapted to multi-dimensional settings. Indeed, with such a choice of  $[\beta]$ , the imaginary part of the extra-diagonal terms of the impedance matrix will not necessarily cancel at the origin. However, for the simplicity of this choice, and because the hysteretic coefficients are usually close for all the elements of the impedance matrix, we will stick to that classical scheme. It should also be noted that, for the construction of a parametric model of the impedance matrix in Sec. 5.3, each realization will correspond to different mechanical properties. Hence, the matrix  $[\beta]$  may be different for each of them, and the diagonal elements of  $[C(a_0)]$  will all start at the origin. However,  $[K_0]$  will be fixed for all trials, so that there will be variations around the mean static value.

#### 5.1.4 Computation of the impedance matrix in SSI problems

In Sec. 3.1.2, several general computational methods were described for impedance matrices, among which FE and BE methods. These methods are also used in SSI problems, and we will particularly show results obtained with MISS, a BE software, developed at the MSSMat Laboratory by Clouteau [2003] and coworkers. However, in this section, we will concentrate on methods that are specific to SSI: Sieffert and Cevaer [1992] charts, lumped-parameter models, and experimental measures.

#### Charts

It is common in civil engineering, in order to simplify the work of the designers, to provide them with charts for the soil impedance matrix. This allows them to take into account, in a simplified way, the influence of the behavior of the soil on that of the building. In Sieffert and Cevaer [1992] handbook of impedance functions, several important configurations of the layers and foundation are considered, and, for each of them, the stiffness and damping coefficients are provided in the form of charts, for a given set of geometrical and mechanical parameters. The static stiffness, and the hysteretic damping can be

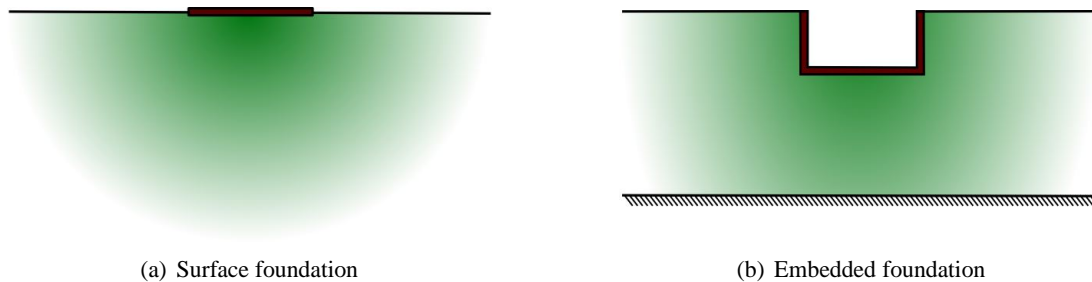


Figure 5.3: (a) A surface foundation over a homogeneous space, and (b) an embedded foundation over a homogeneous layer on rigid bedrock. The proportions for the radius of the foundation  $r$ , the embedment  $D$  and the height of the layer  $H$  are those used for the examples of this dissertation, namely  $H/r = 3$ , and  $D = r$ .

introduced separately, if desired. The data of these charts was compiled from several literature papers, so that it represents a common knowledge of the SSI community.

As an example, we consider here two settings: a circular surface foundation on a homogeneous space, and a circular embedded foundation in a layer of soil on rigid rock (see Fig. 5.3). In the second case, the height of the layer is three times the embedment, the embedment is equal to the radius of the foundation, and in both cases, Poisson's ratio is  $\nu = 1/3$ . In Fig. 5.4 to 5.7, the stiffness and damping coefficients for these two cases are drawn, and compared with the results of other methods. Other configurations that are considered in the handbook are surface and embedded square, rectangular, and strip foundations on homogeneous space.

As these charts are derived from papers in the literature, they also inherit their errors. For example, in Fig. 5.6 and Fig. 5.6, the rocking element of the impedance matrix is limited in frequency to  $a_0 < 3$ , while all other terms are drawn up to  $a_0 = 6$ , which originates in a scaling error in Kausel [1974], that was copied in Sieffert and Cevaer [1992].

### Lumped parameter models

Another approach in providing the engineers with simple means of computing soil impedance matrices consists in identifying lumped-parameter models. This means replacing the soil by a set of springs, dampers, and masses, assembled in an appropriate way, so that the impedance of the dynamical system that is obtained is close to that of the soil. The most basic models of this type introduced only a spring and a damper in parallel, so that they could not represent resonance behaviors, but many more accurate models were introduced over the years. Once the structure of a lumped-parameter model has been decided upon, the coefficients of the springs, dampers and masses have to be provided. Much like the charts seen above, these coefficients are given in tables for different configurations of the soil, and are usually computed by minimization of the difference of impedance of the supposed lumped parameter and the value of an impedance recognized as correct in the SSI community.

These models are usually constructed independently for each element of the impedance matrix, and suppose that the shaking-rocking coupling term is negligible. In Wolf and Somaini [1986] and de Barros and Luco [1990], for each element of the impedance matrix, one internal DOF is considered besides that of the boundary. In Jean et al. [1990], two internal DOFs are used. For these three examples, and for each element of the impedance matrix, the matrices of mass, damping and stiffness are, respectively, in the

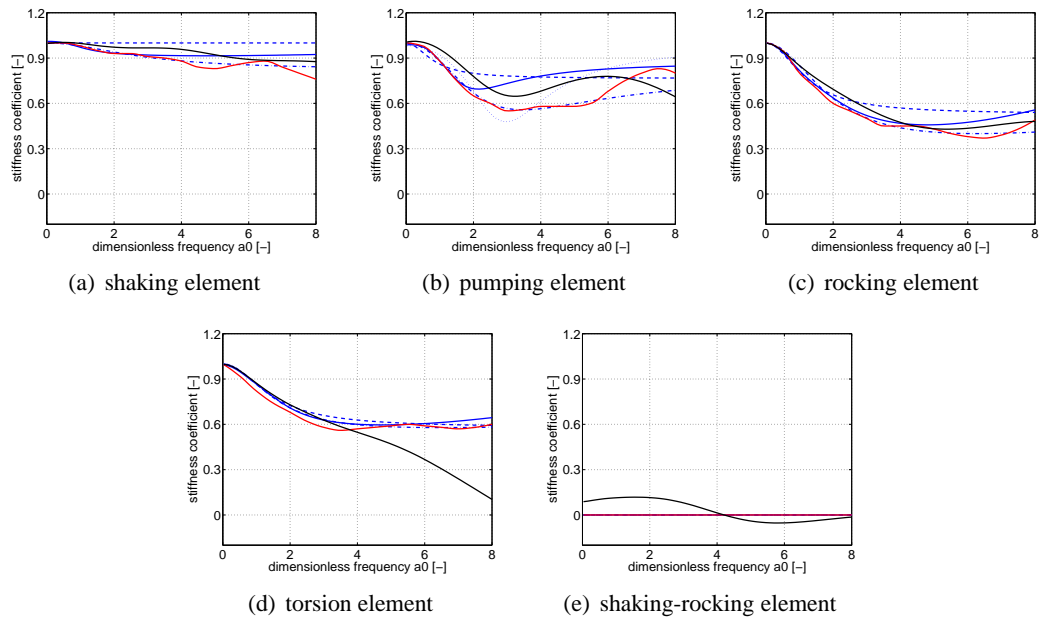


Figure 5.4: Stiffness coefficients of the soil impedance matrix computed with MISS (solid black line), Sieffert and Cevaer [1992] charts (solid red line), and the lumped parameter models of Wolf and Somaini [1986] (dashed blue line), Wu and Lee [2002] (dash-dotted blue line), Jean et al. [1990] (solid blue line), and de Barros and Luco [1990] (dotted blue line, only for pumping).

form

$$[M] = \begin{bmatrix} m_0 & 0 \\ 0 & m_1 \end{bmatrix}, [D] = \begin{bmatrix} d_0 & -d_1 \\ -d_1 & d_1 \end{bmatrix}, \text{ and } [K] = \begin{bmatrix} k & 0 \\ 0 & 0 \end{bmatrix}, \quad (5.18)$$

$$[M] = \begin{bmatrix} m_0 & 0 \\ 0 & m_1 \end{bmatrix}, [D] = \begin{bmatrix} d_0 & -d_1 \\ -d_1 & d_1 \end{bmatrix}, \text{ and } [K] = \begin{bmatrix} k_1 & -k_2 \\ -k_2 & k_2 \end{bmatrix}, \quad (5.19)$$

and

$$[M] = \begin{bmatrix} 0 & 0 & 0 \\ 0 & m_1 & 0 \\ 0 & 0 & m_2 \end{bmatrix}, [D] = \begin{bmatrix} d_1 + d_3 & -d_1 & -d_3 \\ -d_1 & d_2 & -d_5 \\ -d_3 & -d_5 & d_4 \end{bmatrix}, \text{ and } [K] = \begin{bmatrix} k_1 + k_3 & -k_1 & -k_3 \\ -k_1 & k_2 & 0 \\ -k_3 & 0 & k_4 \end{bmatrix}, \quad (5.20)$$

where the first lines and columns of the matrices relate to the DOF on the boundary, and all the coefficients have to be provided for each configuration of the soil and foundation. The fact that the structure of the matrices is chosen beforehand limits the applicability of these methods to particular cases, and generally to narrow bands of frequency, because they cannot capture multiple resonances (see, for example, the case described in Fig. 5.6). Also, the choice of a particular setting over another is often left unexplained.

In Wolf [1991b], a more general approach is developed. The impedance function is expanded in a pole-residue form, and each term of that expansion is modeled by a basic lumped-parameter element. These basic elements can be added in series so as to allow for virtually any degree of refinement of the impedance function. This aspect is very similar to the hidden variables model, where each internal DOF corresponds to a term in the pole-residue expansion of the impedance matrix. In Wolf [1991b], the non-uniqueness issues that were described in Sec. 4.3.1 are also brought up, but in a limited context, and, for one element of the impedance matrix, several equivalent sets of matrices are described. The theory described in this paper was applied and refined<sup>1</sup> in following papers [Wolf, 1991a, Wolf and Paronesso, 1992]

An important drawback with most of these models is that they do not consider the shaking-rocking coupling term. This is a good approximation for surface foundations on homogeneous soils, for example, but not as good for embedded foundations. In Wolf and Somaini [1986], and in subsequent lumped-parameter models by the same group, this coupling is treated in a geometrical manner. An eccentricity, which is really the embedment, is introduced, and the basic models for the three corresponding elements of the impedance matrix (two on the diagonal and one extra-diagonal) are mixed in an appropriate way. This treatment is possible when considering the coupling between only two elements, but seems more complicated if more terms were to be involved.

These difficulties with the shaking-rocking coupling element are rooted in the fact that these lumped-parameter models do not recognize the non-scalar feature of the impedance matrix, and that each of its elements is modeled independently. This means that, when computing the coefficients of the matrices of mass, damping and stiffness, by inverse analysis, the global character of the resonance frequencies is not used, which may result in poorer approximation. More importantly, this means that the consideration of flexible foundations, where all terms of the impedance matrix are coupled, is not possible with these models. Finally, all these papers mention the fact that some of the springs, dampers or masses, have negative coefficients, which seems to go against the physical basis of these lumped-parameter models. Indeed, when considering matrices rather than elements, then these negative coefficients are acceptable as long as the matrices remain positive-definite.

As a conclusion on these lumped-parameter models, it should be mentioned that their main advantage over other simplified methods, charts for example, is that they can readily be used in the time domain.

<sup>1</sup>An error in the formulas of this paper is corrected in Wolf and Paronesso [1991].

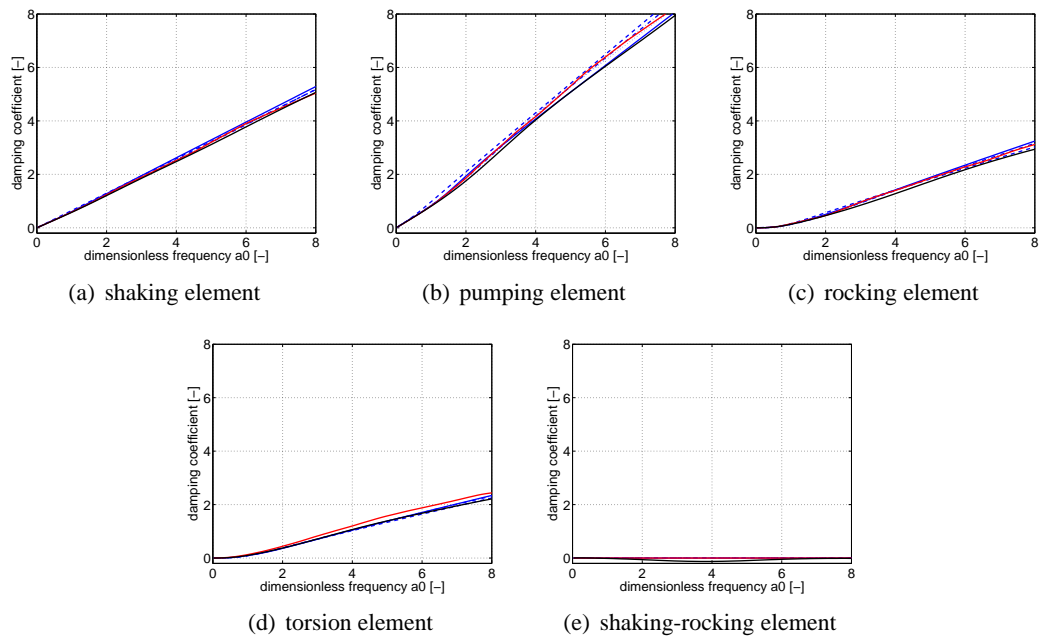


Figure 5.5: Damping coefficients of the soil impedance matrix computed with MISS (solid black line), Sieffert and Cevaer [1992] charts (solid red line), and the lumped parameter models of Wolf and Somaini [1986] (dashed blue line), Wu and Lee [2002] (dash-dotted blue line), Jean et al. [1990] (solid blue line), and de Barros and Luco [1990] (dotted blue line, only for pumping).

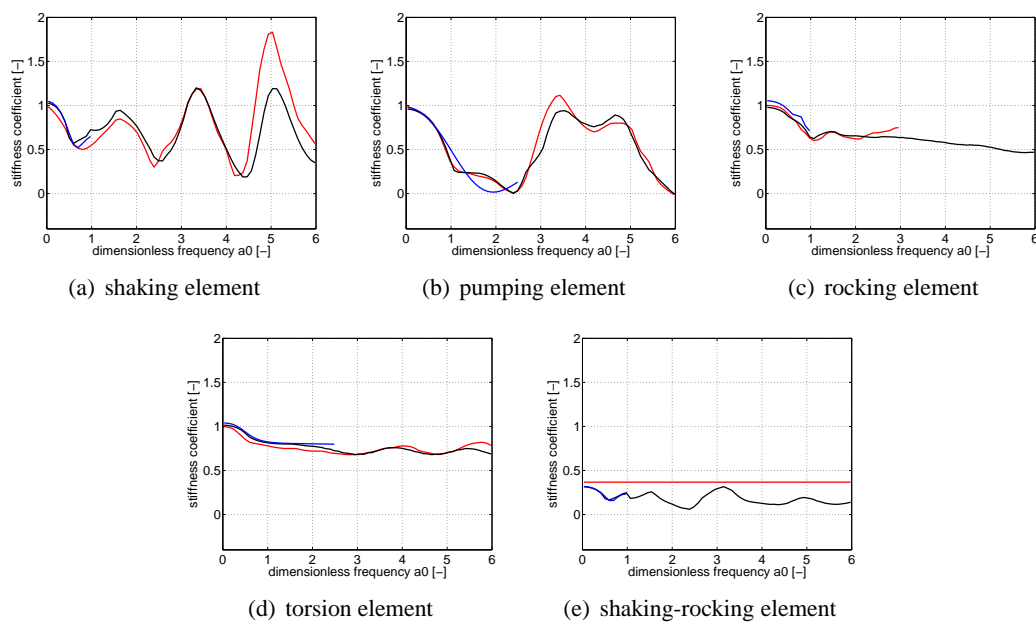


Figure 5.6: Stiffness coefficients of the soil impedance matrix computed with MISS (solid black line), Sieffert and Cevaer [1992] charts (solid red line, up to  $a_0 = 3$  for rocking), and the lumped parameter models of Wolf and Paronesso [1992] (solid blue line, up to  $a_0 = 2.5$  for pumping and torsion, and up to  $a_0 = 1$  for the other elements).

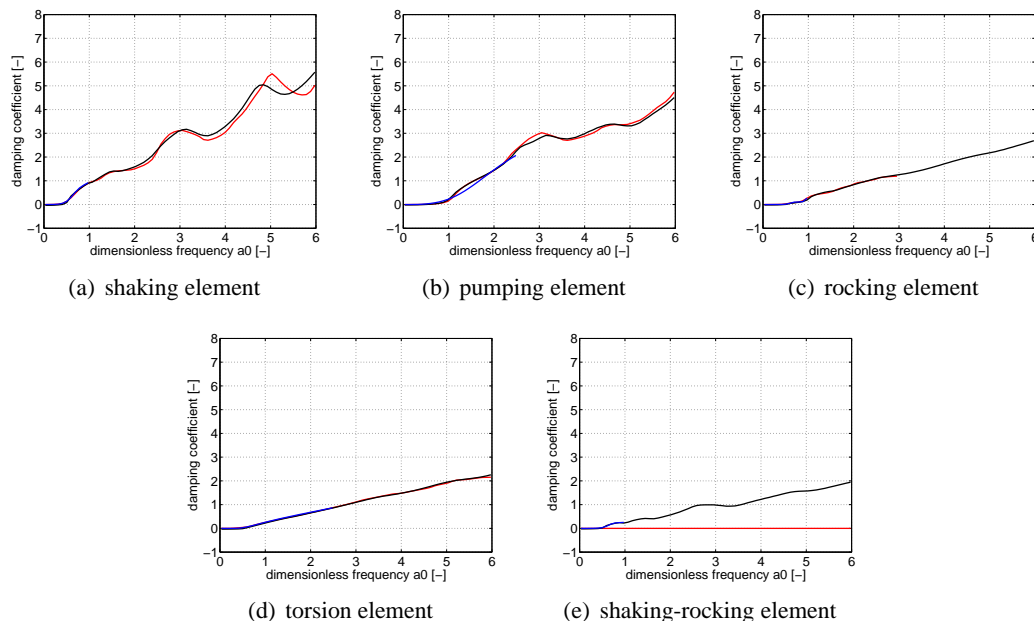


Figure 5.7: Damping coefficients of the soil impedance matrix computed with MISS (solid black line), Sieffert and Cevaer [1992] charts (solid red line, up to  $a_0 = 3$  for rocking), and the lumped parameter models of Wolf and Paronesso [1992] (solid blue line, up to  $a_0 = 2.5$  for pumping and torsion, and up to  $a_0 = 1$  for the other elements).

Indeed, the formulation in terms of mass, damping and stiffness matrix is the same in the frequency and in the time domain. In particular, it means that these models can be used when considering a linear soil coupled with a nonlinear structure, with a resolution in the time domain. This aspect is probably what motivated the important research activity that bursted around these models. More examples of lumped-parameter models can be found in the introductions of Wolf [1991b] and de Barros and Luco [1990].

### Experimental measures of the impedance

Although these simplified models can provide interesting approximations of the impedance of a soil, it has been argued that they cannot replace on-site measurements. The models and computations on which they are based incorporate strong assumptions, particularly concerning damping and homogeneity, that do not represent appropriately the real behavior of the soils. Indeed, in Crouse et al. [1990], forced-vibrations experiments, completed by Spectral Analysis of Surface Waves (SASW) tests and borings, are compared to computation results obtained with a BE method. The comparison is rather disappointing, at both sites used. The authors believe these differences to arise from the simple models used in the construction of the numerical impedance, and to possible errors in the shear velocity profiles measured with the SASW method. In Wong et al. [1988], slightly better results were obtained, particularly for the real part of the impedance, and for the rocking component.

As large-scale on-site tests are too expensive to be performed before every construction, an interesting approach consists in using simplified models of the same type seen above, but with coefficients identified

from experimental results, rather than numerical. This type of approach is considered in Luco and Wong [1992], and allows shear wave velocity and damping profiles to be identified from forced-vibration testing. This gives an alternative method to the SASW for the estimation of the mechanical parameters of a soil. In Glaser [1995], additional structural identification methods for soils are presented, particularly forced-vibration tests, identification from ambient vibration, from the measure of impedance functions, and from the recording of earthquake response.

## 5.2 Probabilistic models and methods in Soil-Structure Interaction problems

We have discussed in the previous section several features particular to the DD technique and the impedance matrices in SSI problems. We now turn to some probabilistic models and methods that were used in that field. This section does not replace Chap. 2, but rather particularizes it to the case of SSI problems. It is mostly based on examples of approaches that were explored in the SSI literature.

### 5.2.1 Probabilistic models for earthquake engineering problems

In this first part, we discuss successively models of the seismic ground motion, and of the soil parameters. They are modeled respectively as random processes indexed, respectively, on time and space, and on space, and these models usually concentrate on the introduction of appropriate correlation functions. The main focus of this section is to illustrate the difficulties related to such models, particularly in terms of identifiability of their parameters.

#### Probabilistic modeling of earthquake ground motions

Because of the complexity of the earth rupture processes and of the soil medium, seismic waves arriving at a given spot on the surface are seemingly random functions of time (see Fig. 5.8 for an example). For the same reasons, the waves arriving at two separate spots are different, and there is usually no apparent pattern to these differences between pairs of points. Seismic ground motions are therefore often modeled as space-time random processes. The variability in space can usually be neglected when the foundation under study is small compared to the scale of fluctuations of the ground motion, but it becomes a major feature when the foundation is extended or lies on different types of soils. One pile of a bridge, for example, might stand on the bottom of a river, and another one on the main land. The seismic motions they will undergo will probably be quite different, and might lead to important additional differential motions.

Two separate scales of fluctuations are sometimes defined for the probabilistic modeling of earthquake ground motion [Krée and Soize, 1986, Chap. 7]: a short one, with a typical duration of a few seconds, related to the occurrence of one particular earthquake, and a longer one, of a few years, related to the period of occurrence at the given site. Some parameters of the problem, mainly those controlling the propagation of the wave from the epicenter of the earthquake to the structure, have an influence for the short-term model, and others, like the total energy released by the earthquake or the distance between the epicenter and the structure, can be supposed deterministic when considering only one event, and modeled as random when considering a series of earthquakes at the same site. In engineering problems, only the short time scale is considered, because the focus is usually on the design of structures submitted to one given earthquake.

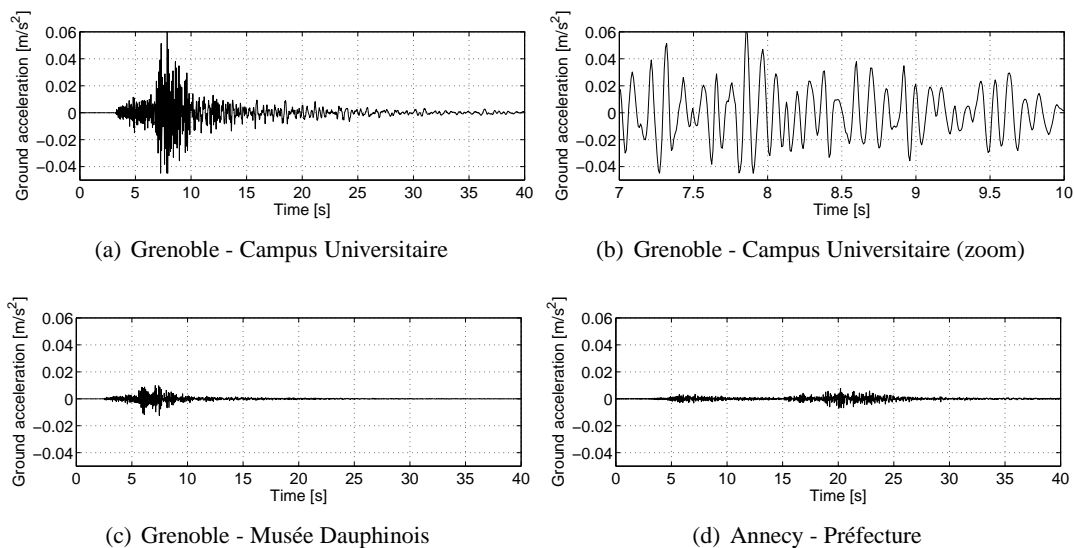


Figure 5.8: Example of an earthquake ground motion: accelerograms recorded during a Magnitude 4.2 earthquake in Grenoble (France) on January 11, 1999 [Ambraseys et al., 2001] (a-b) at the Campus Universitaire site, on soft soil at 18km from the epicenter, (c) at the Musée Dauphinois site, on rock at 18km from the epicenter, and (d) at the Annecy Préfecture site, on soft soil at 100km from the epicenter.

Before the installation of dense instrument arrays, the spatial variation of earthquake ground motions was supposed to derive from the wave passage effect only, which is the fact that the seismic waves arrive at different points of the foundation at different times. The installation of these arrays of seismographs showed that it was a gross oversimplification. One of the first arrays created was the 300 meters-long linear El Centro differential array in California, which is known for having recorded the 1979 Imperial Valley earthquake [Spudich and Cranswick, 1984]. Another array which was extensively studied, because it recorded many small and large magnitude earthquakes, was created in the SMART-1 international project (Strong Motion ARray in Taiwan) at a site in Lotung, Taiwan, in 1980 [Abrahamson et al., 1987]. It consists of 36 seismographs on three concentric circles, with radii 200 meters, 1 kilometer and 2 kilometers respectively, around a central one. In 1985, the smaller LSST array was added in the vicinity, with seismographs both at the surface and down in bore-holes in the soil [Abrahamson et al., 1991]. Many more accelerographs arrays have been installed in the world since then (see Zerva and Zervas [2002] for a recent review with references of the most important arrays), including the European Union-funded EURO-SEISTEST array in Greece [Pitilakis et al., 1994].

Because of their variability in both time and space, the modeling and study of earthquake ground motions is a complicated problem, and interesting simplifications can be obtained by considering mean-square stationarity in time and mean-square homogeneity in space. Unfortunately, experimental evidence goes against these hypotheses. The nonstationary character of the ground motions, for example, can be read directly from any accelerogram (Fig. 5.8), as it is clear that there are alternating short strong motion and long low motion periods. Nevertheless, the records that are used for the evaluation of the characteristics of the motions for the engineering applications are limited in time and focused on the strong motion windows, which can be seen as portions of stationary processes [Kozin, 1988]. Alternatively, as was mentioned in Sec. 2.1.3, the process can be modeled as a stationary process, modulated by a function

of time [Deodatis, 1996]. Another assumption which is usually made when studying earthquake ground motions is that of ergodicity of the time history. This hypothesis, which means that averages taken along one realization of a stationary process are equivalent to ensemble averages, is often necessary because we usually do not have multiple recordings at the same station of earthquakes with the same characteristics. Unfortunately, and for the same reason, the accuracy of that hypothesis is rarely checked.

Earthquake ground motions are therefore often modeled as random processes of time and space, stationary in time and nonhomogeneous in space. The functions defined in Sec. 2.1.2 have to be generalized for that case: the cross-autocorrelation is introduced as  $R(\Delta t; x_1, x_2) = E\{\mathbf{X}(t, x_1)\mathbf{X}(t + \Delta t, x_2)\}$ , and the cross-covariance and cross-correlation functions are defined in a similar manner. The cross-spectral density function, or cross-spectrum, is defined as the Fourier transform, with respect to the lag  $\Delta t$ , of the cross-covariance function. Finally, the cross-spectrum is often encountered in the normalized form of the coherency function, written as

$$\gamma(x_1, x_2, \omega) = \frac{S(x_1, x_2, \omega)}{\sqrt{S(x_1, x_1, \omega)S(x_2, x_2, \omega)}} = |\gamma(x_1, x_2, \omega)| \exp i\theta(x_1, x_2, \omega), \quad (5.21)$$

where  $\theta(x_1, x_2, \omega)$  is the phase spectrum and  $|\gamma(x_1, x_2, \omega)|$  is the lagged coherency. This last name comes from the fact that, if a single type of wave dominates the behavior of the earthquake in the window of time analyzed, then the phase spectrum can be written  $\theta(x_1, x_2, \omega) = -\omega(x_1 - x_2)/c$ , where  $c$  is the apparent propagation velocity along the line connecting the stations, and  $|\gamma(x_1, x_2, \omega)|$  then represents the variability in the recordings once the wave-passage effect has been removed.

Most earthquake ground motions models in the literature [Zerva and Zervas, 2002] are based on a model of the coherency function, but no general agreement seems to arise as to which is the most appropriate. Each site - and each event - seems to require a specific model. Even the numerical treatment performed to evaluate the coherency from the raw data seems to have an impact. The first models that were developed were purely empirical and only intended to fit the data recorded at seismographs arrays. In Harichandran and Vanmarcke [1986], for example, the lagged coherency is developed as a sum of two exponential functions, parameterized by regression from data. In Hoshiya and Ishii [1983], the product of an exponential function of the position and of cosine functions of the depth, is proposed, where two parameters, seemingly not related to physical quantities, have to be fitted to recorded data. Other semi-empirical models postulate a structure of the coherency function from the study of analytical models and fit the parameters from recorded data. In Luco and Wong [1986] for example, the authors used theoretical results of propagation of shear waves in a random medium to introduce their model of coherency. This last model is probably the one that has been most used for soil-structure interaction problems under random loading (see Sec. 5.2.2). Finally, Pais and Kausel [1990] considered an extended seismic rupture zone, and calculated the earthquake ground motion and its incoherence function as the superposition of the seismic waves arriving from different points of the rupture fault, with variable incident angle. It is very difficult to compare these models because they are not all based on parameters with a physical meaning, and when they are, they do not rely on the same ones. Three examples of these coherency models are presented in Fig. 5.9 at  $\omega = 5\text{rad/s}$ , however, comparisons are not obvious because the parameters were not fitted with respect to the same data. Also, as stated in Box 2.1.3, the impact of the choice of one correlation model or another on the design variables of the mechanical problem is not blatant.

The last noteworthy aspect of seismic ground motion modeling concerns the generation of seismic samples for civil engineering design applications. Design codes usually specify the seismic loadings through site-dependent response-spectra, and the link between coherency functions and response-spectra is not trivial. Nevertheless, in Deodatis [1996], an iterative method is proposed to compute earthquake

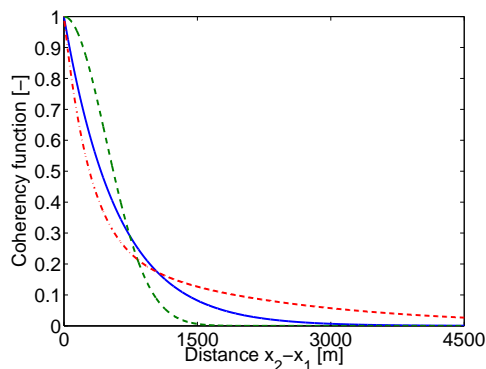


Figure 5.9: Examples of coherency functions in the literature (at  $\omega = 5$  rad/s): Hoshiya and Ishii [1983] model (solid blue line) with parameters  $V_s = 300$  m/s and  $b = 0.1$ , Luco and Wong [1986] model (dashed green line) with parameters  $\gamma/\beta = 2 \times 10^{-4}$ , and Harichandran and Vanmarcke [1986] model (dash-dotted red line) with parameters  $A = 0.736$ ,  $\alpha = 0.147$ ,  $k = 1740$  m,  $b = 2.78$ , and  $f_0 = 1.09$  Hz.

ground motions at several locations with specified coherency and ensuring that the response spectrum at each location checks to the corresponding soil conditions.

### Probabilistic modeling of soils

The complexity of the geological processes creating the soils induces an important spatial variability of their properties. Besides, the experiments used for the identification of soil properties are usually both expensive and inaccurate, so that measures are usually scarce and imprecise. Either these experiments are done in the field, and only the uppermost layer of soil is usually accessible, or some sample of soil is removed and tested in the laboratory, and the reshuffling then affects the link between the measured value and that in the field. Therefore, it seems appealing, as for earthquake ground motions, to model soil properties by random fields. Theoretically, the soils are in constant evolution under the same geological processes that created them, so that this time dependence should be taken into account. In general though, this effect can be neglected at the scales relevant for construction design and engineering applications.

The soil properties are therefore modeled using space-dependent random fields, usually with a trend in the vertical direction, and mean-square homogeneous in the horizontal directions. The vertical trend is very clear (see Fig. 5.10(a) for example), but the homogeneity is not as obvious. Actually, there is even experimental evidence that this hypothesis is erroneous. Toubalem et al. [1999], for example, observed on SMART-1 records that the symmetric excitation of an axisymmetric building yielded an asymmetric response, which necessarily originated from a strong nonuniform trend in the soil characteristics. Still, as it simplifies the representation of the properties, that homogeneity hypothesis is often encountered in the literature. Besides, the vertical trend is usually easier to account for than a possible horizontal trend. Indeed, it is often easier to gather a lot of data at the same spot in the horizontal plane and at varying depths, with bore holes for example, than to sample in the horizontal directions which often involves the displacement of the experimental setup and equipments.

An important difficulty that appears when modeling soil properties and that was not as salient for earthquake ground motions is the influence of the sampling size on the estimation of the soil parameters [Vanmarcke, 1977]. Indeed, the experimental setups that are used produce measures that are not point-

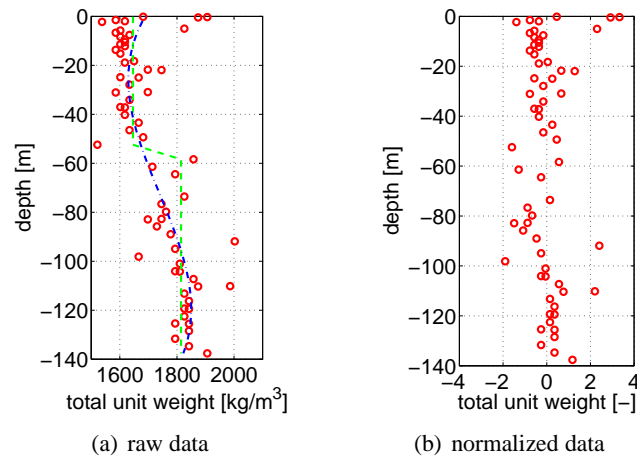


Figure 5.10: Variation of the unit weight with depth in a boring drilled in the Gulf of Mexico at the location of an oil production platform (data taken from Fenton [1997]): (a) raw data (red circles), piece-wise constant trend (green dashed line), and 3rd order polynomial interpolated trend (blue dash-dotted line), and (b) normalized detrended data supposing a piece-wise constant trend.

wise but rather some spatial integrations of point-wise values over the size of the sample. Therefore the estimation of statistical quantities over a data set of measured soil properties is dependent on the size of the samples, and, in particular, the variance of the data set is a decreasing function of the sample size. Moreover, the quantities of interest in engineering, the settlement of a building for example, are usually themselves spatial integrations of the soil properties, so that homogenization questions should be considered when dealing with soil properties modeling.

As already stated in Sec. 2.1.2 for correlation functions, correlation models are usually defined on de-trended and normalized data, so that a model of trend has to be chosen for each data set of soil properties. Considering the example of Fig. 5.10, although the existence of a trend seems obvious, it is difficult to know what type of model of the trend might be adequate. It may be that we have detected the existence of two layers with different properties so that the trend should be constant piece-wise, but it might be some more complicated physical phenomenon so that polynomial interpolation would be more appropriate. Besides, it is often difficult to set apart a trend and a variation taking place over large distances [Vanmarcke, 1977]. In that matter, engineering judgment is often called upon.

Once detrended, the underlying process is usually supposed homogeneous, and various estimators are used to assess the variability of the data set, among which, the correlation function. As the accuracy of that function is highly dependent on the precise evaluation of the trend, which we have seen to be often quite heuristic, another estimator, the semivariogram, is sometimes considered. Very large data sets are necessary to obtain accurate estimations of the correlation function, so that the induced costs prevent most construction projects from obtaining them. Fortunately, it seems like, although the trends are local quantities which depend heavily on the materials actually at the construction site, the correlation structure is more global and transferrable from one site to another [Fenton, 1999a]. Many studies have therefore been launched on large data sets to try to estimate correlation structure models.

The literature on these studies is extensive and only a few examples will be exposed here. In Soulié et al. [1990], the site of an earth dam in Canada is investigated with more than 300 measurements on

25 borings in a radius of 1 kilometer; in Grabe [1994], it is the site of the construction of a high speed train track in an area of 800 square meters in Germany which is studied; and in Fenton [1999b], 143 Cone Penetration Test (CPT) tests are performed on the site of an airport in Norway. From these data sets, the authors try to estimate models of the soil and the parameters that control these models. Two types of model seem to arise [Fenton, 1999a]: finite-scale models, where a finite scale of fluctuation can be identified, and fractal models (or  $1/f$  noise models), where correlations happen over seemingly infinite distances. All the correlation models discussed until now, including the exponential model of Eq. (2.1), were finite-scale models, and state incoherences between two points separated by a large distance. In fractal models, on the other hand, the controlling parameter regulates how the spectral power is distributed between the low- and high- frequencies, but there is seemingly possible correlation between points at very large distances. Although finite-scale models are more classical and the parameter seems to be more amenable to physical interpretation, some studies seem to indicate that these models are more appropriate for soil properties [Grabe, 1994, Fenton, 1999b].

Once a model, and its controlling parameters, have been identified, predictions can be made at unsampled locations. The most classical method until recently seems to have been Kriging, also called Best Linear Unbiased Estimator (BLUE), which is basically a simple least square interpolation of the data set. In its simplest form it does not use the correlation structure discussed above, although some more refined variants have been developed [Goovaerts, 1999]. One of the problems of the Kriging methods, although methods have been proposed [Goovaerts, 2000] to circumvent this difficulty, is that they tend to smooth local variability as they interpolate the data. Another important problem of these approaches is that there is no quantification of the accuracy of the estimated value when the distribution of the data is not known. Usually, a Gaussian distribution is supposed, and confidence intervals hence derived, but that is highly unsatisfactory. A more interesting approach is proposed in Bourdeau and Amundaray [2005], where a bootstrap resampling technique allows the confidence intervals on the estimated values to be derived with no previous knowledge of the underlying distribution. Unfortunately, this method requires a very extensive data set to give accurate results.

An alternative method, without these limitations, and which is gaining increasing acceptance is stochastic simulation. Instead of trying to interpolate the value at the sampled points, the data set is only used to assess the correlation structure, and realizations of the soil are simulated, each of them following that structure. The value of the data at all desired points is provided through an approximated PDF, so that the accuracy of the estimation is given at the same time as the estimated value. This type of approach is used in most SFE methods in geotechnics Auvinet et al. [2000]. The only requirement of the simulation method is a good estimation of the correlation structure, and an important computational capability. In Goovaerts [2001], a more complete comparison of Kriging and simulation methods is presented.

In Fig. 5.11, examples of soil realizations are presented for different fluctuation lengths<sup>2</sup>, based on a particular model of the soil properties field described in Soize [2006] in a general setting, and used for the modeling of soil parameters in Arnst et al. [2006b]. A particular interest of this model is the small number of parameters that it involves, which makes it fit for experimental identification.

### Probabilistic modeling of structures

After this presentation of the probabilistic modeling of the seismic loadings and of the soil properties, we turn to the last important item of SSI problems, the structure. Its main difference with the other two is that it is man-built. This means that both the materials and the design are, or can be, monitored more

---

<sup>2</sup>These figures were drawn using a MATLAB function written by Maarten Arnst.

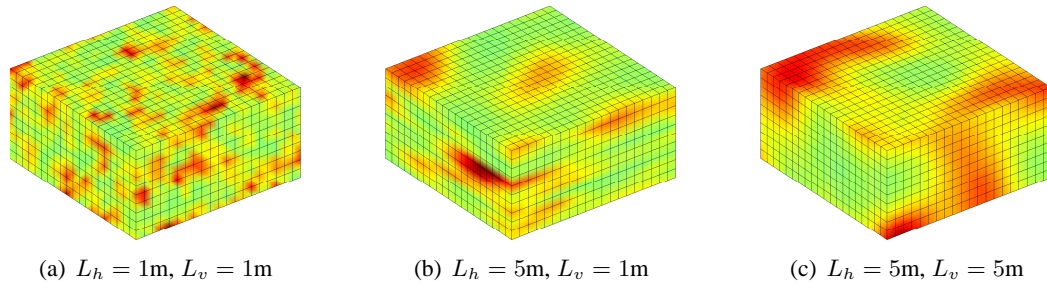


Figure 5.11: Fluctuations of a soil parameter, within a box of dimensions  $20 \times 20 \times 10\text{m}^3$ , for different correlation lengths in the horizontal ( $L_h$ ) and vertical directions ( $L_v$ ), using a model by Soize [2006].

accurately. Therefore, the uncertainties and the variability can be assessed more easily, and limited, so that, in this dissertation, we will disregard them and model the structure as deterministic. Nevertheless, we will see in the next chapters that the approach that will be developed for the probabilistic modeling of SSI problems is compatible with a probabilistic modeling of the structure.

To conclude this section on probabilistic models in SSI problems, the complexity of the identification of these models should be stressed. Most models lack a physical basis that would justify their use in several different settings, or their fitting from several different sites. Also, at each step of the identification, difficulties arise. In the case of soils, particularly, the trend has to be identified, then the correlation, yielding each time approximations and errors, including measurement errors. Finally, the mere quantity of data is far too limited. At best, the validity of these models seems questionable.

## 5.2.2 Probabilistic approaches in SSI problems

In general, the results that have been presented in Sec. 2.2 have been developed and much more used in structural mechanics than in problems of soil mechanics or coupled SSI problems. In structures, two facts ease the resolution of stochastic problems: the boundedness of the domain and the man-made character of the material. The former allows for the use of methods based on SFE, which are not applicable directly to unbounded domains, as in soils, and the latter, as it supposes that the properties of the material are under a certain control, allows for the use of approaches based on small uncertainties like equivalent linearization and perturbation techniques. On the contrary, probabilistic SSI problems seem very complex. Besides, as discussed earlier, the loading also calls for a probabilistic modeling, which complicates the task even more.

Following the path of deterministic SSI, the first attempts at modeling SSI problems in a probabilistic way concentrated on the kinematic interaction aspect. More specifically, the filtering and averaging effects of rigid foundations on a random free-field ground motion were studied, considering a deterministic soil and structure. Only later were the first studies accounting for the variability and the uncertainty of the soil medium attempted. These two types of approaches to stochastic SSI interaction problems are reviewed here.

### Response of a deterministic Soil-Structure Interaction system to a random excitation

This first group of studies concentrated on the impact of a random load on the kinematic interaction. More specifically, a massless foundation on a deterministic soil is considered, and the free-field ground

motion is modeled as a zero-mean random process mean-square homogeneous in space and mean-square stationary in time. The kinematic interaction effect on the input motion is the quantity of interest. The main differences between the works in that field concern the type of coherence function that is chosen for the free-field ground motion and the level of simplification that is considered in the computation of the motion of the foundation from the free-field ground motion. The existence of many different models for the coherence function was discussed in the previous section, and will not be recalled here.

The second difference between the approaches treated in the literature therefore regards the link from the free-field ground motion to the foundation motion. This relation is normally complicated as it requires the knowledge of the impedance function of the soil, but several approximation techniques are used. In Hoshiya and Ishii [1983] and Harichandran [1987], a very simple method is chosen, where the motion of the foundation motion is taken as the average on the interface of the free-field ground motion. In this approach, no rocking of the foundation is considered. A similar approach, based on results by Iguchi [1984] and Scanlan [1976], and taking into account the coupling between rocking and translational movements of the foundation, was thereafter used in Veletsos and Prasad [1989] and Pais and Kausel [1990]. A more complex integral representation, based on Bycroft [1980], is considered in Luco and Wong [1986], Luco and Mita [1987], and Sarkani et al. [1999], but a simplification in the structure of the interface tractions is added to yield a simpler form.

Even though there are differences between these several approaches, they all seem to get to the same conclusion about the effects of the kinematic interaction on the power spectral density of the foundation motion: the creation of rocking of the foundation and an important damping of the higher frequency peaks. In Veletsos and Prasad [1989] and Sarkani et al. [1999], the assessment of inertial interaction is also performed and seems to indicate that inertial interaction effects are usually more important than those of kinematic interaction. Also, whereas kinematic interaction normally yields a reduction of the response, inertial interaction can sometimes increase it, making it more dangerous.

### **Soil-structure interaction problems with uncertain soils**

The study of the SSI problem with random soil is much more recent, and the literature much more limited. Again, most works can be split into two groups, each one with a particular view for the treatment of the unboundedness of the soil. In the first group, the soil is replaced by a simplified model with a small number of parameters that are randomized. Among these simple models are one of Wolf [1994]'s lumped parameters models, a finite column model, and a Winckler spring foundation model. In the second group, the soil is truncated in some way, and modeled using a SFE method. In this type of approach, the problem is the volume of soil that can be considered uncertain while remaining within reasonable bounds of computer time and resources.

In Jin et al. [2000], the soil is replaced by a lumped-parameter model, of a type similar with those described in Sec. 5.1.4. The shear modulus  $G$  and Poisson's ratio  $\nu$  of the soil are considered random and modeled by independent Gaussian random variables. Neither the structure, nor the loading are considered random, although the combination, and comparison, with a random structure was studied in a following paper by the same authors [Lutes et al., 2000]. It was found that the uncertain soil parameters had more impact on the first resonance peaks of the power spectral density of the response of the structure, and for tall structures, whereas the uncertainty on the structure parameters had more influence in the higher frequency range and for smaller structures.

In Toubalem et al. [1995], the soil is replaced by a column with random unit mass and shear modulus, modeled by one-dimensional random fields varying with depth. The covariance function is supposed to follow an exponential model, and the variations are deemed small around the trend. A deterministic

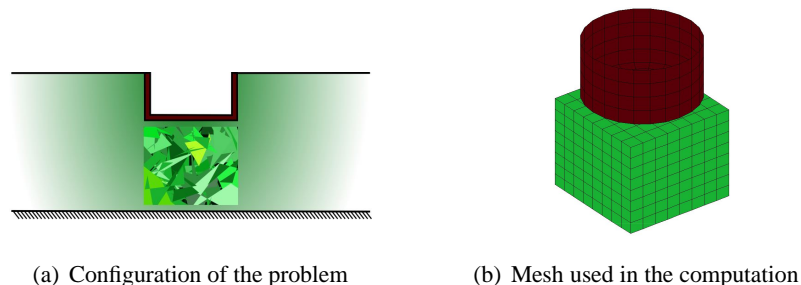


Figure 5.12: (a) configuration of the stochastic parametric problem, and (b) mesh used with software MISSVAR (922 nodes, 1422 elements).

seismic input motion is introduced using prescribed displacement at the base of the column, and the transfer function of the displacement at the top with respect to that prescribed base motion is derived using the perturbation method. This simplified model seems to show that the randomness induces an equivalent damping, the effect of which increases with frequency.

This work is complemented in Toubalem et al. [1999], where the horizontal variability of the soil parameters is considered. The soil is modeled by a Winkler spring foundation, each spring having a different stiffness. The vertical variability is therefore not taken into account anymore. The numerical computations performed seem to show that the horizontal variability is responsible for the strong asymmetry observed in the response of an axisymmetric structure used in the experiments performed for the international project SMART-2 at Hualien, Taiwan. In the transfer function between the displacements at the top of the building with respect to its base, the horizontal variability seems to yield a shift of the first resonance peaks towards the lower frequencies, and a quite important reduction in the amplitude of the higher frequency resonance peaks. The examples of a sewer pipe and of a pile foundation, with the soil replaced by Winkler springs with varying stiffness, are also considered in Breysse et al. [2005]. The consideration of the soil variability is shown to be important in the design of these structures, and the ratio of the correlation length of the soil properties to the typical length of the structure seems to be one of the important controlling parameters. In an older paper [Melerski, 1988], a Winkler type foundation with random stiffness was already used to model the behavior of a massless shell on uncertain soil, but rather strong assumptions (symmetry of the problem, zero Poisson's ratio) gave the results less relevance.

Aside from these very simple models of soils, more precise models of the soil, using SFE representations have been considered, which inherit the deficiencies of deterministic FE methods in modeling unbounded domains. In Savin [1999] and Savin and Clouteau [2002], a method is presented to couple a deterministic unbounded soil, that can be modeled for example using a deterministic BE method, and a bounded volume, where the uncertainty and variability in the parameters are considered more important than in the rest of the soil. The numerical resolution is performed for both using the software MISS [Clouteau, 2003]. In Sec. 5, an application of this method will be presented, for a comparison with the ideas that will be developed herein.

Finally, a very impressive work is presented by Ghiocel and Ghanem [2002], where many parameters of the SSI problem are randomized: the shear modulus at low strains, the shear modulus-shear strain curve, the structural damping, the structural stiffness, and the seismic loading. A SFE method is considered, but, unfortunately, nothing is said of the type of boundary conditions that are considered to take into account the unboundedness of the soil. The methodology is applied to the design of a nuclear plant and

the results seem to indicate that the current design practice of these nuclear plants is overly conservative. This set of random parameter can also include geometrical, such as in Ghanem and Brzakala [1996], where the position of the interface between two layers of soil is randomized.

Of these works, the last two, using SFE methods, seem particularly interesting. The formulation in terms of FE is natural in computational mechanics, and is drafted directly in terms of the classical mechanical variables, so that the choice of random parameters can be readily performed. That correspondence between the random models of the mechanical parameters and the random quantities of interest is indeed one of the main interest of these parametric methods. However, this means that the random models of the parameters have to be appropriate, lest the random model of the quantity of interest lose all meaning. In practice, the identification of such models for soil parameters random fields is arduous, and requires the measurements of underground quantities over very large domains. Also, a limitation of these parametric method that is particularly debilitating in SSI problems is the necessity to mesh the uncertain domain. As the impedance matrix is influenced over large distances by the parameters of the soil, this means that the consideration of uncertainty will give rise to very expensive problems. With respect to these two limitations of the parametric methods, the nonparametric approach is promising. In the next section, we present an application where the features of each method are discussed.

### 5.3 Parametric and nonparametric models of the impedance matrix

We develop in this section two approaches to the random modeling of a mechanical problem: one parametric, using a SFE method, and the nonparametric that was described in this dissertation. The two random problems are built around the same common basis, represented by the deterministic approach, and we analyze the advantages and shortcomings of each method.

The mechanical problem we consider here is that of a circular embedded foundation in a soil layer over a rigid bedrock, which was briefly described in Sec. 5.1.4. We first detail the homogeneous problem, and later derive the corresponding stochastic problems in each of the two approaches. When confronting these two methods, we have to keep in mind that, although they are based on the same homogeneous model, they do not consider the same stochastic problem. Blunt comparison is therefore not possible. They can only be compared in the sense that they both aim at the same purpose, here the safe design of a building. With respect to that goal, and only for this, their appropriateness can be assessed and compared. Also, we will not compare quantitatively the variability between the two methods. Indeed, the marginal laws of the random parameters in the parametric case, and the dispersion parameters in the nonparametric approach, have to be identified with real data, and this was not considered in this dissertation.

#### 5.3.1 The homogeneous problem

We therefore return to the problem of a rigid cylindrical foundation embedded in a homogeneous layer of soil over a rigid bedrock, as seen in Fig. 5.3(b). The radius of the foundation is  $r = 0.5$  m, equal to the embedment height,  $D = 0.5$  m, and the height of the layer of soil is  $H = 1.5$  m. The unit mass is  $\rho = 1$  kg/m<sup>3</sup>, with Lamé's coefficients at  $\underline{\lambda} = 2$  N/m<sup>2</sup>, and  $\underline{\mu} = 1$  N/m<sup>2</sup>, which correspond to Young's modulus  $E = 2.67$  N/m<sup>2</sup>, shear modulus  $G = 1$  N/m<sup>2</sup>, Poisson's ratio  $\nu = 0.33$ , pressure wave velocity  $c_p = 2$  m/s, and shear wave velocity  $c_s = 1$  m/s. The impedance matrix for this problem was already drawn in Fig. 5.6 and Fig. 5.7, as computed by the software MISS, described by a lumped-parameter model by Wolf and Paronesso [1992], and read on the charts of Sieffert and Cevaer [1992]. The impedance functions computed by MISS will be recalled, each time as a solid red line, in the following Fig. 5.13,

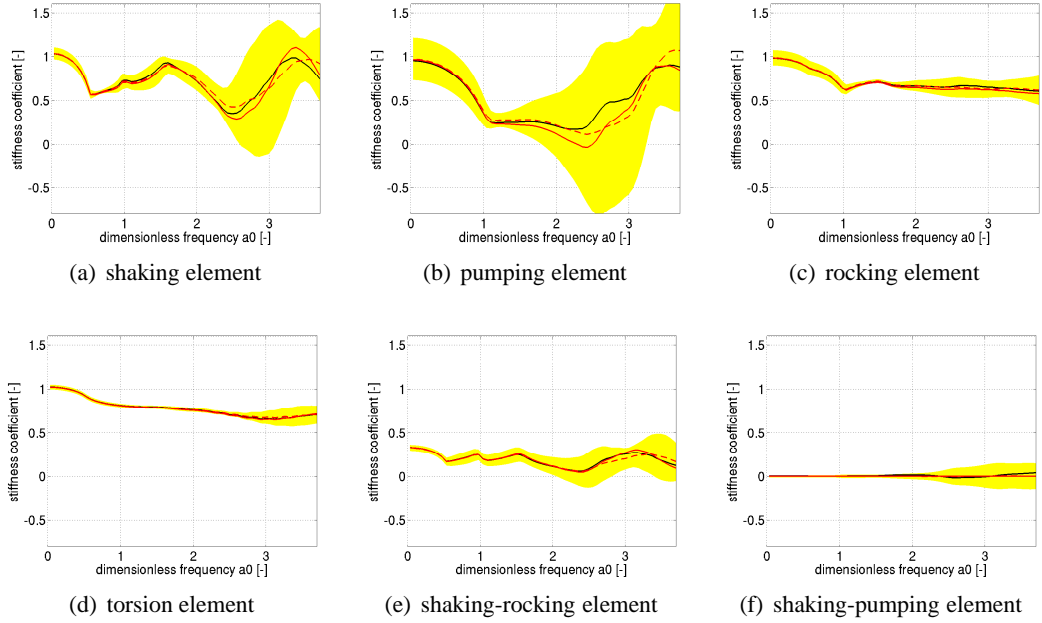


Figure 5.13: Stiffness coefficients of the soil impedance matrix computed with MISSVAR: response without the heterogeneity (solid red line), frequency-wise mean (dashed red line) and 90%-confidence interval (yellow patch) for 200 Monte Carlo trials, and one particular Monte Carlo trial (solid black line).

Fig. 5.14, Fig. 5.19 and Fig. 5.20, for comparison with the parametric probabilistic approach and the nonparametric probabilistic approach.

An important characteristic of systems consisting of a homogeneous layer over a rigid bedrock, is that, for low frequencies, the damping coefficient of the impedance matrix cancels. Because of the presence of the rigid bedrock, body waves cannot escape towards the bottom, while surface waves cannot develop for low frequencies because their extension in height is proportional to the wavelength, or  $1/\omega$ . Hence, below a given cutoff frequency, there is no radiation damping in this system, and it behaves as a simple mass-spring system. Material (hysteretic) damping also has an influence on the imaginary part of the impedance matrix, but it does not appear here in the damping coefficient because of the normalization that was used (see Eq. (5.17)). These cutoff frequencies depend on the type of waves that are considered and are [Gazetas, 1983]

$$\begin{cases} f_{Sc} = \frac{c_s}{4H} \\ f_{Pc} = \frac{c_p}{4H} \end{cases}, \quad (5.22)$$

where  $f_{Sc}$  and  $f_{Pc}$  are, respectively, the cutoff frequencies (in Hz) for shear waves and pressure waves. Alternatively, they can be written in terms of the dimensionless frequency,

$$\begin{cases} a_{0,Sc} = \frac{\pi r}{2H} \\ a_{0,Pc} = \frac{\pi r}{2H} \frac{c_p}{c_s} \end{cases}. \quad (5.23)$$

In our case, these formula yield  $a_{0,cP} = 2a_{0,cS} \approx 1$ . As shaking and torsion generate mainly shear waves, the cutoff frequency should appear at  $a_0 = a_{0,cS} \approx 0.5$ , while for pumping and rocking elements,

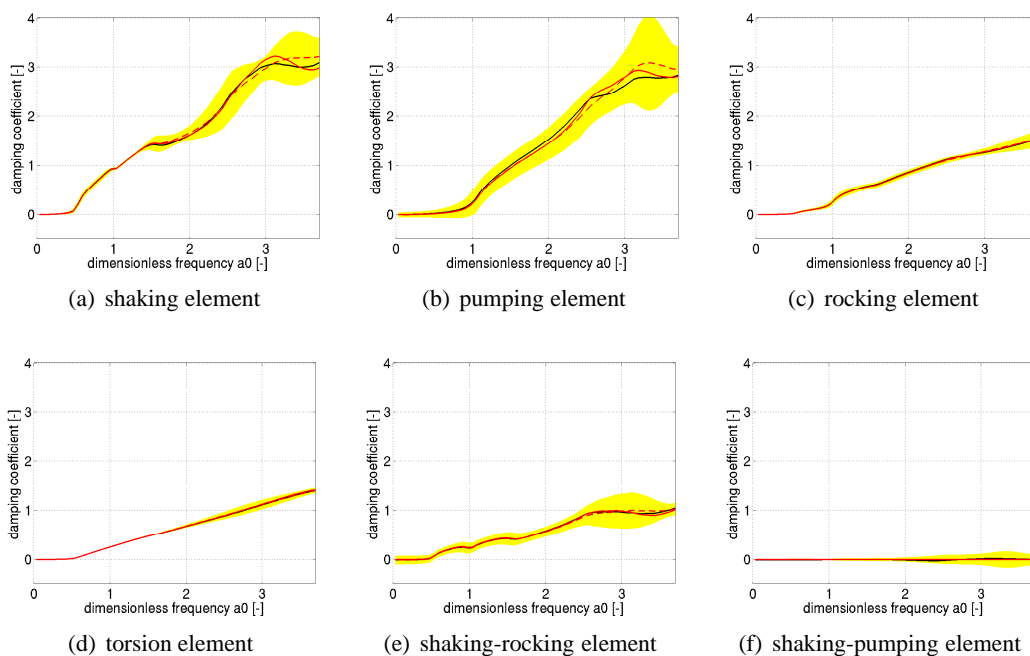


Figure 5.14: Damping coefficients of the soil impedance matrix computed with MISSVAR: response without the heterogeneity (solid red line), frequency-wise mean (dashed red line) and 90%-confidence interval (yellow patch) for 200 Monte Carlo trials, and one particular Monte Carlo trial (solid black line).

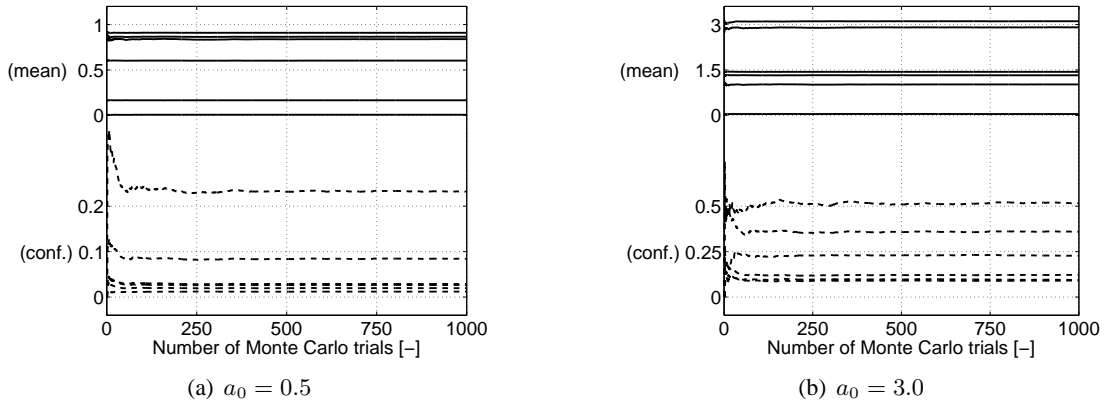


Figure 5.15: Convergence of frequency-wise mean (solid lines) and 90%-confidence intervals (dashed lines) for the amplitude of the elements of the impedance matrix computed using MISSVAR, at frequencies (a)  $a_0 = 0.5$ , and (b)  $a_0 = 3.0$ . Beware that the scales are different for the two frequencies.

which generate more pressure waves, it should appear close to  $a_0 = a_{0,cP} \approx 1$ . These values are in very good accordance with those read in Fig. 5.7. It should be noted, from Eq. (5.22), that the cutoff frequency is a characteristic of the layer rather than of the foundation, the radius in Eq. (5.23) arising only from the definition of the dimensionless frequency.

For the stochastic analyses that will be performed in the following sections based on this homogeneous problem, it is interesting to remind the concept of *zone of influence* [Gazetas, 1983]. For a given stress distribution on the foundation, it indicates approximately the distance from that foundation within which the stresses in the soil are significant. For a circular foundation with radius  $r$ , it is about  $4r$  for vertical translation,  $2r$  for horizontal translation,  $1.25r$  for rocking, and  $0.75r$  for torsion. This zone of influence can be seen as the zone within which the value of the parameters of the soil, and their possible variation, is important for the evaluation of the corresponding elements of the impedance matrix. These zones of influence has been used to explain, in parametric studies of this type of problem, the lack of influence of the height of the layer on the rocking and torsion elements of the impedance.

Although we have modeled this problem as a homogeneous layer over a rigid bedrock, it is obvious that this is a simplification of reality. In a natural setting the parameters of the soil will exhibit variations, and the soil will be largely heterogeneous. A model uncertainty has therefore been introduced. In the parametric approach that is presented in the next paragraph, a bounded volume of soil is meshed and the heterogeneity of the soil is taken into account explicitly in that zone. However, the rest of the soil is still assumed homogeneous, so that there still are model uncertainties. On the contrary, the nonparametric approach does not localize the randomness in the soil, and takes into account the model uncertainties globally.

### 5.3.2 Parametric approach: MISSVAR software

Let us consider first the parametric probabilistic approach. The uncertain soil is modeled using a SFE method, so that it has to be meshed. A bounded subdomain of soil is therefore selected under the foundation and modeled using the SFE method. Implicitly, this means that the rest of the soil is considered deterministically known. The uncertain soil is coupled to the homogeneous soil using a method described

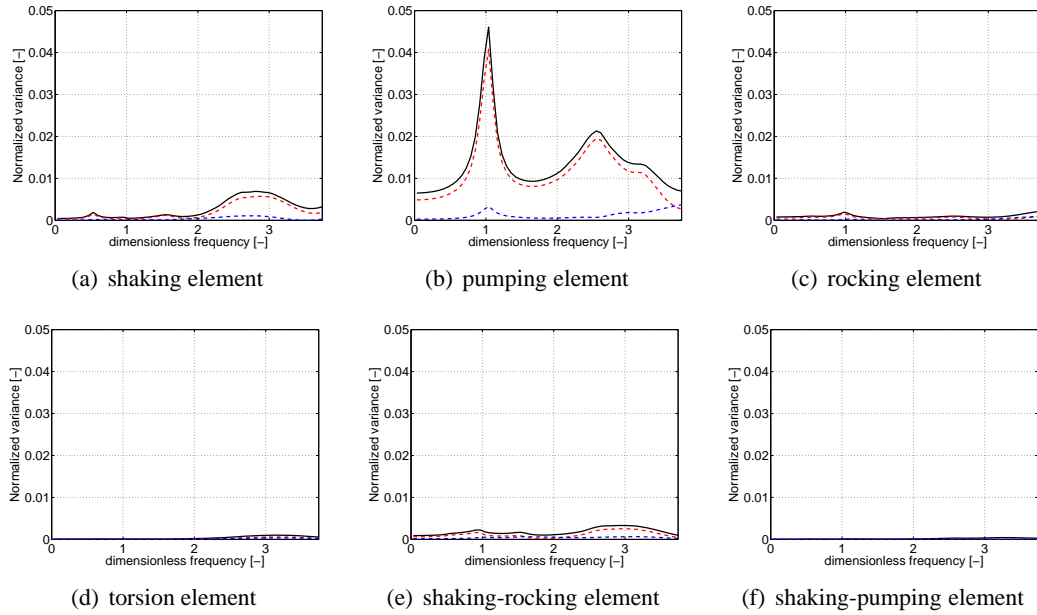


Figure 5.16: Normalized total variance (solid black line) of the elements of the random impedance matrix, and normalized variance for the first two eigenmodes of the covariance matrix. The eigenvalue of the first mode (dashed red line) represents 71% of the trace of the covariance matrix, and the eigenvalue of the second mode (dashed blue line) 14%.

in Savin [1999]. In short, the parameters and displacement fields inside the uncertain domain are seen as the sum of a mean contribution, which is that of the homogeneous case, and of a variation around that mean. The random impedance matrix with respect to the rigid foundation can then be seen as the sum of that in the homogeneous case plus a variation due to the fluctuations of the parameters and displacements fields inside the uncertain domain. This method was implemented in the module MISSVAR of the software MISS [Clouteau, 2003].

The configuration of the problem, as well as the mesh, are represented in Fig. 5.12. The brown part of the mesh in Fig. 5.12(b) represents the foundation, with respect to which we compute the impedance matrix. It is composed of surface elements and is the same as for the homogeneous computation with the software MISS. The green part of the mesh is specific to the stochastic model, and composed of volume elements. The meshing of the boundaries of the soil - air and of the soil layer - rigid bedrock interfaces is not necessary in MISS, so that they do not appear on Fig. 5.12(b). Lamé's coefficients are the only parameters considered random, and they are modeled as the restrictions on bounded intervals of mean-square homogeneous random fields, with mean  $\underline{\lambda} = 2 \text{ N/m}^2$ , and  $\underline{\mu} = 1 \text{ N/m}^2$ , exponential correlation functions with scales of fluctuation  $L = 0.5 \text{ m}$  in all directions, and 60% autocorrelation. Practically, during the probabilistic part of the analysis, these parameters are zero-mean because we consider the superposition of the probabilistic problem on the homogeneous one, where their values are taken as  $\underline{\lambda}$  and  $\underline{\mu}$ . Lamé's coefficients are represented using a KL expansion with 20 terms, with random variables following a zero-mean unit-variance uniform law. The system is solved using the MCS method, with 1000 trials.

It should be noted, on Fig. 5.12(a), that the uncertain subdomain does not intersect the foundation,

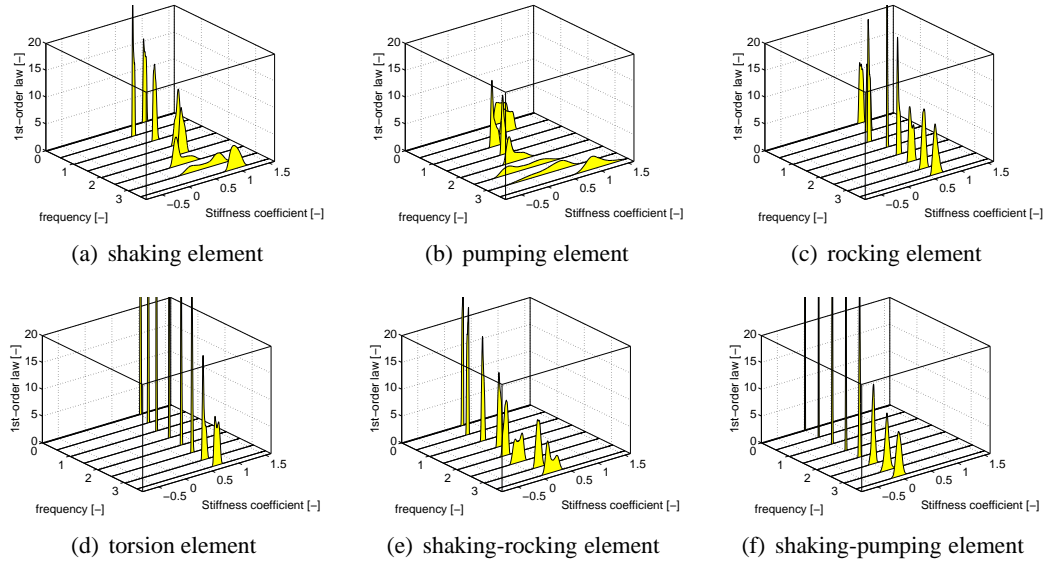


Figure 5.17: Estimation of the first-order marginal law of the stiffness coefficient of the elements of the impedance matrix at several frequencies

nor the bedrock. As the coupling between the homogeneous problem and the stochastic problem is a volume-type coupling, the SFE mesh cannot approach the interfaces, lest numerical problems appear. Although it might be expected, it is not clear whether the existence of this thin homogeneous layer of soil between the foundation and the uncertain soil domain has a strong influence on the probabilistic assessment of the impedance matrix.

Before discussing the model of the impedance matrix obtained with this parametric approach, we study the convergence of the first statistical moments of the elements of the impedance matrix with respect to the number of Monte Carlo trials. The evolution of the estimations of the frequency-wise mean and 90%-confidence intervals, from only the first  $k$  trials, is therefore plotted against  $k$  in Fig. 5.15. Two frequencies are considered:  $a_0 = 0.5$ , where the scattering around the mean is low, and  $a_0 = 3$ , where it is more important. The plots all tend towards a constant value so that the number of Monte Carlo trials seems to be sufficient for the estimation of the first two moments of the impedance matrix. However, more trials will be needed for the appropriate estimation of higher-order moments, or of the first-order marginal laws.

The real and imaginary parts of the frequency-wise mean and 90%-confidence interval are plotted in Fig. 5.13 and Fig. 5.14, respectively. The mean is represented by the dashed red line, while the solid red line represents the elements of the impedance matrix computed in the homogeneous case. The yellow patch represents the frequency-wise confidence interval. It was calculated, not for the complex value, but independently for the real and imaginary parts of each of the elements of the impedance matrix. This way, it gives a feel of the *locus* of the trials of the elements of the impedance matrix. Finally, to give an idea of the dynamical behavior of the trials, the black solid line represents one particular Monte Carlo trial among the 1000 that were drawn. The same trial has been used for all the plots of Fig. 5.13 and Fig. 5.14.

Analyzing the real and imaginary parts of each element of the impedance matrix, it can be observed that there seems to be more variability on the pumping than on any other element, and almost none for

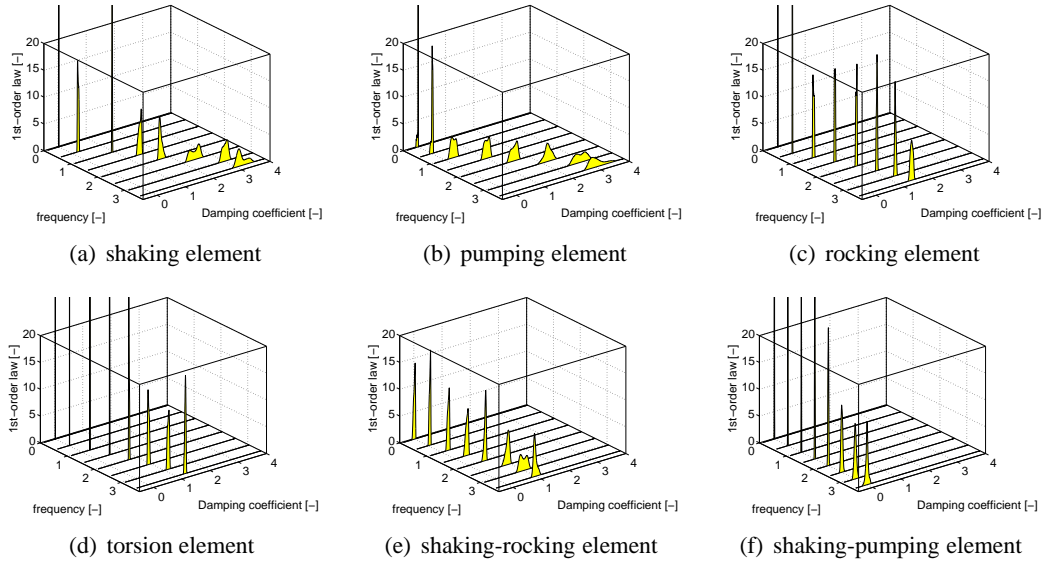


Figure 5.18: Estimation of the first-order marginal law of the damping coefficient of the elements of the impedance matrix at several frequencies.

the torsion. This is due to the geometry of the foundation, which is embedded, with the uncertain soil located only underneath it. As the soil resists more in compression than in shear, the pumping term is very dependent on the characteristics of the soil under the foundation, where it is compressed. On the other hand, the torsion only creates shear in the soil, and more on the sides of the foundation, where the distance from the center of rotation is larger. Therefore the characteristics of the soil underneath the foundation do not influence in a significant manner the dynamics of the torsion element of the impedance matrix. In between, the same type of comments can be made about the shaking and rocking terms. Both are influenced by the soil under the foundation as well as by the sides so that the variability is intermediary between that of the previous two elements.

This can be better seen by representing directly the normalized variance for each of the elements (Fig. 5.16), where the variance is seen as a function of the dimensionless frequency, and the normalization is with respect to the squared mean. Additionally, the covariance of the impedance matrix, seen as a matrix-valued random process indexed on the dimensionless frequencies, can be computed, and its eigenmodes and eigenvalues evaluated. On Fig. 5.16, the normalized variance corresponding to the first two eigenmodes of this covariance matrix are also plotted. The sum of the eigenvalues of these two modes represents 85% of the trace of the covariance matrix. The fact that so few modes of the covariance matrix are actually needed to represent the variance accurately is linked to the scale of fluctuation that was chosen for the model of Lamé's coefficients. These coefficients were expanded using a KL expansion, and an exponential correlation function with a scale of fluctuation of 0.5 m in all directions. This scale of fluctuation is the same as the radius of the foundation. Therefore, it means that the higher terms in the KL expansion represent parameter fields with very rapid fluctuations of their value over space. In a sense, such fields are filtered by the rigid foundation, and their effect on the impedance matrix is mostly averaged. This explains why we see the influence of only a few modes on the variance of the impedance matrix.

We then take a look at estimations of the first-order marginal laws of the elements of the impedance

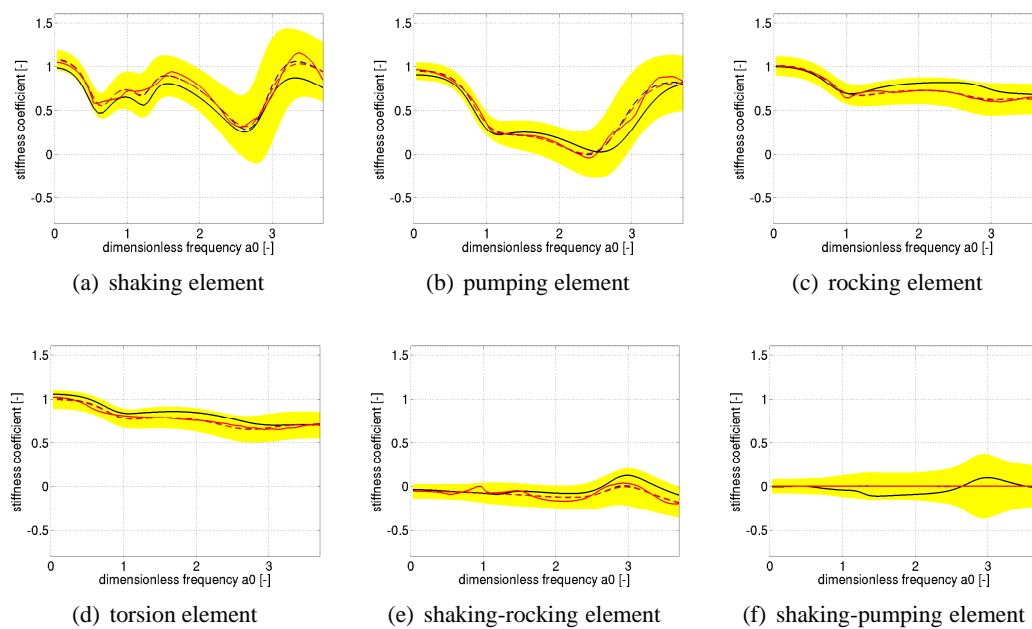


Figure 5.19: Stiffness coefficients of the soil impedance matrix computed with our nonparametric approach: response computed by MISS (solid red line), identified hidden variables model (dashed blue line), frequency-wise mean (dashed red line) and 90%-confidence interval (yellow patch) for 1000 Monte Carlo trials, and one particular Monte Carlo trial (solid black line).

matrix. They are presented in Fig. 5.17 and Fig. 5.18, respectively for the real and imaginary parts. These estimations were performed using the Epanechnikov kernel. Although these first-order marginal laws seem to exhibit interesting dynamical behavior, and particularly bimodal character at higher frequencies, the low number of Monte Carlo trials here does not allow to draw definite conclusions on the matter.

Finally, a short word should be said about the computational cost of such parametric approach for the computation of a probabilistic model of the impedance matrix. On 4 processors of a SGI Altix 350 supercomputer, the computation lasted approximately 3 weeks, for 1000 Monte Carlo trials. As each trial requires the resolution of a complete deterministic problem, the total computational cost grows more or less linearly with the number of Monte Carlo trials. Also the number of elements in the uncertain subdomain of soil induces an important increase of the cost because it has an influence on the computational time of each of the trials.

### 5.3.3 Nonparametric approach

We now turn to the construction of the probabilistic model of the impedance matrix using the nonparametric approach that was introduced in Chap. 3 of this dissertation. As described more particularly in Sec. 3.3, the steps required to construct that model include the computation of a mean model, the identification of the corresponding hidden variables model, and finally the actual construction, using the MCS method. The stochastic problem we consider in this approach is different from the previous one, because we are not required to mesh the uncertain soil, and therefore to bound it. However, we will base our stochastic problem on the same deterministic problem as before, described in Sec. 5.3.1, and it will represent our mean model for the nonparametric approach. Again, the elements of the deterministic impedance matrix are recalled on Fig. 5.19 and Fig. 5.20 in solid red line. Once we have chosen this mean model of the impedance matrix, we then go through the two following steps of the construction process.

Concerning the identification of the hidden variables model corresponding to the impedance matrix of that homogeneous problem, it was described in Sec. 4.1 to be performed in two stages: firstly, the interpolation of the input impedance matrix on a matrix-valued polynomial basis, and secondly, the identification of the matrices of the hidden variables model from that polynomial function. It was mentioned that this segmentation in two stages could induce complications because the positivity of the matrices of the hidden variables model is not enforced during the interpolation step. The system we have here, of a rigid embedded foundation on a homogeneous soil layer on a rigid bedrock, is one of those where these difficulties appear. More specifically, direct interpolation as described in Sec. 4.2 induces a non-positive damping matrix for the hidden variables model. This behavior arises from the combination of two factors:

1. the imaginary part of the diagonal elements of the matrix starts with a plateau at zero before rising, as described in Sec. 5.3.1;
2. the frequency at which this plateau ends is not the same for all the terms of the impedance matrix, namely  $a_{0,S_c}$  is different from  $a_{0,P_c}$ .

As exact interpolation by polynomials of a sharp bend in a function is often not practicable, the former point means that the interpolation process will force the identified impedance to stroll around the target impedance, sometimes above it, and sometimes below. Unfortunately, we saw in the properties of the impedance matrix, in Sec. 3.1.3, that the imaginary part had to remain positive at all frequencies, lest the system be creating energy. We also saw that this was linked to the positivity of the matrices of the

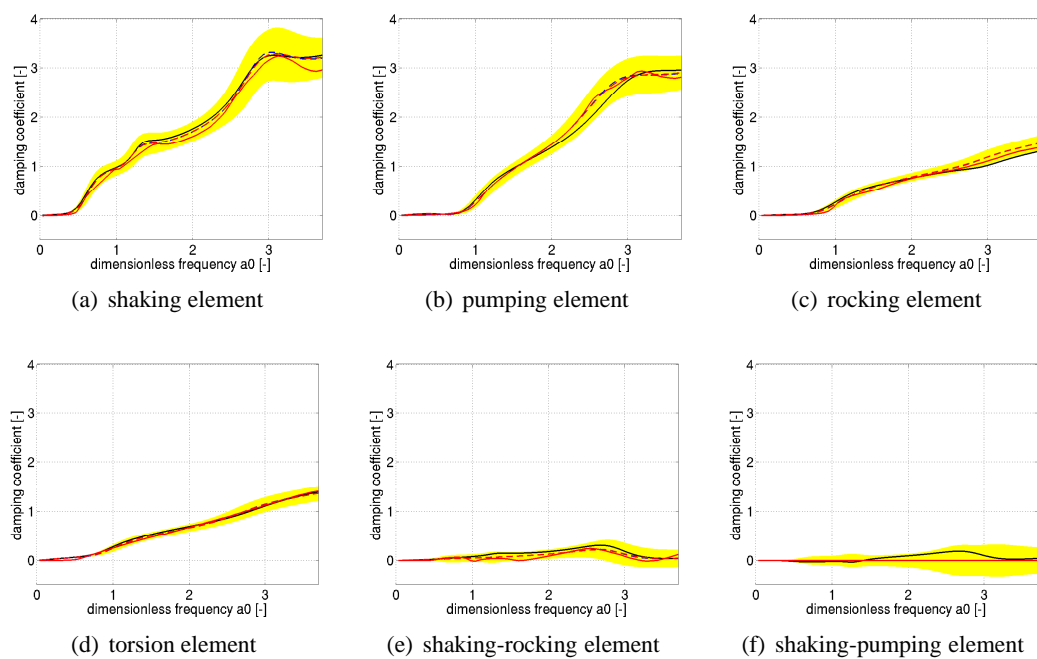


Figure 5.20: Damping coefficients of the soil impedance matrix computed with our nonparametric approach: response computed by MISS (solid red line), identified hidden variables model (dashed blue line), frequency-wise mean (dashed red line) and 90%-confidence interval (yellow patch) for 1000 Monte Carlo trials, and one particular Monte Carlo trial (solid black line).

	Hidden variable number [-]					
	1	2	3	4	5	6
Modal dimensionless frequency [-]	0.65	0.99	1.01	1.27	2.80	2.89
Modal damping [-]	0.38	0.45	0.50	0.15	0.22	0.14

Table 5.2: Modal parameters of the hidden variables model corresponding to a rigid embedded foundation on a homogeneous layer of soil on rigid bedrock.

	Hidden variable number [-]					
	1	2	3	4	5	6
$[D_c]$	$\begin{bmatrix} 0.53 \\ 0.00 \\ 0.00 \\ 0.00 \end{bmatrix}$	$\begin{bmatrix} 0.00 & 0.00 \\ 0.72 & 0.00 \\ 0.00 & 0.00 \\ 0.00 & -0.41 \end{bmatrix}$	$\begin{bmatrix} 0.00 \\ 0.00 \\ 0.57 \\ 0.00 \end{bmatrix}$	$\begin{bmatrix} 0.14 \\ 0.00 \\ 0.00 \\ 0.00 \end{bmatrix}$	$\begin{bmatrix} 0.00 & 0.00 \\ 0.19 & 0.00 \\ 0.00 & 0.00 \\ 0.00 & -0.18 \end{bmatrix}$	$\begin{bmatrix} 0.13 & -0.03 \\ 0.00 & 0.00 \\ -0.10 & -0.12 \\ 0.00 & 0.00 \end{bmatrix}$
$[K_c]$	$\begin{bmatrix} 0.38 \\ 0.00 \\ 0.00 \\ 0.00 \end{bmatrix}$	$\begin{bmatrix} 0.00 & 0.00 \\ 0.44 & 0.00 \\ 0.00 & 0.00 \\ 0.00 & -0.32 \end{bmatrix}$	$\begin{bmatrix} 0.00 \\ 0.00 \\ 0.44 \\ 0.00 \end{bmatrix}$	$\begin{bmatrix} 0.36 \\ 0.00 \\ 0.00 \\ 0.00 \end{bmatrix}$	$\begin{bmatrix} 0.00 & 0.00 \\ 1.82 & 0.00 \\ 0.00 & 0.00 \\ 0.00 & -0.72 \end{bmatrix}$	$\begin{bmatrix} 1.57 & -0.05 \\ 0.00 & 0.00 \\ 0.04 & -0.40 \\ 0.00 & 0.00 \end{bmatrix}$

Table 5.3: Coupling part of the damping matrix  $[D_c]$  and stiffness matrix  $[K_c]$  of the hidden variables model corresponding to a rigid embedded foundation on a homogeneous layer of soil on rigid bedrock. The lines of the matrices correspond, in that order, to the shaking, the pumping, the rocking, and the torsion.

hidden variables model. This means that the identification process will be prone to return a non-positive matrix for the hidden variables model when presented with an impedance matrix with a sharp bend in the imaginary part, following a large frequency band where it was cancelled. The second point adds to this complexity because the interpolation process places a pole close to each of the bends (approximately  $a_0 = 0.5$  and  $a_0 = 1$ ), and, in its attempt at improving the accuracy, wrongly creates a residue for the first pole ( $a_0 = 0.5$ ) for elements which bend at the second pole ( $a_0 = 1$ ), like the rocking element.

To circumvent these problems, we introduced another stage in the identification process, after the interpolation step, and before the identification of the matrices of the hidden variables model. In that stage, we fix the poles that were identified in the interpolation process, manually decouple those that should physically not be coupled, and re-run the interpolation only for coefficients of the matrix-valued numerator ( $[\underline{N}(\omega)]$  in Eq. (4.2)). As the poles are fixed, this interpolation is linear-in-the-parameters, and can be performed with simpler methods than those that were presented previously (we simply used the function LINSQL in MATLAB). The manual decoupling of the poles was performed by forcing an appropriate zero for the elements of  $[\underline{N}(\omega)]$  that required it. Here, we forced a zero at the second pole ( $a_0 = 1$ ) for the shaking and torsion elements, and one at the first pole ( $a_0 = 0.5$ ) for the pumping and rocking elements. Finally, when this is not sufficient, in the sense that the damping matrix is still non-positive after such treatment, appropriate elements of  $[D_\Gamma]$  can be artificially inflated. In all the examples that were considered with this method, this last measure was seldom required, and when needed, extremely small modifications of  $[D_\Gamma]$  were necessary to make it positive definite. As shown on Fig. 5.19 and Fig. 5.20, the result of the identification of the impedance matrix computed with MISS (solid red

line) with the impedance of the corresponding hidden variables model (dashed blue line) is visually very satisfactory.

The characteristics of the identified hidden variables model are presented as in Sec. 4.4, in the form of tables summarizing the modal quantities of the hidden part of the model, and the coupling damping and stiffness submatrices for each hidden variable. Six hidden variables were identified for this problem. The values of the modal dimensionless frequency  $a_{0\ell}$  and modal damping  $\zeta_\ell$ , for  $1 \leq \ell \leq 6$ , are given in Table 5.2, where it is recalled that the diagonal elements of the hidden part of the matrices of damping and stiffness are such that  $d_\ell = 2a_{0\ell}\zeta_\ell$  and  $k_\ell = a_{0\ell}^2$ . When the rank of the coupling damping and stiffness submatrices (its number of columns in Table 5.3) is larger than 1, these diagonal elements are repeated. In Table 5.3, for each hidden variable, the columns of the coupling damping and stiffness submatrices are described. Here, a condensed form was chosen in the sense that null columns were erased, and that only four DOFs of the rigid foundation are shown. The former choice of adding or quitting null columns in  $[D_c]$  and  $[K_c]$  does not change the mean model of the impedance, but it does have an impact on the probabilistic model, which will be studied further along. The latter choice of representing only the four DOFs of shaking, pumping, rocking and torsion comes from the fact that the mean model is axisymmetric, so that the identification is performed on a  $4 \times 4$  impedance matrix. When considering the probabilistic model, however, the matrices of the hidden variables model are extended to represent all 6 DOFs of the foundation.

Once the hidden variables model has been identified from the mean model, the dispersion parameter has to be selected. All three dispersion parameters were chosen here equal,  $\delta_{[M]} = \delta_{[D]} = \delta_{[K]} = \delta = 0.1$ , however it is recalled that, in further studies, this value should be identified in an appropriate manner, as indicated in Sec. 3.2.2. Monte Carlo trials of the matrices of the hidden variables model can then be drawn, the corresponding samples of the impedance matrix computed, and statistical quantities of the random impedance matrix estimated. The frequency-wise mean and 90%-confidence intervals are therefore plotted on Fig. 5.19 and Fig. 5.20 as a dashed red line and a yellow patch.

Before we go further, we plot, as in the parametric case, the convergence of the frequency-wise mean and 90%-confidence interval in Fig. 5.21, for 1000 Monte Carlo trials, and two different frequencies (as before,  $a_0 = 0.5$  and  $a_0 = 3$ ). The convergence seems to be satisfactory, so this number of Monte Carlo trials is deemed sufficient for the estimation of the first moments of the random impedance matrix.

Concerning the variations of the random impedance matrix around the mean, we plot, as for the parametric approach, the normalized variance for each of the elements of the impedance matrix. The contributions of the first modes of the covariance matrix to that normalized variance are also plotted. Contrarily to the previous case, there does not seem to be a large coupling of the modes for different elements of the matrix, and no mode is really dominating the covariance matrix. The first mode participates only for 17% of the trace of the covariance, and the first five only for 55% as a group. This is due to the way the randomness is introduced in the model here. As described in Sec. 3.2.3, for a matrix of size  $n$ ,  $n(n-1)/2$  Gaussian and  $n$  Gamma independent random variables are drawn and mixed in a complex way. There is *a priori* no reason to observe strong correlations between variances for different elements of the impedance matrix. However, smaller correlations appear due to the condensation of the dynamic stiffness matrix on the boundary, and we can observe them on the higher-order modes of the covariance matrix, which are not represented here.

On this same graph, another set of variance and modes are represented in thin lines. They correspond to a probabilistic model of the impedance matrix constructed with the same dispersion parameters and slightly different mass, damping, and stiffness matrices. The matrices for the alternative model were constructed from those of the original model by duplicating each hidden variable, but with no coupling in mass, damping, nor stiffness. This corresponds to adding to each of the submatrices of Table 5.3

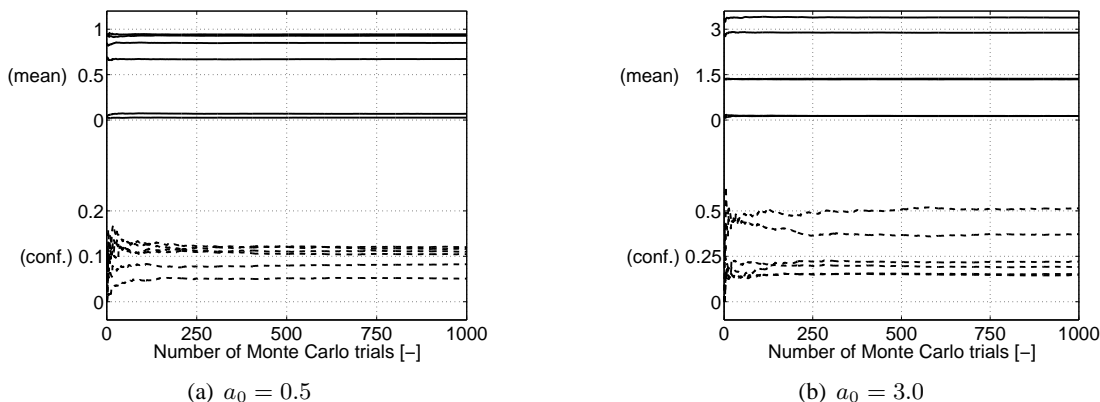


Figure 5.21: Convergence of frequency-wise mean and 90%-confidence intervals for the amplitude of the elements of the impedance matrix computed with the nonparametric method, at frequencies (a)  $a_0 = 0.5$ , and (b)  $a_0 = 3.0$ . Beware that the scales are different for the two frequencies.

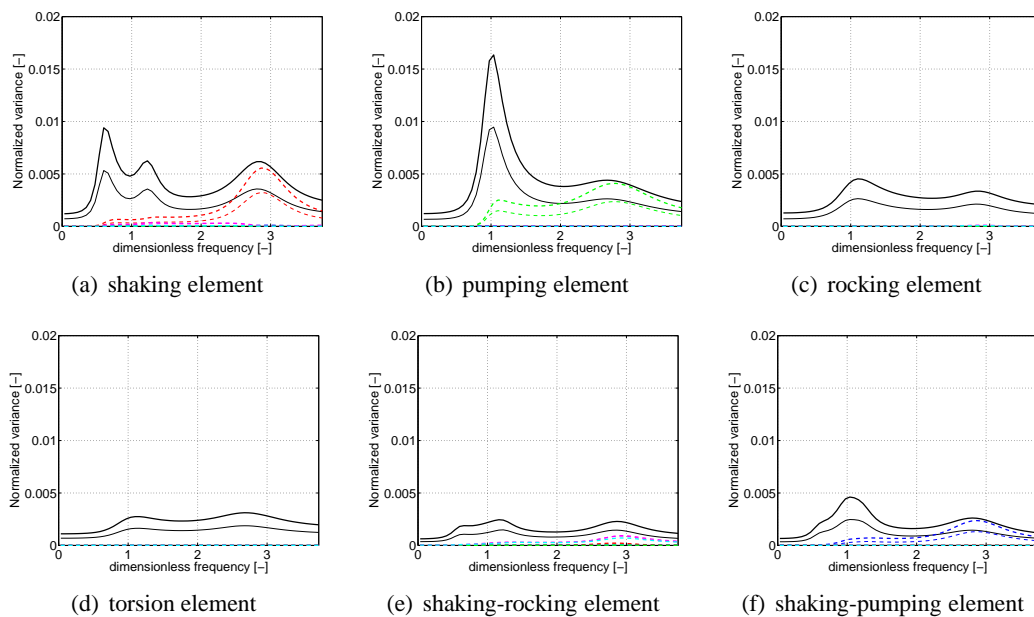


Figure 5.22: Normalized total variance (solid black line) of the elements of the random impedance matrix, and normalized variance for the first five eigenmodes of the covariance matrix (dashed red, blue, green, magenta, and cyan lines), for the normal model (thick lines), and the extended model (thin lines).

an empty column. Obviously, the mean value of the impedance is not modified. However, we see in Fig. 5.22 that it does modify the variance, towards less variability. This, again, originates from the way the random matrices are drawn. By adding columns, we change the size of the matrices, therefore adding random variables to the representation, without changing the mean impedance matrix. As these random variables are independent, this results in a model of the random impedance matrix that is less variable around its mean. This means that the identification of the dispersion parameter is not independent of the choice of the mean model. This fact was also observed in Arnst et al. [2006a].

Next, we plot in Fig. 5.23 and Fig. 5.24 the estimations of the first-order marginal laws at several frequencies of the random impedance matrix constructed using the nonparametric approach. As the number of Monte Carlo trials is higher here than before, the estimation is probably more accurate. This time, we do not observe any sign of bimodality in the estimated laws.

Finally, one of the salient features of the nonparametric approach to the modeling of uncertainty is its low computational cost. Here, the identification of the hidden variables model, as well as the drawing of the 1000 Monte Carlo trials, was a matter of minutes on a regular laptop.

### 5.3.4 Comparisons

Before starting with this section it should be reminded that the comparison of the approaches has to be performed subtly because, although they are based on the same deterministic model, the two stochastic models are different. In particular, the randomness is localized in the parametric approach while it is not in the nonparametric. The probabilistic models of the impedance matrix can therefore not be expected to be equivalent. Also, it should be reminded that neither the parameters of the probabilistic model of Lamé's parameters (the scales of fluctuation) in the parametric approach, nor the dispersion parameters in the nonparametric approach, have been identified properly. This means that, in particular, the amplitude of the variance, or the size of the confidence intervals, cannot be compared directly. As a general pattern, we expect to find similarities between the two approaches when the model errors are low compared to the errors on the parameters, or when the mean model has little sensibility to the latter type of errors. Here, the main model error that is dealt with is the homogeneity of the soil, so that we should find affinities for the elements of the impedance matrix that are more influenced by the soil below the foundation, where the model error is lower. For the other elements, disparities should be more important.

This said, a first remark should go to the adequacy of the dynamics of the variance functions in Fig. 5.16 and Fig. 5.22. They both anticipate more variability on the shaking and pumping terms of the impedance matrix, and this is in concordance with sensibility results studied in Gazetas [1983]. Also, the peaks of the variance seem to occur in both cases at the same frequency, which seems to validate the existence of internal resonance modes, and the identification of the hidden variables model in the nonparametric case. In the parametric case, the variance of the pumping is much higher than the other terms, but it is due to the location of the uncertain domain, right under the foundation, where it influences much more the pumping term than the others. In the nonparametric case, the variance is more equilibrated in the elements, which seems to go along with the concept that the uncertainty for that model is not localized.

A nice feature of the parametric approach, that is not accessible in the nonparametric approach, is the possibility to relate the probabilistic model of the uncertain parameters to the stochastic model of the impedance matrix. This may be useful in the design stage of a foundation, when trying to understand the physical phenomena taking place inside the soil. However, this feature is related to our capability to identify these models of the parameters in the soil, which is feeble at best. The dispersion parameter, on the contrary, is well suited for identification. There is only one dispersion parameter for each of the

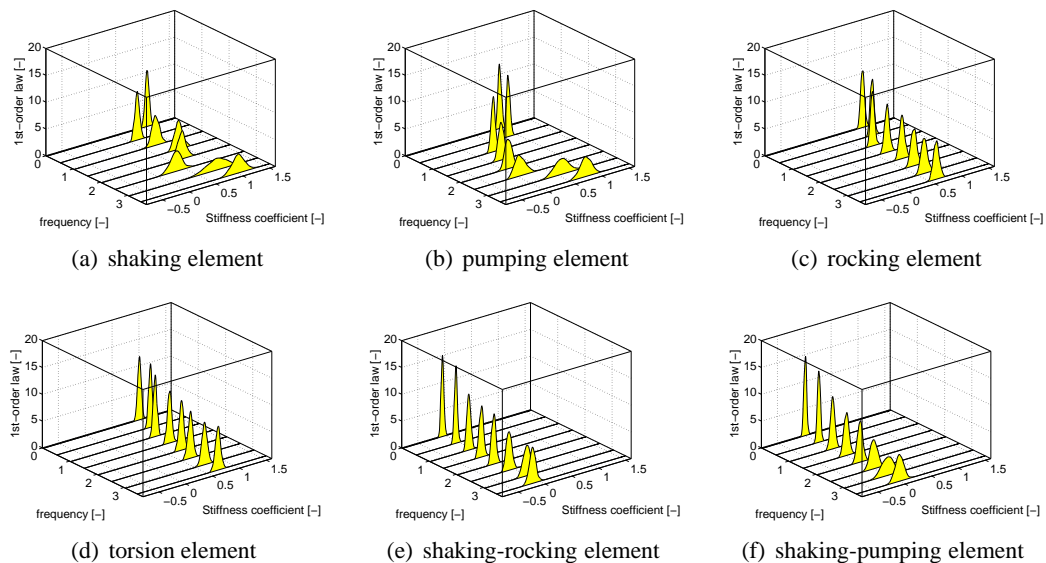


Figure 5.23: Estimation of the first-order marginal law of the stiffness coefficient of the elements of the impedance matrix at several frequencies.

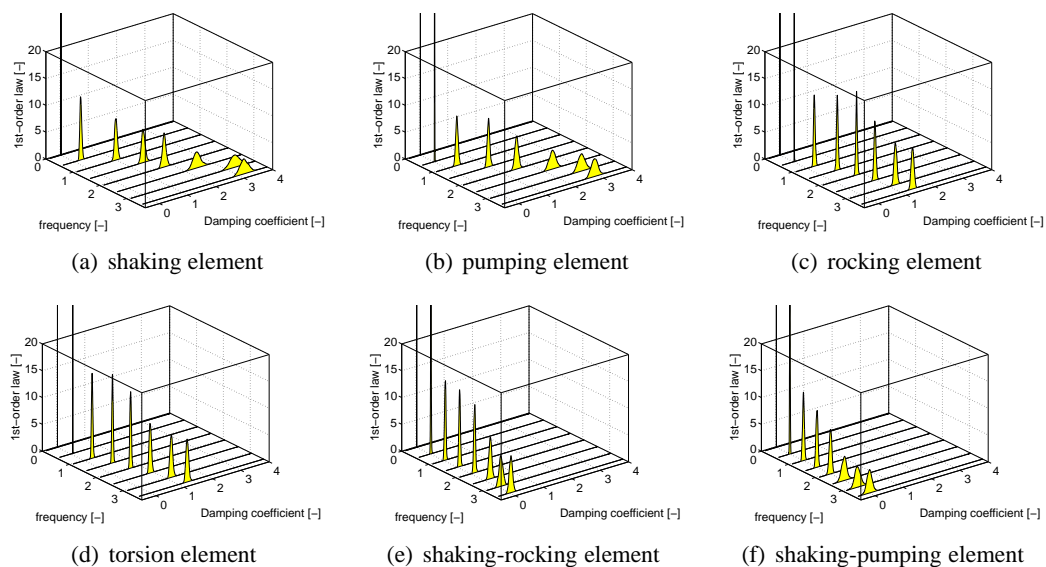


Figure 5.24: Estimation of the first-order marginal law of the damping coefficient of the elements of the impedance matrix at several frequencies.

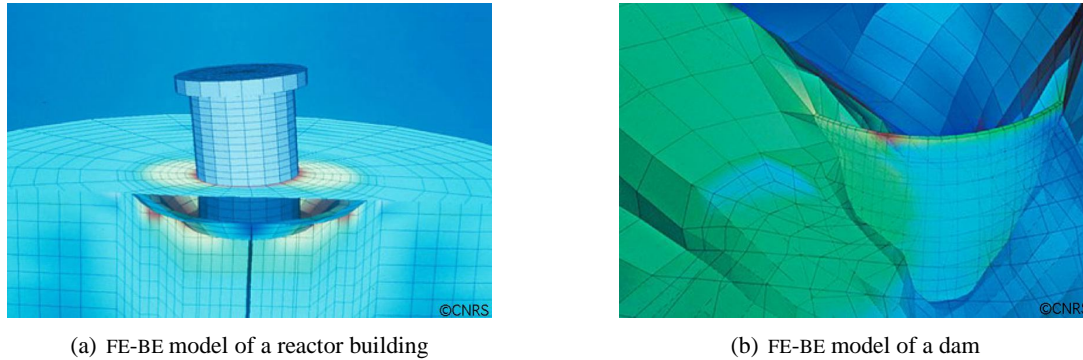


Figure 5.25: Typical structures studied by EDF: mixed FE-BE models of (a) a reactor building with its soil and (b) a dam with the soil and water.

matrices of the hidden variables model, and an identification process would not require any underground investigation, because these parameters are linked to the impedance matrices that are measured at the ground level, on the foundations.

Finally, considering the numerical costs associated with each of the methods, the nonparametric approach has an unequivocal advantage. Not considering the cost of the construction of the mean model, which is the same in both cases, the construction of the nonparametric model with 1000 Monte Carlo trials was a matter of minutes, while it was a matter of days in the parametric case, also for 1000 Monte Carlo trials.

## 5.4 Design of a building using a stochastic impedance matrix

The previous application presented the construction of probabilistic models of the soil impedance matrix. However, this type of model is not interesting *per se*, because the quantities of interest for design applications lie rather in the structure than in the soil. We study here, on an industrial building, the impact that the randomness of the impedance matrix has on the quantities of interest for its design. In particular we will consider the maximum acceleration at the top of the building, and other quantities could have been equivalently observed. As this thesis was conducted in collaboration with the I&R department of the company EDF, we first present their needs in terms of seismic design, and the position of this dissertation with respect to others that were conducted in related fields with the same company.

### 5.4.1 Industrial needs

EDF is the main electricity operator in France, and, as such, builds and operates nuclear plants and dams (Fig. 5.25). These sensible structures are submitted to a very strict and constraining regulation concerning, in particular, the seismic risk. Even though that risk is very limited in metropolitan France, the designers of these structures have to consider the possibility of occurrence of rather large earthquakes, and to assess the resistance of the structures in those cases. When considering the SSI problems associated with the assessment of the seismic behavior of nuclear plants and dams, and as was discussed earlier, the variability in the soils and the randomness of the seismic motions may be particularly influent and, nevertheless, difficult to take into account. A classical approach consists in using security coefficients

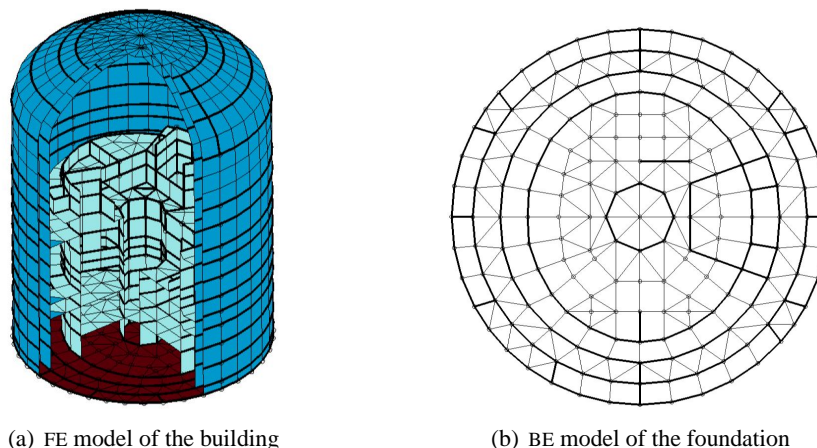


Figure 5.26: FE model of the structure and corresponding BE model for the foundation.

to avoid errors due to the uncertainty on these parameters. However, for the levels of reliability that are required for these structures, this approach may yield a design that is overly conservative. Considering that the costs associated with the construction, or rehabilitation, of the nuclear plants and dams are very high, EDF R&D and the Service d'Études et Projets Thermiques et Nucléaires (SEPTEN), which are respectively the I&R department and the Design department of EDF, are therefore interested in the construction of refined models of the SSI problem. With these, the goal is to be able to localize the areas where particular attention is required, and to lower the requirements on less critical zones.

The interest for stochastic approaches in SSI problems of EDF R&D and the SEPTEN is not new, and several Ph.D. theses were realized under their patronage. At the University of Bordeaux I, Antoinet [1995] used a SFE approach to quantify the impact of the variability of the soil properties on the settlement of the foundation of a nuclear plant. The works of Toubalem [1996] at the École Centrale de Lyon and of Savin [1999] at the École Centrale Paris, which were mentioned in Sec. 5.2.2, were also conducted with their collaboration. It is also interesting to note that the needs of EDF in France parallel those of the nuclear industry in the United States, where stochastic SSI problems are also the subject of attention [Ghiocel and Ghanem, 2002].

#### 5.4.2 The classical deterministic approach

We present in this section an example of the deterministic computation of the maximum acceleration at the top of the building. Although we have chosen the maximum acceleration as a quantity of interest, any other could have been equivalently derived, provided that the FE model of the building allowed its computation. The model of the building, the model of the soil, and the model of the earthquake loading are successively described. Then, the impedance matrix is computed, and the global problem solved to yield the acceleration at the top of the reactor building.

The building we consider for this application is a model of reactor building (Fig. 5.26(a)), with the shape of a cylinder closed by a semi-spherical top. It is composed of a double wall, and the interior structure is also represented. The height of the building is 75 m and the radius of the cylinder is approximately 25 m. The FE model uses 2578 nodes and 7429 elements, and was designed using the softwares OpenFEM [2006] and SDT [Balmès and Leclère, 2003]. We will study this SSI problem on a frequency

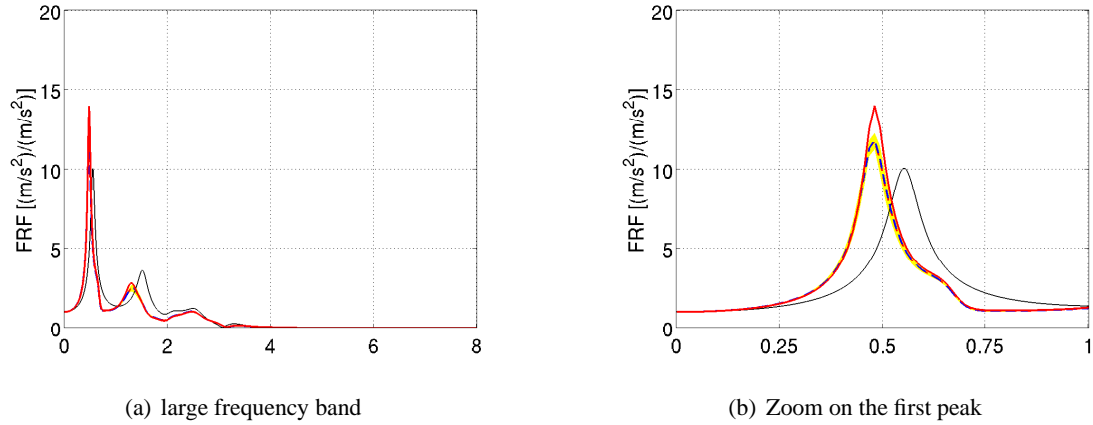


Figure 5.27: Ratio of the amplitude of the displacement at the upmost node of the building to the amplitude of a displacement imposed on the foundation (thin black line), and to the amplitude of a plane SH-wave propagating in the soil, polarized in the direction of the observation (deterministic case in solid red line, hidden variables model in dashed blue line, mean of the probabilistic model in dashed red line, and 90%-confidence interval in yellow patch).

	$h$ [m]	$\rho$ [kg/m <sup>3</sup> ]	$c_p$ [m/s]	$c_s$ [m/s]	$E$ [GPa]	$G$ [GPa]	$\nu$ [-]	$\lambda$ [GPa]	$\mu$ [GPa]	$\beta$ [-]
Layer 1	10.5	2400	2807	1235	10.10	3.66	0.38	11.59	3.66	5%
Layer 2	10.5	2500	3721	1741	20.60	7.57	0.36	19.48	7.57	5%
Layer 3	19.5	2400	3715	1577	16.60	5.97	0.39	21.17	5.97	5%
Substratum	$\infty$	2500	3797	1992	26.00	9.92	0.31	16.19	9.92	5%

Table 5.4: Thickness  $h$ , unit mass  $\rho$ , pressure velocity  $c_p$ , shear velocity  $c_s$ , Young's modulus  $E$ , shear modulus  $G$ , Poisson's ratio  $\nu$ , Lamé's coefficients  $\lambda$  and  $\mu$ , and hysteretic damping coefficient  $\beta$  of the layers and substratum of soil.

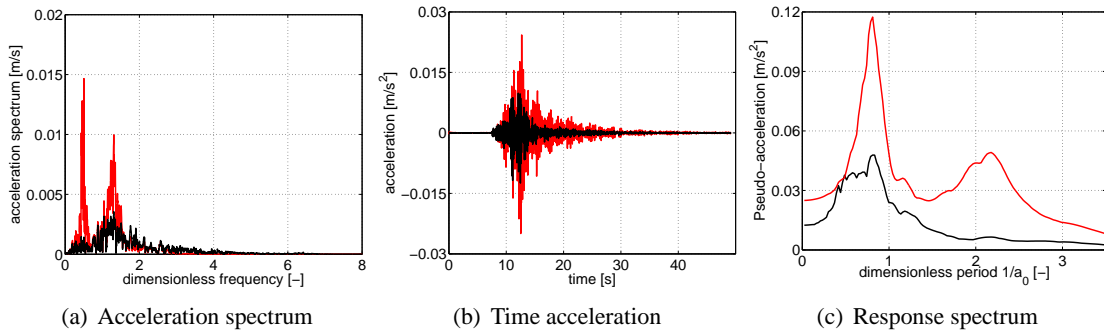


Figure 5.28: (a) Spectrum, (b) time history, and (c) pseudo-acceleration response spectrum for the input accelerogram (black line) and the acceleration at the top of the building (red line), in the direction of polarization of the incoming seismic wave.

band of  $a_0 \in [0.1, 8]$ , or  $f \in [0.5, 64]$  Hz, which is larger than what is usually required in this type of problem. In that band, and apart from the rigid body movements, we consider 200 fixed-interface modes of the structure, which is also more than necessary to represent the behavior of a building excited by a seismic signal. We consider a constant modal viscous damping over all modes of  $\zeta = 7\%$ . On Fig. 5.27, the ratio of the amplitude of the displacement at the upmost node of the building to the amplitude of a displacement imposed on the foundation, is represented in a thin black line. This ratio is useful when designing the building without considering the SSI effects. The peaks indicate the modes that will be the most important for the computation of the displacement (and acceleration) at the top of the building. Here, those peaks correspond to bending modes of the exterior wall, to which the DOF we are considering belongs.

The BE mesh of the foundation corresponding to the FE mesh of the structure, and which is used for the computation of the soil impedance matrix, is drawn on Fig. 5.26(b). It represents a circular, rigid, surface foundation. The soil at the site of this building is composed of three relatively stiff layers over a substratum. The mechanical parameters of these layers and of the substratum are given in Table 5.4. The presence of a softer layer between the second layer and the substratum should be signaled, but it was shown in a previous study [Savin, 1999] to have little influence on the overall behavior of the SSI system. The soil impedance matrix is computed using the software MISS, and the stiffness and damping coefficients are respectively plotted on Fig. 5.29 and Fig. 5.30, in solid red line. The conventions of Eq. (5.16) and Eq. (5.17) are used for the normalization.

Finally, we consider the model of the seismic signal used to load the structure. We chose the ground motion that was described in Fig. 5.8, and recorded on January 11, 1999, at the Musée Dauphinois site, near Grenoble, in France. It represents a Magnitude 4.2 earthquake, and the motion was recorded at 18 km from the epicenter, on a rock site. In Fig. 5.28, we recall its time history, along with its acceleration spectrum, which is the Fourier transform of the time acceleration. The seismic wave is modeled as a plane SH-wave propagating vertically. As discussed in Sec. 5.1.2, there is no kinematic interaction for this problem, because the foundation is rigid and on the surface level. Therefore the vector  $[c_0(\omega)]$  is equal to the surface free-field displacement vector of the input earthquake, and the load vector  $[F^s(\omega)]$

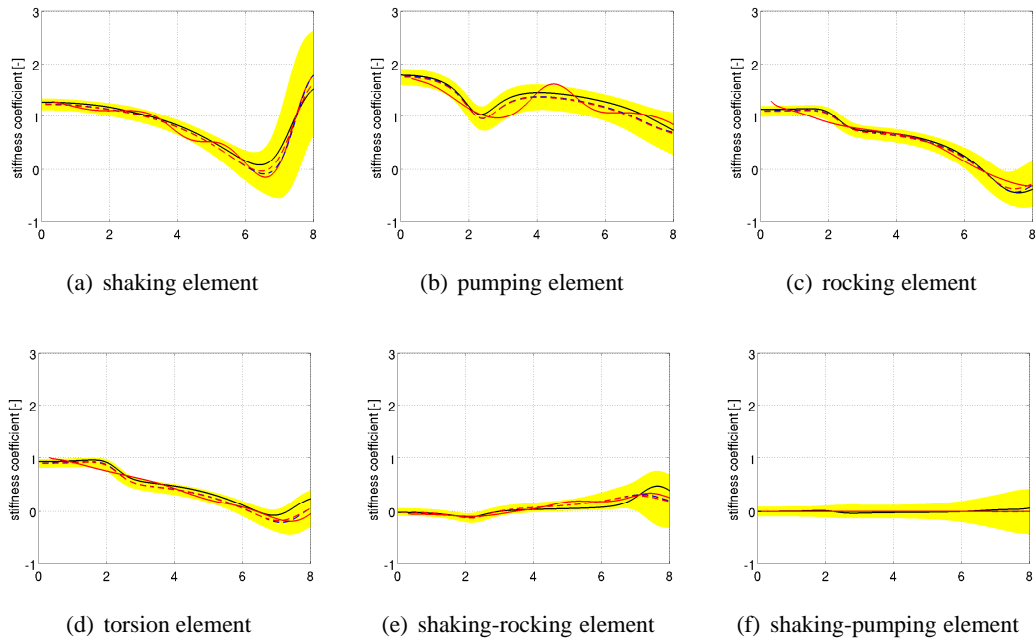


Figure 5.29: Stiffness coefficients of the soil impedance matrix computed with our nonparametric approach: impedance computed by MISS (solid red line), identified hidden variables model (dashed blue line), frequency-wise mean (dashed red line) and 90%-confidence interval (yellow patch) for 1000 Monte Carlo trials, and one particular Monte Carlo trial (solid black line).

can be computed as

$$[F^s(\omega)] = [Z^s(\omega)] \begin{bmatrix} 1 \\ 0 \\ 0 \\ 0 \\ 0 \\ 0 \end{bmatrix} a(\omega), \quad (5.24)$$

where  $[Z^s(\omega)]$  is given in the basis of the rigid body displacements of the foundation,  $a(\omega)$  is the spectrum of the accelerogram, plotted in Fig. 5.28(a), and the geometrical vector indicates that the model SH-wave is polarized along the first horizontal direction, and generates translation only along that direction, and no rocking or torsion.

Using these models of the soil, the structure and the loading, we solve the coupled problem in the frequency domain. First, the ratio of the amplitude of the displacement at the upmost node of the building to the amplitude of the model SH-wave,  $a(\omega)$ , is represented in Fig. 5.27 in a solid red line. Comparing with the problem without SSI (in thin black line), we observe the usual shift of the peaks towards the lower frequencies, the amplification in amplitude of the first peak, and the reduction in amplitude of the following. We then compute the acceleration spectrum of the top node of the building, in the direction of polarization of the seismic wave (Fig. 5.28(a)). Comparing it to the spectrum of the earthquake, we see that it was filtered around the resonance frequencies of the first two bending modes of the building. By inverse Fourier transform, we then go back to the time domain, and plot the acceleration history of the top

	Hidden variable number [-]		
	1	2	3
Modal dimensionless frequency [-]	2.40	7.62	9.29
Modal damping [-]	0.09	0.14	0.30

Table 5.5: Modal parameters of the hidden variables model corresponding to a rigid circular surface foundation over a horizontally-layered soil.

node of the building (Fig. 5.28(b)). Compared with the acceleration history of the input earthquake, we observe a longer duration of the oscillations, and a large amplification. The pseudo-acceleration response spectrum of a given signal, and for a given frequency, is the acceleration of a 1-DOF system resonating at the given frequency, were it to be excited by the given signal. It is useful when designing a secondary system, modeled as a 1-DOF system, connected to a principal one, when the dynamical behavior of the latter can be supposed not to be influenced by that of the former. This pseudo-acceleration response spectrum is plotted in Fig. 5.28(c), both for the input seismic accelerogram, and for the acceleration at the top of the building.

### 5.4.3 Probabilistic model of the response of the building

We now turn to a probabilistic modeling of this problem. Specifically, we consider the soil uncertain, and model the soil impedance matrix with the nonparametric method described in this dissertation. The building itself is still modeled in the same deterministic manner, following the discussion of Sec. 5.2.1. Concerning the seismic signal, we keep using the same surface recording, so that the equivalent load  $[F^s(\omega)]$  on the foundation is a random process, defined by Eq. (5.24). In doing this, we implicitly suppose that the incident wave remains a plane SH-wave propagating vertically, which may be arguable in the case of a heterogeneous soil. As in the previous example, we go through the three steps of our method: the computation of a mean model of the impedance matrix, the identification of the corresponding hidden variables model, and finally the determination of the probabilistic model using the MCS method. Again, we choose the deterministic impedance matrix of the previous section as our mean model, and move one to the last two steps.

This time, the identification of the hidden variables model is simpler than in the previous application, because there are no cutoff frequencies to be dealt with. The method described in Sec. 4.2, is therefore directly used, and yields a hidden variables model with three hidden variables. The corresponding stiffness and damping coefficients are plotted in dashed blue line on Fig. 5.29 and Fig. 5.30. Comparing with the impedance of the mean model (in solid red line), we observe some discrepancies around  $a_0 = 4$ , particularly for the pumping term. Since we are considering an horizontal seismic excitation, this should not influence severely the response. There are also some differences in the rocking and torsion elements in the lower frequency band, which induce some apparent damping in the FRF of Fig. 5.27 between the mean model and the hidden variables model. The modal parameters of the hidden variables model, as well as the damping and stiffness coupling matrices are represented in Table 5.5 and Table 5.6. The previous commentaries about the form of the matrices presented in Table 5.3 (number of columns and channels) are also valid and the condensed form is still used.

Once this hidden variables model has been identified, we can compute the probabilistic model of the soil impedance matrix. We draw 1000 Monte Carlo trials of the mass, damping, and stiffness matrices of the hidden variables model, using, as before  $\delta_{[M]} = \delta_{[D]} = \delta_{[K]} = \delta = 0.1$ . The random impedance

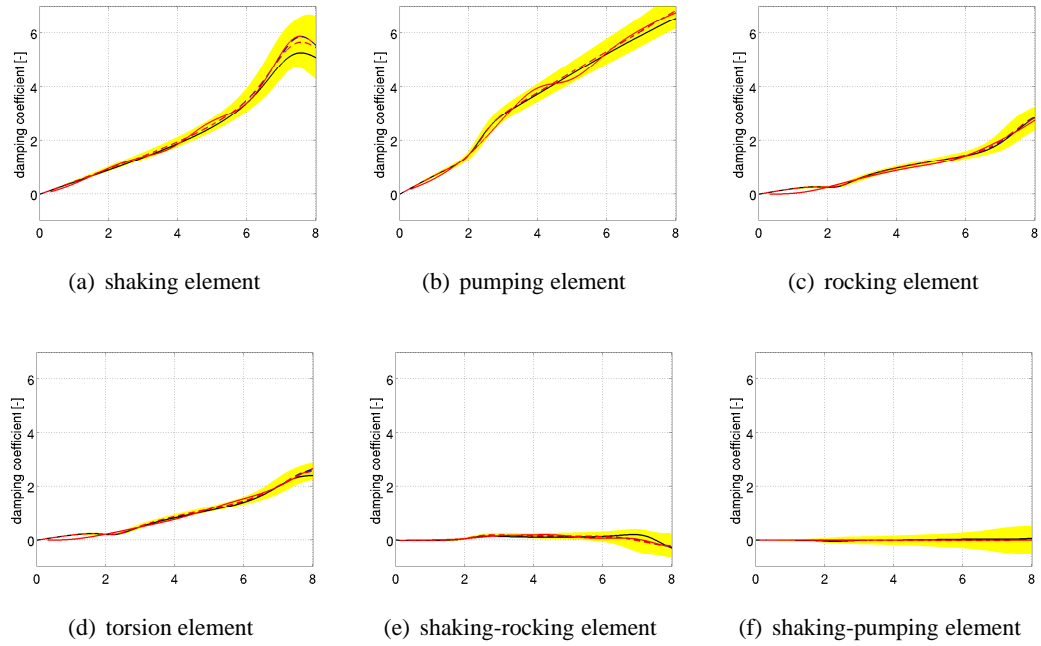


Figure 5.30: Damping coefficients of the soil impedance matrix computed with our nonparametric approach: impedance computed by MISS (solid red line), identified hidden variables model (dashed blue line), frequency-wise mean (dashed red line) and 90%-confidence interval (yellow patch) for 1000 Monte Carlo trials, and one particular Monte Carlo trial (solid black line).

	Hidden variable number [-]											
	1				2				3			
$[D_c]$	0.0	0.0	0.1	0.2	0.0	0.0	0.0	0.0	-0.2	0.0	0.1	0.0
	-0.5	0.0	0.0	0.0	0.0	0.0	0.0	-0.2	0.0	-0.4	0.0	0.0
	0.0	0.0	-0.4	0.0	0.1	0.0	0.3	0.0	0.0	0.0	0.2	0.0
	0.0	-0.4	0.0	0.0	0.0	-0.1	0.0	0.0	0.0	0.0	0.0	0.0
$[K_c]$	0.00	0.00	-0.4	0.3	-6.7	0.0	0.6	0.0	-4.4	0.0	0.5	0.0
	-1.3	0.0	0.0	0.0	0.0	0.0	0.0	-1.2	0.0	-0.9	0.0	0.0
	0.0	0.0	-0.3	0.2	1.0	0.0	3.4	0.0	1.5	0.0	2.1	0.0
	0.0	-0.2	0.0	0.0	0.0	-3.3	0.0	0.0	0.0	0.0	0.0	1.3

Table 5.6: Coupling part of the damping matrix  $[D_c]$  and stiffness matrix  $[K_c]$  of the hidden variables model corresponding to a rigid circular surface foundation over a horizontally-layered soil.

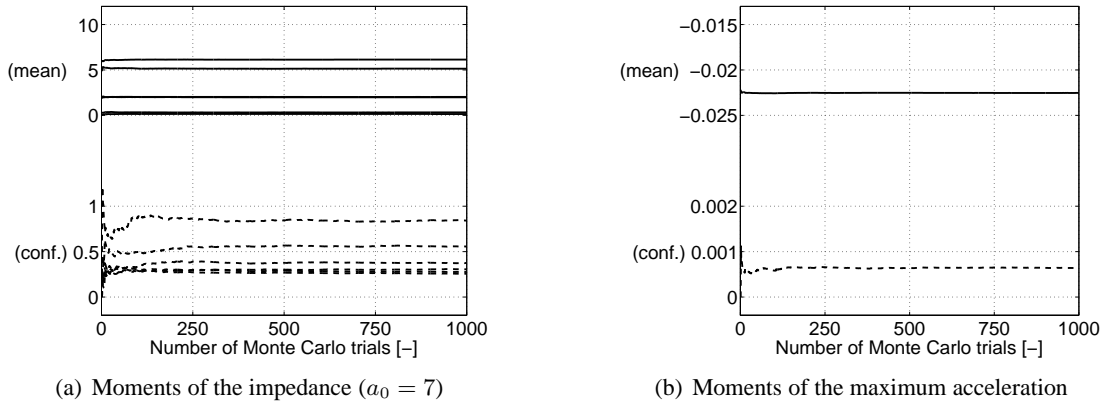


Figure 5.31: Convergence of the mean and the 90%-confidence interval of (a) the elements of the soil impedance matrix, for  $a_0 = 7$ , and (b) for the maximum acceleration at the top of the building.

matrix can then be derived, and the frequency-wise mean and 90%-confidence intervals for the stiffness and damping coefficients are plotted in Fig. 5.29 and Fig. 5.30. The convergence of the first two moments of the elements of the impedance matrix, for  $a_0 = 7$ , are plotted in Fig. 5.31(a), and seems to be reached.

As we are interested here in the laws of the acceleration of the top node of the structure, and in the PDF of the maximum acceleration, we solve the coupled SSI problem for each of the samples of the impedance matrix. The frequency-wise mean and 90%-confidence intervals of the ratio of the amplitude of the displacement at the upmost node of the building to the amplitude of the model SH-wave are represented in Fig. 5.27. It is notable that the solid red line, which corresponds to the homogeneous problem, lies above the confidence interval. However, it is not entirely due to an apparent damping induced by the consideration of randomness in the soil, but rather to the error introduced in the identification of the mean model. To not take falsely into account that error, which will be discussed in the conclusions, we will therefore compare, for the remainder of this application, the probabilistic model with the hidden variables model rather than the homogeneous one.

We then plot in Fig. 5.32 the random model for the acceleration on top of the building, as well as the homogeneous one (in solid red line) and the hidden variables model (in dashed blue line), for comparison. Again, the decrease in the amplitude of the random model with comparison to the deterministic one is due to the error in the identification of the hidden variables model. The mean of the trials and the hidden variables model are, however, almost identical. It is also interesting to note that the phase of the acceleration seems to be very little influenced by the randomness of the soil. Indicatively, on the same figure, the results obtained for the 90%-confidence interval for the acceleration at the top of the building, for a random model of the soil impedance matrix constructed using a dispersion parameter  $\delta = 0.3$ , are also plotted.

Finally, we look at probabilities of failure. If we consider for example a failure due to high accelerations at the top of the building, we can plot for the appropriate DOF, an estimation of the PDF, and of the cumulative density function, of the maximum acceleration. On the latter, we can read the estimation of the acceleration corresponding to any desired quantile. For example, there is a 95% chance that the acceleration be below  $22.9 \text{ mm/s}^2$ , and a 99% chance that it be below  $23.0 \text{ mm/s}^2$  (in absolute value). With the soil impedance model computed with  $\delta = 0.3$  these values become, respectively,  $30.6 \text{ mm/s}^2$

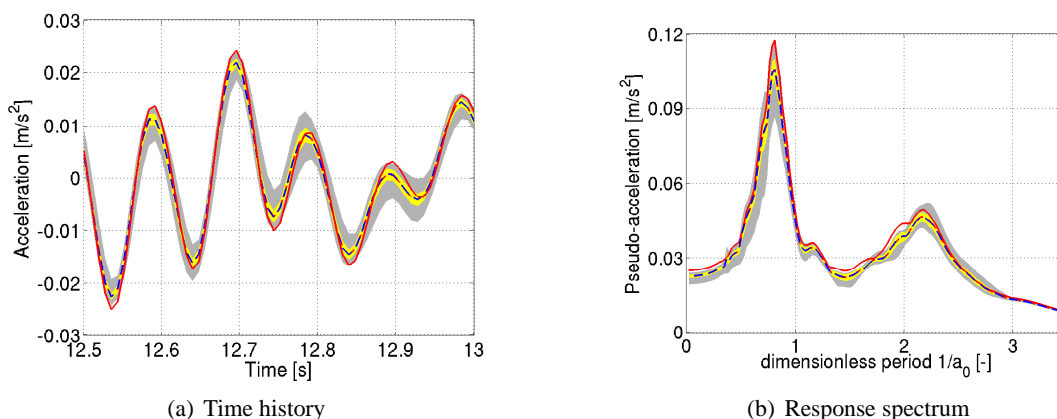


Figure 5.32: (a) Time history, and (b) pseudo-acceleration response spectrum for the acceleration at the top of the foundation for the deterministic study (solid red line), the hidden variables model (dashed blue line), and the probabilistic model (mean in red dashed line, for  $\delta = 0.1$ , and 90%-confidence interval in yellow patch for  $\delta = 0.1$  and grey patch for  $\delta = 0.3$ ) of the impedance.

and  $30.8 \text{ mm/s}^2$ . However, these considerations should be treated with care, because the convergence of these very high quantiles takes a large number of Monte Carlo trials (Here, it was checked for these two quantiles for 1000 Monte Carlo trials, although it is not plotted here). More simply, it can be checked that the mean is slightly below the value for the hidden variables model for  $\delta = 0.1$ , and drops further for  $\delta = 0.3$ .

As a conclusion, it should be noted that, apart from the generation of the random soil matrices, all the computations that were presented in this application are very common tools for the earthquake engineers. The computational costs are higher than a regular design analysis because the problem must be solved for each Monte Carlo trial of the impedance matrix, but subsequently the designer obtains a PDF for his quantity of interest rather than a sole deterministic value. Even if the quantity as the mean of the Monte Carlo trials is equal to the quantity computed using a deterministic model, the additional information, including the sensibility of that design quantity to uncertainties on the model or the data, may be invaluable. However, here, the accuracy of the identification of the hidden variables model seems to be poor, and diminishes the interest of the method for that particular example. Thus, this issue will have to be the object of future study, as will be discussed in the next, and last, section.

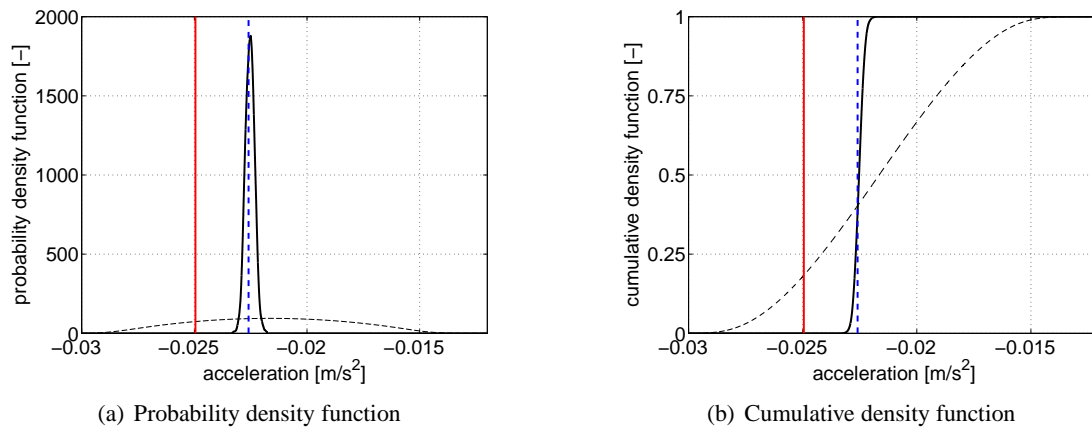


Figure 5.33: Estimations of the probability density function and cumulative density function for the maximum acceleration at the top of the building for the probabilistic model of the impedance matrix (with  $\delta = 0.1$  in thick solid black line, and with  $\delta = 0.3$  in thin dashed black line), and corresponding values for the mean model (solid red line) and the hidden variables model (dashed blue line).



# Chapter 6

## Conclusions and perspectives

This dissertation introduced a novel approach to the probabilistic modeling of impedance matrices. After an introduction on general matters concerning the impedance matrices, the DD techniques, and the issues and features of probabilistic modeling in mechanics, a review was presented (Chap. 2) of existing methods for the probabilistic modeling of mechanical problems. Of these, most were shown to be poorly adapted to the consideration of variability in large or very uncertain domains, and the nonparametric approach was then hinted at. In the following chapter (Chap. 3) a formal definition of the impedance matrix was given in a general context, along with some of its most salient properties, and the hidden variables model and the nonparametric approach for the probabilistic modeling of impedance matrices were introduced. The latter and the content of Chap. 4, which presents the identification of the hidden variables model, constitute the two main novelties of this dissertation. Finally, in Chap. 5, the issues described in the previous chapters are particularized in the case of SSI problems, and two major applications are presented.

In the following brief sections, we try to critically summarize the main interests and drawbacks of the items that were introduced in this dissertation.

### **Features of the hidden variables model of the impedance matrix**

The first tool that was extensively used in this dissertation is the hidden variables model of the impedance matrix, that was introduced by Chabas and Soize [1987]. We used it here to create probabilistic models of impedance matrices, but it is really a deterministic model that can be valuable in other situations. We have tooled it up, in this dissertation, with a new identification method that works for scalar impedance functions as well as matrix-valued impedances.

Theoretically, the views behind this hidden variables model and the lumped-parameter models that were presented in Sec. 5.1.4 are very similar. The idea is to replace whichever impedance function by an approximation in terms of the impedance of a simpler system of masses, dampers and springs. This really corresponds to the problem of approximating a given function by the ratio of two polynomials of the frequency. A great interest of these models is the possibility to use the approximated system directly in the time domain. Likewise, the mass, damping, and stiffness matrices of the hidden variables model are serviceable in the time domain. This is interesting, for example, to couple the domain that is represented by the impedance to a nonlinear structure.

The strength in our approach, with comparison to the lumped parameter models, is the possibility to consider the problem entirely in a matrix setting. This is made possible by the results of Sec. 4.3.2, that are entirely novel to this thesis. The consideration of the matrix-structure of the impedance means that the poles, that are global quantities, will be identified for all elements at the same time. It also means that coupling in the matrix is naturally taken into account, while the lumped parameters models have to devise specific schemes to consider it (see for example Wolf and Somaini [1986]). Further, we expect

to be able to identify the hidden variables model of flexible foundations, while the lumped parameters models are stuck with the rigidity hypothesis, which limits the coupling between the elements of the impedance matrix.

### **Features of the nonparametric approach to the probabilistic modeling of the impedance matrix**

In the conclusion of Chap. 2, we advocated the interest of the nonparametric approach to the modeling of large mechanical systems with significant model uncertainties and parametric errors, with comparison to more classical parametric methods. The application in Sec. 5.3 confirmed that view on several points. For large systems, the meshing of the large domain is indeed a very debilitating inconvenience. For a heterogeneous soil, the assumption of homogeneity outside the meshed domain induces large model errors that cannot be taken into account with a parametric method. This yields, as in the application presented, strong asymmetry in the variances of the different elements of the impedance matrix. Besides, when considering a large meshed domain, the computational costs may rise very rapidly. In comparison, the nonparametric method for the probabilistic modeling of the impedance matrix is numerically cheap, and can take into account the model errors introduced by the consideration of a homogeneous soil rather than a more realistic heterogeneous one.

Another important factor that should be considered when choosing a modeling method is the possibility to identify its parameters. In the parametric methods, the parameters are those that allow the representation of the random fields to be created. They include, among other, the choice of a type of correlation function, with the associated correlation lengths, and the choice of a type of set of first-order marginal laws. The inverse problem to determine these parameters requires a large data set of samples of the random field, spanning the entire support of the field. While it might seem feasible in some cases, it is rather ambitious in the case of soils, where such large scale experiments are very expensive, and the requirement to measure the parameters including in depth is rather hindering. The literature on that matter therefore offers many conflicting models, with little clues as to which should be elected. On the contrary, the identification of the parameters of the nonparametric approach, which are the dispersion parameters  $\delta$  for each of the matrices, seems more practicable. The main aspect is that this identification involves only the measurements of impedance matrices, which are performed on the subsurface, and are therefore more easily workable.

### **Issues, and possible improvements, of the identification process of the hidden variables model**

In the two applications that were presented in this dissertation (Sec. 5.3 and Sec. 5.4), we presented the identification of soil impedance matrices for two different mechanical systems. In the first example, the straight identification yielded either non-positive matrices for the hidden variables model, or unstable poles, depending on the chosen number of hidden variables, so that a more complicated identification process had to be set. In the second example, the direct identification was possible, but the approximation could not be improved further than with three hidden variables, lest the identified system be, again, unstable.

These issues in the identification process arise because we have chosen to separate that process into an interpolation stage, workable with any scheme in the literature, and a more specific identification step, where the matrices of the hidden variables model are determined. This separation seemingly impedes us from enforcing conditions on the matrices at the level of the interpolation. Although the blunt signature may not be enforceable directly, there are, however, some possibilities. For example, the positivity of the hidden part of the damping matrix is directly related to the stability of the system, and, in [Strelitz,

1977], a method is described to enforce the stability of a rational polynomial function at the level only of the coefficients of the polynomials. More generally, the particular identification method that we have chosen for the applications in this dissertation can provide a very elegant way to enforce some of these conditions. The formulation of the identification in terms of the Eq. (4.12), in particular, allows us to introduce constraints such as that of Strelitz.

Alternatively, the non-positivity of the damping matrices arising during the identification of the hidden variables models of the impedance matrix of certain mechanical systems might come from the main hypothesis that was performed in the derivation of the hidden variables model. In Sec. 4.3.1, we suppose that the hidden part of the damping matrix could be diagonalized in the same basis as the hidden parts of the mass and stiffness matrices. Although often accepted in structural mechanics this hypothesis might be too strong for some of the applications considered. In Hasselman [1976] and Park et al. [1992], two criteria are given to determine the appropriateness of that hypothesis, depending on the separation of the modes on the frequency line, and the modal damping. For the problems for which that hypothesis is not fitting, an fruitful approach might consist in identifying an initial set of matrices with a non-positive (diagonal) damping matrix, and update it under particular constraints to yield a set of positive matrices. In Beattie and Smith [1992], such an iterative process is presented, where a matrix is updated under the constraints of a given sparsity pattern and signature, while minimizing the mean-square difference between the old and new matrices. However, a main difference with our case is that we need to update the damping matrix under constraints, while minimizing the modifications in terms of the impedance matrix.

### **Consideration of a correlated loading**

In the application of Sec. 5.4, the load that is used in the resolution of the coupled SSI problem corresponds to a seismic free-field ground motion, following the scheme of Fig. 5.2. Physically, the seismic waves propagate inside the heterogeneous soil before hitting the building so that they should really be modeled by a random field. Furthermore, this field should be heavily correlated with the random impedance matrix. If probabilistic models of the seismic motions are readily available in the literature, the way to correlate these models to our probabilistic model of the impedance matrix is not obvious.

One trail might be to follow the leads of the designers of the lumped parameters models, and to impose the seismic excitation as a displacement at the basis of the lumped model rather than as a load at the foundation level. By doing this, the seismic is conceptually seen to go through the soil system. However, this goes against the typical approach in earthquake engineering, and would require the computation of the appropriate model of the input motion. Attempts in that direction are presented, for example, in de Barros and Luco [1990] and in a series of papers by Wu and Chen [2001, 2002] and Wu and Lee [2002], where massless lumped-parameters models are developed.

### **Further applications**

In spite of these difficulties in the identification process, the methods described in this dissertation are very promising. The very generic character of the hidden variables model, as well as its connections to matrices of mass, damping and stiffness, that are very familiar for the mechanicians, allows us to plan further applications. Among them, an interesting opening would be the consideration of the hidden variables model corresponding to impedance matrices of complicated systems, such as flexible foundations or pile groups. The hidden variables approach would beneficially complement the work of Taherzadeh and Clouteau [2006], and help detect the meaningful physical parameters controlling the soil-pile group-superstructure interaction problems.

Another possible application of the tools presented in this dissertation is the identification of the hidden variables model, and possibly the construction of the probabilistic model, of unorthodox impedance matrices. By unorthodox, we mean impedance matrices that were not computed numerically, nor measured experimentally. The charts of Sieffert and Cevaer [1992] are one such example. The way the hidden variables model is identified, and the probabilistic model constructed, indeed allows the use of such charts to be considered as a mean model. This might find application, although remote, in possible probabilistic design codes. As these codes are more based on charts than on complicated numerical computations or experimental measures, our approach might offer a device to complement usual deterministic charts with probabilistic equivalents. The dispersion parameters would, however, have to be specified for each type of soil or class of problem, much like is done today with, for example, the security coefficients.

Finally a last important generalization of the constructions described here concerns the identification of measured experimental impedance matrices. The interpolation method (Sec. 4.2) we used in the applications is based on a LLS minimization, which is not appropriate for that type of identification. Other schemes, possibly stochastic (see the discussion in Sec. 4.1.1), would have to be considered, and implemented. However, the capability to identify experimental hidden variables model, and nonparametric probabilistic models of experimental impedance matrices, would really open the way to the experimental identification of the dispersion parameters.

# Appendix A

## Mathematical notations and definitions

### A.1 Notations

We present here some of the main notations that are used in this dissertation. It is recalled that the implicit summation over repeated indices is used throughout. It is also stressed that vectors are put within brackets, as the matrices, although we try to differentiate them by using, respectively, lower case and upper case. Bold fonts are reserved for random quantities, in upper case, and to continuous fields, in lower case.

Let  $[x] = (x_1, \dots, x_n)$  be a vector of the euclidian space  $\mathbb{R}^n$ , equipped with the usual scalar product  $([x], [y])_{\mathbb{R}} = [x]^T [y]$  and the associated euclidian norm  $\|[x]\|_{\mathbb{R}} = ([x], [x])_{\mathbb{R}}^{1/2}$ . The hermitian space  $\mathbb{C}^n$  is equipped with the hermitian scalar product  $([x], [y])_{\mathbb{C}} = ([x], \overline{[y]})_{\mathbb{R}}$  and its associated norm  $\|[x]\|_{\mathbb{C}} = ([x], [x])_{\mathbb{C}}^{1/2} = ([x], \overline{[x]})_{\mathbb{R}}^{1/2}$ , where  $\overline{[x]}$  is the complex conjugate of  $[x]$ . Let  $\mathbb{K}$  be  $\mathbb{R}$  or  $\mathbb{C}$  when equivalent relations exist in both cases.  $\mathbb{M}_{mn}(\mathbb{K})$  is the space of  $n \times m$  matrices  $[A]$  whose elements  $A_{ij}$  are in  $\mathbb{M}_n(\mathbb{K})$ . The vectors of  $\mathbb{K}^n$  are identified to the column matrices in  $\mathbb{M}_{n1}(\mathbb{K})$ .  $[I_{nm}]$  is the identity matrix in  $\mathbb{M}_{nm}(\mathbb{K})$ , whose elements are such that  $I_{ii} = 1$  and  $I_{ij, j < i} = 0$ , and  $[0_{nm}]$  denotes the null matrix in  $\mathbb{M}_{nm}(\mathbb{K})$ , whose elements are all equal to 0. When  $n = m$ ,  $\mathbb{M}_n(\mathbb{K}) = \mathbb{M}_{nn}(\mathbb{K})$ ,  $[I_n] = [I_{nn}]$  and  $[0_n] = [0_{nn}]$ . The determinant, the trace, the transpose and the adjoint of a matrix  $[A]$  in  $\mathbb{M}_n(\mathbb{K})$  are denoted  $\det[A]$ ,  $\text{tr}[A] = \sum_{j=1}^n A_{jj}$ ,  $[A]^T$  and  $[A]^* = \overline{[A]}^T$ . The subset of  $\mathbb{M}_n(\mathbb{K})$  of symmetric matrices (verifying  $[A] = [A]^T$ ) is denoted  $\mathbb{M}_n^S(\mathbb{K})$ . The subset of  $\mathbb{M}_n^S(\mathbb{K})$  of positive definite matrices (respectively semi-positive definite), such that  $([A][x], [x])_{\mathbb{R}} > 0$  (respectively  $([A][x], [x])_{\mathbb{R}} \geq 0$ )  $\forall [x] \in \mathbb{K}^n \setminus \{[0_{n1}]\}$ . With the Frobenius (or Hilbert-Schmidt) norm, defined for a matrix  $[A]$  in  $\mathbb{M}_n(\mathbb{K})$  by  $\|[A]\|_F = (\text{tr}\{[A][A]^*\})^{1/2}$ , the set  $\mathbb{M}_n(\mathbb{K})$  is a Hilbert space. The subset of  $\mathbb{M}_n(\mathbb{K})$  of the non-singular (invertible) matrices is denoted  $\mathbb{M}_n^*(\mathbb{K})$ .

### A.2 Probability theory

#### Basic principles

In mathematics, probabilities are not defined directly for the values of the random variable that is considered. Rather, they are defined on a space of the causes that imply these values. In practice, that space is never defined precisely and is easily forgotten. However, its existence is linked to the discussion of Sec. 1.2.2, where we considered whether a random variable was intrinsically random, or we did not know how to represent its complicated behavior. That approach means that two principles are required: one to define probabilities on the space of causes, and one to relate these to the probabilities on the values of the random variable itself. These two principles are the probability principle and the causality principle.

Let us therefore consider a variable, the state of which we are interested in. The state of this variable,

in a set  $\mathcal{F}$ , depends on the state of the parameters that variables depends on, in a set  $\mathcal{A}$ . The elements of the set  $\mathcal{A}$  are referred to as causes, and those of  $\mathcal{F}$  as consequences. The probability principle consists in defining a probabilistic space as the triplet  $(\mathcal{A}, \mathcal{T}, P)$ , where

- $\mathcal{A}$  is the set of causes for the state of the variable of interest,
- $\mathcal{T}$  is a  $\sigma$ -field<sup>1</sup> of elements of  $\mathcal{A}$ ,
- and  $P$  is a probability measure<sup>2</sup>, on  $(\mathcal{A}, \mathcal{T})$ .

Denoting  $X$  the application from  $\mathcal{A}$  to  $\mathcal{F}$  that links each cause to its consequence, the causality principle then consists in introducing

- a  $\sigma$ -field  $\mathcal{B}_F$  of the elements of  $\mathcal{F}$ , such that  $X$  is measurable<sup>3</sup>,
- and a probability  $P_X$ , such that

$$\forall B \in \mathcal{B}_F, P_X(B) = P[X^{-1}(B)]. \quad (\text{A.1})$$

The application  $X$  can then be considered a random variable defined on  $(\mathcal{A}, \mathcal{T}, P)$ , with values in  $(\mathcal{F}, \mathcal{B}_F)$ . It is then denoted  $\mathbf{X}$  and the probability  $P_X$  on  $(\mathcal{F}, \mathcal{B}_F)$  is called the law of the random variable  $\mathbf{X}$ . That law is the measure of probability that is considered in practice.

### Second-order random variables in $\mathbb{R}^n$

Most random variables encountered in mechanical applications are second-order random variables with values in  $\mathbb{R}^n$ . We will define them here, and introduce the quantities that are most often used to quantify uncertainty of parameters: mathematical expectation, or mean, covariance, correlation, and standard deviation.

Let us therefore choose an integer  $n$ , and consider a random variable  $[\mathbf{X}] = (\mathbf{X}_1, \dots, \mathbf{X}_n)$  defined on a probabilistic space  $(\mathcal{A}, \mathcal{T}, P)$ , with values in  $\mathbb{R}^n$ . The law of the random variable  $[\mathbf{X}]$  is the probability measure  $P_{[\mathbf{X}]}(dx)$  on  $\mathbb{R}^n$ , where  $dx = dx_1 dx_2 \dots dx_n$ , and such that,  $\forall B \in \mathcal{B}_{\mathbb{R}^n}$ ,

$$\int_B P_{[\mathbf{X}]}(dx) = P_{[\mathbf{X}]}(B), \quad (\text{A.2})$$

where  $\mathcal{B}_{\mathbb{R}^n}$  is the Borel algebra<sup>4</sup> on  $\mathbb{R}^n$ . For a given  $1 \leq \ell \leq n$ , the marginal law  $P_{\mathbf{X}_\ell}$  of  $\mathbf{X}_\ell$  is the probability law  $P_{\mathbf{X}_\ell}(dx_\ell)$  on  $\mathbb{R}$  of the random variable  $\mathbf{X}_\ell$ , and,  $\forall B_\ell \in \mathcal{B}_{\mathbb{R}}$ , the Borel algebra on  $\mathbb{R}$ ,

$$P_{\mathbf{X}_\ell}(B_\ell) = P_{[\mathbf{X}]}(\mathbf{X}_1 \in \mathbb{R}, \dots, \mathbf{X}_\ell \in B, \dots, \mathbf{X}_n \in \mathbb{R}). \quad (\text{A.3})$$

<sup>1</sup>The set  $\mathcal{T}$  of elements of  $\mathcal{A}$  is said to be a  $\sigma$ -field, or  $\sigma$ -algebra, if  $\emptyset \in \mathcal{T}$ ,  $A \in \mathcal{T}$ ,  $A \in \mathcal{T} \implies \mathcal{A} \setminus A \in \mathcal{T}$ , and  $A_n \in \mathcal{T}, n \geq 1, \implies \cup_{n \geq 1} A_n \in \mathcal{T}$

<sup>2</sup>The application  $P$  from  $(\mathcal{A}, \mathcal{T})$  to the real interval  $[0, 1]$  is said to be a probability measure on  $(\mathcal{A}, \mathcal{T})$  if  $P(\mathcal{A}) = 1$ , and, for any family of non-overlapping events  $(A_n)_{n \geq 1}$  in  $\mathcal{T}$ ,  $P(\cup_{n \geq 1} A_n) = \sum_{n \geq 1} P(A_n)$ .

<sup>3</sup>The application  $X$  from  $\mathcal{A}$  to  $\mathcal{T}$  is measurable if  $\forall B \in \mathcal{B}_F, X^{-1}(B) \in \mathcal{T}$ , where  $\mathcal{T}$  and  $\mathcal{B}_F$  are  $\sigma$ -fields on  $\mathcal{A}$  and  $\mathcal{T}$ , and  $X^{-1}(B) = \{a \in \mathcal{A}, X(a) \in B\}$

<sup>4</sup>The Borel algebra on  $\mathbb{R}^n$  is the minimal  $\sigma$ -field on  $\mathbb{R}^n$  containing all the open sets. It can be generated by all the products of intervals in the form  $] - \infty, a_1[ \times \dots \times ] - \infty, a_n[$ , with  $(a_1, \dots, a_n)$  spanning  $\mathbb{R}^n$ .

The law  $P_{[\mathbf{X}]}$  may be defined by the cumulative distribution function  $x \mapsto F_{[\mathbf{X}]}(x)$  on  $\mathbb{R}^n$ , with values on the real interval  $[0, 1]$ , and such that

$$F_{[\mathbf{X}]}(x) = P_{[\mathbf{X}]}(B_x) = \int_{y \in B_x} P_{[\mathbf{X}]}(dy), \quad (\text{A.4})$$

with  $B_x = ]-\infty, x_1] \times \dots \times ]-\infty, x_n] \in \mathcal{B}_{\mathbb{R}^n}$ . Alternatively, when it exists (and it will always be the case in practical applications), the density of the measure  $P_{[\mathbf{X}]}(dx)$  with respect to  $dx$  is called the PDF of the random variable  $[\mathbf{X}]$ . It is denoted  $p_{[\mathbf{X}]}(x)$ , and we have

$$P_{[\mathbf{X}]}(dx) = p_{[\mathbf{X}]}(x)dx, \quad (\text{A.5})$$

and  $p_{[\mathbf{X}]} \in L^1(\mathbb{R}^n, \mathbb{R}^+)$ , the space of Lebesgue-integrable functions defined on  $\mathbb{R}^n$  with values in  $\mathbb{R}^+$ .

For  $1 \leq p < +\infty$ , the random variable  $[\mathbf{X}]$  is said to be of order  $p$  if

$$\mathbb{E}\{\|[\mathbf{X}]\|^p\} = \int_{\mathcal{A}} \|X(a)\|_{\mathbb{R}^n}^p dP(a) = \int_{\mathbb{R}^n} \|x\|_{\mathbb{R}^n}^p P_{[\mathbf{X}]}(dx) < +\infty. \quad (\text{A.6})$$

For a random variable  $[\mathbf{X}]$  of order  $p \geq 1$ , we define the mean as  $[m_{[\mathbf{X}]}] = \mathbb{E}\{[\mathbf{X}]\} = \int_{\mathbb{R}^n} x P_{[\mathbf{X}]}(dx)$ . For second-order random variables, we can also define the correlation matrix  $[R_{[\mathbf{X}]}] = \mathbb{E}\{[\mathbf{X}][\mathbf{X}]^T\}$  and the covariance matrix  $[C_{[\mathbf{X}]}] = \mathbb{E}\{([\mathbf{X}] - [m_{[\mathbf{X}]}])([\mathbf{X}] - [m_{[\mathbf{X}]}]^T)\}$ . The covariance matrix is the correlation matrix of the zero-mean random variable  $([\mathbf{X}] - [m_{[\mathbf{X}]}])$ , and both these matrices are positive definite with finite trace. For  $1 \leq \ell \leq n$  the covariance of the random variable  $\mathbf{X}_\ell$  is called the variance, and its square root the standard deviation. The zeros in the correlation matrix correspond to orthogonal random variables, and those of the covariance matrix correspond to uncorrelated random variables.

### Classical Probability Density Functions

In this section, we present a few classical PDFs. We define them for simplicity in the case  $n = 1$ , but multidimensional generalizations also exist. In our case, both the mean and the covariance are real scalars, the latter positive.

**The uniform law** The uniform law on the real interval  $[a, b]$  is defined by the PDF

$$p_{\mathbf{X}}(x) = \begin{cases} \frac{1}{b-a}, & \text{for } x \in [a, b] \\ 0, & \text{for } x < a, \text{ or } x > b. \end{cases} \quad (\text{A.7})$$

The uniform distribution is the one that maximizes the entropy under the one and only constraint of known bounded support.

**The normal law** The normal, or Gaussian, law on  $\mathbb{R}$ , of the random variable  $\mathbf{X}$ , of mean  $m_{\mathbf{X}}$  and positive variance  $\sigma_{\mathbf{X}}^2$  is defined by the PDF

$$p_{\mathbf{X}}(x) = \frac{1}{\sigma_{\mathbf{X}}\sqrt{2\pi}} \exp\left(-\frac{(x - m_{\mathbf{X}})^2}{2\sigma_{\mathbf{X}}^2}\right) \quad (\text{A.8})$$

This law is the most often encountered in the literature. Among the reasons why are its simplicity, its definition from only its mean and variance (or covariance matrix in a multidimensional setting), the

nullity of its cumulants of order superior to 2, and, particularly, the central limit theorem. This theorem states that the joint probability of a large set of independent second-order identically distributed random variables tends to be distributed normally. Since physical parameters are influenced by many natural phenomena, the central limit theorem is often used to justify the normality of a physical parameter. However the independence of the natural phenomena is not always easy to demonstrate, so that the normal distribution should be used with care. In particular, when the values of a parameter are known not to span the entire real line (the mass, for example, is always positive), the normal distribution is not appropriate. The normal law is also the law that maximizes the entropy under the constraint of known mean and standard deviation.

**The log-normal law** The log-normal distribution is the distribution of any random variable whose logarithm is normally distributed. For a random variable of mean  $m_{\mathbf{X}} = \exp(m + \sigma/2)$  and variance  $\sigma_{\mathbf{X}}^2 = (\exp(\sigma^2) - 1) \exp(2m + \sigma^2)$ , its PDF is

$$p_{\mathbf{X}}(x) = \frac{1}{x\sigma\sqrt{2\pi}} \exp\left(-\frac{(\ln x - m)^2}{2\sigma^2}\right) \quad (\text{A.9})$$

It is sometimes used to bypass the difficulty mentioned above for the modeling of positive physical parameters. The central limit theorem justifies the log-normal law when considering the influence of the product, rather than the sum, of infinitely many independent identically distributed random variables.

**The Gamma law** Considering a shape parameter  $k > 0$ , and a scale parameter  $\theta > 0$ , the PDF of the Gamma distribution is defined for  $x > 0$  by

$$p_{\mathbf{X}}(x) = x^{k-1} \frac{\exp^{-x/\theta}}{\theta^k \Gamma(k)}, \quad (\text{A.10})$$

where  $\Gamma(k) = \int_0^{+\infty} t^{k-1} \exp^{-t} dt$ .

**The (symmetric) triangular law** The symmetric triangular law on the interval  $[a, b] \in \mathbb{R}$  is defined by

$$p_{\mathbf{X}}(x) = \begin{cases} \frac{4(x-a)}{(b-a)^2}, & \text{for } x \in [a, \frac{(a+b)}{2}] \\ \frac{4(b-x)}{(b-a)^2}, & \text{for } x \in ]\frac{(a+b)}{2}, b] \\ 0, & \text{for } x < a, \text{ or } x > b. \end{cases} \quad (\text{A.11})$$

These five PDFs are drawn in Box 2.1.1, with the parameters chosen so as to impose a same mean ( $m_{\mathbf{X}} = 2$ ) and standard deviation ( $\sigma_{\mathbf{X}} = 1$ ) for all of them. Namely, for the uniform law,  $a = 0.27$  and  $b = 3.73$ , for the normal law,  $m_{\mathbf{X}} = 2$  and  $\sigma_{\mathbf{X}} = 1$ , for the log-normal law,  $m = 0.58$ , and  $\sigma = 0.47$ , for the Gamma law,  $k = 4$  and  $\theta = 5$ , and for the symmetric triangular law  $a = 0.59$  and  $b = 3.41$ .

## Stochastic processes

The random variables are the equivalent in probability theory of parameters. We define here the stochastic processes, which are the equivalent of functions. Let us therefore consider, for a positive integer  $d$ , an open subset  $T$  of  $\mathbb{R}^d$ . A stochastic process defined on  $(\mathcal{A}, \mathcal{T}, P)$ , indexed by  $T$ , with values in  $\mathbb{R}^n$  is an application from  $T$  to  $L^0(\mathcal{A}, \mathbb{R}^n)$ ,  $t \mapsto [\mathbf{X}(t)] = [\mathbf{X}_1(t), \dots, \mathbf{X}_n(t)]$ . In practice, the name stochastic

process is reserved for the case  $d = 1$ , as when considering random functions of time, and for  $d \geq 2$  we use the name stochastic field, as when considering random functions of space. For any  $a \in \mathcal{A}$ , the application  $t \mapsto \mathbf{X}(t, a)$  from  $T$  to  $\mathbb{R}^n$  is called a sample of the random process.

If the set of all non-empty and non-ordered subsets of  $T$  is denoted  $I$ , for any  $i = \{t_1, \dots, t_m\} \in I$ , the application  $a \mapsto \mathbf{X}_i(a) = [\mathbf{X}(t_1, a), \dots, \mathbf{X}(t_m, a)]$  is a random variables on  $(\mathcal{A}, \mathcal{T}, P)$  with values in  $(\mathbb{R}^n)^m$ . Its law is denoted  $P_{\mathbf{X}_i}$ . When  $i$  spans  $I$ , the set of all these laws constitutes the system of marginal laws of the random process  $[\mathbf{X}]$ .

If we consider a group  $G$  of transformations of  $T$ , such that the identical transformation be in  $G$  and  $G$  be stable by composition, and that, for any  $g \in G$ , the random processes  $[\mathbf{X}(t)]$  and  $[\mathbf{X}(g(t))]$  have the same system of marginal laws, then the random process  $[\mathbf{X}(t)]$  is said to be stationary with respect to  $G$ . The most usual example of stationarity is for  $T = \mathbb{R}^d$  and the group  $G$  of translations  $t \mapsto t + \tau$ , which defines classical stationarity on  $\mathbb{R}^d$ .

In physical applications, we will consider only second-order random processes, because they correspond to stochastic representations of quantities with finite energy. These processes are such that  $t \mapsto [\mathbf{X}(t)] \in L^2(\mathcal{A}, \mathbb{R}^n)$ . The mean, autocorrelation, and covariance are introduced similarly as in the case of multidimensional random variables. They are defined respectively on  $T$ ,  $T \times T$ , and  $T \times T$ , and are  $[m_{[\mathbf{X}]}(t)] = E\{[\mathbf{X}(t)]\}$ ,  $[R_{[\mathbf{X}]}(t, t')] = E\{[\mathbf{X}(t)][\mathbf{X}(t')]^T\}$ , and  $[C_{[\mathbf{X}]}(t, t')] = E\{([\mathbf{X}(t)] - [m_{[\mathbf{X}]}(t)])([\mathbf{X}(t')] - [m_{[\mathbf{X}]}(t')])^T\}$ . A second-order random process is said to be mean-square continuous if the application  $t \mapsto [\mathbf{X}(t)]$  is continuous from  $T$  to  $L^2(\mathcal{A}, \mathbb{R}^n)$ . A necessary and sufficient condition for mean-square continuity is that the autocorrelation be continuous on  $T \times T$ . A random process is said to be mean-square stationary if its mean is constant on  $T$ , and its autocorrelation function depends only on the time lag  $[R_{[\mathbf{X}]}(t, t')] = [R_{[\mathbf{X}]}(t + u, t' + u)]$ , for all  $(t, t', u) \in T^3$ . Stationarity implies mean-square stationarity but the converse is not true. When it exists, the Fourier transform of the autocorrelation function is called the Spectral Density function, and denoted  $[S_{[\mathbf{X}]}(\omega)]$ . For  $1 \leq i, j \leq n$ , when  $[S_{\mathbf{X}_i}(\omega)]$  and  $[S_{\mathbf{X}_j}(\omega)]$  are not zero, the coherency is defined as

$$\gamma = \frac{|S_{\mathbf{X}_i \mathbf{X}_j}(\omega)|^2}{[S_{\mathbf{X}_i}(\omega)][S_{\mathbf{X}_j}(\omega)]}. \tag{A.12}$$

### Classical examples of stochastic processes

**Gaussian process** A process  $[\mathbf{X}(t)]$  indexed on  $T \subset \mathbb{R}^d$ , with values in  $\mathbb{R}^n$  is said to be Gaussian, if all the probability measures of its system of marginal laws are Gaussian.

**Markov process** A Markov, or memoryless, process is a process for which knowledge on previous values does not add information for the determination of the future values. More precisely, for a given  $B \in \mathcal{B}_{\mathbb{R}^n}$ , and  $t_2 < t_1 < t < +\infty$ , if  $P\{[\mathbf{X}(t)] \in B \mid [\mathbf{X}(t_1)] = x_1, [\mathbf{X}(t_2)] = x_2\}$  is the probability of the event  $\{[\mathbf{X}(t)] \in B\}$  conditional on the value of  $[\mathbf{X}]$  at time  $t_1$  being  $x_1$ , and at time  $t_2$  being  $x_2$ , we have

$$P\{[\mathbf{X}(t)] \in B \mid [\mathbf{X}(t_1)] = x_1, [\mathbf{X}(t_2)] = x_2\} = P\{[\mathbf{X}(t)] \in B \mid [\mathbf{X}(t_1)] = x_1\} \tag{A.13}$$

This process is particularly important when considering the Fokker-Planck equation.

**Wiener process** A Wiener process  $\mathbf{W}(t)$  defined on  $(\mathcal{A}, \mathcal{T}, P)$ , indexed on  $\mathbb{R}^+$ , with values in  $\mathbb{R}$ , is a Gaussian stochastic process with independent increments. For  $0 \leq s < t < +\infty$ , the increment

$\Delta W_{st} = \mathbf{W}(s) - \mathbf{W}(t)$  is a second-order Gaussian random variable with covariance  $C_{\Delta W_{st}} = (s - t)$ . It is non-stationary, and its paths are almost surely continuous and non-differentiable. It is used for  $\hat{\text{Ito}}$  stochastic differential equation.

### Classical examples of correlation functions

Most correlation structures for stationary random processes are defined with reference to a scale of fluctuation  $\tau$  (with the dimension of time for random processes and length for random fields). This scale allows to compare the strength of different correlation functions. The values of a random processes at two times separated by less than that scale of fluctuation can be considered heavily correlated, while for times further apart, they will be considered close to uncorrelated. More details on the different meanings of this scale of fluctuation in Vanmarcke [1977] and the examples of correlation structures in Table A.1 in Popescu [1995].

The correlation function most often encountered in the literature for stationary random processes is the exponential correlation function. It depends on the positive delay  $\Delta t = |t_1 - t_2|$ , where  $t_1$  and  $t_2$  are the times at which the random process is evaluated, and is defined by

$$\rho(\Delta t) = \exp\left(-2\frac{\Delta t}{\tau}\right). \quad (\text{A.14})$$

Other common correlation functions can be found in the Table A.1

Name	Correlation function
Exponential	$\exp\left(-2\frac{\Delta t}{\tau}\right)$
Squared exponential	$\exp\left(-\pi\left(\frac{\Delta t}{\tau}\right)^2\right)$
Cosine Decaying	$\exp\left(-\frac{\Delta t}{\tau}\right) \cos\left(\frac{\Delta t}{\tau}\right)$
Modulated exponential	$\exp\left(-4\frac{\Delta t}{\tau}\right) \left(1 + 4\frac{\Delta t}{\tau}\right)$
Triangular	$\begin{cases} 1 - \frac{\Delta t}{\tau} & , \text{ for } \Delta t \leq \tau \\ 0 & , \text{ for } \Delta t > \tau \end{cases}$

Table A.1: Definition of a few classical correlation functions.

# List of Figures

1	Variance normalisée (trait plein noir) du terme de pompage de la matrice d'impédance pour un modèle (a) paramétrique, et (b) non-paramétrique, et contribution des premiers modes de la matrice de covariance (traits discontinus). . . . .	v
2	Spectre de plancher en haut du bâtiment-réacteur pour un modèle déterministe (ligne continue rouge), un modèle à variables cachées (ligne discontinue bleue), et un modèle probabiliste (moyenne en ligne rouge discontinue et intervalle de confiance à 90%, en jaune pour $\delta = 0.1$ et en gris pour $\delta = 0.3$ ) de l'impédance. . . . .	v
1.1	General mechanical problem posed on the entire domain $\Omega$ and corresponding decomposed problem posed on subdomains $\Omega_1$ and $\Omega_2$ interacting through their common boundary $\Gamma$ . . . . .	2
1.2	A domain $\Omega_\ell$ and its boundary of interest $\Gamma$ . . . . .	3
1.3	2-DOFs series system. . . . .	4
1.4	(a) real part, (b) imaginary part, (c) amplitude, and (d) phase of the impedance in Eq. (1.10), for $\mu = 1$ , $\xi = 0.5$ (solid lines) or $\xi = 1$ (dashed lines), $\zeta = 0.05$ (red and magenta lines) or $\zeta = 0.2$ (blue and cyan lines), and $\alpha_k = 0.5$ (cyan and magenta lines) or $\alpha_k = 1$ (blue and red lines). The black solid line is the same as the red dashed line, with $\mu = 0.5$ . . . . .	5
2.1	Example of an earthquake ground motion recorded during a Magnitude 4.2 earthquake in Grenoble (France) on January 11, 1999 [Ambraseys et al., 2001] at the Campus Universitaire site. . . . .	12
2.2	PDFs and tails of the cumulative distribution functions for some distributions with the same mean ( $\mu = 2$ ) and standard deviation ( $\sigma = 1$ ): Normal (dash-dotted blue line), lognormal (dashed green line), Gamma (solid red line), uniform (solid magenta thin line), and symmetric triangular (cyan dashed thin line). . . . .	13
2.3	(a) Correlation function and (b) normalized spectral density function for several models with the same scale of fluctuation ( $\tau = 1$ s): exponential model (solid blue line), squared exponential model (dashed green line) and triangular model (dash-dotted red line). . . . .	15
2.4	Realizations of an exponentially-correlated stationary Gaussian random process ( $\tau = 2$ s) synthesized by (a) the spectral representation method and (b) the KL expansion. Two paths are presented for each method, along with the modes used for the first of the two paths. . . . .	17
2.5	(a) Example of a failure function $g$ in the plane of the parameters $(\mathbf{Y}_1, \mathbf{Y}_2)$ , corresponding safe set and failure set, and reliability index $\beta$ , and (b) FORM approximation of the same failure function and corresponding safe and failure sets. . . . .	26
2.6	Failure surface, safe and failure sets, and reliability index for (a) a series structure and (b) a parallel structure. . . . .	27
3.1	Setting of the Boundary Value Problem: (bounded) domain $\Omega$ and boundary $\Gamma$ with respect to which the impedance will be defined. . . . .	30

4.1	(a) Real part, (b) imaginary part, (c) amplitude, and (d) phase of the (1,1)-, (2,2)-, and (1,2)-elements of an example of impedance matrix (solid red line), and corresponding identified functions with 4 hidden state variables (dashed blue line), and 3 hidden state variables (dash-dotted blue line). The resonance frequencies of the input impedance are at 0.2, 0.4, 0.7, and 0.9 rad/s. . . . .	58
4.2	Real part of the (1,1)-, (2,2)-, and (1,2)-elements of the input impedance matrix (solid red line), and corresponding identified functions on $B^*$ with 4 hidden variables (dotted magenta line), on $B_L$ with 2 (dotted blue line) and 4 hidden variables (dashed blue line), and on $B_H$ with 2 (dotted green line) and 4 hidden variables (dashed green line). . . . .	61
4.3	Real part of the (1,1)-, (2,2)-, and (1,2)-elements of the noisy input impedance matrix (solid red line), and corresponding identified functions (dashed blue line) in the case $\alpha = 0.05$ (low noise). . . . .	62
4.4	Real part of the (1,1)-, (2,2)-, and (1,2)-elements of the noisy input impedance matrix (solid red line), and corresponding identified functions (dashed blue line) in the case $\alpha = 0.3$ (high noise). . . . .	62
4.5	Real part of the (1,1)-, (2,2)-, and (1,2)-elements of the input impedance matrix for the original system (solid red line), for the system with non-diagonal $[\tilde{D}_h]$ (solid magenta line), and for the hidden variables model identified from the latter (dashed blue line). . . . .	63
5.1	A typical soil-structure interaction problem: a building $\Omega_b$ resting on a soil $\Omega_s$ , and excited by a seismic wave. The displacement field in the soil $\mathbf{u}$ is usually decomposed in an incident displacement field $\mathbf{u}_i$ and a scattered displacement field $\mathbf{u}_d$ , such that $\mathbf{u} = \mathbf{u}_i + \mathbf{u}_d$ . . . . .	68
5.2	Decomposition of the SSI problem: computation of the equivalent seismic load $\mathbf{F}^s$ , computation of the soil impedance $[Z_s]$ , and resolution of the global problem on the structure. . . . .	70
5.3	(a) A surface foundation over a homogeneous space, and (b) an embedded foundation over a homogeneous layer on rigid bedrock. The proportions for the radius of the foundation $r$ , the embedment $D$ and the height of the layer $H$ are those used for the examples of this dissertation, namely $H/r = 3$ , and $D = r$ . . . . .	74
5.4	Stiffness coefficients of the soil impedance matrix computed with MISS (solid black line), Sieffert and Cevaer [1992] charts (solid red line), and the lumped parameter models of Wolf and Somaini [1986] (dashed blue line), Wu and Lee [2002] (dash-dotted blue line), Jean et al. [1990] (solid blue line), and de Barros and Luco [1990] (dotted blue line, only for pumping). . . . .	75
5.5	Damping coefficients of the soil impedance matrix computed with MISS (solid black line), Sieffert and Cevaer [1992] charts (solid red line), and the lumped parameter models of Wolf and Somaini [1986] (dashed blue line), Wu and Lee [2002] (dash-dotted blue line), Jean et al. [1990] (solid blue line), and de Barros and Luco [1990] (dotted blue line, only for pumping). . . . .	77
5.6	Stiffness coefficients of the soil impedance matrix computed with MISS (solid black line), Sieffert and Cevaer [1992] charts (solid red line, up to $a_0 = 3$ for rocking), and the lumped parameter models of Wolf and Paronesso [1992] (solid blue line, up to $a_0 = 2.5$ for pumping and torsion, and up to $a_0 = 1$ for the other elements). . . . .	78

5.7	Damping coefficients of the soil impedance matrix computed with MISS (solid black line), Sieffert and Cevaer [1992] charts (solid red line, up to $a_0 = 3$ for rocking), and the lumped parameter models of Wolf and Paronesso [1992] (solid blue line, up to $a_0 = 2.5$ for pumping and torsion, and up to $a_0 = 1$ for the other elements). . . . .	79
5.8	Example of an earthquake ground motion: accelerograms recorded during a Magnitude 4.2 earthquake in Grenoble (France) on January 11, 1999 [Ambraseys et al., 2001] (a-b) at the Campus Universitaire site, on soft soil at 18km from the epicenter, (c) at the Musée Dauphinois site, on rock at 18km from the epicenter, and (d) at the Annecy Préfecture site, on soft soil at 100km from the epicenter. . . . .	81
5.9	Examples of coherency functions in the literature (at $\omega = 5$ rad/s): Hoshiya and Ishii [1983] model (solid blue line) with parameters $V_s = 300$ m/s and $b = 0.1$ , Luco and Wong [1986] model (dashed green line) with parameters $\gamma/\beta = 2 \times 10^{-4}$ , and Harichandran and Vanmarcke [1986] model (dash-dotted red line) with parameters $A = 0.736$ , $\alpha = 0.147$ , $k = 1740$ m, $b = 2.78$ , and $f_0 = 1.09$ Hz. . . . .	83
5.10	Variation of the unit weight with depth in a boring drilled in the Gulf of Mexico at the location of an oil production platform (data taken from Fenton [1997]): (a) raw data (red circles), piece-wise constant trend (green dashed line), and 3rd order polynomial interpolated trend (blue dash-dotted line), and (b) normalized detrended data supposing a piece-wise constant trend. . . . .	84
5.11	Fluctuations of a soil parameter, within a box of dimensions $20 \times 20 \times 10\text{m}^3$ , for different correlation lengths in the horizontal ( $L_h$ ) and vertical directions ( $L_v$ ), using a model by Soize [2006]. . . . .	86
5.12	(a) configuration of the stochastic parametric problem, and (b) mesh used with software MISSVAR (922 nodes, 1422 elements). . . . .	88
5.13	Stiffness coefficients of the soil impedance matrix computed with MISSVAR: response without the heterogeneity (solid red line), frequency-wise mean (dashed red line) and 90%-confidence interval (yellow patch) for 200 Monte Carlo trials, and one particular Monte Carlo trial (solid black line). . . . .	90
5.14	Damping coefficients of the soil impedance matrix computed with MISSVAR: response without the heterogeneity (solid red line), frequency-wise mean (dashed red line) and 90%-confidence interval (yellow patch) for 200 Monte Carlo trials, and one particular Monte Carlo trial (solid black line). . . . .	91
5.15	Convergence of frequency-wise mean (solid lines) and 90%-confidence intervals (dashed lines) for the amplitude of the elements of the impedance matrix computed using MISSVAR, at frequencies (a) $a_0 = 0.5$ , and (b) $a_0 = 3.0$ . Beware that the scales are different for the two frequencies. . . . .	92
5.16	Normalized total variance (solid black line) of the elements of the random impedance matrix, and normalized variance for the first two eigenmodes of the covariance matrix. The eigenvalue of the first mode (dashed red line) represents 71% of the trace of the covariance matrix, and the eigenvalue of the second mode (dashed blue line) 14%. . . . .	93
5.17	Estimation of the first-order marginal law of the stiffness coefficient of the elements of the impedance matrix at several frequencies . . . . .	94
5.18	Estimation of the first-order marginal law of the damping coefficient of the elements of the impedance matrix at several frequencies. . . . .	95

5.19	Stiffness coefficients of the soil impedance matrix computed with our nonparametric approach: response computed by MISS (solid red line), identified hidden variables model (dashed blue line), frequency-wise mean (dashed red line) and 90%-confidence interval (yellow patch) for 1000 Monte Carlo trials, and one particular Monte Carlo trial (solid black line). . . . .	96
5.20	Damping coefficients of the soil impedance matrix computed with our nonparametric approach: response computed by MISS (solid red line), identified hidden variables model (dashed blue line), frequency-wise mean (dashed red line) and 90%-confidence interval (yellow patch) for 1000 Monte Carlo trials, and one particular Monte Carlo trial (solid black line). . . . .	98
5.21	Convergence of frequency-wise mean and 90%-confidence intervals for the amplitude of the elements of the impedance matrix computed with the nonparametric method, at frequencies (a) $a_0 = 0.5$ , and (b) $a_0 = 3.0$ . Beware that the scales are different for the two frequencies. . . . .	101
5.22	Normalized total variance (solid black line) of the elements of the random impedance matrix, and normalized variance for the first five eigenmodes of the covariance matrix (dashed red, blue, green, magenta, and cyan lines), for the normal model (thick lines), and the extended model (thin lines). . . . .	101
5.23	Estimation of the first-order marginal law of the stiffness coefficient of the elements of the impedance matrix at several frequencies. . . . .	103
5.24	Estimation of the first-order marginal law of the damping coefficient of the elements of the impedance matrix at several frequencies. . . . .	103
5.25	Typical structures studied by EDF: mixed FE-BE models of (a) a reactor building with its soil and (b) a dam with the soil and water. . . . .	104
5.26	FE model of the structure and corresponding BE model for the foundation. . . . .	105
5.27	Ratio of the amplitude of the displacement at the upmost node of the building to the amplitude of a displacement imposed on the foundation (thin black line), and to the amplitude of a plane SH-wave propagating in the soil, polarized in the direction of the observation (deterministic case in solid red line, hidden variables model in dashed blue line, mean of the probabilistic model in dashed red line, and 90%-confidence interval in yellow patch). . . . .	106
5.28	(a) Spectrum, (b) time history, and (c) pseudo-acceleration response spectrum for the input accelerogram (black line) and the acceleration at the top of the building (red line), in the direction of polarization of the incoming seismic wave. . . . .	107
5.29	Stiffness coefficients of the soil impedance matrix computed with our nonparametric approach: impedance computed by MISS (solid red line), identified hidden variables model (dashed blue line), frequency-wise mean (dashed red line) and 90%-confidence interval (yellow patch) for 1000 Monte Carlo trials, and one particular Monte Carlo trial (solid black line). . . . .	108
5.30	Damping coefficients of the soil impedance matrix computed with our nonparametric approach: impedance computed by MISS (solid red line), identified hidden variables model (dashed blue line), frequency-wise mean (dashed red line) and 90%-confidence interval (yellow patch) for 1000 Monte Carlo trials, and one particular Monte Carlo trial (solid black line). . . . .	110

- 
- 5.31 Convergence of the mean and the 90%-confidence interval of (a) the elements of the soil impedance matrix, for  $a_0 = 7$ , and (b) for the maximum acceleration at the top of the building. . . . . 111
- 5.32 (a) Time history, and (b) pseudo-acceleration response spectrum for the acceleration at the top of the foundation for the deterministic study (solid red line), the hidden variables model (dashed blue line), and the probabilistic model (mean in red dashed line, for  $\delta = 0.1$ , and 90%-confidence interval in yellow patch for  $\delta = 0.1$  and grey patch for  $\delta = 0.3$ ) of the impedance. . . . . 112
- 5.33 Estimations of the probability density function and cumulative density function for the maximum acceleration at the top of the building for the probabilistic model of the impedance matrix (with  $\delta = 0.1$  in thick solid black line, and with  $\delta = 0.3$  in thin dashed black line), and corresponding values for the mean model (solid red line) and the hidden variables model (dashed blue line). . . . . 113



# List of Tables

4.1	Modal parameters of the input system and of the identified systems. . . . .	57
4.2	Coupling damping matrix, $[D_c]$ of the input system and of the identified systems. The columns are organized so as to correspond to increasing modal frequencies, like in Table 4.1. . . . .	59
4.3	Coupling stiffness matrix, $[K_c]$ of the input system and of the identified systems. The columns are organized so as to correspond to increasing modal frequencies, like in Table 4.1. . . . .	60
5.1	Values of the elements of the static stiffness matrix $[K_0]$ for a rigid circular surface and embedded foundations. $G$ is the shear modulus, $\nu$ is Poisson's ratio, $r$ is the radius of the foundation, $H$ is the height of the first layer, and $D$ is the embedment height. . . . .	73
5.2	Modal parameters of the hidden variables model corresponding to a rigid embedded foundation on a homogeneous layer of soil on rigid bedrock. . . . .	99
5.3	Coupling part of the damping matrix $[D_c]$ and stiffness matrix $[K_c]$ of the hidden variables model corresponding to a rigid embedded foundation on a homogeneous layer of soil on rigid bedrock. The lines of the matrices correspond, in that order, to the shaking, the pumping, the rocking, and the torsion. . . . .	99
5.4	Thickness $h$ , unit mass $\rho$ , pressure velocity $c_p$ , shear velocity $c_s$ , Young's modulus $E$ , shear modulus $G$ , Poisson's ratio $\nu$ , Lamé's coefficients $\lambda$ and $\mu$ , and hysteretic damping coefficient $\beta$ of the layers and substratum of soil. . . . .	106
5.5	Modal parameters of the hidden variables model corresponding to a rigid circular surface foundation over a horizontally-layered soil. . . . .	109
5.6	Coupling part of the damping matrix $[D_c]$ and stiffness matrix $[K_c]$ of the hidden variables model corresponding to a rigid circular surface foundation over a horizontally-layered soil. . . . .	110
A.1	Definition of a few classical correlation functions. . . . .	124



# List of Acronyms

<b>AR</b>	Auto-Regressive
<b>ARMA</b>	Auto-Regressive, Moving Average
<b>BE</b>	Boundary Element
<b>BLUE</b>	Best Linear Unbiased Estimator
<b>BVP</b>	Boundary Value Problem
<b>CPT</b>	Cone Penetration Test
<b>DD</b>	Domain Decomposition
<b>DOF</b>	Degree-of-Freedom
<b>EDF</b>	Électricité de France
<b>FE</b>	Finite Element
<b>FFT</b>	Fast Fourier Transform
<b>FORM</b>	First-Order Reliability Method
<b>FRF</b>	Frequency Response Function
<b>HV</b>	Hidden Variable
<b>IRF</b>	Impulse Response Function
<b>KL</b>	Karhunen-Loève
<b>KUL</b>	Katholieke Universiteit Leuven
<b>LLS</b>	Linear Least Squares
<b>LS</b>	Least Squares
<b>LTI</b>	Linear Time Invariant
<b>MA</b>	Moving Average
<b>MCS</b>	Monte Carlo Sampling
<b>MDOF</b>	Multiple-Degrees-of-Freedom
<b>MIMO</b>	Multiple-Input, Multiple-Output
<b>NLS</b>	Nonlinear Least Squares

- PC** Polynomial Chaos
- PDF** Probability Density Function
- PML** Perfectly Matched Layer
- SASW** Spectral Analysis of Surface Waves
- SEPTEN** Service d'Études et Projets Thermiques et Nucléaires
- SBE** Stochastic Boundary Element
- SDOF** Single-Degree-of-Freedom
- SFE** Stochastic Finite Element
- SISO** Single-Input, Single-Output
- SORM** Second-Order Reliability Method
- SSI** Soil-Structure Interaction
- SVD** Singular Value Decomposition

# Bibliography

- Abrahamson, N. A., Bolt, B. A., Darragh, R. B., Penzien, J., and Tsai, Y. B. (1987). The SMART-1 accelerograph array (1980-1987): a review. *Earthquake Spectra*, 3:263–287.
- Abrahamson, N. A., Schneider, J. F., and Stepp, J. C. (1991). Empirical spatial coherency functions for application to soil-structure interaction analyses. *Earthquake Spectra*, 7(1):1–27.
- Allemang, R. J. and Brown, D. L. (1998). A unified matrix polynomial approach to modal identification. *Journal of Sound and Vibration*, 211(3):301–322.
- Ambraseys, N., Smit, P., Sigbjörnsson, R., Suhadolc, P., and Margaris, B. (2001). Internet-site for european strong-motion data. <http://www.isesd.hi.is/>.
- Antoinet, É. (1995). *Intégration de la variabilité spatiale dans l'estimation probabiliste du tassement et du devers de grands ouvrages*. PhD thesis, Université Bordeaux I, Bordeaux, France.
- Arnst, M., Clouteau, D., and Bonnet, M. (2005). Identification of probabilistic structural dynamics model: application to Soize's nonparametric model. In Soize and Schuëller [2005], pages 823–828.
- Arnst, M., Clouteau, D., and Bonnet, M. (2006a). Identification of non-parametric probabilistic models from measured frequency transfer functions. submitted to *Computer Methods in Applied Mechanics and Engineering*.
- Arnst, M., Ta, Q. A., Clouteau, D., and Bonnet, M. (2006b). Identification of random field models for elastic moduli from spectral analysis of compression wave experiments. In *Proceedings of the International Conference on Noise and Vibration Engineering (ISMA2006)*.
- Auvinet, G., Mellah, R., Masrouri, F., and Rodriguez, J. F. (2000). La méthode des éléments finis stochastiques en géotechnique. *Revue Française de Géotechnique*, 93:67–79.
- Balmès, E. (1996). Frequency domain identification of structural dynamics using the pole/residue parametrization. In *Proceedings of the International Modal Analysis Conference*.
- Balmès, E. and Leclère, J.-M. (2003). *Structural Dynamics Toolbox 5.1 (for use with MATLAB)*. SD-Tools, Paris, France. <http://www.sdtools.com>.
- Beattie, C. A. and Smith, S. W. (1992). Optimal matrix approximants in structural identification. *Journal of Optimization Theory and Applications*, 74(1):23–56.
- Bernard, P. (1998). Stochastic linearization : what is available and what is not. *Computers & Structures*, 67(1-3):9–18.
- Bourdeau, P. L. and Amundaray, J. I. (2005). Non-parametric simulation of geotechnical variability. *Géotechnique*, 55(2):95–108.
- Bressey, D., Niandou, H., Elachachi, S., and Houy, L. (2005). A generic approach to soil-structure interaction considering the effects of soil heterogeneity. *Géotechnique*, 55(2):143–150.

- Bultheel, A., Cuyt, A., van Assche, W., van Barel, M., and Verdonk, B. (2005). Generalizations of orthogonal polynomials. *Journal of Computational and Applied Mathematics*, 179:57–95.
- Bultheel, A., van Barel, M., and van Gucht, P. (2004). Orthogonal basis functions in discrete least squares rational approximation. *Journal of Computational and Applied Mathematics*, 164-165:175–194.
- Burczyński, T. (1994). Stochastic boundary element methods: computational methodology and applications. In Spanos, P. D. and Wu, Y.-T., editors, *Probabilistic structural mechanics: advances in structural reliability methods*, pages 42–55. International Union of Theoretical and Applied Mathematics, Springer-Verlag.
- Bycroft, G. N. (1980). Soil-foundation interaction and differential ground motions. *Earthquake Engineering and Structural Dynamics*, 8(5):397–404.
- Caughey, T. K. (1963a). Derivation and application of the Fokker-Planck equation to discrete nonlinear dynamic systems subjected to white random excitation. *Journal of the Acoustical Society of America*, 35(11):1683–1691.
- Caughey, T. K. (1963b). Equivalent linearization techniques. *Journal of the Acoustical Society of America*, 35(11):1706–1711.
- Chabas, F. and Soize, C. (1987). Modeling mechanical subsystems by boundary impedance in the finite element method. *La Recherche Aérospatiale (english edition)*, 5:59–75.
- Chalko, T. J., Gershkovich, V., and Haritos, N. (1996). Direct simultaneous modal approximation method. In *Proceedings of the 14th International Modal Analysis Conference*, volume 2, pages 1130–1136, Dearborn, Michigan, USA.
- Champeney, D. C. (1973). *Fourier transforms and their applications*, volume 1 of *Techniques of physics*. Academic Press, London.
- Clouteau, D. (2000). Interaction sol structure. Course notes of the master dynamique des structures et des systèmes couplés, École Centrale Paris, Châtenay-Malabry, France. in french.
- Clouteau, D. (2003). *Miss 6.3 : Manuel Utilisateur : version 2.2*. École Centrale Paris, Châtenay-Malabry, France. in french.
- Clouteau, D. and Aubry, D. (2001). Computational soil structure interaction. In Hall, W. S. and Oliveto, G., editors, *Boundary element methods for soil-structure interaction*. Kluwer Academic.
- Craig, R. R. and Bampton, M. C. (1968). Coupling of substructures for dynamic analyses. *AIAA Journal*, 6(7):1313–1319.
- Crandall, S. H. (1963). Perturbation techniques for random vibration of nonlinear systems. *Journal of the Acoustical Society of America*, 35(11):1700–1705.
- Crandall, S. H. (2001). Is stochastic equivalent linearization a subtly flawed procedure ? *Probabilistic Engineering Mechanics*, 16:169–176.
- Crandall, S. H. (2006). A half-century of stochastic equivalent linearization. *Structural Control and Health Monitoring*, 13(1):27–40.

- Crouse, C. B., Hushmand, B., Luco, J. E., and Wong, H. L. (1990). Foundation impedance functions: theory vs. experiment. *Journal of Geotechnical Engineering ASCE*, 116(3):432–449.
- Şafak, E. (2006). Time-domain representation of frequency-dependent foundation impedance functions. *Soils Dynamics and Earthquake Engineering*, 26(1):65–70.
- Dautray, R. and Lions, J.-L. (1990). *Mathematical Analysis and Numerical Methods for Science and Technology*. Springer-Verlag.
- de Barros, F. C. and Luco, J. E. (1990). Discrete models for vertical vibrations of surface and embedded foundation. *Earthquake Engineering and Structural Dynamics*, 19(2):289–303.
- Deodatis, G. (1996). Non-stationary stochastic vector processes: seismic ground motion applications. *Probabilistic Engineering Mechanics*, 11:149–168.
- Der Kiureghian, A. (1996). Structural reliability methods for seismic safety assesment: a review. *Engineering Structures*, 18(6):412–424.
- Dessombz, O., Thouverez, F., Laîné, J.-P., and Jézéquel, L. (2001). Calcul des valeurs et vecteurs propres d'une structure stochastique par projection sur un chaos polynomial. calcul de fonctions de transfert stochastiques. In Batoz, J.-L., Ben Dhia, H., and Chauchot, P., editors, *Actes du 5ème Colloque National en Calcul des Structures*, volume 2, pages 983–990.
- Dienstfrey, A. and Greengard, L. (2001). Analytic continuation, singular-value expansions, and Kramers-Kronig analysis. *Inverse Problems*, 17(5):1307–1320.
- Ditlevsen, O. D. and Bjerager, P. (1986). Methods of structural systems reliability. *Structural Safety*, 3:195–229.
- Dominguez, J. (1993). *Boundary elements in dynamics*. Computer Mechanics Publications.
- Favre, J.-L. (1998). Errors in geotechnics and their impact on safety. *Computers & Structures*, 67(1):37–45.
- Favre, J.-L. (2000). Les différents types d'erreurs et leur prise en compte dans les calculs géotechniques. *Revue Française de Géotechnique*, 93:11–20. in french.
- Fenton, G. A. (1997). Probabilistic methods in geotechnical engineering. Workshop presented at ASCE GeoLogan'97 Conference.
- Fenton, G. A. (1999a). Estimation for stochastic soil models. *Journal of Geotechnical and Geoenvironmental Engineering*, 125(6):470–485.
- Fenton, G. A. (1999b). Random field modeling of CPT data. *Journal of Geotechnical and Geoenvironmental Engineering*, 125(6):486–498.
- Franco, G. E., Betti, R., and Longman, R. W. (2006). On the uniqueness of solutions for the identification of linear structural systems. *Journal of Applied Mechanics*, 73(1):153–162.
- Franco, G. E., Yu, J., and Betti, R. (2004). Uniqueness of solutions for the identification of linear reduced order structural systems. In *Proceedings of the 2004 ASME International Mechanical Engineering Congress and Exposition*, Anaheim, California USA.

- Gazetas, G. (1983). Analysis of machine foundation vibrations: state of the art. *Soils Dynamics and Earthquake Engineering*, 2(1):2–42.
- Ghanem, R. G. and Brzakala, W. (1996). Stochastic finite-element analysis of soil layers with random interface. *Journal of Engineering Mechanics*, 122(4):361–369.
- Ghanem, R. G. and Spanos, P. D. (1991). *Stochastic Finite Elements: A Spectral Approach*. Springer-Verlag.
- Ghiocel, D. M. and Ghanem, R. G. (2002). Stochastic finite-element analysis of seismic soil-structure interaction. *Journal of Engineering Mechanics*, 128(1):66–77.
- Givoli, D. (1992). *Numerical Methods for Problems in Infinite Domains*. Studies in Applied Mechanics. Elsevier.
- Givoli, D. and Keller, J. B. (1989). A finite element method for large domains. *Computer Methods in Applied Mechanics and Engineering*, 76:41–66.
- Glaser, S. (1995). System identification and its application to estimating soil properties. *Journal of Geotechnical and Geoenvironmental Engineering*, 121(7):553–560.
- Golub, G. H. and van Loan, C. F. (1983). *Matrix computations*. Johns Hopkins University Press.
- Goovaerts, P. (1999). Geostatistics in soil science: state-of-the-art and perspectives. *Geoderma*, 89:1–45.
- Goovaerts, P. (2000). Estimation or simulation of soil properties? an optimization problem with conflicting criteria. *Geoderma*, 97:165–186.
- Goovaerts, P. (2001). Geostatistical modeling of uncertainty in soil science. *Geoderma*, 103:3–26.
- Grabe, J. (1994). Spatial variation of soil stiffness: spectral density approach. *Soils Dynamics and Earthquake Engineering*, 13(1):25–29.
- Grigoriu, M. (2000). Stochastic mechanics. *International Journal on Solids and Structures*, 37:197–214.
- Guillaume, P., Pintelon, R., and Schoukens, J. (1996). Parametric identification of multivariable systems in the frequency domain - a survey. In *Proceedings of the 21st International Conference on Noise and Vibration Engineering (ISMA)*, pages 1069–1082, Leuven, Belgium.
- Harari, I. (1998). A unified variational approach to domain-based computation of exterior problems of time-harmonic acoustics. *Applied Numerical Mathematics*, 27(4):417–441.
- Harichandran, R. S. (1987). Stochastic analysis of rigid foundation filtering. *Earthquake Engineering and Structural Dynamics*, 15:889–899.
- Harichandran, R. S. and Vanmarcke, E. H. (1986). Stochastic variation of earthquake ground motion in space and time. *Journal of Engineering Mechanics*, 112(2):154–174.
- Hasselmann, T. K. (1976). Modal coupling in lightly damped structures. *AIAA Journal*, 14(11):1627–1628.
- Heylen, W., Lammens, S., and Sas, P. (1997). *Modal analysis theory and testing*. Katholieke Universiteit Leuven, Leuven, Belgium.

- Hicks, M. (2005). Risk and variability in geotechnical engineering. *Géotechnique*, 55(1-2):1–188.
- Horn, R. A. and Johnson, C. R. (1990). *Matrix analysis*. Cambridge University Press.
- Hoshiya, M. and Ishii, K. (1983). Evaluation of kinematic interaction of soil-foundation systems by a stochastic model. *Soils Dynamics and Earthquake Engineering*, 2:128–134.
- Ibrahim, R. A. (1987). Structural dynamics with parameter uncertainties. *Applied Mechanics Review*, 40(3):309–328.
- Iguchi, M. (1984). Earthquake response of embedded cylindrical foundation to SH and SV waves. In *Proceedings of the Eighth World Conference on Earthquake Engineering*, volume 3, pages 1081–1088, San Francisco, CA. Englewood Cliffs, N.J. : Prentice-Hall.
- Jaynes, E. T. (1957). Information theory and statistical mechanics. *Physical Review*, 106(4):620–630.
- Jean, W.-Y., Lin, T.-W., and Penzien, J. (1990). System parameters of soil foundations for time domain dynamic analysis. *Earthquake Engineering and Structural Dynamics*, 19(4):541–553.
- Jin, S., Lutes, L. D., and Sarkani, S. (2000). Response variability for a structure with soil-structure interactions and uncertain soil properties. *Probabilistic Engineering Mechanics*, 15:175–183.
- Johnson, E. A., Proppe, C., Jr, B. F. S., Bergman, L. A., Székely, G. S., and Schuëller, G. I. (2003). Parallel processing in computational stochastic dynamics. *Probabilistic Engineering Mechanics*, 18:37–60.
- Karhunen, K. (1946). Über lineare methoden in der warhscheinlichkeitsrechnung. *Annales Academiae Scientiarum Fennicae, Series AI: Mathematica-Physica*, 37:3–79.
- Kausel, E. (1974). Forced vibrations of circular foundations on layered media. Technical Report R 74-11, Massachusetts Institute of Technology.
- Kleiber, M. (1999). Computational stochastic mechanics. *Computer Methods in Applied Mechanics and Engineering*, 1-4:1–353.
- Kline, S. J. (1985). The purposes of uncertainty analysis. *Journal of Fluids Engineering*, 107(2):153–160.
- Koutsourelakis, P.-S., Pradlwarter, H. J., and Schuëller, G. I. (2004). Reliability of structures in high dimensions, part I: algorithms and applications. In Print.
- Kozin, F. (1988). Autoregressive moving average models of earthquake records. *Probabilistic Engineering Mechanics*, 3(2):58–63.
- Kramers, H. A. (1927). La diffusion de la lumière par les atomes. In *Resoconto del Congresso Internazionale dei Fisici*, volume 2, pages 545–557, Como, Italy. in french.
- Krée, P. and Soize, C. (1986). *Mathematics of Random Phenomena: Random Vibrations of Mechanical Structures*. D. Reidel Publishing Company.
- Kronig, R. d. (1926). On the theory of dispersion of x-rays. *Journal of the Optical Society of America*, 12(6):547–557.

- Lemaire, M. (2005). *Fiabilité des structures - couplage mécano-fiabiliste statique*. Génie Civil. Hermès - Lavoisier. in french.
- Lemaire, M., Favre, J.-L., and Mébarki, A., editors (1995). *Applications of Statistics and Probability - Civil Engineering and Reliability, Proceedings of the ICASP7 Conference*, Paris, France. A. A. Balkema Publishers.
- Leuridan, J. M. and Kundrat, J. A. (1982). Advanced matrix methods for experimental modal analysis - a multi-matrix method for direct parameter extraction. In *Proceedings of the 1st International Modal Analysis Conference*, pages 192–200.
- Levy, E. C. (1959). Complex curve fitting. *IRE Transactions on Automatic Control*, 4:37–43.
- Lévy, P. (1948). *Processus stochastiques et mouvement brownien*. Gauthier-Villars et Cie, Paris. Suivi d'une note de M. Loève. in french.
- Lin, Y. K. and Cai, G. Q. (1995). *Probabilistic structural dynamics: advanced theory and applications*. McGraw-Hill.
- Lin, Y. K., Kozin, F., Wen, Y. K., Casciati, F., Schuëller, G. I., Der Kiureghian, A., Ditlevsen, O. D., and Vanmarcke, E. H. (1986). Methods of stochastic structural dynamics. *Structural Safety*, 3:167–194.
- Loève, M. (1955). *Probability theory, foundation, random sequences*. The University series in higher mathematics. D. Van Nostrand, New-York.
- Luco, J. E. and Mita, A. (1987). Response of circular foundation to spatially random ground motion. *Journal of Engineering Mechanics*, 113(1):1–15.
- Luco, J. E. and Wong, H. L. (1986). Response of a rigid foundation to spatially random ground motion. *Earthquake Engineering and Structural Dynamics*, 14:891–908.
- Luco, J. E. and Wong, H. L. (1992). Identification of soil properties from foundation impedance functions. *Journal of Geotechnical Engineering ASCE*, 118(5):780–795.
- Lumb, P., editor (1971). *Statistics and Probability in Civil Engineering, Proceedings of the 1st International Conference on Applications of Statistics and Probability to Soil and Structural Engineering (ICASP)*, Hong-Kong. Hong-Kong University Press.
- Lutes, L. D., Sarkani, S., and Jin, S. (2000). Response variability of an SSI system with uncertain structural and soil properties. *Engineering Structures*, 22:605–620.
- Mace, B. R., Worden, K., and Manson, G. (2005). Uncertainty in structural dynamics. *Journal of Sound and Vibration*, 288(3):423–790.
- Magoulès, F. and Harari, I. (2006). Absorbing boundary conditions. *Computer Methods in Applied Mechanics and Engineering*, 195(29-32):3551–3902.
- Manohar, C. S. and Ibrahim, R. A. (1999). Progress in structural dynamics with stochastic parameter variations: 1987 to 1996. *Applied Mechanics Review*, 52(5):177–192.
- Manolis, G. D. (2002). Stochastic soil dynamics. *Soils Dynamics and Earthquake Engineering*, 22:3–15.

- Manolis, G. D. and Karakostas, C. Z. (2003). A Green's function method to SH-wave motion in a random continuum. *Engineering Analysis with Boundary Elements*, 27:93–100.
- Mehta, M. L. (1991). *Random matrices*. Academic Press. revised and enlarged second edition.
- Melerski, E. (1988). Thin shell foundation resting on a stochastic soil. *Journal of Structural Engineering*, 114(12):2692–2709.
- Mignolet, M. P. (1993). Simulation of random processes and fields by arma models: A review. In Cheng, A. H.-D. and Yang, C. Y., editors, *Computational Stochastic Mechanics*, pages 149–173. Elsevier.
- Ohayon, R. and Soize, C. (1998). *Structural Acoustics and Vibration*. Academic Press.
- OpenFEM (2006). *OpenFEM. A finite element toolbox for Matlab and Scilab*. SDTools and INRIA.
- Pais, A. L. and Kausel, E. (1990). Stochastic response of rigid foundations. *Earthquake Engineering and Structural Dynamics*, 19:611–622.
- Park, S., Park, I., and Ma, F. (1992). Decoupling approximation of nonclassically damped structures. *AIAA Journal*, 30(9):2348–2351.
- Paronesso, A. (1997). *Rational approximation and realization of generalized force-displacement relationship of an unbounded medium*. PhD thesis, École Polytechnique Fédérale de Lausanne, Lausanne, Switzerland.
- Pecker, A. (2006). Dynamique des structures et des ouvrages. Course Notes (in french).
- Pellisetti, M. F. and Schuëller, G. I. (2006). On general purpose software in structural reliability - an overview. *Structural Safety*, 28:3–16.
- Pellisetti, M. F., Schuëller, G. I., Pradlwarter, H. J., Calvi, A., Fransen, S., and Klein, M. (2006). Reliability analysis of spacecraft structures under static and dynamic loading. *Computers & Structures*, 84:1313–1325.
- Pierce, L. B. (2001). Hardy functions. Junior paper, Princeton University. <http://www.princeton.edu/lbpierce/>.
- Pintelon, R., Guillaume, P., Rolain, Y., and van Hamme, H. (1994). Parametric identification of transfer functions in the frequency domain - a survey. *IEEE Transactions on Automatic Control*, 39(11):2245–2260.
- Pintelon, R., Rolain, Y., Bultheel, A., and van Barel, M. (2004). Frequency domain identification of multivariable systems using vector orthogonal polynomials. In *Proceedings of the 16th International Symposium on Mathematical Theory of Networks and Systems*, Leuven (Belgium).
- Pintelon, R. and Schoukens, J. (2001). *System identification: a frequency domain approach*. IEEE Press, Piscataway.
- Pitilakis, D. (2006). *Effects of the soil nonlinearity on soil-structure interaction*. PhD thesis, École Centrale Paris, Châtenay-Malabry, France.

- Pitilakis, D., Lopez-Caballero, F., Modaresi, A., and Clouteau, D. (2005). Study of the soil-structure interaction using an equivalent linear and an elastoplastic soil model: comparative results. In *Proceedings of the Satellite Conference on Recent Developments in Earthquake Geotechnical Engineering, 16th International Conference on Soil Mechanics and geotechnical Engineering*, pages 183–190, Osaka, Japan.
- Pitilakis, K., Hatzidimitriou, D., Bard, P.-Y., and Manos, G. (1994). EURO-SEISTEST: Volvi-Thessaloniki - a european test site for engineering seismology, earthquake engineering and seismology. In Savidis [1994], pages 3–10.
- Popescu, R. (1995). *Stochastic variability of soil properties: data analysis, digital simulation, effects on system behavior*. PhD thesis, Princeton University, Department of Civil Engineering and Operations Research, Princeton, New Jersey.
- Pradlwarter, H. J. and Schuëller, G. I. (1992). Equivalent linearization - a suitable tool for analyzing MDOF-systems. *Probabilistic Engineering Mechanics*, 8:115–126.
- Pradlwarter, H. J. and Schuëller, G. I. (1997). On advanced Monte Carlo simulation procedures in stochastic structural dynamics. *International Journal on Non-Linear Mechanics*, 32(4):735–744.
- Puel, G. (2004). *Sur une théorie des méconnaissances en dynamique des structures*. PhD thesis, École Normale Supérieure, Cachan, France.
- Rackwitz, R. (2001). Reliability analysis - a review and some perspectives. *Structural Safety*, 23(4):365–395.
- Robert, C. P. and Casella, G. (1999). *Monte Carlo statistical methods*. Springer Texts in Statistics. Springer-Verlag.
- Roberts, J. B. and Spanos, P. D. (1990). *Random vibration and statistical linearization*. John Wiley & Sons, New-York.
- Sanathanan, C. K. and Koerner, J. (1963). Transfer function synthesis as a ratio of two complex polynomials. *IEEE Transactions on Automatic Control*, AC-9(1):56–58.
- Sarkani, S., Lutes, L. D., Jin, S., and Chan, C. (1999). Stochastic analysis of seismic structural response with soil-structure interaction. *Structural Engineering and Mechanics*, 8(1):53–72.
- Savidis, S. A., editor (1994). *Proceedings of the 2nd International Conference on Earthquake Resistant Construction and Design*, Berlin, Germany. Geotechnical Institute, Technical University Berlin, A. A. Balkema Publishers.
- Savin, É. (1999). *Influence de la variabilité spatiale en interaction sismique sol-structure*. PhD thesis, École Centrale Paris, Châtenay-Malabry, France.
- Savin, É. and Clouteau, D. (2002). Elastic wave propagation in a 3D unbounded random heterogeneous medium coupled with a bounded medium. Applications to seismic soil-structure interaction. *International Journal for Numerical Methods in Engineering*, 54(4):607–630.
- Scanlan, R. H. (1976). Seismic wave effects on soil-structure interaction. *Earthquake Engineering and Structural Dynamics*, 4(4):379–388.

- Schuëller, G. I. (1997). A state-of-the-art report on computational stochastic mechanics. *Probabilistic Engineering Mechanics*, 12(4):197–321.
- Schuëller, G. I. (2001). Computational stochastic mechanics - recent advances. *Computers & Structures*, 79:2225–2234.
- Schuëller, G. I., Pradlwarter, H. J., and Koutsourelakis, P.-S. (2004). A critical appraisal of reliability estimation procedures for high dimensions. *Probabilistic Engineering Mechanics*, 19:463–474.
- Shannon, C. E. (1948). A mathematical theory of communication. *The Bell System Technical Journal*, 27:379–423, 623–656.
- Shinozuka, M. (1972). Monte carlo solution of structural dynamics. *Computers & Structures*, 2(5-6):855–874.
- Shinozuka, M. and Deodatis, G. (1996). Simulation of multidimensional gaussian stochastic fields by spectral representation. *Applied Mechanics Review*, 49(1):29–53.
- Sieffert, J.-G. and Cevaer, F. (1992). *Handbook of impedance functions. Surface foundations*. Ouest Éditions.
- Simos, N. and Costantino, C. J. (2004). Soil spatial variability effect on soil-structure interaction studies: enveloping uncertainties in structural response. In Celebi, M., Todorovska, M. I., Okawa, I., and Iiba, M., editors, *Proceedings of the Third UJNR Workshop on Soil-Structure Interaction*.
- Sobczyk, K. and Trębicki, J. (1999). Approximate probability distributions for stochastic systems: maximum entropy method. *Computer Methods in Applied Mechanics and Engineering*, 168(1-4):91–111.
- Socha, L. (2005). Linearization in analysis of nonlinear stochastic systems: Recent results—part i: Theory. *Applied Mechanics Review*, 58(3):178–205.
- Socha, L. and Pawleta, M. (2001). Are statistical linearization and standard equivalent linearization the same methods in the analysis of stochastic dynamic systems? *Journal of Sound and Vibration*, 248(2):387–394.
- Socha, L. and Soong, T. T. (1991). Linearization in analysis of nonlinear stochastic systems. *Applied Mechanics Review*, 10(10):399–422.
- Soize, C. (1988a). Problèmes classiques de dynamiques stochastiques : méthodes d'études. In *Traité Sciences Fondamentales*, volume A, chapter 1346. Techniques de l'Ingénieur, Paris, France. in french.
- Soize, C. (1988b). Steady-state solution of Fokker-Planck equation in higher dimension. *Probabilistic Engineering Mechanics*, 3(4):196–206.
- Soize, C. (1994). *The Fokker-Planck equation for stochastic dynamical systems and its explicit steady state solutions*. Series on Advances in Mathematics for Applied Sciences. World Scientific Publishing Co.
- Soize, C. (2000). A nonparametric model of random uncertainties for reduced matrix models in structural dynamics. *Probabilistic Engineering Mechanics*, 15:277–294.

- Soize, C. (2001). Maximum entropy approach for modeling random uncertainties in transient elastodynamics. *Journal of the Acoustical Society of America*, 109(5):1979–1996.
- Soize, C. (2005). Random matrix theory for modeling uncertainties in computational mechanics. *Computer Methods in Applied Mechanics and Engineering*, 194:1333–1366.
- Soize, C. (2006). Non-gaussian positive-definite matrix-valued random fields for elliptic stochastic partial differential operators. *Computer Methods in Applied Mechanics and Engineering*, 195:26–64.
- Soize, C. and Schuëller, G. I., editors (2005). *Eurodyn 2005: Proceedings of the 6th International Conference on Structural Dynamics*, Paris, France. Millpress.
- Soulié, M., Montes, P., and Silvestri, V. (1990). Modelling spatial variability of soil parameters. *Canadian Geotechnical Journal*, 27(5):617–630.
- Spudich, P. and Cranswick, E. (1984). Direct observation of rupture propagation during the 1979 Imperial Valley earthquake using a short baseline accelerometer array. *Bulletin of the Seismological Society of America*, 74(6):2083–2114.
- Strelitz, S. (1977). On the Routh-Hurwitz problem. *American Mathematical Monthly*, 84(7):542–544.
- Taherzadeh, R. and Clouteau, D. (2006). Soil-pile group and superstructure interaction under seismic loading. In *Proceedings of the 1st European Conference on Earthquake Engineering and Seismology*.
- Takagi, T. (1925). On an algebraic problem related to an analytic theorem of Caratheodory and Fejer and on an allied theorem of Landau. *Japanese Journal of Mathematics*, 1:83–93.
- Toubalem, F. (1996). *Interaction sol-structure en milieux stochastiques*. PhD thesis, École Centrale de Lyon, Ecully, France.
- Toubalem, F., Thouverez, F., and Labbé, P. (1995). Contribution in the study of a transfer function in a medium with random characteristics. In Lemaire et al. [1995], pages 1197–1201.
- Toubalem, F., Zeldin, B., Thouverez, F., and Labbe, P. (1999). Vertical excitation of stochastic soil-structure interaction systems. *Journal of Geotechnical and Geoenvironmental Engineering*, 125(5):349–356.
- Tsynkov, S. V. (1998). Numerical solution of problems on unbounded domains. a review. *Applied Numerical Mathematics*, 27:465–532.
- Turkel, E. (1998). Special issue on absorbing boundary conditions. *Applied Numerical Mathematics*, 27(4):327–560.
- Udwadia, F. E., Sharma, D. K., and Shah, P. C. (1978). Uniqueness of damping and stiffness distributions in the identification of soil and structural systems. *Journal of Applied Mechanics*, 45(1):181–187.
- van Barel, M. and Bultheel, A. (1992). A parallel algorithm for discrete least squares rational approximation. *Numerische Mathematik*, 63:99–121.
- van Barel, M. and Bultheel, A. (1993). Discrete least squares approximation with polynomial vectors. Technical Report TW190, Katholieke Universiteit Leuven, Leuven (Belgium).

- van de Wouw, N. (1999). *Steady-state behaviour of stochastically excited nonlinear dynamic systems*. PhD thesis, Technische Universiteit Eindhoven, Eindhoven.
- Vanmarcke, E. H. (1977). Probabilistic modeling of soil profiles. *Journal of the Geotechnical Engineering Division, Proceedings of the ASCE*, 103(GT11):1227–1246.
- Veletsos, A. S. and Prasad, A. M. (1989). Seismic interaction of structures and soils: stochastic approach. *Journal of Structural Engineering*, 115(4):935–956.
- Wolf, J. P. (1985). *Dynamic soil-structure interaction*. Prentice-Hall, Inc., Englewood Cliffs, N. J.
- Wolf, J. P. (1988). *Soil-structure interaction analysis in time domain*. Prentice-Hall, Inc., Englewood Cliffs, N. J.
- Wolf, J. P. (1991a). Consistent lumped-parameter models for unbounded soil: frequency-independent stiffness, damping and mass matrices. *Earthquake Engineering and Structural Dynamics*, 20(1):33–41.
- Wolf, J. P. (1991b). Consistent lumped-parameter models for unbounded soil: physical representation. *Earthquake Engineering and Structural Dynamics*, 20(1):11–32.
- Wolf, J. P. (1994). *Foundation vibration analysis using simple physical models*. Prentice-Hall, Inc., Englewood Cliffs, N. J.
- Wolf, J. P. and Paronesso, A. (1991). Errata: consistent lumped-parameter models for unbounded soil. *Earthquake Engineering and Structural Dynamics*, 20(6):597–599.
- Wolf, J. P. and Paronesso, A. (1992). Lumped-parameter model for a rigid cylindrical foundation embedded in a soil layer on rigid rock. *Earthquake Engineering and Structural Dynamics*, 21:1021–1038.
- Wolf, J. P. and Somaini, D. R. (1986). Approximate dynamic model of embedded foundation in time domain. *Earthquake Engineering and Structural Dynamics*, 14(5):683–703.
- Wolf, J. P. and Song, C. (1996). *Finite-element modelling of unbounded media*. Wiley, Chichester.
- Wolf, J. P. and Song, C. (2001). The scaled boundary finite-element method - a fundamental solution-less boundary-element method. *Computer Methods in Applied Mechanics and Engineering*, 190(42):5551–5568.
- Wong, H. L., Trifunac, M. D., and Luco, J. E. (1988). A comparison of soil-structure interaction calculations with results of full-scale forced vibration tests. *Soils Dynamics and Earthquake Engineering*, 7(1):22–31.
- Wu, W.-H. and Chen, C.-Y. (2001). Simple lumped-parameter models of foundation using mass-spring-dashpot oscillators. *Journal of the Chinese Institute of Engineers*, 24(6):681–697.
- Wu, W.-H. and Chen, C.-Y. (2002). Simplified soil-structure interaction analysis using efficient lumped-parameter models for soil. *Soil and Foundations*, 42(6):41–52.
- Wu, W.-H. and Lee, W.-H. (2002). Systematic lumped-parameter models for foundations based on polynomial-fraction approximation. *Earthquake Engineering and Structural Dynamics*, 31(7):1383–1412.

- 
- Yamazaki, F. and Shinozuka, M. (1988). Digital generation of non-gaussian stochastic fields. *Journal of Engineering Mechanics*, 114(7):1183–1197.
- Zerva, A. and Zervas, V. (2002). Spatial variation of seismic ground motions: an overview. *Applied Mechanics Review*, 55(3):271–297.
- Zienkiewicz, O. C., Taylor, R. L., and Zhu, J. Z. (2005). *The finite element method*, volume 1. Butterworth-Heinemann, sixth edition.



## Abstract

In many application fields, as in civil engineering or aeronautics, engineers have to deal with design problems where the structure is coupled to an unbounded domain. For these problems, only the structure is of interest, and the behavior of the exterior domain is taken into account through its equivalent stiffness, in statics, or its impedance matrix, in dynamics. The models for the unbounded domains considered in these applications are usually coarse and the information available on their properties scarce and polluted. This leads to errors in the estimation of the behavior of the structure, which may partially be taken into account by using probabilistic approaches.

We present, in this Ph.D. thesis a probabilistic model of impedance matrices, which generalizes the nonparametric approaches introduced recently by Soize for the predictions of vibrations in random structures. The construction of this probabilistic model first requires the construction of a deterministic model, so-called hidden variables model, that verifies the basic properties of impedance matrices, among which the causality. The hidden variables model has to be identified from numerical results or experimental measures, and the identification procedure is also developed in this thesis.

Two applications are presented. Our nonparametric model of the impedance matrix is first compared to a parametric model, on a classical problem in dynamic soil-structure interaction, to illustrate the main differences between the two approaches. Then, it is used in a more industrial seismic design problem, to show the practical application of the nonparametric probabilistic model of impedance matrices

## Résumé

Dans de nombreux domaines d'application, comme en génie civil ou en aéronautique, les ingénieurs sont confrontés à des problèmes de dimensionnement de structures en contact avec un domaine non-borné. Pour ces problèmes, seule la structure intéresse réellement les ingénieurs, et le domaine extérieur n'a d'importance que par sa raideur équivalente, en statique, ou sa matrice d'impédance, en dynamique. Par ailleurs, les domaines infinis considérés dans ces applications sont souvent mal connus ou complexes à modéliser. Cela entraîne des erreurs et incertitudes pour les estimations faites sur la structure, qui peuvent être en partie prises en compte par des approches probabilistes.

On propose donc dans cette thèse un modèle probabiliste des matrices d'impédance, qui généralise l'approche non-paramétrique proposée récemment par Soize pour les prédictions des vibrations de structures aléatoires. La construction de ce modèle probabiliste nécessite tout d'abord la construction d'un modèle déterministe approché, dit à variables cachées, des matrices d'impédance suivant leurs propriétés de base, dont, notamment, la causalité. Ce modèle doit être identifié à partir de calculs numériques ou de mesures, et la procédure d'identification est également développée dans le cadre de la thèse.

Deux applications sont proposées. Le modèle non-paramétrique de matrice d'impédance est d'abord comparé, sur un cas simple d'interaction dynamique sol-structure, à un modèle paramétrique pour illustrer les principales différences entre les approches. Ensuite, un cas plus industriel de dimensionnement sismique permet d'envisager l'utilisation pratique du modèle probabiliste non-paramétrique.